

Evaluation and Optimization of Natural Gas Liquefaction Process with Exergy-Based Methods: A Case Study for C3MR

vorgelegt von

M.Sc.

Eko Primabudi

von der Fakultät III – Prozesswissenschaften

der Technischen Universität Berlin

zur Erlangung des akademischen Grades

Doktor der Ingenieurwissenschaften

- Dr.-Ing. -

genehmigte Dissertation

Promotionsausschuss

Vorsitzender : Prof. Dr. Frank Behrendt

Gutachterin : Prof. Dr. Tetyana Morozyuk

Gutachter : Prof. Dr. Vittorio Verda

Tag der wissenschaftlichen Aussprache: 28. März 2019

Berlin 2019

Acknowledgements

Doing research is an exciting task but doing it in four years as a doctoral student in lovely Berlin settings made it even more challenging. That's why I would like to say my deepest gratitude to all people who contributed to this work. First of all, I would like to thank my supervisor Prof. Tetyana Morozuk, who accepted me as her student and believed in me to accomplish the grueling Ph.D. works, for her encouragement on taking this path. I would also like to thank Prof. George Tsatsaronis for your kindness to provide me assistance, supervision, and peace of mind, especially during our conferences. I am so grateful to have you both in as my supervisors. Secondly, I would like to thank my beloved mother who always let me express myself and supports me in every way possible. My lovely wife who has made unimaginable sacrifices to support my Doctoral degree, my sisters Poppy and Fenty who always be my inspiration, Wisataone team: Faru and Reza, we'll make our dreams come true! Berlin family, Chandra, Luky, Mita, Neni, Alavi, and Aufi who have been my best mates throughout my Ph.D. time. Lunch and hangout friends from TU Berlin: Turfa, Bayu, Fauzan, Yitzhak, Imam, and Bagas. Colleagues of the institute: Jing, Gigi, Saeed, Renzo, Alex, Stefan, Yahya, Steffi and Elisa who have always inspired and motivated me day in and out. Thank you for the productive lunchtime discussions, productivity boost, both technically and non-technically. I would also not forget to mention Jan, Michael and Miriam, for our encounters and their meaningful insights that have opened up the path for my choice to pursue Ph.D. Above all and the most importantly, thanks to God the Almighty for each of His blessings.

Eko Primabudi

Berlin,

February 28th, 2019 22:47

This work is dedicated to my late Father and late Grandfather,
Abdul Aziz and Zoelkarnain Idris.

May God honor them and grant them peace.

Abstract

Propane pre-cooled mixed refrigerant process, known as C3MR, is the leading technology in the LNG market based on the capacity installed. In this study, exergy-based methods were implemented in order to obtain optimal operation conditions. The C3MR process is modeled with 4.5 MTPA production capacity using Aspen Plus process simulator, which is connected to the exergy and exergoeconomic analysis routines, programmed with Microsoft Excel VBA and Python. The exergy efficiency in the base case is 53.3%, whereas the total cost of product was obtained at 109.3 \$/GJ. Furthermore, metaheuristic method such as genetic algorithm (GA) is a popular technique to solve an optimization problem without requiring gradient information of the objective function. It is shown that GA produced a better result when performed sequentially by carefully selecting the design variables according to the results of exergy and exergoeconomic analyses. In comparison with the conventional GA procedure, this approach produced a better performance in terms of exergy efficiency by 3%. Likewise, the sequential approach was applied to minimize the total cost of product, where it was obtained at 92.9 \$/GJ, where the costs of investment account for 70% from the total costs of product. The optimization also revealed that minimizing the exergy destruction in the heat exchangers resulted in high costs of investment, such as in MHX, where the costs were twice as high as in the base case. Additionally, multi-objective optimization of C3MR was carried out with two objective functions: (a) maximizing the exergy efficiency and (b) minimizing the total cost of the product. The result shows that the range of Pareto feasible solutions is between 58% to 64% for exergy efficiency and between 93 to 120 \$/GJ for the specific cost of product. When the exergetic efficiency is maximized at 64.4%, the total cost of product will increase from 93 \$/GJ to 118.5 \$/GJ. The thesis demonstrates the approach for performing optimizations in the LNG process with the aid of exergy-based methods and how the approach can be beneficial to produce an efficient optimization procedure.

Zusammenfassung

C3MR ist die führende Technologie auf dem LNG-Markt, basierend auf der installierten Kapazität. In dieser Studie wurden Exergie-basierte Verfahren implementiert, um optimale Betriebsbedingungen zu erhalten. Der C3MR-Prozess wird mit Produktionskapazität von 4,5 Millionen Tonnen pro Jahr unter Verwendung des Aspen Plus Prozesssimulators modelliert, der an die Exergie- und Exergoökonomischen Analyseroutinen verknüpft ist. Nach dem Ergebnis beträgt der exergetische Wirkungsgrad im Basisfall auf 53,3 % während die Gesamtkosten des Produkts bei 109,3 \$/GJ liegt. Darüber hinaus sind die Metaheuristik wie zum Beispiel der genetische Algorithmus (GA) eine beliebte Technik, um ein Optimierungsproblem zu lösen, ohne dass eine Gradienteninformation der Zielfunktion erforderlich ist. Es wird gezeigt, dass GA ein besseres Ergebnis liefert, wenn es sequentiell durchgeführt wurde, indem die Optimierungsvariablen entsprechend den Ergebnissen von Exergie-basierte Methoden sorgfältig ausgewählt wurden. Im Vergleich zum konventionellen GA-Verfahren erzielte dieser Ansatz eine um 3 % bessere Leistung hinsichtlich des exergetischen Wirkungsgrads. Wird der sequentielle Ansatz angewandt, erzielt die Optimierung der Gesamtkosten bei 92,9 \$/GJ, in denen 70 % davon die Investitionskosten entsteht. Außerdem wurde die Multikriterielle Optimierung mit zwei Zielfunktionen durchgeführt: (a) Maximierung des exergetischen Wirkungsgrads und (b) Minimierung der Gesamtkosten des Produkts. Das Ergebnis zeigt, dass der Bereich der durch Pareto-realisierbaren Lösungen für den exergetischen Wirkungsgrad zwischen 58 % und 64 % und für die spezifischen Produktkosten zwischen 93 und 120 \$/GJ beträgt. Wenn der exergetische Wirkungsgrad bei 64,4 % maximiert ist, wird die Gesamtkosten des Produkts von 93 \$/GJ im Basisfall auf 118,5 \$/GJ gestiegen sind. Die Dissertation führt den Ansatz zur Auswertung und Optimierung des LNG-Prozesses mithilfe Exergie-basierter Methoden vor und wie der Ansatz für ein effizientes Optimierungsverfahren vorteilhaft sein kann.

Contents

Abstract.....	i
Zusammenfassung	ii
Contents	iii
List of Figures.....	viii
List of Tables.....	xi
Nomenclature.....	xiii
1. Introduction	1
1.1. Natural Gas and Liquefied Natural Gas (LNG) Industry	1
1.2. Exergy-based Methods	4
1.3. Exergy Analysis for Liquefaction Processes	5
1.4. Motivation	7
1.5. Research Objectives	8
1.6. Outline of the Thesis.....	9
2. The Liquefied Natural Gas	11
2.1. History of the liquefaction of gases	11
2.2. Natural Gas Production	11
2.3. Liquefaction Process of Natural Gas.....	15

2.3.1.	Overview of the process	15
2.3.2.	Mixed Refrigerant Cycle	17
2.3.3.	Cascade Refrigeration Cycle	18
2.3.4.	PRICO® Process	21
2.3.5.	LIMUM®1 and LIMUM®3	21
2.3.6.	Propane Pre-Cooled Mixed Refrigerant (C3MR).....	23
2.3.7.	Air Products' SMR and Nitrogen Recycle Process	25
2.3.8.	Dual Mixed Refrigerant (DMR).....	26
2.4.	LNG Storage	27
3.	Exergy-based Methods for Energy Systems	30
3.1.	Exergy Analysis	30
3.1.1.	Physical Exergy	32
3.1.2.	Chemical exergy.....	33
3.1.3.	Exergy Balance.....	34
3.2.	Economic Analysis	36
3.2.1.	Total Capital Investment (TCI)	36
3.2.2.	Economic Evaluation	39
3.2.3.	Carrying Charges and Total Revenue Requirement	39

3.2.4.	Total Revenue Requirement	40
3.3.	Exergoeconomics	41
3.3.1.	The Cost Balance and Auxiliary Equations	43
3.3.2.	The Cost Rate of Exergy Destruction and Exergy Losses	44
3.3.3.	Exergoeconomic Factor and the Relative Cost Difference	44
4.	Optimization of the LNG Process.....	46
4.1.	Deterministic Algorithm.....	47
4.2.	Stochastic algorithm.....	49
4.2.1.	Genetic Algorithm	51
4.3.	Multi-objective Optimization	53
4.3.1.	Multi-objective Genetic Algorithm.....	55
4.4.	Optimization of LNG Process – Literature Survey	56
4.4.1.	Single Objective Optimization	56
4.4.2.	Multi-Objective Optimization	59
5.	Base Case Analysis of C3MR Process.....	61
5.1.	Process Modeling and Simulation.....	61
5.2.	Exergy Analysis of C3MR Process.....	66
5.3.	PEC Estimations.....	72

5.3.1.	Compressors.....	72
5.3.2.	Heat Exchangers.....	72
5.3.3.	Coolers.....	74
5.3.4.	Vapor-Liquid Separators.....	75
5.3.5.	J-T Valves	76
5.4.	Economic Analysis	76
5.4.1.	Fixed Capital Investment (FCI)	77
5.4.2.	Other Outlays.....	78
5.4.3.	Fuel and O&M Costs.....	81
5.4.4.	Estimation of TRR	83
5.5.	Exergoeconomic Analysis	86
6.	Single-Objective Optimization of C3MR.....	92
6.1.	Optimization Workflow	92
6.2.	Maximizing the Exergy Efficiency	93
6.2.1.	Optimization of Mixed Refrigerant Cycle (OF1 and OF2)	93
6.2.2.	Optimization of Precooling Cycle (OF3).....	99
6.2.3.	Conventional GA Optimization (OF4).....	101
6.3.	Minimizing the Total Cost of Product (OF5 and OF6)	104

6.3.1.	Comparison Between Base Case, OF3 And OF5.....	110
6.3.2.	The Solutions to the Design Variables	112
7.	Multi-Objective Optimization.....	115
7.1.	Optimization Workflow	115
7.2.	Objective Functions and Decision Variables.....	118
7.3.	Optimization results.....	120
7.3.1.	The effect of design variables	124
8.	Summary and Conclusions.....	128
	Bibliography	131
	Appendix A: Exergy Balance Equations.....	144
	Appendix B: Exergoeconomic Balance	147
	Appendix C: Optimization Modules	153
8.1.	Exergy and Exergoeconomic Analysis in VBA.....	153
8.2.	Aspen Plus Automation (VBA).....	157
8.3.	Initialization of the Optimization	162
8.4.	Genetic Algorithm in Python	166

List of Figures

Figure 1.1 – Relative cost of LNG transportation and cost of pipeline transmission as a function of distance.....	3
Figure 1.2 – LNG trade volumes 1990 – 2017.....	3
Figure 1.3 – The share of liquefaction processes used in the existing LNG Plants.....	4
Figure 2.1 - A typical scheme of natural gas pre-treatment with liquefaction plant	13
Figure 2.2 – Flowsheet for fractionation columns of NGL Recovery Unit.....	15
Figure 2.3 – Schematic process of (a) Linde Process and (b) Claude Process	17
Figure 2.4 – Cascade refrigeration cycle.....	18
Figure 2.5 – Simplified flowsheet and the cooling curve of Klimenko process.	19
Figure 2.6 – Conoco Phillips optimized cascade cycle.....	20
Figure 2.7 – Linde/Statoil’s MFC [®] and MFC [®] 3 Process.....	21
Figure 2.8 – Black & Veatch PRICO [®] Process.....	22
Figure 2.9 – LIMUM [®] 3 liquefaction process for medium-scale LNG plant	22
Figure 2.10 – General flowsheet of AP-C3MR.....	24
Figure 2.11 – Nitrogen recycle process with two or three expanders.....	25
Figure 2.12 – Shell’s proprietary DMR process	28

Figure 3.2 – Illustration of exergoeconomic balance of k^{th} component	42
Figure 4.1 – Pseudo code of genetic algorithms	51
Figure 4.2 – The roulette wheel selection crossover	53
Figure 4.3 –NSGA-II optimization procedure	56
Figure 5.1 – Process flowsheet of C3MR process in Aspen Plus	63
Figure 5.2 – Calculation of the change of state with departure function	66
Figure 5.3 – Distribution of \dot{Z} at the component level and general category.....	87
Figure 6.1 – Optimization workflow of GA using Python, VBA and Aspen Plus	92
Figure 6.2 – Exergy destruction comparison between the base case, OF1, and OF2.....	97
Figure 6.3 – Progress of the exergy efficiency optimization with OF1 and OF2	98
Figure 6.4 – T-Q diagram of MHX1 and MHX2 of base case, OF1, and OF2	99
Figure 6.5 – Exergy destruction for the base case, OF1, OF2, and OF3.....	101
Figure 6.6 – GA progression of OF4 in comparison with OF2 and OF3.....	102
Figure 6.7 – Exergy destruction comparsion between OF3 and OF4.....	104
Figure 6.8 – Exergoeconomics optimization workflow.....	106
Figure 6.9 – The comparison of the objective functions between OF5 and OF6	108
Figure 6.10 – Comparison of $\dot{C}_D + \dot{Z}_k$ between the base case, OF3, and OF5.....	114
Figure 7.1 – Multi-objective optimization workflow	116

Figure 7.2 – Progression of C3MR multi-objective optimization towards Pareto front ...	120
Figure 7.3 – Pareto frontier of multi-objective optimization for C3MR process.....	122
Figure 7.4 – Exergy Destruction in OF3, OF5 and OF7.....	123
Figure 7.5 – Distribution of $\dot{C}_D + \dot{Z}_k$ from all OF7 scenarios.....	125
Figure 7.6 – Distribution of the \dot{E}_D , $\dot{C}_{D,tot}$ and \dot{Z}_{tot} from all OF7 scenarios.....	125

List of Tables

Table 2.1 - Typical Composition of Raw Natural Gas.....	12
Table 3.1 – Items of total capital investment (TCI).....	37
Table 5.1 – Process design variables of the base case simulation.....	62
Table 5.2 – Initial mass fraction of the base case simulation.....	64
Table 5.3 – Thermodynamic base-case data of process material streams.....	68
Table 5.4 – Energy consumption within the components of C3MR process.....	70
Table 5.5 – Exergy analysis of C3MR components.....	71
Table 5.6 – Cost estimations of compressors	73
Table 5.7 – Cost estimation of heat exchangers ($A_{\text{ref}} = 672.43 \text{ m}^2$).....	74
Table 5.8 – Cost estimation of coolers.....	75
Table 5.9 – Cost estimation of vapor-liquid separators.....	76
Table 5.10 – Cost estimation of J-T valves ($\alpha = 0.67$).....	77
Table 5.11 – Parameters and assumptions used in TRR calculation.....	79
Table 5.12 – Calculations of AFUDC in million US\$	81
Table 5.13 – Estimation of Total Capital Investment of the base case.....	82
Table 5.14 – Year-by-year revenue requirement analysis in million US\$	85
Table 5.15 – Specific cost associated with thermal and mechanical exergy	89

Table 5.16 – The results of exergoeconomic analysis for base case	91
Table 6.1 – Genetic algorithm parameters for the optimization.....	95
Table 6.2 – The lower and upper bound of the design variables for OF1 and OF2.....	96
Table 6.3 – The solutions for design variables of OF1 and OF2.....	98
Table 6.4 – Lower and upper bound of the design variables for OF3	100
Table 6.5 – Exergy analysis of the solution from OF4.....	103
Table 6.6 – The optimized design variables of OF3 and OF4.....	105
Table 6.7 – Overview of the exergy and exergoeconomic optimization results	107
Table 6.8 – Exergoeconomic analysis of the solution from OF5.....	109
Table 6.9 – Comparison of exergoeconomic analysis between the optimized cases.....	111
Table 6.10 – The optimized solutions for design variables OF3 and OF5	113
Table 7.1 – Overview of the analysis results of multi-objective optimization.....	122
Table 7.2 – Design variables from all multi-objective optimization scenarios	126
Table 7.3 – Exergoeconomic analysis results of all OF7 scenarios	127

Nomenclature

Abbreviations

AFUDC – allowance for funds used during construction

APCI – Air Products and Chemicals Inc.

C3MR – propane pre-cooled mixed refrigerant cycle

CC – carrying charges

CELF – constant escalation levelized factor

CEPCI – chemical engineering plant cost index

CI – cost index

COP – coefficient of performance

CRF – capital recovery factor

DMR – dual mixed refrigerant cycle

FC – fuel cost

FCI – fixed capital investment

GHG – greenhouse gas

IPCC – Intergovernmental Panel on Climate Change

LIMUM – Linde Multistage Mixed Refrigerant

LNG – liquefied natural gas

MACRS – modified accelerated cost recovery system

MCHE – main cryogenic heat exchanger

MFC – mixed fluid cascade

MHX – main cryogenic heat exchanger

MR – mixed refrigerant

MRC – mixed refrigerant compressors

MRCOL mixed refrigerant coolers

MRCOMP – compressors

MRFL – mixed refrigerant flash tanks

MRMIX – mixed refrigerant mixers

MRTV – mixed refrigerant throttling valve

MTPA – million ton per annum
 NG – natural gas
 NGCC – natural gas combined cycle
 NGL – natural gas liquids
 NGTV – natural gas throttling valve
 OMC – operation and maintenance cost
 PEC – purchased equipment cost
 PF – precooling flash tanks
 PHX – precooling heat exchanger
 PRICO – poly-refrigeration integrated cycle operation
 PROPC – precooling compressors
 PROPC – precooling compressors
 PROPCOL – precooling coolers
 PROPMIX – propane mixers
 PROPTV – propane throttling valve
 SMR – single mixed refrigerant
 TCI – total capital investment
 TRR – total revenue requirement
 VBA – Visual Basic Application

Symbols

A	heat transfer surface area (m ²)
\dot{C}	cost rate associated with exergy transfer cost per unit of exergy (\$/h)
c	specific cost rate of exergy transfer (\$/GJ)
e	specific exergy (kJ/kg)
f	exergoeconomic factor (%)
h	specific enthalpy (kJ/kg)
i_{eff}	effective annual discount rate (%)
n	time period (years)
\dot{Q}	heat transfer duty (MW)
p	pressure (bar)
r	relative cost difference (%)
s	specific entropy (kJ/kg K)
T	Temperature (K)

U	overall heat transfer coefficient (W/m ² K)
v	Specific volume (m ³ /kg)
W	Work (MW)
y	exergy destruction ratio (%)
y^*	exergy destruction rate (%)
ε	exergy efficiency (%)
\dot{Z}	cost rate associated with investment and operation and maintenance (\$/h)

Subs- and Superscript

BM	bare module
ce	common equity
CH	chemical exergy
d	debt
D	exergy destruction
e	effluent
el	electricity
F	exergy of fuel
i	influent
j	stream of matter, year
k	k th component of the system
L	levelized value
OTXI	other taxes and insurance
P	product
PH	physical exergy
ps	preferred stock
r	real escalation
ref	reference state
tot	total system

1. Introduction

1.1. Natural Gas and Liquefied Natural Gas (LNG) Industry

Climate change issue and the demand for a cleaner fuel to produce energy has been taking center stage since the beginning of the 21st century. Fossil energy sources are deemed to be one of the leading causes of climate change, environmental pollution, and even political instability throughout the globe. Currently, some of the developed countries such as Germany and Switzerland attempt to shift their energy policy towards a cleaner and more sustainable options. The strategy, known as “Energiewende” is roughly translated as the energy transition scheme. Fundamentally, the policy aims to gradually minimize the usage of fossil fuels as the primary energy source and turns to a cleaner, sustainable resources such as wind, solar and hydropower. It is envisioned that in 2060 Germany would cut 80-95% of their greenhouse gas emissions (compared with 1990) by increasing energy efficiency and boosting utilization of renewables [1]. Natural gas plays a crucial role to support the long-term vision of energy transition; not only due to its lower CO₂ emissions relative to the other fossil fuels but also because it can be deployed rapidly for peak-shaving purposes or fill the production gap from solar and wind power generation. Renewables are currently impeded with intermittency problems, which can be solved by generating power from natural gas.

Under the new policies scenario, natural gas consumption is estimated to increase by 45%, of which most of the demand comes from China, India and other Asian countries [2]. In the 5th assessment report of IPCC, it is also mentioned that the natural gas combined-cycle (NGCC) would be the ideal substitute for coal-fired power generation systems. It is estimated that approximately 50% of specific GHG emissions of the world could be reduced when the substitutions were fully implemented [3]. Furthermore, natural gas is expected to

dominate the energy system in the future where a highly seasonal of renewable energy production persists. Therefore, improving and maintaining the gas infrastructure is as crucial as the transition towards sustainable energy itself. Low-density characteristic of natural gas poses a challenge for the production, storage, and distribution, especially when it is compared to oil. Pipeline infrastructure is limited and could not transport the natural gas from remote sites, where most of the reserves are located. In this case, liquefied natural gas (LNG) has created greater flexibility to transport natural gas to long-distance buyers. The cost to transport LNG is, in fact, cheaper than onshore pipeline transport when the gas needs to be delivered to the destination over 3000 km, as shown in Figure 1.1. At a relatively shorter distance, the LNG shipping is even a much better option compared to the offshore pipeline. The leading LNG players such as Indonesia, Malaysia, Qatar, Japan, and South Korea have a solid case to support the presence of LNG in their energy policy mix.

The growth in LNG trade has been steadily increasing by over 6% per year, where the strongest demands mainly come from China, Japan, and South Korea. In 2017 alone, at least 293.1 million tonnes of LNG were traded globally [1] along with the additional LNG facilities, which were recently commissioned in Australia and the United States. On the long term the LNG supply to the Asia Pacific region, particularly China, is expected to be high with even a stronger demand growth. China had recently become the second largest LNG importers in the world after Japan at 37.8 MT in 2017. it is estimated that China needs to import LNG at the level of more than 68 million tonnes per annum (MTPA) by 2023, eventually surpassing Japan as the largest LNG importers [2]. As reported by the International Gas Union [1] , there are 369.4 MTPA capacity are operating globally, with 92 MTPA additional capacity are currently being constructed. By 2023, it is estimated that the growth of liquefaction capacity would increase by 23%.

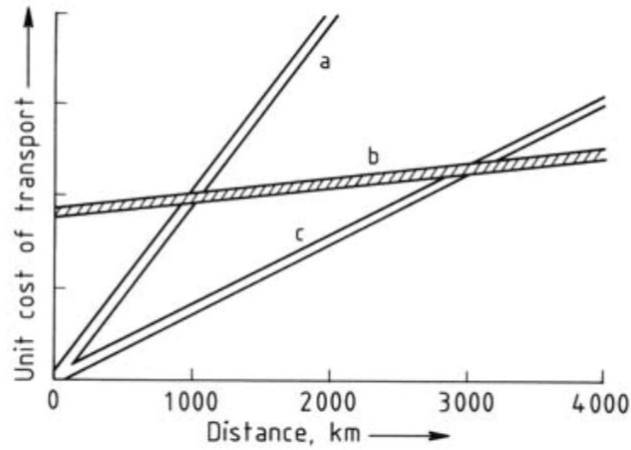


Figure 1.1 – Relative cost of LNG transportation and cost of pipeline transmission as a function of distance with a) Off-shore pipeline (900-mm diameter); b) LNG transportation with liquefaction onshore (125 800 m³); c) Onshore pipeline (1000-mm diameter) [3]

In terms of the liquefaction technology, Air Product and Chemicals Inc. (APCI) and Shell are instrumental in combining the idea of cascade liquefaction processes to the mixed refrigeration process by proposing propane with mixed refrigerant for the Brunei LNG plant, which came to operation in 1972. The propane pre-cooled mixed refrigerant AP-C3MR™ (further called C3MR), accounted for 43% of the global market share [1]. By using C3MR as the basis of liquefaction technologies the LNG industry has evolved with an improved design that can accommodate a larger capacity and cost-effective at the same time. The development has led to the extension of C3MR, such as the AP-C3MR/Split-MR® and the AP-X®, which currently accounted for 17% and 13%, respectively [1].

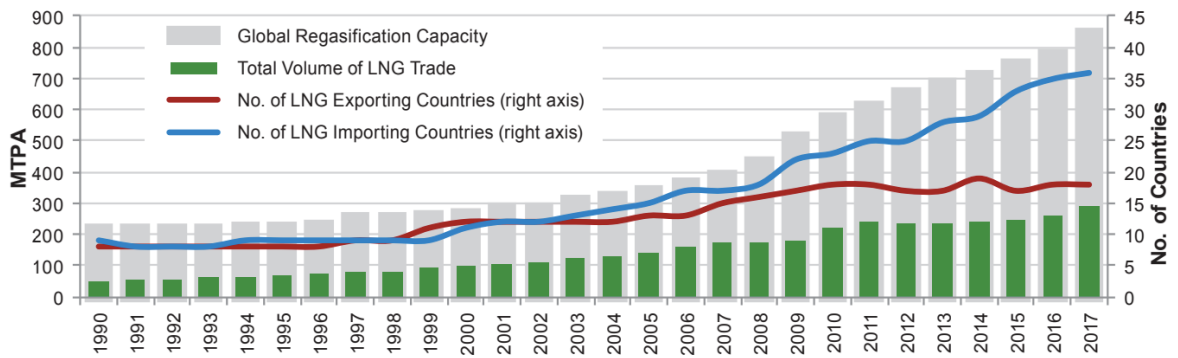


Figure 1.2 – LNG trade volumes 1990 – 2017 [1]

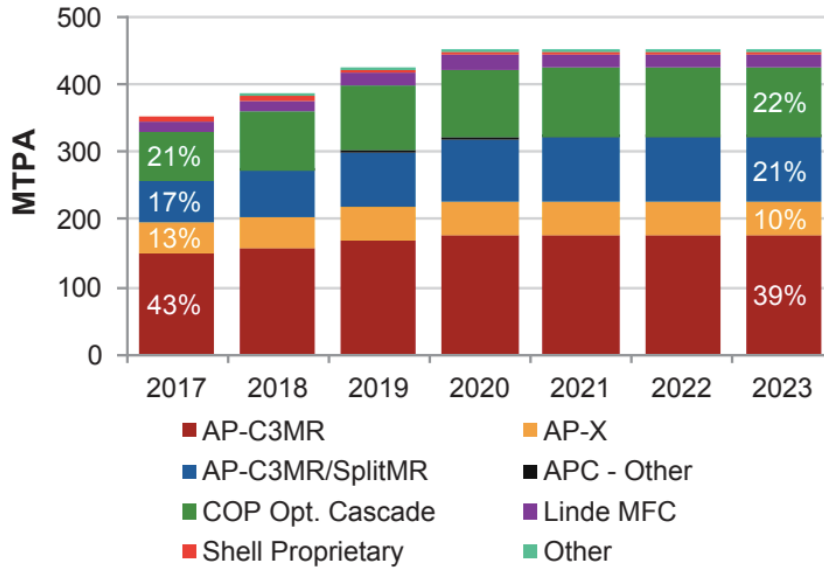


Figure 1.3 – The share of liquefaction processes used in the existing LNG Plants [1]

1.2. Exergy-based Methods

The first law of thermodynamics can be applied to evaluate an energy system by means of the energy balance formulations in order to provide useful information regarding the system's performance. The method is indeed useful when evaluating and comparing similar systems, e.g., two different designs of shell and tube heat exchangers. However, the approach using the first law fails to provide information about the quality of energy and therefore cannot be applied to compare the performance of two different energy systems, e.g., a C3MR process and a natural gas combined-cycle (NGCC). This is where the concept from the second law of thermodynamics complements the first law method and extend it to a property known as exergy, as a result from the combination of the first and the second law concept. It embodies not only the quantity but also the quality of the energy. The exergy of an energy carrier is a thermodynamic property that depends on (a) the state of the carrier being considered; and (b) the state of the environment. The exergy analysis complements the energy analysis by providing information about the magnitude, location, and true inefficiencies of the system [4]. Exergy analysis plays an essential role as the modern approach to evaluate energy systems. Inspired from the concept of the second law of

thermodynamics, the exergy analysis can determine the real thermodynamic value of an energy carrier, and it is able to reveal the real inefficiency of the energy system, known as the irreversibility. In the application of exergy analysis, the term is also known as exergy destruction; an important parameter that defines the deteriorating quality of energy in a particular process. By using exergy analysis, the source of real inefficiencies in the process can be identified, and the opportunities for improvement can be clearly defined.

The combination of exergy analysis with economic considerations resulted in a method called exergoeconomics, which rests on the notion that exergy is the only rational basis for assigning costs to the interactions of an energy system experiences with its surroundings and to their sources of inefficiencies within it [5]. Exergy is used in this method as a basis to associate the costs with the exergy streams of a particular system. This approach eliminates the need to have a separate analysis for exergy and economics of the LNG plants, making it a convenient tool to uncover the optimization opportunity with regards to the irreversibilities and costs. The exergy-based methods are ideally suited to evaluate and identify the real thermodynamic inefficiencies as well as to understand the cost structure of the LNG plant.

1.3. Exergy Analysis of Liquefaction Processes

One of the earliest works using exergy analysis for the low-temperature process was conducted in 1980 by Chiu and Newton [6]. The authors compared the results from two LNG processes, a single-pressure mixed refrigerant, and a C3MR cycle. The irreversibility here is termed as the “exergy dissipation.” It was also shown that the flash (LNG is partially vaporized before storage) mode in C3MR generated less total irreversibility compared to the subcooling mode. The authors also mentioned the potential of future applications by combining the exergy and economic analyses to optimize the entire process. Ahern [7] reviewed the potential of exergy analysis to assess the design and performance of cryogenic systems, including for the LNG. Zheng, Uchiyama, and Ishida [8] compared the exergy

destruction (previously termed as exergy loss) of two types of LNG power systems using the energy-utilization diagram. Liu and You [9] proposed a method to predict the exergy value of LNG system, in which the temperature and pressure part of the total exergy are decomposed. One of the earliest studies for multistage cascade liquefaction process using exergy analysis was conducted by Kanoğlu [10]. The author formulated the exergy balance for each component of the process while defining the exergy efficiency as the minimum work divided by the actual work of the cycle. Likewise, Remelje and Hoadley [11] applied exergy analysis to three small-scale LNG processes; the SMR, the new LNG scheme, and the cLNG technology. The result shows that the exergy analysis is a suitable tool to compare the performance of different systems with SMR being the lowest specific energy consumption at 5.10 kW h/kmol. Recently, Vatani and Mehrpooya [12] conducted the energy and exergy analyses to the five most popular liquefaction technology: Cascade Process with SMR process of Linde's LIMUM[®]1 and AP-SMR[™], C3MR, DMR and Linde's MFC[®]. Their work was subsequently extended [13] by implementing the advanced exergy analysis based on the methodology presented by Tsatsaronis and Morosuk [14].

Several notable works from Morosuk and Tsatsaronis [15–18] focused on the advanced exergy analysis of LNG regasification plant and refrigeration machines. The analyses proposed a distinctive approach for low temperature systems, where the physical exergy is split into endogenous/exogenous and avoidable/unavoidable parts, making the calculations more accurate than merely applying a conventional exergy analysis [19,20]. The former is affected by the performance of a single component while the latter is affected by the interaction of the single component with the inefficiencies of other components within the particular system. The information of avoidable/unavoidable exergy destruction can also be split using the advanced analysis. Additionally, Morosuk and Tsatsaronis [21] proposed a slightly different treatment for a system that operates below and crossing the environment temperature. The authors asserted that the physical exergy should be split into the mechanical and thermal part since they represent two different sides of the exergy balance.

For instance, the mechanical part in a heat exchanger is typically related to pressure change is the exergy of fuel, whereas the thermal part is related to the exergy of product, in which the benefit of the cold temperature process is truly gained [21].

1.4. Motivation

Over 41% of the total cost within the LNG value chain is related to the liquefaction plant [22–24], which incurred from the investment, operation, and maintenance of various components such as the heat exchangers and the compressors. Since the construction of the plant is capital intensive, engineers have to make sure that the design variables are configured such that the plant is cost-efficient while at the same time maintaining high efficiency. Exergy analysis can provide a convenient method to identify the real inefficiencies of energy systems, while exergoeconomic analysis allows the cost analysis to be assigned to the exergy streams. The results of the analyses should give valuable information on how to improve the system in the presence of real design and operational constraints. These methods, known as exergy-based analyses, are able to locate the components which have the most significant potential for improvement and hence, revealing the right path to the process optimization. In total, the C3MR process from APCI, including the extension process such as AP-X[®], accounts for 73% of the global LNG facilities. The dominance of the process in the LNG industry for years to come is indisputable.

While there are several studies that have addressed the evaluation and optimization of C3MR process [25–27], none of them so far are comprehensively devoted to the exergy-based methods combined with a systematic approach to optimization. These studies, however, do not address the conflicting objectives between the efficiency and the cost of product, which should be beneficial to the process evaluation of the C3MR. High exergy efficiency might lead to operational cost savings; however, it would also increase the investment costs to the required components. Conversely, low cost of product with the less efficient plant would not be a desirable scenario either since the plant owners always want a liquefaction plant that

has an optimum thermodynamic efficiency. Furthermore, the accurate exergy-based analyzed for liquefaction systems, i.e., the system that partially operates below and crossing the ambient temperature, should deal with the splitting the physical exergy into thermal and mechanical parts. This method was not implemented in any of these studies. Based on this motivation, a thorough and systematic study with regards to the thermodynamic performance and the cost optimization of C3MR is conducted using the principle of exergy-based analyses. Ultimately, it is hoped that this thesis would be constructive to the existing engineering stack that is related to the evaluation and optimization of the LNG process.

1.5. Research Objectives

The thesis focused on providing a comprehensive workflow from the modeling, process simulation, exergy-based analyses, to the optimization procedure. C3MR is selected as the case study due to its dominant application in the current and future LNG market, where the interactions between variables and components are known to be relatively high. The exergy and exergoeconomic analyses outline the information at component level, i.e., the exergetic value of each stream and the cost associated with it. Subsequently, the possible improvement for the system is outlined and used as the basis to guide the optimization strategy. In this thesis, a state-of-the-art, metaheuristic optimization technique called genetic algorithm (GA) is implemented and adjusted to suit the exergy-based methods for the LNG process.

Accordingly, the goals of the thesis are to (1) Develop the process modeling and investigate the thermodynamic performance of C3MR process using exergy analysis; (2) Acquire high resolution analysis by applying exergoeconomic method to reveal the cost formations of the components and the overall system; (3) Create an efficient and reliable approach to a single and multi-criteria optimization problem based on the exergy and exergoeconomic analyses; and (4) Optimize the thermodynamic and cost-effective performance of liquefaction process, especially when dealing with mixed refrigerant system.

1.6. Outline of the Thesis

In Chapter 2, a brief history of the LNG industry and natural gas production are introduced. Subsequently, the core concept of the gas liquefaction is explained, followed by the description of the state-of-the-art in the liquefaction technology, including the propane pre-cooled mixed refrigerant process. In chapter 3, the concept of exergy, starting from its inception to the development of the exergy analysis is briefly described. The framework of the economic analysis for energy systems is also presented, followed by the methodology of the exergoeconomics principle, which combines the exergy and the economic analyses, providing a clear approach to determine the interdependencies between the exergy and the economics of the LNG plant.

Chapter 4 presents the optimization techniques that can be applied to the energy systems, starting from the deterministic to the stochastic algorithms, including the main idea of genetic algorithm (GA). The application of GA and several other approaches in the multi-objective optimization field is also described. Finally, a number of studies that are related to the evaluation and optimization of the LNG process are discussed.

Chapter 5 provides the base case evaluation of the C3MR process, which includes the process modeling, exergy analysis. The calculation of purchased equipment costs and the economic analysis based on the total revenue requirement (TRR) method are also presented. The last section of this chapter discusses the application of exergoeconomic analysis to the C3MR process. All results are used as the basis for the system optimization that is described in detail in the subsequent chapters.

In Chapter 6, the single-objective optimization workflow for C3MR process is described with two different objectives: (a) to maximize the exergy efficiency and (b) to minimize the total cost of product. Several different strategies are implemented to achieve the objectives, where the results are compared and discussed in detail.

The multi-objective optimization, which was applied using a different approach compared to single-optimization cases, are described in Chapter 7. The adjustment of the selection procedure from a conventional GA operator to a multi-objective optimization purpose, i.e., the non-domination and the crowding distance parameters, are explained. The result of this section is to find the Pareto front, an optimum curve that draws the tradeoff between the exergy efficiency and the total cost of product.

2. The Liquefied Natural Gas

2.1. History of the Liquefaction of Gases

The emerging interest of gas liquefaction can be traced back to the 17th century when Robert Boyle discovered the inverse relationship between the pressure and the volume of ideal gases at a fixed temperature. The experiment continued and progressed for the next century, during which Michael Faraday was able to liquefy some gases such as chlorine, nitrous oxide, cyanogen, and ammonia by applying considerable pressure and low temperature during the winter time [28].

One of the pioneering attempts to liquefy natural gas was carried out in West Virginia, United States. Afterwards, in 1941, the first liquefied natural gas (LNG) plant is built in Cleveland and was continued with the LNG shipment by the first LNG carrier called the Methane Pioneer in 1959 [29]. In total there were 8 LNG cargos transported from Lake Charles, Louisiana to Canvey Island in the United Kingdom, which also happened to be the first LNG regasification terminal. In the subsequent year, the construction of the first large-scale, commercial LNG facility of 1 MTPA was initiated in Arzew, Algeria and officially transported its first cargo to the Canvey Island in 1964. The total cost of the LNG project was estimated to be US\$89 million, and the FOB price for the first cargo was 53 cents/MMBtu. Interestingly the delivered price was 76 cents/ MMBtu² suggesting the freight was a far more significant component of the cost build up than it is today [30].

2.2. Natural Gas Production

The composition of natural gas mainly comprises methane (CH_4) with the rest of the chemical components vary considerably according to their gas fields, as shown in Table 2.1. Typically, the extracted gas from the field contains a considerable concentration of impurities such as hydrogen sulfide (H_2S) and carbon dioxide (CO_2). Additionally, it may

contain water vapor from a trace amount to saturation as well as trace quantities of mercury. All of the impurities have to be separated in order to protect the LNG equipment from corrosion and preventing gas hydrate formation, which will cause clogging in the pipeline. Before entering the liquefaction unit, the raw natural gas feed has to be dehydrated and cleaned from impurities. First and foremost, the raw gas is fed to a slug catcher unit, in which the settling liquids from the flow lines are separated and collected. The side product of this process is C5+ and heavier hydrocarbons known as natural gas condensate, where the economic value has its own significance in the energy market. Subsequently, natural gas stream flows through the acid gas removal unit, where the acid gases such as H₂S and CO₂ are separated due to its corrosive effects. In large-scale production, chemical absorption is typically applied with monoethanolamine (MEA), or diethanolamine (DEA), usually referred to as amines, as a solvent to strip the acid gases. Other acid gas treatment process includes adsorption, membrane separation, and cryogenic removal. H₂S is removed by an amine solvent to meet the total sulfur product specification, typically 4 ppmv. CO₂ is removed to 50 ppmv to avoid CO₂ freezing in the main exchangers in the liquefaction plant [24].

Table 2.1 - Typical Composition of Raw Natural Gas [3]

Component	Molar Fraction
Hydrocarbons	0.75 – 0.99
Methane	0.01 – 0.15
Ethane	0.01 – 0.10
Propane	0.00 – 0.02
n-Butane	0.00 – 0.01
Isopentane	0.00 – 0.01
Hexane	0.00 – 0.01
Heptane and higher hydrocarbons	0.00 – 0.001
Non-Hydrocarbons	0.00 – 0.25
Nitrogen	0.00 – 0.15
Carbon Dioxide	0.00 – 0.30
Hydrogen Sulfide	0.00 – 0.30
Helium	0.00 – 0.05

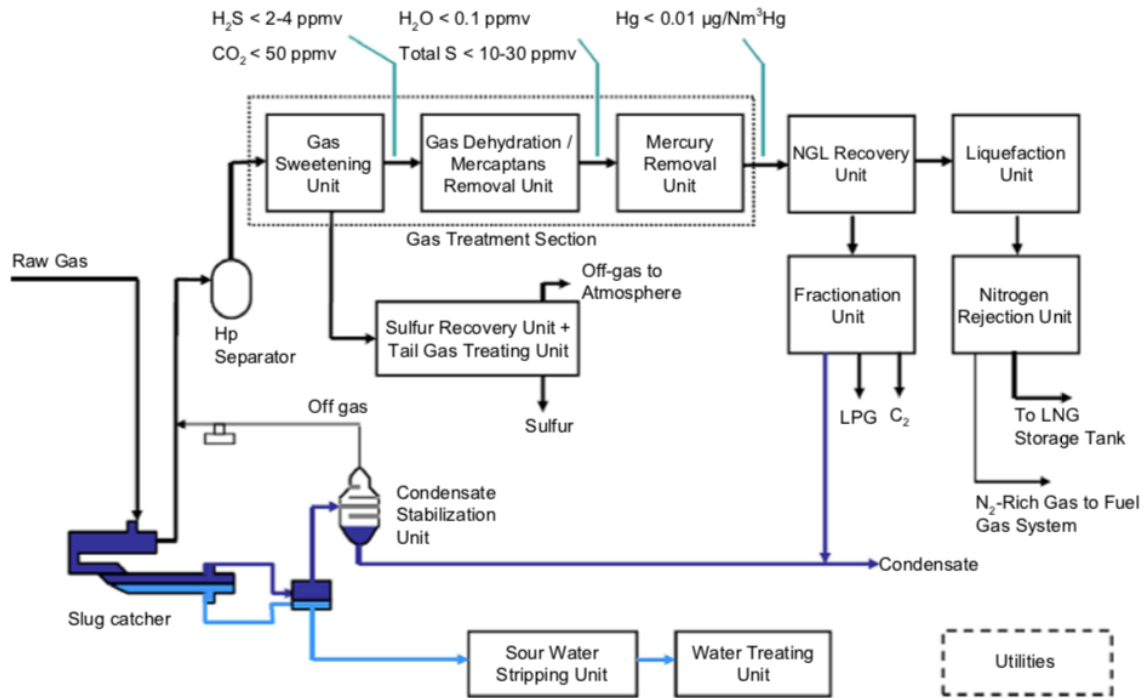


Figure 2.1 - A typical scheme of natural gas pre-treatment with liquefaction plant [24]

It is also essential to remove the water vapor from the raw gas since the liquefaction process involves low temperature process below water freezing point. It may also form gas hydrates that will cause blockages and the undesirable reactions with the sour gases [31]. Water removal starts from the wellhead, yet a dedicated dehydration unit is still necessary due to the strict limitation of water content for the LNG feed. A typical technology for the treatment depends on the raw gas composition. The most common practice is to use molecular sieve adsorption, which is able to remove water content from the natural gas to below 0.1 ppmv [32]. Another impurity is mercury, which also has to be removed to protect the aluminum parts for the LNG heat exchangers. Mercury has caused numerous aluminum exchanger failures. It amalgamates with aluminum, resulting in a mechanical failure and gas leakage. At the current experience, removal to less than 0.01 $\mu\text{g}/\text{Nm}^3$ or 1 part per trillion of natural gas is desirable [33]. The removal unit contains either a regenerative adsorbent such as special type of molecular sieve [34] or a non-regenerative sorbent such as

elemental sulfur dispersed within a porous carrier, which should be replaced after several years of application [35].

Subsequently, the raw gas is subsequently treated in the natural gas liquids (NGLs) recovery unit to extract the NGL components. It consists of the heavier gaseous hydrocarbons such as ethane, propane, and isobutane as well as a small fraction of C5+. The term “rich gas” in the LNG industry means that the raw gas composes of a higher concentration of NGL, typically at 5-32%. Removal of the NGL components would also eliminate the need for a scrubber column in the liquefaction plant, which typically is used to remove aromatics and heavy hydrocarbons to avoid waxing in the main exchanger [24]. Several NGL removal techniques are already implemented in the oil and gas industry, such as the lean oil process, the Joule-Thomson process, the refrigeration process, and the turboexpansion processes. The NGL have higher boiling points compared to methane, hence the main idea of the extraction process is to control the dew point of the gas, such that the NGL will liquefy and separate itself from the natural gas. When the raw gas pressure is low, however, an external refrigeration cycle is necessary to achieve the separation. Often times a high recovery of NGL is favored due to its economic value, which can be achieved using turbo-expander. Instead of using a Joule-Thomson valve, the cold temperature is produced by the expansion with turbo-expander, which not only generate a colder temperature, but also useful work to drive compressors [24]. The major breakthrough for turboexpanders came when the design and materials made it possible for condensation to occur inside the expander. The fraction condensed can be up to 50% by weight. However, the droplets must generally be 20 microns in diameter, or less, as larger droplets would cause rapid erosion of internal components [31]. Although it is the most efficient NGL recovery configuration, the cost is also higher than the other techniques [36].

After separation from the natural gas, the NGLs have to be separated to a single component, based on their respective boiling points. This process is known as fractionation, where NGL

are further separated by heating the mixed NGL stream and processing them through a series of distillation towers. Fractionation takes advantage of the differing boiling points of the various NGL components [24]. The typical scheme is shown in Figure 2.2. The NGL stream is fed through a series of distillation columns which consist of deethanizer, depropanizer, and debutanizer column [31].

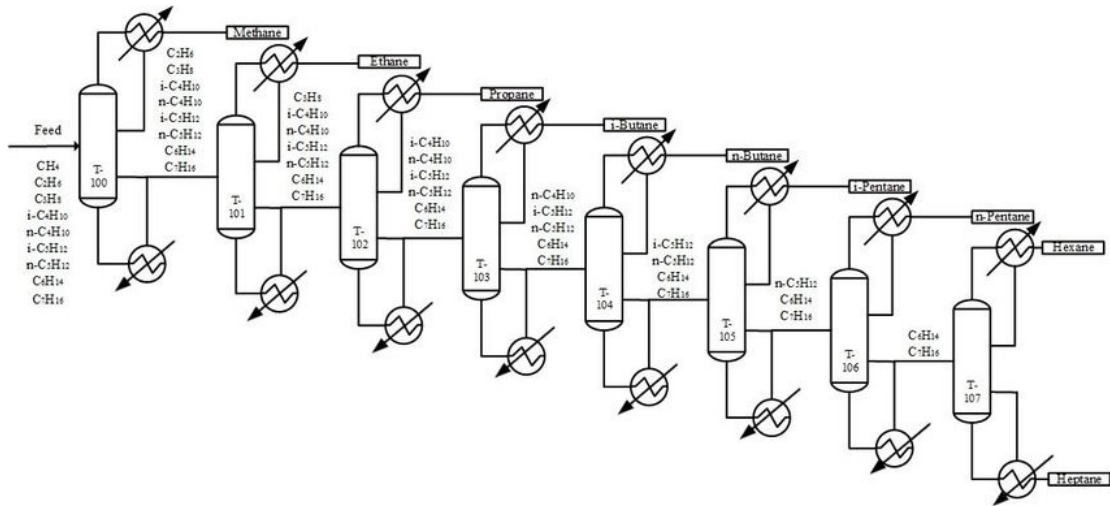


Figure 2.2 – Flowsheet for fractionation columns of NGL Recovery Unit

2.3. Liquefaction Process of Natural Gas

2.3.1. Overview of the process

In the LNG value chain, the natural gas liquefaction is the most critical part in connection with the design, operational and economics significance. In order to achieve the low temperature condition required for LNG, a process needs to apply the cryogenic technology using various cycle designs and a range of working fluid selection. LNG is non-toxic, colorless, odorless and virtually non-flammable in its liquid form. Nevertheless, there is also safety risk involved, just like other fuels. LNG vapor may become flammable and explosive when mixed with air within the range of 5 to 15%. Furthermore, the accumulation of LNG vapor in a confined space will displace air, which would create a dangerous location for a

human to breathe. As mentioned earlier, the purpose of liquefying the natural gas is to create a condition such that at approximately a temperature of -160°C and ambient pressure the LNG is safe and compact to be transported within a long distance.

The development of the cryogenic technology itself kickstarted when Carl von Linde and William Hampson, both independently patented a process to liquefy air. The process is conducted by applying the principle of isothermal compressions followed by isenthalpic expansion within the Joule-Thomson (J-T) valve. The method has a significant advantage since no moving parts required, minimizing the need for thermal insulation and avoiding mechanical complications [37,38]. A pre-cooling stage was also invented, resulting in a significantly better yield. At the same time, a French engineer named Georges Claude also developed another method which differs from the Linde process. In this cycle, an isothermal compression and a series of heat exchangers are configured with an expander which introduced between the heat exchangers, making it more energy efficient. Figure 2.3 shows the process configuration of the two processes.

Soon after, they were able to separate the liquefied air such as oxygen, nitrogen and inert gases. By the early 1900s, the liquefied gas market began to emerge with Linde, and Claude's Air Liquide company became the global market leader for industrial gases and even collaborated with each other [39]. The natural gas liquefaction is made possible by the continuous development of these technologies. The advancement of the LNG process is motivated by the needs of transporting a reliable source of fuel to a long distance, which today has created a global market with tight competition with other energy sources. The competitive edge is obviously closely related to the energy and cost efficiency in every part of the LNG value chain.

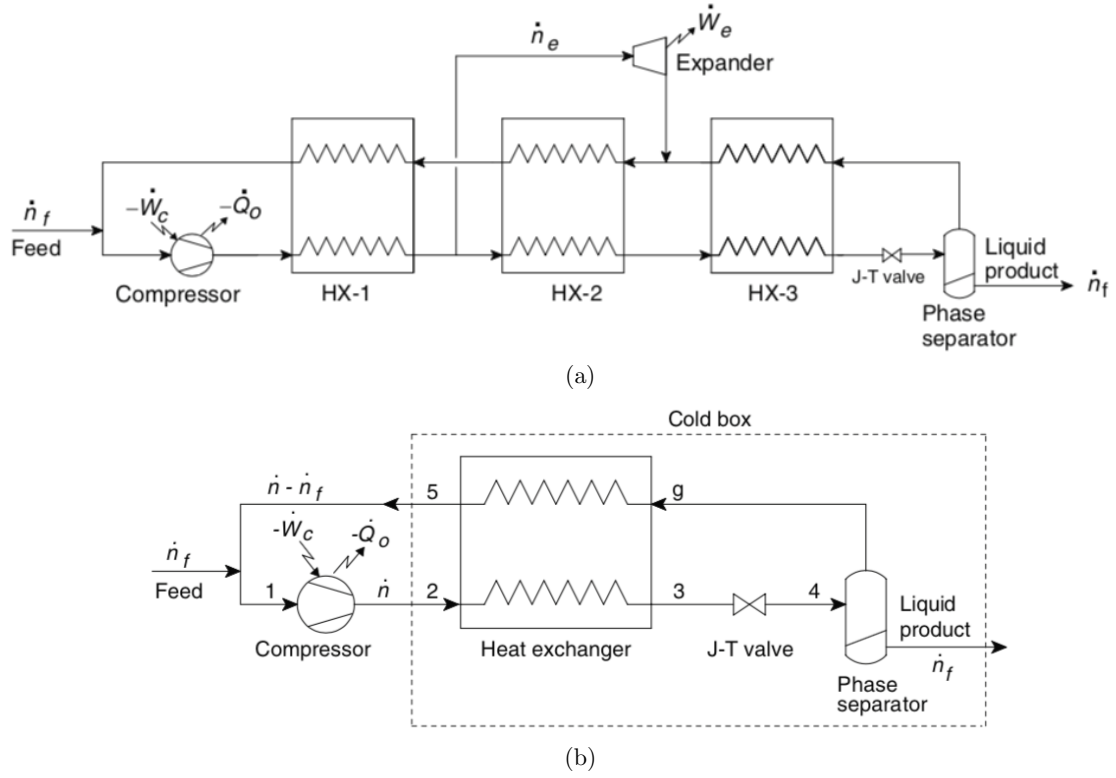


Figure 2.3 – Schematic process of (a) Linde Process and (b) Claude Process [38]

2.3.2. Mixed Refrigerant Cycle

During the early emergence of the natural gas industry, it was Klimenko who proposed the first mixed refrigerant system for liquefaction of natural gas based on the cascade cycle [40]. The refrigerant used by an original design by Klimenko is taken directly from the natural gas, which comprises a mixture of hydrocarbons and nitrogen. In the previous concept by Linde and Claude, the heat exchangers experience substantial exergy destruction, which compensated by additional pre-cooling. By utilizing the potential of mixed refrigerant, the destruction can be minimized and thus eliminating the need for pre-cooling and/or expansion [40]. The simplified flowsheet and the cooling curve are depicted in Figure 2.5. The flowsheet shows that the liquefied natural gas is collected in several steps between the heat exchangers, whereas the boil-off gas is recycled to back to the compressor. The development of the cycle started out around the 1960s in present-day Russia (USSR) and

quickly adopted throughout the liquefaction industry [40]. However, the cycle is deemed uneconomical due to more components required such as several separators and J-T valves. The new cycle is further developed afterwards, which slightly differs than the original concept by providing a specialized refrigerant mixture and thus removing the separators.

2.3.3. Cascade Refrigeration Cycle

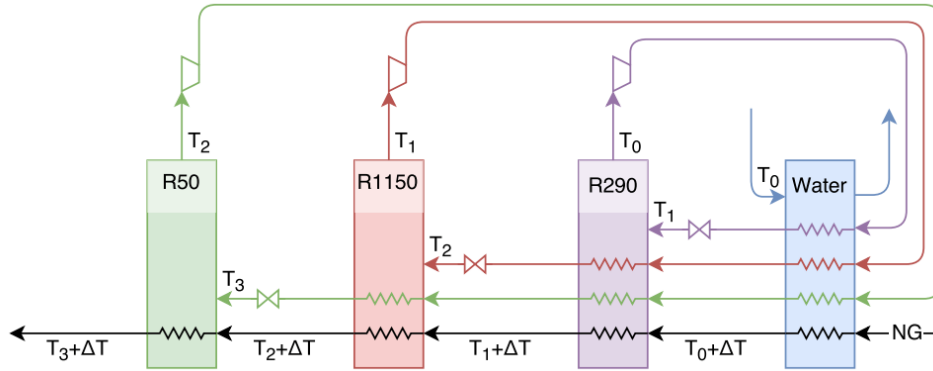


Figure 2.4 – Cascade refrigeration cycle [41]

The first commercial LNG plant in Algeria was implemented by multiple pure refrigerants, configured in a cascade refrigeration cycle, as illustrated in Figure 2.4. Economics of scale at that time showed that the cascade cycle is most suited to large train capacities since the low heat exchanger area and low power requirement offset the cost of having multiple components [42]. Natural gas is liquefied in the main heat exchanger using either fin plate or coil wound type heat exchanger. The low temperature condition is generated from three interconnected cycles, in which a gradual temperature reduction is achieved at the last state. Propane (R290), Ethylene (R1150) and Methane (R50) are used as the refrigerants, separately configured in their own compression and expansion stages. The refrigerants are selected based on their boiling points; from the highest to the lowest (Propane at -42°C , Ethylene at -103.7°C and Methane at -161.5°C) hence the name cascade cycle. Although it has a lower specific energy consumption compared to the C3MR process, it produces less

LNG throughput by some margin. Furthermore, several plate-fin or coil-wound heat exchangers required for each refrigerant, resulting in higher initial investment costs.

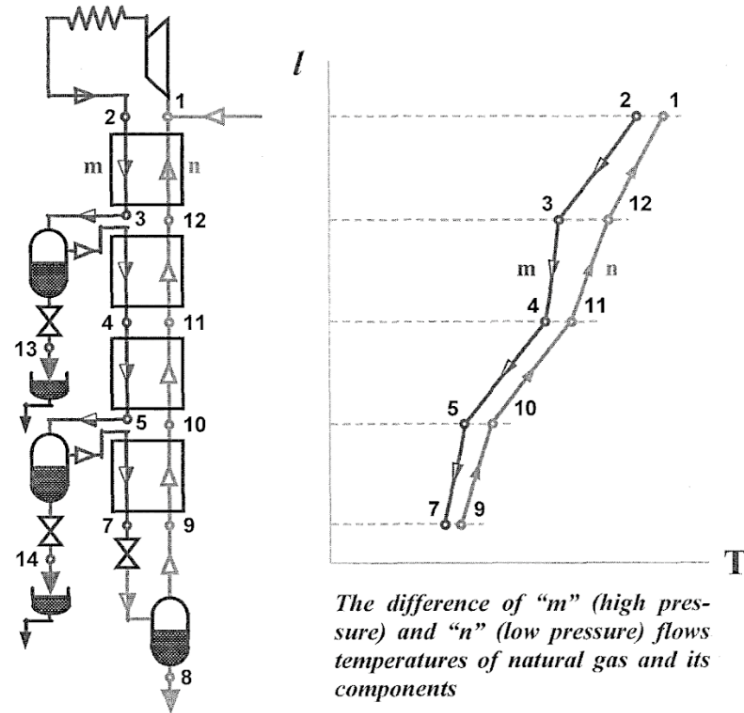


Figure 2.5 – Simplified flowsheet and the cooling curve of Klimenko process [40].

The basic cascade cycle configuration has been adjusted to minimize the cost and the specific energy consumption of the plant, such as the optimized cascade developed by Conoco Phillips [43]. It is asserted that the cycle has better flexibility when operating in various feed gas composition, which is a notable disadvantage in the classic cascade cycle. The plant that implements the Conoco Phillips three-stage cascade LNG process is located in Kenai, Alaska, built in 1969. Figure 2.6 shows the flowsheet of the optimized cascade LNG process. Propane is the first stage of the cooling cycle where the feed gas, ethylene, and methane are precooled. The cycle adopts the concept of compression and J-T effect to produce low temperature. The feed gas passes through the second heat exchanger where Ethylene is used as the refrigerant. Finally, by the same principle, the third cycle liquefies the natural gas in the methane cold box. The operation of the plant also takes the recycling vapor from LNG

tankers and storage in order to enhance the throughput yield. This process has also been applied in Egypt, Angola, and several other LNG projects in Australia [44]. The most recent commissioned project is Corpus Christi LNG in the United states, which consist of three liquefaction trains and has a total capacity of 4.5 MTPA.

Another variant is the Mixed-Fluid Cascade® (MFC) invented by Linde and Statoil which is being implemented in Statoil LNG Hammerfest, Norway with a single train of 4.3 MTPA capacity. The cold and high variation of the ambient temperature in the arctic is the primary motivation to modify the classic cascade process, where three different stages with multi-component refrigerants are used. It is claimed that the process can accommodate up to 10 MTPA in a single train, although the proven commercial operation to date is only Hammerfest LNG. The second generation of MFC is being developed in order to make the design relevant to the warmer climate, where propane is used as a pre-cooling refrigerant [45].

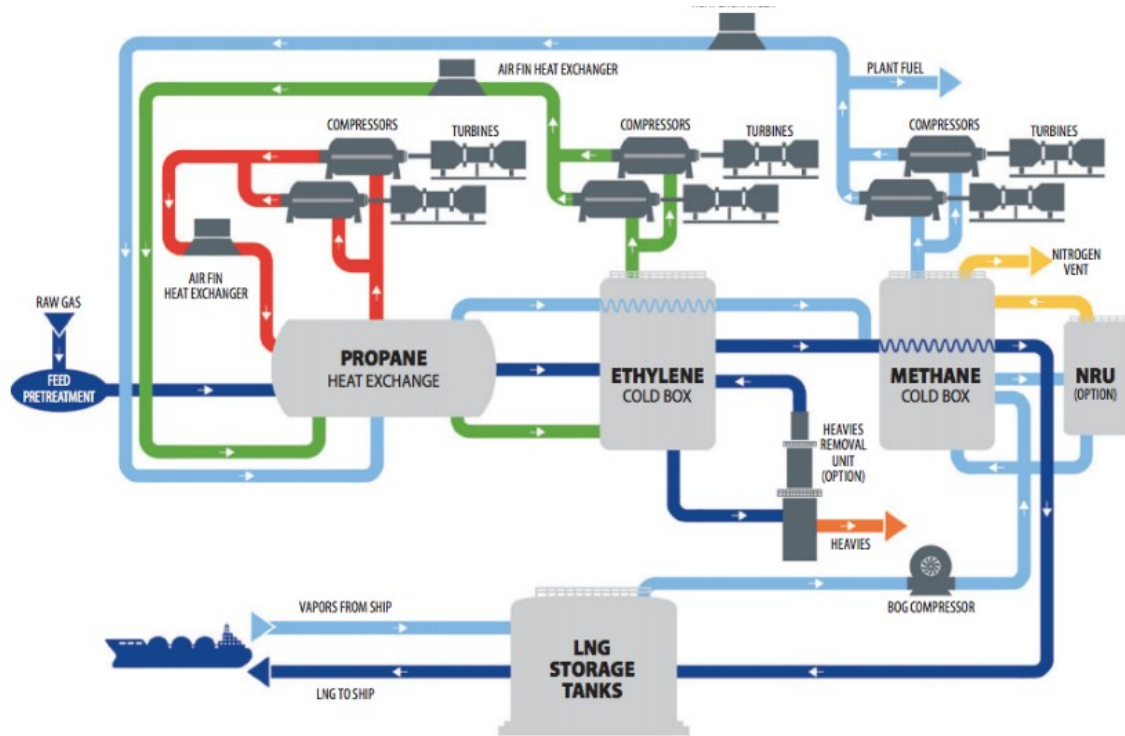


Figure 2.6 – Conoco Phillips optimized cascade cycle [43]

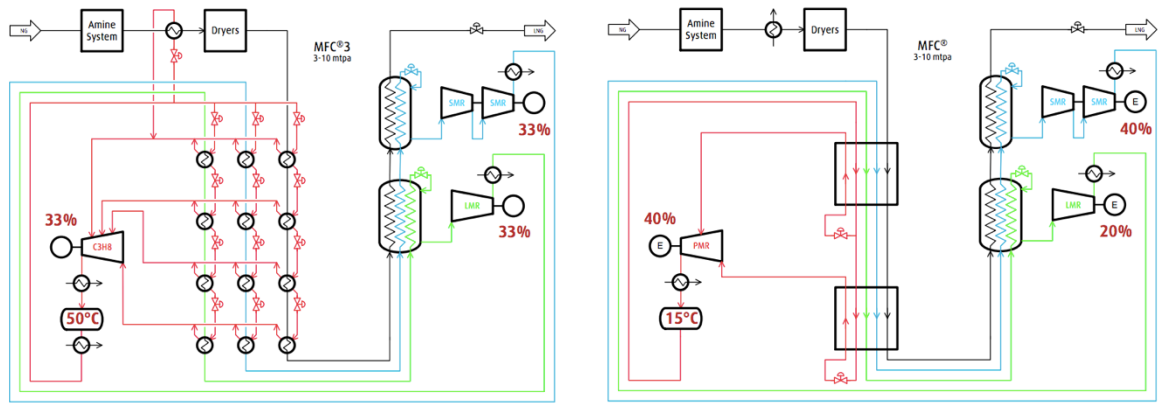


Figure 2.7 – Linde/Statoil's MFC® and MFC®3 Process [46]

2.3.4. PRICO® Process

The poly-refrigeration integrated cycle operation, simply known as PRICO® process invented by Black and Veatch uses a single mixed refrigerant to produce LNG for a small-scale purpose such as peak-shaving plant, vehicle fuel supply, and gas distribution systems. The first implementation of this process actually took place in 1971 at Skikda plant, Algeria, for a base load purpose. At present there are at least 21 LNG plants are using this process while 16 more plants are in the design and/or construction phase [47]. The process design is shown in Figure 2.8, exhibiting its simplicity and ease of operation and maintenance. Feed gas is initially pre-cooled to separate and collect the remaining NGL, whereas a closed loop of a mixed refrigerant stream is used to liquefy the natural gas inside the cold box. PRICO process is the first proven technology for an emerging floating LNG technology (FLNG) Hilli Episeyo in nearshore waters off the coast of Cameroon, which was successfully commissioned in 2016.

2.3.5. LIMUM®1 and LIMUM®3

Linde has developed its own single mixed refrigerant process to capture the emerging small to the mid-scale LNG market. The Linde Multistage Mixed Refrigerant, commercially called LIMUM® comprises two stages centrifugal compression with intercooling, after which the

mixed refrigerant is partially condensed. Afterward, it flows through a plate-fin heat exchanger where the refrigerant from the first and the second stage is mixed and eventually completely condensed after the J-T expansion. Moreover, NGL separation and liquefaction of feed gas also take place within the heat exchanger. The technology has been implemented for LNG plants in Kollsnes (Norway) and Kwinana (Australia) with a capacity of 0.04 MTPA and 0.06 MTPA, respectively.

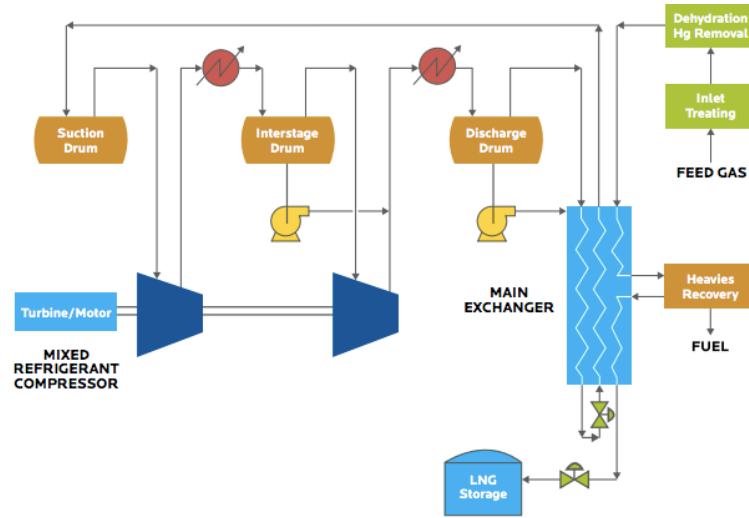


Figure 2.8 – Black & Veatch PRICO® Process [48]

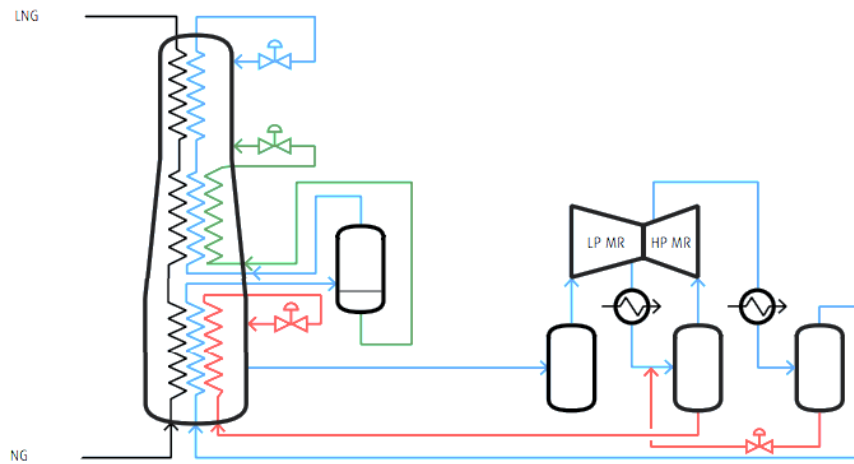


Figure 2.9 – LIMUM®3 liquefaction process for medium-scale LNG plant [46]

The second generation, LIMUM®3, uses a coil wound heat exchanger with a slightly different flow arrangement. At the bottom part of the heat exchanger, the condensed refrigerant is used to precool the feed gas and to condense the lighter mixture of compressed refrigerant. In the middle part, the liquefaction takes place using the boiling refrigerant while the lightest mixture sub-cools the liquefied natural gas in the upper part. LIMUM®3 has been successfully implemented and currently operated in several LNG trains in China, Stavanger (Norway) and Bintulu (Malaysia) with the capacity ranging from 0.3 to 0.65 MTPA [46].

2.3.6. Propane Pre-Cooled Mixed Refrigerant (C3MR)

C3MR is one of the proprietary liquefaction technologies from Air Products and Chemicals, Inc., which is intended for medium to large-scale, base load LNG plants. Various accounts [1,6,22,49] reported that it is the most popular liquefaction technology based on capacity installed. Early contributors to C3MR include Lee Gaumer and Chuck Newton who invented the process [6] for Air Products in 1973 [6,50,51]. Analogous to SMR process, it also uses a mixed refrigerant as the working fluid for liquefaction and subcooling stage. An additional propane cycle is added to the system to precool both the natural gas and the mixed refrigerant. Brunei LNG is the first commercial plant to implement the process in 1973, followed by Bontang LNG in East Borneo, Indonesia. Many LNG projects with the total installed capacity over 150 MTPA have been or will be built worldwide with the C3MR technology. A simplified process flowsheet of the C3MR is shown in Figure 2.10. Propane serves as the precooling medium for the natural gas and the mixed refrigerant, which configured in a separate cycle. Both streams are pre-cooled to about -30 to -35°C in the precooling stage. Although not visible in the figure, the compression is conducted in three to four pressure levels with interstage cooling. The precooling stage for the propane cycle typically uses multiple kettle-type evaporators made of the lower cost carbon steel, which require relatively large plot space [3,49]. Subsequently, the mixed refrigerant is partially condensed, and through a series of J-T expansion, it is liquefied and finally subcooled inside

the main cryogenic heat exchanger (MCHE). The liquefaction of natural gas takes place inside the MCHE by removing the heat to the mixed refrigerant, where the final LNG temperature reaches -162°C . The typical substances used in the mixed refrigerant are methane, ethane, propane, butane, and nitrogen, which can be easily extracted from the natural gas stream. The mixed refrigerant is completely vaporized after the subcooling process and sent back to compressors, which typically have a high outlet pressure between 45 to 48 bar, depending on the mixture composition.

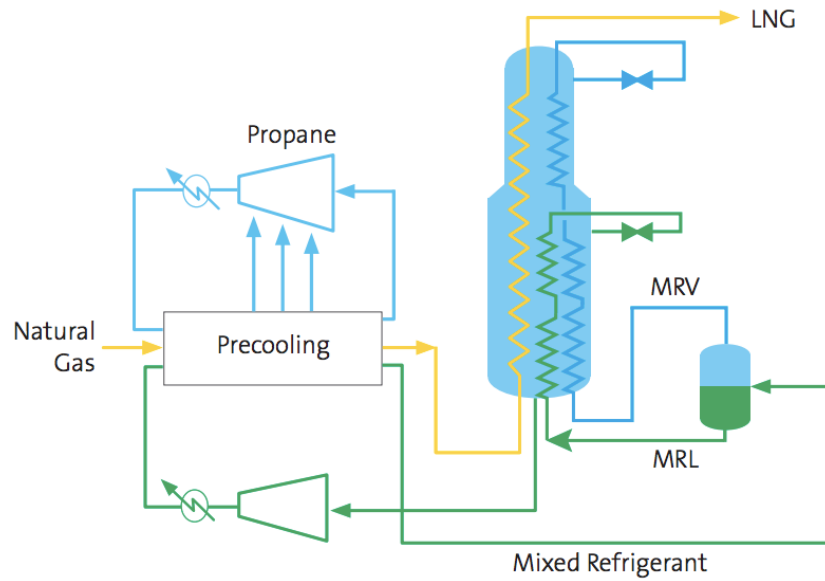


Figure 2.10 – General flowsheet of AP-C3MR [52]

With the maturity of the industry, there is a higher demand for a larger LNG processing capacity, since the specific cost can be lowered with a larger capacity. In the last 25 years, the C3MR cycle has evolved to several significant developments such as:

1. AP-XTM process is pioneered to Qatar LNG by combining C3MR and nitrogen expander cycle, which is discussed in the previous sub-section, to deliver additional refrigeration duties after MCHE stage. The process is implemented for processing capacity up to 8 MTPA.

2. Large capacity trains over 5 MTPA can be designed using the C3MR/SplitMR[®] compressor/driver arrangement. The available power of each gas turbine driver and its helper motor or turbine is fully utilized for LNG production with a minimum number of refrigerant compressor casings [24]. It has been installed in several projects, such as for the capacity expansion of Bontang LNG.

2.3.7. Air Products' SMR and Nitrogen Recycle Process

For small-scale LNG plants, Air Products offers two technologies: Nitrogen recycle (AP-NTM) and single mixed refrigerant process (AP-SMRTM). Nitrogen recycle process is adopted from the concept of the Brayton cycle, where the low temperature is generated by compressing and expanding nitrogen through a turbo-expander [49,53]. The process can be arranged into several compression/expansion stages according to the capacity requirement, as it is shown in Figure 2.11. A hybrid cycle using nitrogen and methane as the working fluids is currently being proposed [53]. The principle of AP-SMRTM is somewhat similar to LIMUM[®]3.

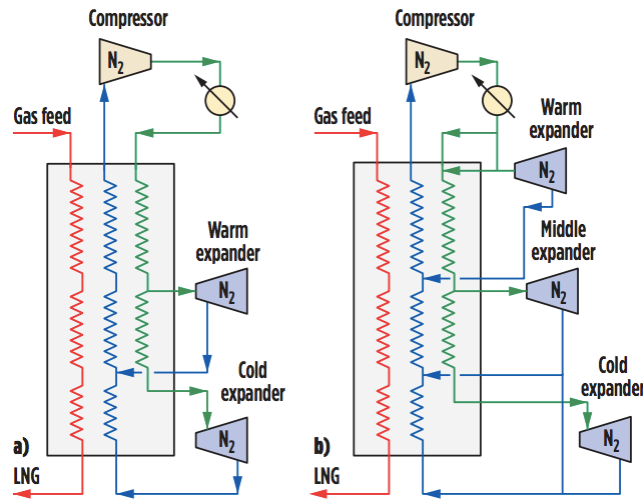


Figure 2.11 – Nitrogen recycle process with two or three expanders [53]

The liquefaction takes place in a coil wound heat exchanger, which consists of three main steps: (1) Precooling to cool the natural gas to around -30°C ; (2) Liquefaction where the natural gas starts to liquefy at around -120°C ; and (3) Subcooling where the liquefied natural gas subsequently cools down to -150°C . The process is attractive due to a straightforward operation and minimum requirement of components to implement the process. The capital cost difference between the two systems is almost comparable. In terms of operation and maintenance, SMR is recommended for plants with a relatively stable production with higher operating hours, while nitrogen recycle offers better performance with production variability with low operating hours. Thus it is more suitable for peak-shaving plants [54].

2.3.8. Dual Mixed Refrigerant (DMR)

Instead of using a single component as the precooling stage, the dual mixed refrigerant is designed with two mixed refrigerants in a separate cycle. Linde plc first started DMR concept [55] using ethane and propane as the first working fluid are used for the precooling purpose, and with methane, ethane, nitrogen, and propane in the second working fluid for the liquefaction. The development of DMR was motivated by the requirement of low energy consumption and high LNG production within a range of varying ambient temperature conditions. Furthermore, the temperature variations of the cooling water due to changing seasons can cause imbalances in the various refrigeration cycles of the regular cycles [56,57].

DMR requires a more complex configuration and additional equipment, albeit having a lower energy consumption, especially compared to the C3MR process. In DMR technology designed by the Royal Dutch Shell plc, the precooling stage uses coil wound heat exchanger instead of traditional shell and tube or plate-fin heat exchanger as in C3MR. C3MR and DMR are able to match the boiling curve of the mixed refrigerant with the condensation curve of natural gas, which translates to high efficiency for the plant. The heat exchangers are commonly half the height and size of the heat exchangers used in a single mixed refrigerant (SMR) process due to the split of the cooling duty into two cycles [24]. The

configuration of the Shell DMR is illustrated in Figure 2.12. A number of studies reported that the C3MR cycle is the most efficient, while others asserted that DMR is more efficient [11]. A comparison study by Nibbelke et al. [58] and Bradley et al. [59] reported by that the specific energy consumption of DMR is 4-9% lower than C3MR whereas the capital cost of DMR is 5% higher than C3MR. In fact, Shell DMR has only been implemented in Sakhalin LNG plant, Russia. The process is chosen due to its precooling flexibility to adapt to the arctic conditions, a problem that would occur when propane is used in this type of climate. At this location, increasing the proportion of propane creates a heavier refrigerant mix for the first cycle in the summer months, which cools the gas to -40°C , while adding ethane yields a lighter mix for winter, cooling gas to -65°C [59].

Analogous to AP-XTM, there is an ongoing development of DMR in order to process larger liquefaction capacity between 7 to 11 MTPA. Shell proposes the extension based on DMR or C3MR to form a new concept called parallel mixed refrigerant (PMR). The immense processing capacity is achieved by arranging a precooling cycle followed by two parallel circuits of liquefaction cycles. Nonetheless, PRM is designed for a project with a considerable amount of natural gas supply, which might be possible in a handful of countries.

2.4. LNG Storage

After the liquefaction and end flash process, the LNG stream is sent to the storage, typically close to the berth (for a base-load plant) before shipping it to regasification terminals. The storage tank consists of an inner and outer part which constructed using different materials. The inner tank is typically manufactured with 9% nickel steel, and the outer tank is composed of reinforced concrete and pre-stressed concrete. The 9% nickel steel is widely used as a material for the inner tank since it has the strength and toughness enough for the cryogenic purposes [60]. There is also alternative construction such as membrane tanks, metal-lined tanks, and the all-concrete LNG (ACLNG) tank [61].

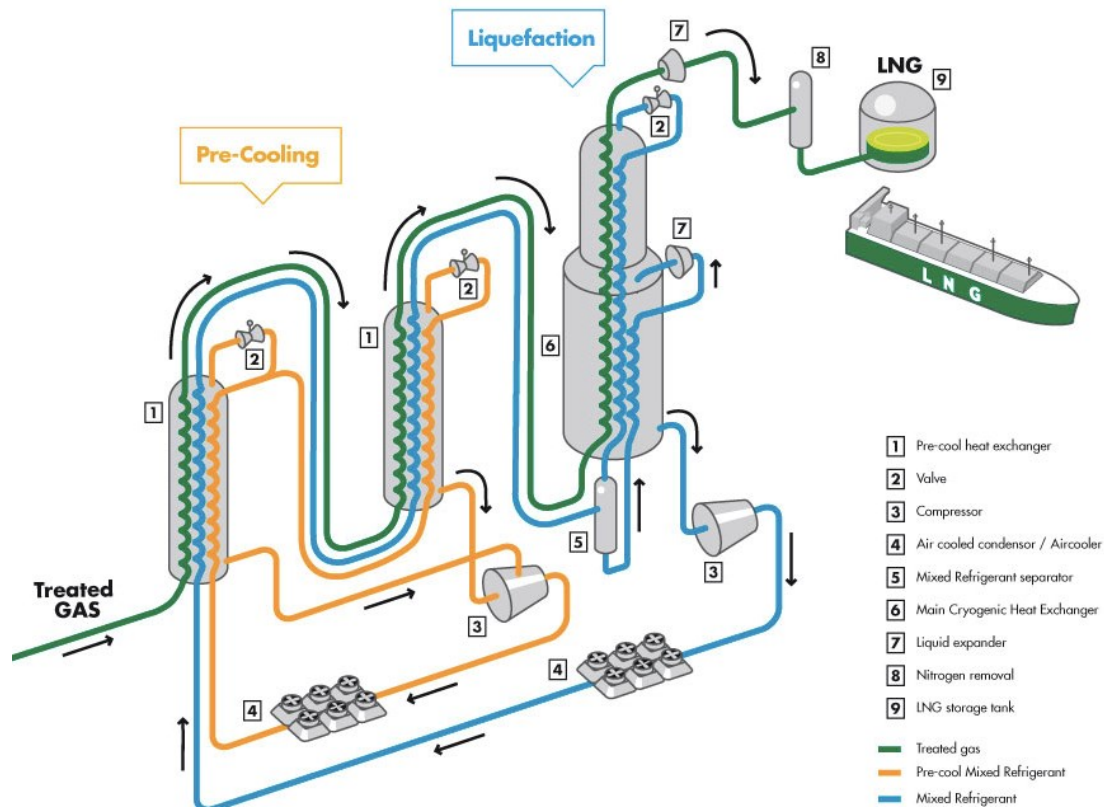


Figure 2.12 – Shell's proprietary DMR process [62]

In the storage, the operating pressure is set slightly above the ambient pressure at 0.10 to 0.24 bar gauge. Methane, the primary composition of LNG, has the lowest boiling point among other hydrocarbons and therefore will take a quantity of heat equal to its latent heat of vaporization when stored. Overtime, the concentration of heavier hydrocarbons will increase and the composition of LNG changes due to transfer for shipment, during which the boiling point of stored LNG becomes higher. This would cause a plug formation in the pumps and pipes, particularly when the partial pressure of Butane in the boiloff gas from the comparatively warm LNG in the pump gets high enough, because the Butane will condense out of the vapor phase while returning to the tank and then solidify forming a semi-porous solid blockage of the line [63]. The vaporization of LNG due to the transfer or external heat entering the tank is known as boil-off gas (BOG). Unique treatment needs to

be taken in order to manage the boil-off gas released from the storage to maintain the LNG quality. In offshore operations, BOG is re-liquified through a refrigeration cycle, while in onshore plants it is routed to the system and used as the fuel gas. From the energy perspective, the use of BOG as fuel gas is the most efficient way to recover BOG. However, there is a constraint for the amount of fuel gas necessary for an LNG plant. Kurle et al. [64] asserted that this strategy would not increase the total plant revenue, while Zellouf and Portannier [65] investigated the possibility to minimize the BOG production in offshore LNG operations.

The state-of-the-art LNG process design can be classified according to the capacity requirement of the plant. A large-scale liquefaction capacity involves a more complicated process with more components, such as in the case of C3MR or DMR. For this purpose, they are more efficient than AP-SMRTM or PRICO, which is intended to be used in the small to the mid-range LNG plant. The number of components will also determine the investment costs of the plant, which is one of the main concerns for plant owners. Therefore, the selection of the liquefaction process needs to consider not only in terms of efficiency and ease of operation but also in terms of the economics of the process.

3. Exergy-based Methods for Energy Systems

3.1. Exergy Analysis

The method of exergy analysis adopted the concept of the second law of thermodynamics and the entropy generation, which ultimately provides: (a) A measure to judge the magnitude of 'energy waste' in relation to the 'energy' supplied or transformed in the total plant and in the component being analyzed; (b) a measure for the quality or usefulness of energy from the thermodynamic viewpoint; and (c) a variable to define rational efficiencies for energy systems [4] This method applies the second law of thermodynamics by taking into account the irreversibilities of a real energy system [4,66]. The exergy-based method quantifies them by means of exergy destructions and exergy losses.

The first law mentions that the energy always conserved and cannot be destroyed, only transforms into different forms. In contrast with energy, a part of exergy in a real process from one state to another is always destroyed as the result of irreversibility. A process is called irreversible if by no means the system and its respective surrounding can be reinstated to their initial states [67]. The concept of exergy is closely related to the second law of thermodynamics, where the destroyed part of exergy during a process, known as the exergy destruction, is related to the relationship between the system and its environment. When a system is brought to a state of thermodynamic equilibrium with its environment, the value of its exergy is zero. At this condition, the thermal, mechanical and chemical equilibrium is satisfied. This condition is called dead states since there is no potential to produce any useful work, whereas the equilibrium in which only thermal and mechanical are considered, is referred to restricted dead state [67].

The term exergy itself is first coined in 1956 by Rant in his paper *Exergie, ein neues Wort für Technische Arbeitsfähigkeit* [68]. In his term, a brief definition for exergy can be

considered as the technical availability to do useful work, and the term was generally accepted in the scientific community, rather than the one proposed by Keenan. Szargut used the following statement to describe the term “Exergy is the amount of work obtainable when some matter is brought to a state of thermodynamic equilibrium with the common components of its surrounding nature by means of reversible processes, involving interaction only with the above mentioned components of nature” [69]. In fact, the concept is rather similar to the Gibbs free energy equation, where it describes the amount of available work for an isothermal and isobaric process. The exergy, however, measures the available work until a system reaches equilibrium with its surroundings, irrespective of the thermodynamic process. In applied thermodynamics, the exergy concept combines the concept of the first law, which establishes the flow of energy balance, with the second law, which quantifies the available work and the exergy destructions of the system. This method is known as exergy analysis, which calculates the quantity and quality of energy as well as the irreversibilities with respect to the surroundings [66].

In their early inception exergy analysis was mostly applied to the energy conversion systems. One of the earliest works related to the exergy analysis comes from Hans-Georg [70] analyzed the exergy loss from heat transfer of a nuclear reactor, whereas Siegel [71] conducted the exergy analysis to the heterogeneous nuclear power reactor. Hendrix [72] applied exergy analysis coupled with the optimization for the regenerative feedwater heaters. Thirumaleshwar [73] applied the exergy analysis to a modified Brayton-cycle-based helium cryorefrigerator system. Maloney and Burton [74] conducted the second law analysis, which is analogous to the exergy analysis, with a case study of catalytic reformer ethylene plants in the petrochemical industry. Flower and Linnhoff [75] followed a similar approach to the industrial process networks of nitric acid and sulphuric acid, while Shapiro and Kuehn [76] evaluated a solid waste recovery system to characterize the use of solid waste for supplementary fuel purposes. Gaggioli [77] wrote about the application of second law which relates to the term available energy, dead state and the calculation of entropy generation.

He then continued the works with the mathematical formulation of available thermal energy and chemical available energy. Discourses regarding the general methodology for exergy analysis can be traced back to Evans (1969), Haywood [78], Brzustowski and Golem [79], Ahern (1980) [80] and Tsatsaronis [66]. Furthermore, Szargut [69] has also contributed to the development of exergy analysis, especially in providing the methods to calculate standard chemical exergy [69,81]. Lee et al. [82] conducted exergy and exergoeconomic analyses in fuel-cell-based combined heat and power plant, while Petrakopoulou [83,84] performed comprehensive exergy-based methods including the exergoenvironmental analysis in the area of carbon capture and storage. Tsatsaronis and his research group have also proposed advanced exergy-based analyses [85], which produces a high-resolution output with additional parameters such as the avoidable/unavoidable part of exergy. The analysis is also able to detect whether the sources of irreversibilities are exogenous or endogenous [15,18,20,83,84].

3.1.1. Physical Exergy

Fundamentally, the total exergy of a stream into four separate forms: kinetic exergy E_k^{KN} , potential energy E_k^{PT} , physical exergy E_k^{PH} , and chemical exergy E_k^{CH} . Kinetic and potential exergy are equal to kinetic and potential energy, respectively.

$$E_k = E_k^{KN} + E_k^{PT} + E_k^{PH} + E_k^{CH} \quad (3.1)$$

The kinetic and potential part of exergy in a system are often assumed to be negligible, leaving the physical exergy as the maximum theoretical useful work from initial state to the restricted dead state, and the chemical exergy as the maximum theoretical useful work from the restricted dead state to the state in which a complete equilibrium with the environment is reached [67].

When dealing with low-temperature systems, it is necessary to split the physical exergy into thermal and mechanical parts, since the fuel and product of the particular system might

not have the same direction when brought to rest relative to its surroundings. The separation is particularly useful in analyzing a component, in which the incoming and outgoing streams cross the environment temperature, which takes place in the low temperature energy system. They can be expressed as [21]

$$e_k^{PH} = e_k^T + e_k^M \quad (3.2)$$

$$e_k^T = (h - h_{T_o, p_i}^*) - T_o(s - s_{T_o, p_i}^*) \quad (3.3)$$

$$e_k^M = (h_{T_o, p_i}^* - h_o) - T_o(s_{T_o, p_i}^* - s_o) \quad (3.4)$$

where h_{T_o, p_i}^* and s_{T_o, p_i}^* represent the enthalpy and entropy of the system k at a particular pressure p_i and environment temperature T_o . The thermal exergy e_k^T is referred to the maximum theoretical work as the system k brought from its initial temperature T_i to T_o at the initial pressure. Likewise, the mechanical exergy e_k^M is the maximum theoretical work as the system k brought from its initial pressure at p_i to p_o at the environment temperature.

3.1.2. Chemical exergy

The chemical exergy represents the difference of chemical potential between a system and the environment. The standard environment is associated with the standard chemical exergy of a substance at a reference state, typically at ambient temperature and pressure (298.15 K and 1.03125 bar). The values for the standard chemical exergy that are widely accepted and applied for exergy analysis are based on the model developed by Ahrendts [86] and Szargut [69]. Assuming an ideal gas behavior, chemical exergy of a substance k at an environment temperature T_o and pressure p_o can be defined as

$$\bar{e}_k^{CH} = \bar{R}T_o \ln \left(\frac{p_o}{x_k^e p_o} \right) \quad (3.5)$$

Where \bar{R} is the universal gas constant and x_k^e is the mole fraction of the k -th substance of an ideal gas mixture in the environment.

The notation of $\left(\frac{p_o}{x_k p_o}\right)$ is the ratio between environment pressure and partial pressure, which equals to

$$\bar{e}_k^{CH} = -\bar{R}T_o \ln(x_k^e) \quad (3.6)$$

The chemical exergy of an ideal mixture is therefore given by

$$\bar{e}_{mix}^{CH} = \bar{R}T_o \sum_K x_k \ln\left(\frac{x_k^e}{x_k}\right) \quad (3.4)$$

Using the standard model, \bar{e}_{mix}^{CH} can be calculated as a function of the molar chemical exergy of the k^{th} chemical constituent of the mixture at its standard reference state denoted by \bar{e}_k^{CH} . Therefore,

$$\bar{e}_{mix}^{CH} = \sum_K x_k \bar{e}_k^{CH} + \bar{R}T_o \sum_K x_k \ln(x_k) \quad (3.8)$$

3.1.3. Exergy Balance

The total exergy balance of a system is defined as exergy of fuel that equals to the sum of exergy of product, the exergy of destruction and exergy of loss [67]

$$\dot{E}_{F,tot} = \dot{E}_{P,tot} + \dot{E}_{D,tot} + \dot{E}_{L,tot} \quad (3.9)$$

where the exergy loss, $\dot{E}_{L,tot}$, is related to the exergy of streams that are not going to be used further and rejected out of the system (to the environment). In a closed system where there are only outgoing streams that are related to the exergy of products, the exergy loss is equal to zero. The same rule applies when applying the equation 3.1 to a particular component in a system. The approach is more appropriate than using the input-output relationship, in which the definition can be misleading and results in incorrect information regarding the irreversibilities. The exergy of fuel, $\dot{E}_{F,k}$ and exergy of product, $\dot{E}_{P,k}$ are calculated based on the fuel and product approach.

According to Lazzaretto and Tsatsaronis [87], the exergy of fuel is defined to be equal to

- all the influent exergy of the respective material streams supplied to the component (including the exergy of energy streams supplied to the component); plus
- the exergy removals between influent and effluent of the respective material streams; minus
- all the exergy increase from the streams between influent and effluent that are not associated with the purpose of the component.

Likewise, the exergy of product is defined to be equal to

- all the effluent exergy of the respective material streams, including the exergy streams generated in the component plus
- all the exergy increases between influent and effluent that are not associated with the purpose of the component.

Subsequently, the exergy efficiency of component k , of each component can be calculated using the equation below. The exergy efficiency of a system can be determined using the same calculation.

$$\varepsilon = \frac{\dot{E}_{P,k}}{\dot{E}_{F,k}} = 1 - \frac{\dot{E}_{D,k}}{\dot{E}_{F,k}} \quad (3.10)$$

Other useful parameters in exergy analysis are the exergy destruction ratio y_k and the exergy destruction rate y_k^* . They can be used to compare the magnitude of exergy destruction for each component in a system and identify the potential for improvements.

$$y_k = \frac{E_{D,k}}{E_{F,sys}} \quad (3.11)$$

$$y_k^* = \frac{E_{D,k}}{E_{D,sys}} \quad (3.12)$$

3.2. Economic Analysis

Estimation of the costs associated with all equipment is essential in evaluating the feasibility of the energy conversion systems. The thermodynamic performance for such systems is laid out by exergy analysis and by combining it with economic analysis, engineers are able to obtain the information of the specific costs per exergy unit that are related to all material streams. The method is known as exergoeconomics, which was introduced by Tsatsaronis [5,88]. It has been successfully applied to many case studies that involve the energy conversion process. The method is also able to reveal the cost associated with the total exergy of fuel, total exergy of product, and most importantly, the exergy destructions at the component level, thus unfold the optimization opportunity to a higher level. One of the methods of economic analysis, which were applied in the thesis, is based on the total revenue requirement (TRR). In principle, it comprises of four main steps [67,89]:

1. Estimation of total capital investment (TCI) as shown in Table 3.1.
2. Integration of the economic, financial, operating and market input parameters to the cost estimation.
3. Calculation of TRR.
4. Calculation of the levelized fuel costs, the levelized cost associated with investment and operation and maintenance, and the carrying charges.

3.2.1. Total Capital Investment (TCI)

The basis of TCI estimation is based on the PEC calculation, which varies from process to process. Initially, the PEC for each component is estimated, and the rest of the key parameters for TCI are calculated based on these values as indicated in Table 3.1. Additionally, effects of the equipment characteristics such as the material of construction, pressure and temperature specifications are also taken into account. Therefore, TCI can be expressed as

$$TCI = DC + IC + OO \quad (3.13)$$

The best option for estimating the cost of the equipment is to obtain it directly from a vendor's quotation. For large capacity projects, at least the costs of most expensive equipment should be obtained from a vendor for the sake of the analysis. If the vendor quotations are not available, estimation of the costs from past purchase orders, quotations from experienced professional cost estimators or by calculating them using the extensive cost databases created mostly by the companies, is the second-best option. Furthermore, if the two best options are not available due to the high cost or time requirements for such estimation, then the purchased equipment cost (PEC) can also be estimated using the purchased-equipment base cost charts C_B available in the literatures [67,89].

Table 3.1 – Items of total capital investment (TCI) [67]

I.	Fixed Capital Investment (FCI)
A.	Direct costs (DC)
1.	Onsite costs (ONSC)
	Purchased equipment cost (PEC)
	PEC installation (20-90% of PEC)
	Piping (10-70% of PEC)
	Instrumentation and control (6-40% of PEC)
	Electrical equipment and materials (10-20% of PEC)
2.	Offsite costs (OFSC)
	Land (0-10% of PEC)
	Civil, structural and architectural work (15-90% of PEC)
	Service facilities (30-100% of PEC)
B.	Indirect costs (IC)
1.	Engineering and supervision (25-75% of PEC)
2.	Construction costs (15% of DC)
3.	Contingencies (5-20% of FCI)
II.	Other Outlays (OO)
A.	Startup costs
B.	Working capital
C.	Cost of licensing, research and development
D.	Allowance for funds used during construction (AFUDC)

The PEC calculation starts by estimating the module cost, which is given by

$$C_{PE} = C_B f_d f_m f_T f_p f_{BM} \quad (3.14)$$

The base cost C_B is corrected by including them as factors such as design f_d , material f_m , pressure f_p and temperature f_T . Bare module factors f_{BM} is also added to estimate the final purchased equipment costs C_{PE} .

The PEC can also be estimated by considering the cost chart of reference equipment and a scaling exponent factor to α at its own capacity or size. The effect of size on PEC using the cost chart is expressed as

$$C_{PE,A} = C_{PE,ref} \left(\frac{X_A}{X_{ref}} \right)^\alpha \quad (3.15)$$

where X_A and X_{ref} represent the capacity or size related to the equipment item A and the reference equipment, respectively. The term α refers to exponent sizing, taken from the slope of the data correlation line of the respective PEC against the equipment size. In the absence of other reference cost information, an exponent factor of 0.6 may be used. The approach is known as the six-tenths rule [67,90].

Since the cost charts are generally taken from the previous years (original), the estimated cost data needs to be brought to the year of which the economic analysis is conducted (reference year). In order to this, a so-called cost index approach is applied to the following equation

$$C_{PE,ref.year} = C_{PE,original} \left(\frac{Cost\ Index_{ref.year}}{Cost\ Index_{original}} \right) \quad (3.16)$$

The purpose of the equation is to take the inflation of all factors involved in the PEC into account. In practice, the cost indexes can be obtained from various references such as the

Chemical Engineering Plant Cost Index (CEPCI) and Marshall and Swift Equipment Cost Index (M&S).

3.2.2. Economic Evaluation

The cost estimation of the energy system is typically levelized on an annual basis by considering the future value of money. A variable is defined to express the amount of annual rate of return within a certain number of compounding period p within a year, which is called the annual effective rate of return (i_{eff}).

$$i_{eff} = \left(1 + \frac{i}{p}\right)^p - 1 \quad (3.17)$$

where i is the annual rate of return.

Furthermore, CRF is the capital recovery factor to obtain the ratio of the constant annuity of equal amounts of TCI during the n lifetime of the energy system, which can be formulated as

$$CRF = \frac{i_{eff}(1 + i_{eff})^n}{(1 + i_{eff})^n - 1} \quad (3.18)$$

where i_{eff} represents the annual effective rate of return and n is, in the case of energan y system, is the economic lifetime of the plant in years.

3.2.3. Carrying Charges and Total Revenue Requirement

Carrying charges include insurance, storage costs, interest charges on borrowed funds and other similar costs. Initially, the total capital investment TCI can be used as the basis for the calculation of levelized carrying charges CC_L .

$$CC_L = TRR_L - (FC_L + OMC_L) \quad (3.19)$$

Where TRR_L represents the annualized amount of money that is collected from the product sales in to compensate all expenses during the plant operational lifetime adequately. In order to determine the levelized fuel cost FC_L and levelized operation and maintenance OMC_L , a constant escalation levelized factor ($CELF$) is introduced. Escalation of fuel costs and operation and maintenance costs over an n -year period results in a non-uniform cost schedule in which the expenditure at any year is equal to the previous year expenditure multiplied by nonuniform costs $(1 + r_n)$, where r_n is the nominal escalation rate. It indicates the correlation between the expenses of the first year and equivalent annuity. Since the fuel price growth is expected to increase faster than the operation and maintenance costs, the two variables are calculated separately [67,91].

$$FC_L = FC_0 \times CELF = FC_0 \frac{k_{FC}(1 - k_{FC}^n)}{(1 - k_{FC})} CRF \quad (3.20)$$

$$OMC_L = OMC_0 \times CELF = OMC_0 \frac{k_{OMC}(1 - k_{OMC}^n)}{(1 - k_{OMC})} CRF \quad (3.21)$$

Where k_{FC} and k_{OMC} are the function of i_{eff} and average annual nominal escalation rate for fuel cost r_{FC} and operation and maintenance cost r_{OMC} , respectively. It is given by

$$k_{FC} = \frac{1 + r_{FC}}{1 + i_{eff}} \quad (3.22)$$

with the same formulation applies to k_{OMC} .

3.2.4. Total Revenue Requirement

The annual total revenue requirement (TRR) of a thermal plant is defined as the revenue which must be gained in a specified year, coming from the sale of all the products of the plant in order to compensate the system operating company for the expenses acquired in the same specified year and to ensure the sound economic plant operation. TRR of j^{th} year using current dollar value is calculated as the sum of the eight annual amounts: total capital recovery (TCR); minimum return on investment (ROI); income taxes (ITX); other taxes

and insurance (OTXI); fuel costs (FC); and operating and maintenance costs (O&M) as expressed in the Equation 3.30 [67,89].

$$TRR_{j,current} = TCR_j + ROI_{j,ce} + ROI_{j,ps} + ROI_{j,d} + ITX_j + OTXI_j + FC_j + O\&M_j \quad (3.23)$$

Where the subscript ce, ps, and d refer to the return of investment for common equity, preferred stock, and debt, respectively. Ultimately, the total revenue requirement TRR_p is calculated as the sum of the year-by-year TRR at constant dollar by considering the real escalation rate and real rates of return. The value is converted to the levelized value TRR_L according to Equation 3.31 [67,89].

$$TRR_p = \sum_{y=1}^N TRR_{y,constant} \quad (3.24)$$

$$TRR_L = CRF \times TRR_p \quad (3.25)$$

3.3. Exergoeconomics

The exergoeconomic analysis is particularly useful to combine the exergy and economic considerations, where the costs can be assigned to the exergy streams of the corresponding energy systems. The method is accomplished by formulating the cost balance based on the exergy balance and assigning the specific costs to all exergy streams within the system. Several studies with regards to this field used the term thermoeconomic in the early days, i.e., from Frangopoulos [92,93], Wall [94], Valero and Lozano [95], while El-Sayed and Gaggioli [96] wrote a review of the methodology, to which they called the second law costing. The earliest works that used the term exergoeconomics, which also establish the general methodology of the analysis, can be found in Hesselmann [97], Tsatsaronis [88,98], Tsatsaronis, Tawfik and Gallaspy [99], Tsatsaronis, Lin and Pisa [100,101]. Furthermore, the introduction of the specific exergy costing approach (SPECO) from Tsatsaronis and Lazaretto [4,87] has established a systematic approach to exergoeconomic analysis. According to the methodology, each exergy additions and removals can be defined by

formulating the fuel and product of the components. The costs, which is obtained from the basic principle of economic analysis, can be associated with all corresponding exergy streams. For instance, the cost of exergy destruction of a component shows how the costs incurred by the exergy destruction with the relationship of the specific cost of fuel.

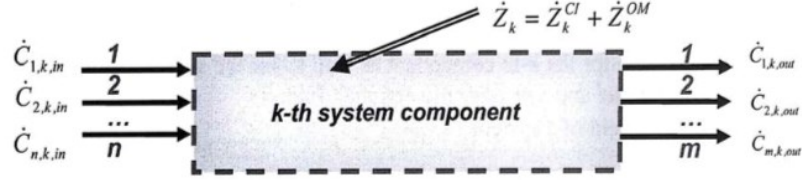


Figure 3.1 – Illustration of the exergoeconomic balance of k^{th} component [67]

The exergoeconomic analysis starts with the formulation of exergoeconomic balance, which can be expressed as

$$\sum_{m=1}^M c_{m,in,k} \dot{E}_{m,in,k} + \dot{Z}_k = \sum_{n=1}^N c_{m,out,k} \dot{E}_{m,out,k} \quad (3.26)$$

The balance can be explained by illustrating a k^{th} component in Figure 3.3. Each of the incoming streams has an exergy rate $\dot{E}_{F,k}$ and a specific cost of fuel per exergy unit $c_{F,k}$. The cost rate associated with the product is in this case the outgoing stream, which consists of the exergy rate $\dot{E}_{P,k}$ as well as the specific cost of product per exergy unit $c_{P,k}$. Additionally, \dot{Z}_k comprises the costs rate of the capital investment \dot{Z}_k^{CI} and the operation and maintenance \dot{Z}_k^{OM} of the respective component.

The cost rate of a k^{th} component, denoted as \dot{Z}_k , is derived from the economic analysis, which associates the with its purchased equipment costs, carrying charges and with operation and maintenance. It is one of the major parameter in exergoeconomics that can be expressed as

$$\dot{Z}_k = \frac{CC_L + OMC_L}{\tau} \frac{C_{PE,k}}{\sum C_{PE,k}} \quad (3.27)$$

Where the τ is the average plant capacity factor, and $C_{PE,k}$ are the purchased equipment cost of component k .

3.3.1. The Cost Balance and Auxiliary Equations

There are two main steps for performing an exergoeconomic analysis: (1) formulation of the cost balances; and (2) formulation of the auxiliary equations. The cost balances are expressed similar to the exergoeconomic balance, which, instead of merely taking the input-output relationship, is based on the fuel and product approach [87].

$$c_{P,k}\dot{E}_{P,k} = c_{F,k}\dot{E}_{F,k} + \dot{Z}_k \quad (3.28)$$

The exergoeconomic balance of the total system is expressed as

$$c_{F,k}\dot{E}_{F,tot} + \sum_{k=1}^K \dot{Z}_k - \dot{C}_{L,tot} = c_{P,tot}\dot{E}_{P,tot} \quad (3.29)$$

$\dot{C}_{L,sys}$ is the cost rate of exergy loss that corresponds to the monetary loss of the outgoing exergy streams from the system to the environment that will not be further used.

The cost balances formulation consists of the specific cost of all streams involved in each component, which can only be solved if the number of streams equal to the number of equations. Therefore, auxiliary costing equations for every component are required. The general rule is when the number of the outgoing streams of a particular component is higher than one ($n > 1$), then $n-1$ auxiliary equations are required. The auxiliary equations in the exergoeconomic analysis are defined based on the F and P rules [87,102], i.e.:

F rule: According to the F-rule for the formulation of auxiliary equations, the total cost associated with the removal of exergy from an exergy stream in a component is equal to the cost at which the removed exergy was supplied to the same stream in upstream components.

P rule: Based on the P-rule, each exergy unit supplied to any stream associated with product of the component has basically the same specific cost of product c_p .

Since in a complex energy system there are multiple components and streams involved, forming a system of linear equations is necessary in order to solve the equations efficiently. In practice, it is not uncommon that one must formulate a copious amount of cost balances and auxiliary equations. Note that exergy and economic analysis must be performed before proceeding to the exergeconomic analysis.

3.3.2. The Cost Rate of Exergy Destruction and Exergy Losses

The cost rate of exergy destruction is defined as the specific cost of fuel of the component k multiplied by its exergy destruction rate

$$\dot{C}_{D,k} = c_{F,k} \dot{E}_{D,k} \quad (3.30)$$

and for the overall system, it is given by

$$\dot{C}_{D,tot} = c_{F,tot} \sum \dot{E}_{D,k} \quad (3.31)$$

Furthermore, the exergy loss of the overall system ($\dot{E}_{L,tot}$) can be accounted from the result of the heat transfer to the surroundings or rejected streams to the environment and this is not further used in the overall system [89]. The cost rate associated with the exergy loss can be expressed as

$$\dot{C}_{L,tot} = c_{F,tot} \sum \dot{E}_{L,tot} \quad (3.32)$$

3.3.3. Exergoeconomic Factor and the Relative Cost Difference

The optimization opportunity in terms of exergoeconomic can be primarily evaluated when considering the two key parameters: the cost rate of investment \dot{Z}_k and the cost rate of exergy destruction $\dot{C}_{D,k}$. In order to evaluate the magnitude of the cost contributions from

these parameters, exergoeconomic factor f_k is a convenient indicator. A high value of f_k indicates that the cost of capital investment of the component dominates the total cost of the component, and vice versa. Exergoeconomic factor is given by

$$f_k = \frac{\dot{Z}_k}{\dot{C}_{D,k} + \dot{Z}_k} \quad (3.33)$$

Another useful parameter is the relative cost difference, where it indicates the relative increase of the cost of product in a component or a system

$$r_k = \frac{c_{P,k} - c_{F,k}}{c_{P,k}} \quad (3.34)$$

Exergy-based methods, which comprises exergy and exergoeconomic analysis is a convenient tool when applied to energy systems for extracting high-resolution information concerning the costs and the exergetic values. The analysis allows the calculation of exergy destructions at the component level as well as the costs associated with it, hence revealing the possibilities for systems improvements. Ultimately, the exergy efficiency and the total cost of product prove to be the most critical parameters on the process evaluation and optimization in terms of thermodynamic performance and cost objectives.

4. Optimization of the LNG Process

In the mathematical description, a general optimization problem is defined as

$$\underset{x \in \mathbb{R}^n}{\text{minimize}} \quad f_i(x) \quad (i = 1, 2, \dots, M), \quad (4.1)$$

$$\text{subject to} \quad h_j(x) = 0 \quad (j = 1, 2, \dots, J), \quad (4.2)$$

$$g_k(x) \leq 0 \quad (k = 1, 2, \dots, K), \quad (4.3)$$

where $f_i(x)$ is the objective function, $h_j(x)$, where x has the equality constraints and/or $g_k(x)$ is referred to as the inequality constraints.

The classification of the problem above can also be seen from a various different perspective. For instance, based on the function forms it can be either linear or nonlinear. Depending on the design variables, the problem can be convex or non-convex, discrete or continuous, and many more. Another classification can be defined according to the number of objectives, which comprises two categories: the single optimization and multi-objective optimization. In terms of the algorithm, there is no clear way to categorize the optimization technique since they depend on the type of problem. Each problem is unique and often intertwine between one type to another. Nevertheless, the optimization algorithm can be categorized according to the convergence characteristics into two broad categories: deterministic and stochastic approach. The method is called deterministic when the problem is solved by providing an explicit mathematical model, through which the model will always give the same solution. On the other hand, the stochastic approach attempts to solve optimization problems by involving random variables in order to search for the best solution for the objective function. Furthermore, the algorithm is characterized by an iterative procedure in the whole range of possibilities and aiming to create a faster convergence. Although the approach does not guarantee a globally optimum solution, the stochastic algorithm can be

easily replicated and requires no derivative information, regardless of the problem type and complexity.

Energy systems are typically characterized by its nonlinearity and multimodal nature. Often the problems also involve integer variables. Therefore a treatment using a mixed integer non-linear programming (MINLP) has to be included. Principally, optimization of the energy systems can be performed by applying either a deterministic and stochastic algorithm, or in a number of studies [103–106], by combining the two approaches in order to find a globally optimum solution.

4.1. Deterministic Algorithm

Deterministic approaches typically provide mathematical guarantees for convergence to a globally optimum solution in a finite number of steps for optimization problems involving specific mathematical structure [107]. They can be applied using the gradient information of the objective function, such as the classic Newton-Rhapson, quasi-Newton or gradient descent method. When the objective function is discontinuous, a free-gradient method can be applied such as Hooke-Jeeves search [108] or Nelder-Mead downhill simplex [109]. However, most of the problems in energy systems are non-convex, which means that there are multiple local optima that do not necessarily can be interpreted as the globally optimum solution. In this case, the performance of the classic Newton or gradient descent method can be severely hindered. In this section, some of the well-known approaches for the deterministic algorithm is presented, including their capability in dealing with non-convexity.

There are several conventional techniques that are widely used in convex, constrained nonlinear problems, for instance, the quasi-Newton method [110–112] as an improved version from Newton’s method to find local optima. Interior point method [113] and sequential quadratic programming (SQP) [114,115] are quite popular techniques, which are available

in MATLAB built-in solver as `fmincon`. Partitioning procedure or known as Benders decomposition [116] was initially introduced for a large-scale mixed integer linear programming with all integer variables of the 0 or 1 class. A generalized Benders decomposition (GBD) method was then developed by Geoffrion [117] in order to extend its capability to convex nonlinear programming (NLP) and mixed integer nonlinear programming (MINLP). Branch and bound, introduced by Land and Doig [118], was initially intended for integer linear programming (ILP). The method was also applicable later on to nonlinear programming, as demonstrated by Lawler and Wood [119]. Improved versions were presented to solve convex ILP problems by Gupta and Ravindran [120] and for MINLP by Quesada and Grossmann [121]. An outer approximation algorithm for MINLP class was introduced by Duran and Grossmann [122] with the idea of developing an equivalent linear representation of the the MINLP and applied relaxation. The idea is similar to the GBD approach, where at each iteration of the MINLP solution, the upper bound and the lower bound are generated. Another method to solve the MINLP problem is the extended cutting plane (ECP) algorithm which was developed by Westerlund and Pettersson [123]. The approach is based on the pioneering work of cutting plane method for NLP class by Kelley [124]. The ECP methods have some advantages such as the simplicity and robustness of the solution. The disadvantage with the convergence speed is at least partially avoided in weakly non-linear problems [123].

Global non-convex optimization is a hard problem, and it is still ongoing active research. Non-convex problems also prove to be hard to solve analytically, not only because of local optima but also when dealing with saddle point; that is when the derivatives at all orthogonal directions are zero but does not belong to the extremum of the function. This is the point where minima or maxima cannot be clearly defined. One of the techniques was proposed to overcome the issue is by applying saddle-free Newton method [125]. The popular branch and bound technique also found its way to non-convex optimization problems, with Branch-And-Reduce Optimization Navigator (BARON) [126] being the state-of-the-art for

MINLP solver, while Belotti et al. [127] proposed an alternative with bounds tightening and branching strategies. Other approach developed by Androulakis et al. [107] offers a modified branch and bound global optimization α BB, which is a type of spatial branch and bound method where the concept of a convex relaxation of the original non-convex is performed. Curtis and Overton [128] proposed an SQP gradient sampling method to be applied in non-convex cases, while an algorithm using the outer approximation [122] for tackling the non-convex problems was also developed by Kocis, Viswanathan, and Grossmann [129,130].

4.2. Stochastic algorithm

The deterministic algorithms are traditionally aimed at the locally optimum problems, which then developed into a more advanced technique to solve more complicated optimization problems. When they are applied to a high dimensional and non-convex function that is very complex, the computational time would be very expensive, and sometimes the solutions could become inconsistent and unreliable. These issues have generated the interests of the scientific community to find an alternative method, which ultimately paved the way for stochastic algorithms. The most distinctive feature in the stochastic algorithm is they require no derivate information from the objective functions, thus creating a more straightforward workflow when dealing with a highly complex optimization problem. The term stochastic is derived from Greek “stokhazestai” (meaning to aim or to guess) embodies the core definition of the algorithm, which always involves random variables and iterative process. The stochastic algorithm should not be confused with stochastic programming, an optimization modeling approach which involves some degree of uncertainties. Another vital principle of the stochastic algorithm is: (a) the diversification of search space in order to search for the best path to an optimum solution, and (b) the intensification or exploitation of the search around the current solution, when it is found to be a good one. Furthermore, the method approximates the best solution in a reasonable computational time at the expense of lower accuracy. Therefore, it does not

guarantee globally optimum solutions but good enough to be accepted as the near-optimum solutions.

In general, there are two types of stochastic algorithms: Heuristics and Metaheuristics. Heuristics is a knowledge-based approach that applies an iterative process in the search space of a particular problem. Since it is based on the experts' knowledge, the approach is problem-specific and relies on the rule of thumb, hence cannot be replicated to a different type of optimization problems. The concept of heuristics followed by the development of a higher-level algorithm, which is designed to be adaptive to all optimization problems. However, the concept had not been really taken place in the scientific community until the full concept of genetic algorithm (GA) is popularized by Holland [131] in his seminal work in the 1970s. It is conceptualized as an artificial system with intelligence, which is adaptive, can replicate itself, and has the ability to learn from its environment (in this case, mathematical models). During the same years, a similar method known as the Evolutionary strategy (ES) was established by Schwefel and Rechenberg [132,133]. In fact, these approaches are now classified as an evolutionary algorithm (EA) since they are inspired by the Darwinian theory of evolution. There are other related methods, such as differential evolution [134] and gene expression programming [135]. Specific to GA, the procedure involves genetic operators within its iteration loops, such as mutation and crossover. These will be discussed further in the next section.

Simulated annealing was initially proposed by Kirkpatrick [136] to solve combinatorial optimization problems by mimicking the concept of annealing in metallurgy. The process involves heating and progressive cooling of a metal to obtain a near-optimum crystal form, which related to the minimum energy level at a given temperature [137]. Ant colony optimization (ACO) [138] was inspired by the route used by ant colonies to discover the best direction while foraging for food. The colony that finds the most efficient route will collect more food and thus will leave pheromone trails and will be followed by the rest of

the colonies. ACO has also been successfully applied to multi-objective optimization problems [139]. Similarly, particle swarm optimization was developed by Kennedy et al. [140] works according to the natural phenomena such as bird flocking, fish schooling and swarming theory. The concept is similar to evolutionary algorithm and ant colony though it does not feature operators such as crossover or mutation nor pheromone density. The particles are spread randomly throughout the search space of a given objective function, and their paths are adjusted through the iterative process. The particle that has moved towards the best location will attract other particles, where a fraction of random trajectory character is kept. Most recently, several new metaheuristic methods have also emerged such as the Bat-inspired algorithm, harmony search and symbiotic organism search [141–143].

4.2.1. Genetic Algorithm

```

Input:  $Population_{Size}$ ,  $Problem_{Size}$ ,  $P_{crossover}$ ,  $P_{mutation}$ 
Output:  $OF_{Best}$ 

Population  $\leftarrow$  InitializePopulation( $Population_{Size}$ ,  $Problem_{Size}$ )
EvaluatePopulation(Population)
 $OF_{Best} \leftarrow$  GetBestSolution(Population)

While (StopCondition())
    Parents  $\leftarrow$  SelectParents(Population,  $Population_{Size}$ )
    Children  $\leftarrow \emptyset$ 
    For ( $Parent_1$ ,  $Parent_2 \in$  Parents)
        Offspring1, Offspring2, Crossover( $Parent_1$ ,  $Parent_2$ ,  $P_{crossover}$ )
        Offspring Mutate(Offspring1,  $P_{mutation}$ )
        Offspring Mutate(Offspring2,  $P_{mutation}$ )
    End
    EvaluatePopulation(Children)
     $OF_{Best} \leftarrow$  GetBestSolution(Children)
    Population Replace(Population, Children)
End

Return ()

```

Figure 4.1 – Pseudo code of genetic algorithms [144]

The GA is a metaheuristic optimization method is by an intelligent search procedure combined with the so-called genetic operators which consist of selection, crossover and mutation operator. The algorithm runs in a specified number of iteration loop, eliminating

the “least-fit” individuals during its selection process which will make the fittest individual thrive and survive for the next iteration. The method is prevalent due to its effectiveness to escape from local optima and offers simplicity with its implementation. In practice, GA is more likely to produce a near-optimum solution, instead of reaching to a globally optimum point, due to the computational limitations. The path is obviously not replicable since a certain degree of randomness is involved in the process. Moreover, the genetic operators have to be carefully adjusted to create a faster convergence towards the best solution. Nonetheless, the strongest point of GA is the ability to escape from local minima/maxima regardless of the optimization problems.

The framework of genetic algorithm is presented with the pseudo-code in Figure 4.1. The algorithm starts with the random initialization of the design variables that consist of several individuals, collectively known as the population. The population of each iteration is evaluated and ranked based on their objective function values (in GA term, they referred to as the fitness values). The next population for subsequent iteration is generated by crossover operators, in which the individuals from the previous iteration are selected as parents, and then the crossovers are performed to produce new generations (offspring) according to the property of their parents. The purpose of this step is to “intensify” the selection of individuals that have the best fitness. Furthermore, the lower ranks of the population are discarded and replaced with the new offspring. At a certain degree the population with the best fitness, known as the elitist strategy, are kept for the next iteration. In order to explore or “diversify” the feasible solution of the subjective space, some variables in the new generation are mutated as an attempt to avoid local minima and early convergence in the process. Aside from the initial design variables, the quality GA solution depends on several critical parameters such as the number of iterations, the population size, the number of elites and the mutation rate. The original GA proposed by Holland represents the variables as binary strings of 0s and 1s. Afterwards, a modified version that proposed real-valued or continuous GA started to be applied in several case studies [145–147].

There are several operator methods available for selecting the crossover operator, such as fitness proportionate (roulette wheel) selection, tournament selection, steady state selection, and Boltzmann selection. The comparison between the selection operators is discussed in Yadav and Sohal [148]. The purpose is to increase the chance of selecting the best individuals as parents, while at the same time still giving an opportunity for the lower rank to be selected. In roulette wheel selection, for example, the fitness function of each individual is associated proportionally with a probability of selection. Hence, the best individual will have a bigger chance to be selected during the random selection. On the other hand, the tournament selection applies different principle by randomly group individuals in a tournament scheme to compete with each other based on their fitness. Goldberg and Deb [149] asserted that the roulette wheel selection is significantly slower than rank selection and tournament selection, with the latter is preferable than others in terms of computational time. Zhong et al. [150] also reported that tournament selection is preferable than the roulette wheel after conducting a test with 7 different functions. The crossover method with the roulette wheel selection is illustrated in Figure 3.3.

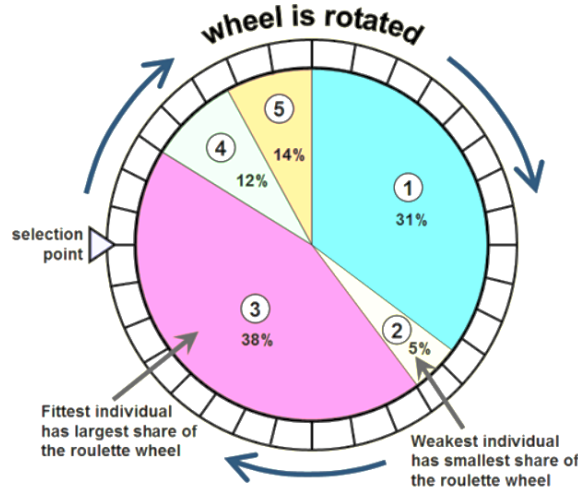


Figure 4.2 – The roulette wheel selection crossover [151]

4.3. Multi-objective Optimization

Unlike single optimization, a single global optimum in multi-objective optimization (MOO) problems are hardly present unless when the objective functions are not in conflict with each other. Therefore, the approaches that are used to solve multi-objective optimization problems depend on the user perception to the objective functions. The first approach is a priori articulation of preference which implies that the desired outcome of each objective function is determined prior to performing the optimization. Weighted sum belongs to this category since weights are assigned to each function based on the preference of the user before running the optimization. Ultimately, the objective functions are simplified to a single objective problem, known as the utility function, with a weighted sum function. Instead of assigning arbitrary weights, physical programming [152] uses preference functions in the calculation, which consists of eight preference classes according to their desirability. Another method is the Lexicographic method, which also treats MOO as a single utility function and set the priorities to each of the objectives. The first objective is chosen as the most important, which is then optimized. Afterwards, the second objective is optimized without decreasing the quality of the solution obtained for the first objective [153]. The procedure continues for the rest of the objective functions. The effectivity of this method depends on how accurately one is able to approximate the preference function [154].

In most of the cases, if not all, the priority scale between one objective to another is undefined or rather vague. The solution for this is to provide the decision maker with all possibilities at the Pareto optimum frontier, a limit where an objective function cannot be improved further without worsening at least one of the other objectives. The approach is referred to as a posteriori articulation of preference, which is carried out by selecting a single solution from a set of mathematically equivalent solutions [154]. The main goal in this approach is to map out the Pareto optimum frontier so that the decision making for preferences can be commenced thereafter. Normal boundary intersection (NBI) is an algorithm to approximate Pareto optimum points, where it is initially intended for NLP problems. The global Pareto optimum may not be found by using NBI. However it is still

useful in constructing a smoother approximation of the Pareto boundary [155]. By simplifying the preference classes, a modified version of physical programming was proposed by Guenov et al. [156] to generate Pareto optimum frontier and thus suitable for a posteriori approach. Furthermore, an additional algorithm is proposed to remove non-Pareto and local solutions. Normalized normal constraint method [157] introduced a Pareto filter algorithm to eliminate unnecessary non-Pareto and local solutions. It is an improvement of standard constrain method [158] in terms of numerical scaling.

4.3.1. Multi-objective Genetic Algorithm

With the advent of metaheuristic methods, researchers started to explore the application of GA for MOO cases, since the search algorithms involve iterative process and can be tweaked to move towards global Pareto optimality. In fact, GA can be a very practical approach for multi-objective problem, with some modifications to the core algorithm. Although to some extent the approach for multi-objective is similar to the single-objective optimization, the basic principle of the GA operators for this case are substantially modified. Assigning weights to each objective would not be acceptable since the optimization procedure needs to have a range of selection of non-dominated solutions, known as Pareto frontiers. Therefore, there is no need to assign arbitrary weights to objective functions. In minimization objectives, a solution $x^{opt} \in X$ is Pareto optimum if there does not exist another point, $x \in X$, such that $F(x) \leq F(x^{opt})$, and $F_j(x) < F_j(x^{opt})$ for at least one function [154]. In the metaheuristics application, the result might not be Pareto optimum but close enough to the optimum boundary. This condition is known as weakly Pareto optimum.

There are several proposed algorithms on implementing GA for MOO purpose. For instance, vector evaluated genetic algorithm (VEGA) developed by Schaffer [159], Multi-objective GA (MOGA) developed by Fonseca and Flemming [160] and Strength Pareto approach (SPEA) by Zitzler et al. [161], which was quickly followed by several improvement strategies

proposed in SPEA2 [162]. A non-dominated sorting genetic algorithm (NSGA) developed by Srinivas and Deb [163] proposed the non-domination front in each iteration to replace the conventional GA selection operator. The sorting method carries the most critical part of the algorithm, which will determine the subsequent selection process. Instead of sorting individuals based on single-objective, it applies the sorting procedure based on the non-domination property of each individual. Some of the drawbacks of NSGA method, such as expensive computational time and lack of elitist strategy led to the development of NSGA-II, which is also developed by Deb et al. [164]. This technique can be used to create a full Pareto-front in only a single execution, something that is impossible to do with simulated annealing, for instance [137]. In this version, two important operators are introduced: non-dominated sorting and crowding distances. The former selects the population based on the non-domination properties to assign the individuals' frontier, while the latter acts as a mechanism to ensure diversity of Pareto solutions on the search space of the objectives. At a given number of iterations, the population is ranked and selected accordingly, resulted in solutions from all frontiers which will converge towards Pareto optimum frontier. Elitism can also be included in the non-dominated sorting to accelerate the convergence. The MOO workflow of NSGA-II is explained in Figure 4.3.

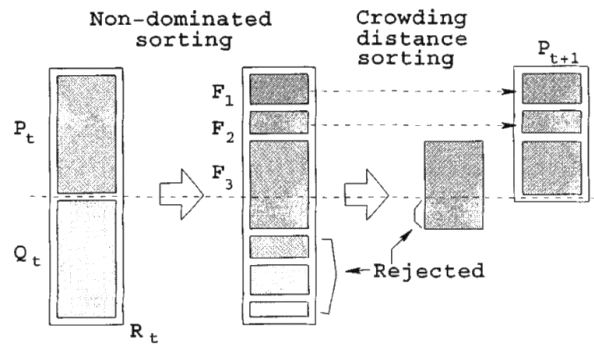


Figure 4.3 –NSGA-II optimization procedure [164]

4.4. Optimization of LNG Process – Literature Survey

4.4.1. Single Objective Optimization

Several publications have discussed the process optimization for liquefaction cycles albeit not exclusively coupled with the exergy-based methods. For instance, Alabdulkarem et al. [165] applied the GA optimization method to C3MR process with Matlab built-in toolbox, where energy consumption set as the objective function. There are 22 optimization variables within two-stage optimization based on the separated cycle of C3MR. Four different pinch temperatures of main heat exchanger were also analyzed. The optimized composition resulted in 9.08% power consumption savings. Sanavandi and Ziabasharhagh [27] performed the optimization of the C3MR with energy consumption chosen as the objective function. HYSYS optimizer functions and a self-initiated method entitled as “Observation of governing trend in mixed refrigerant cooling curve behavior by an approach to maximization of possible fit in cryogenic heat exchangers composite curve” were used for the optimization. The author set 10 variables to the optimization, including MR composition, discharge pressure, and pre-cooling outlet temperature. It is reported that at optimized condition the energy consumption has decreased by 5.35% from its initial condition at 1028.94 kJ/kg_{LNG} to 973.93 kJ/kg_{LNG}. In addition, exergy analysis was also performed using input/output relationship, with 6.36% improvement obtained after the optimization. Al-Sobhi and Elkamel [166] investigated a multi-product system that includes LNG, GTL, and methanol production network, in which the C3MR process is implemented. The main goal is to maximize profit by simulating the upstream and downstream network simultaneously and finding the right amount of natural gas distributed along each production line. The simulation and economic analysis were carried out using Aspen Plus and Aspen Economic Analyzer, while linear programming was used for the optimization model.

Similarly, Wang et al. [25] performed four different objective functions to C3MR and C3MR with split propane (C3MR-SP) process. The objective functions include shaft work, two different exergy efficiency expressions, and operational expenditure (OPEX). They considered the pressure and flowrate of refrigerants, the composition of mixed refrigerants (MR), and the outlet temperature of the main cryogenic heat exchangers as the decision

variables. The ultimate goal is to see which objective function that require the least total shaft work. The exergy analysis was conducted using an input/output relationship without special treatment to the streams that cross the environment temperature. According to their results, maximizing the exergy efficiency will produce the most optimum solution. In his extended study, Wang et al. [167] revisited C3MR and dual-mixed refrigerant (DMR) optimization and selected four different objective functions: total shaft work consumption, total cost investment (TCI), total annualized cost (TAC), and total capital cost of compressors and main cryogenic exchangers (MCHEs). A similar approach with the previous study was applied for the exergy analysis. The author intended to find the most efficient objective function by ultimately looking at the minimum shaft work and overall heat transfer coefficient and area (UA) of MCHEs. The results showed a trade-off between economic objectives and energy consumption. Hatcher [168], on the other hand, constructed and tested 8 different objective functions using Aspen HYSYS “BOX” method, including net present value (NPV) and shaft work of C3MR process. The author’s main focus was on evaluating the robustness of various objective functions according to design and operational expenses, as well as the scenario when the gas feed decreases. They found that from a design perspective, minimizing the cost of compressors should be chosen, whereas from an operational perspective, minimizing the net present value (NPV) should be favored as the objective function.

In a small-scale LNG process, Khan et al. [169] used non-linear programming combined with energy analysis applied to a single mixed refrigerant cycle. The design variables manipulated were the refrigerant composition and flow rate, suction and evaporation pressures, and refrigerant vaporization. Xu et al. [170] optimized the exergy efficiency in PRICO process using GA and Aspen Plus as the simulator. MR composition was chosen as design variables, and the author also investigated the effect of the environment temperature to the system performance. The process was optimized in four different ambient conditions ranging from -10°C to 40°C. The optimizations resulted in the exergy efficiency between 39.6% to 42.3%.

The author asserts that when ambient temperature increases, the concentrations of methane, ethylene, and propane should decrease, while isopentane should increase. The exergy analysis in this paper, however, was not implemented rigorously. The author only considered the exergy efficiency as the reversible work divided by the real shaft work, with the former is defined using the inlet/outlet relationship.

4.4.2. Multi-Objective Optimization

There are publications that focused on multi-objective optimization for energy conversion plants albeit not exclusively focused on the LNG processes. For example, using exergy-based methods, Ahmadi and Dincer [171] optimized the gas turbine power plant by including exergy efficiency, the total cost of the system and cost of environmental impact. As the extension of the previous study, Ahmadi et al. [172] implemented an evolutionary algorithm to multi-objective optimization of combined cycle power plants with additional evaluation of supplementary firing. The authors set the exergy efficiency, total cost rate of the system and CO₂ emissions of the overall plant as the objective functions. Zhao [173] evaluated the thermodynamic performance and specific cycle cost of two different arrangement of supercritical CO₂ Brayton cycles. The author also conducted multi-objective optimization for the parameters mentioned above, where it was found that heat source temperature, turbine inlet temperature, and cycle pressure ratio are the key variables for the exergy efficiency. Fergani et al. [174] applied a multi-objective particle swarm optimizer for multi-criteria exergy-based optimization (exergy, exergoeconomic and exergoenvironmental analyses) of an Organic Rankine Cycle for waste heat recovery in the cement industry. Wang et al. [175] used Mixed-integer nonlinear programming and differential evolution technics for multi-objective optimization of coal-fired power plants. Since publications [171–175] are not dealing with LNG plants, the obtained results are not discussed here. Using the C3MR process as the study case, Ghorbani et al. [176] recently reported the multi-objective optimization for the exergetic performance and total cost of product. However, the accurate

exergy-based analyzed for liquefaction systems (operate partially below and crossing the ambient temperature) should deal with the splitting the physical exergy into thermal and mechanical parts, which was not implemented in any of these studies.

5. Base Case Analysis of C3MR Process

5.1. Process Modeling and Simulation

Prior to the exergy-based analyses and optimization, the C3MR process was modeled and simulated using Aspen Plus with the initial variables for the base case were adopted from Hill [26]. Furthermore, several assumptions for the simulation were taken, such as:

1. Pressure drop in the heat exchangers was assumed to be 3%. For simplification, it was assumed that there is no pressure drop in the precooling cycle.
2. Isentropic efficiency was assumed to be 78% for precooling compressors, and 75% for MR compressors, while all compressors were assumed to have a 90% mechanical efficiency [26,177].
3. Vapor-liquid separators and mixers were assumed to have no pressure drops, and operated were operated without heat duty.
4. The LNG processing capacity for the base case simulation was designed at 4.5 MTPA.
5. Base case variables for the MR compositions are based on Venkatarathnam [38] and Gaumer et al. [50,178] and were modified accordingly for the sake of process convergence. All variables used for the base case are summarized in Table 5.1.
6. The natural gas feed is assumed to be pre-processed; meaning the pre-treatment facility including dehydration, sweetening, NGL and condensate recovery units are excluded in the process simulation and further analyses.

The process flowsheet of C3MR created with Aspen Plus is depicted in Figure 5.1. Propane and mixed refrigerant (MR) serve as the working fluids in its own, separate cycle. Initially, natural gas feed and MR streams are pre-cooled to about -33°C with propane cycle. Propane is compressed using a four-stage compression with intercooling (PROP-C1 to PROP-C4)

while the MR is compressed in the three-stage process (MR-C1 to MR-C3). Four heat exchangers represent precooling of propane cycle (PHX1 to PHX4), and two heat exchangers (MHX1 and MHX2) represent the main cryogenic heat exchanger of MR cycle. The composition of natural gas feed and MR are listed in Table 5.2.

After the pre-cooling stage, the MR is separated into liquid and vapor streams before entering the main cryogenic heat exchanger. The heat exchanger itself is modeled as two separate components with different temperature profile: MHX1 and MHX2. The vapor part of the MR stream flows to both MHX1 and MHX2, while the liquid part only flows to MHX1. By taking advantage of Joule Thomson effect, the temperature MR streams are further decreased in J-T valves (MRTV-1 and MRTV-2), before finally mixed together to be used as the cold stream for MHX1. At the outlet of MHX1 and MHX2, the natural gas is cooled down to -127°C and -139°C, respectively. Ultimately, the natural gas is depressurized to near ambient pressure, at which it is liquefied to -160°C. LNG is stored at near-ambient pressure since it simplifies storage handling and transport.

Table 5.1 – Process design variables of the base case simulation

Specification	Value
Natural gas mass flow rate	158.42 kg/s
Natural gas feed temperature	300 K
Natural gas feed pressure	65 bar
LNG temperature	113 K
LNG pressure	1.2 bar
MR compressors discharge pressure	2.5 – 5.1 – 7.2 – 14.3 bar
Propane compressors discharge pressure	7.5 – 17.5 – 48.6 bar
Compressors Isentropic efficiency	75%-78%
Compressors mechanical efficiency	90%
Pressure drops of natural gas and MR in heat exchangers	3%
Pressure drops of within the heat exchangers of precooling cycle	0%

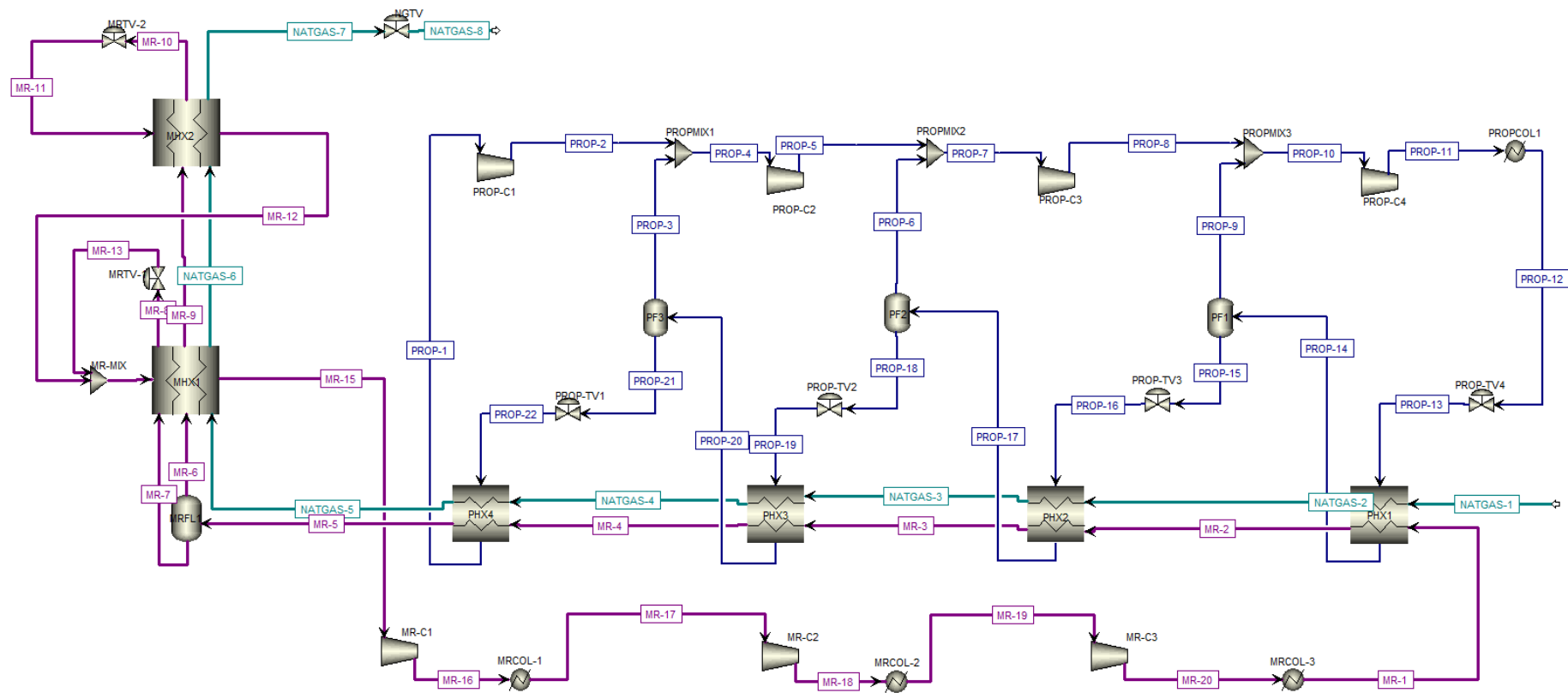


Figure 5.1 – Process flowsheet of C3MR process in Aspen Plus

Table 5.2 – Initial mass fraction of the base case simulation

Component	Natural gas	Mixed refrigerant
Propane	0.021	0.213
Nitrogen	0.041	0.07
Methane	0.875	0.418
Ethane	0.055	0.299
N-Butane	0.005	0
I-Butane	0.003	0

The thermodynamic properties in the simulation were calculated with the Peng-Robinson equation of state [179]. This is one of the most widely used equations of state (EOS) in the natural gas process since the equations are suitable for nonpolar substances while still able provide accurate predictions of vapor-liquid equilibria [180,181]. Several studies of LNG technology have been reported to use the equation as well [11,47,169,170]. The EOS from Peng-Robinson is given by

$$p = \frac{RT}{v - b} - \frac{a}{v(v + b) + b(v - b)} \quad (5.1)$$

Where p is pressure, T is temperature and v is the volume of the considered substance. As a cubic equation, it can also be expressed as

$$Z^3 - (1 - B)Z^2 + (A - 3B^2 - 2B)Z - (AB - B^2 - B^3) = 0 \quad (5.2)$$

where,

$$A = \frac{ap}{R^2T^2} \quad (5.3)$$

$$B = \frac{bp}{RT} \quad (5.4)$$

$$Z = \frac{pv}{RT} \quad (5.5)$$

Parameter a and b are related to the critical temperature T_c and critical pressure p_c , where

$$a = 0.45724 \frac{R^2T_c^2}{p_c} \alpha \quad (5.6)$$

$$b = 0.07780 \frac{RT_c}{p_c} \quad (5.7)$$

with α is a dimensionless function of reduced temperature $T_r = \frac{T}{T_c}$ and acentric factor ω as given by

$$\alpha = \sqrt{1 + \kappa(1 - T_r^{\frac{1}{2}})} \quad (5.8)$$

$$\kappa = 0.37464 + 1.54226\omega - 0.26992\omega^2 \quad (5.9)$$

By applying thermodynamic relationships, the fugacity coefficient component k of a mixture can be calculated in order to obtain the vapor liquid equilibrium $f^V = f^L$.

$$\ln \frac{f_k}{x_k p} = \frac{b_k}{b} (Z - 1) - \ln(Z - B) - \frac{A}{2\sqrt{2}B} \left(\frac{2 \sum_i x_i a_{ik}}{a} - \frac{b_j}{b} \right) \ln \left(\frac{Z + 2.414B}{Z - 0.414B} \right) \quad (5.10)$$

For mixtures, the conventional van der Waals one-fluid combining rules are applied [181]

$$a = \sum_i \sum_j x_i x_j a_{ij} \quad (5.11)$$

$$b = \sum_i x_i b_i \quad (5.12)$$

$$a_{ij} = (1 - k_{ij})(a_i a_j)^{1/2} \quad (5.13)$$

Where k_{ij} is an empirically determined binary interaction coefficient characterizing the binary formed by component i and component j , tabulated in the literature [182].

Similarly, enthalpy and entropy of a component can be obtained using the departure function

$$h_{T,p} - h_{T,p}^{ideal} = RT_c \left[T_r(Z - 1) - 2.078(1 + \kappa)\alpha^{1/2} \ln \left(\frac{Z + 2.414B}{Z - 0.414B} \right) \right] \quad (5.14)$$

$$s - s_{T,p}^{ideal} = R \left[(Z - B) - 2.078\kappa \left(\frac{1 + \kappa}{\sqrt{T_r}} - \kappa \right) \ln \left(\frac{Z + 2.414B}{Z - 0.414B} \right) \right] \quad (5.15)$$

The value of enthalpy and entropy are calculated from a reference state, either from a reference state of an ideal gas or real fluid. The schematic of the calculation is best explained in Figure 5.2. Using ideal gas reference state, we can obtain [182]

$$h = h_{T,p} - h_{T,p}^{ideal} + \int_{T_{ref}}^T c_p dT + h_{ref}^{ideal} \quad (5.16)$$

$$s = s_{T,p} - s_{T,p}^{ideal} + \int_{T_{ref}}^T \frac{c_p}{T} dT - R \ln \frac{p}{p_{ref}} + s_{ref}^{ideal} \quad (5.17)$$

5.2. Exergy Analysis of C3MR Process

Once the process modeling has been established, the enthalpy and entropy values of all streams were used to calculate the physical and chemical exergies, as presented in Table 5.3. The environment temperature and pressure considered in the analysis are 298.15 K and 1.013 bar, respectively. The exergy balance of each component was formulated and computed for each component according to Equation 3.1. Instead of using input-output relationship, the principle of “exergy of fuel / exergy of product” approach [47,87,102] was adopted to the exergy balance formulations, with further details are presented in Appendix A. The exergy of product is defined as the desired by a component or a system being considered, while the exergy of fuel is the exergetic resources consumed to generate the exergy of product [183].

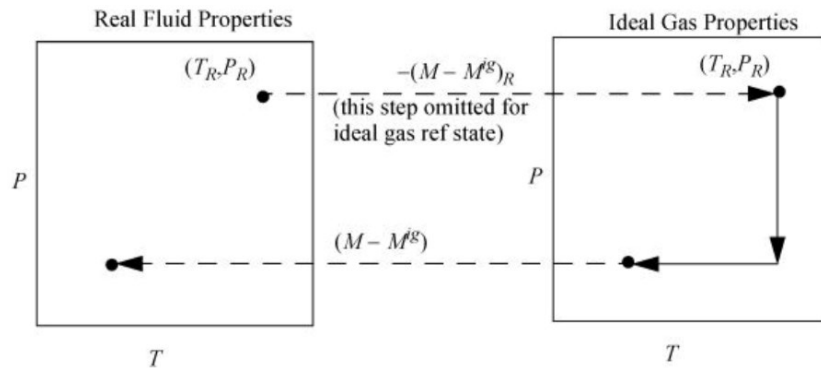


Figure 5.2 – Calculation of the change of state with departure function [182]

Referring to the process flowsheet in Figure 5.1, the pre-cooling cycle consists of the precooling compressors (PROPC1, PROPC2, PROPC3, and PROPC4), four series of heat exchangers (PHX1, PHX2, PHX3, PHX4), mixers (PROPMIX-1, PROPMIX-2, PROPMIX-3) and throttling valves (PROP-TV1, PROP-TV2, PROPTV-3, PROPTV-4). Likewise, the MR cycle consists of MR compressors (MR-C1, MR-C2, MR-C3), a main cryogenic heat exchanger (MHX1 and MHX2), a mixer (MR-MIX) and throttling valves (MR-TV1 and MR-TV2). In addition, the cooler for propane (PROPCOL-1) and cooler for MR (MRCOL-2 and MRCOL-3) are considered as dissipative components since they do not give positive effect to the system and only resulted in exergy destructions. Therefore, there is no exergy of fuel and nor product defined to these components. The flash separators are not analyzed since there are no exergy gained nor exergy removals caused by the components since both cycles are configured in a closed loop. The thermodynamic properties of the process streams including the exergy values are tabulated in Table 5.3.

The exergy analysis was subsequently carried out by extracting information from the exergy streams, resulting in a more detailed analysis for each component as well as the total system. The exergy efficiency of the base case is calculated at 53.4%, while the total exergy destruction is 111.52 MW. The exergy of fuel of the system consists of two parts: (a) The total work required for the compressors, as shown in Table 5.4; and (b) The mechanical exergy destruction related to the pressure drops of the natural gas feed. Likewise, the exergy of product is the addition between the inlet (NATGAS-1) and the outlet (NATGAS-8) of gas streams as a result of the liquefaction process.

Table 5.3 – Thermodynamic base-case data of process material streams

Stream ID	m	T	p	h	s	x	e ^{CH}	E ^T	E ^M	E ^{PH}
	[kg/s]	[K]	[bar]	[kJ/kg]	[kJ/kg-K]		[kJ/kg]	[kW]	[kW]	[kW]
MR-1	301.84	305	48.2	-2974.43	-6.26	1	46234.84	62.26	99775.25	99837.51
MR-2	301.84	291	46.74	-3032.58	-6.45	0.907	46234.84	185.97	99158.25	99344.22
MR-3	301.84	279	45.33	-3108.24	-6.71	0.735	46234.84	1315.82	98535.7	99851.51
MR-4	301.84	257	43.96	-3228.68	-7.15	0.497	46234.84	5553.83	97904.18	103458
MR-5	301.84	240	42.63	-3307.31	-7.46	0.358	46234.84	10572.31	97264.47	107836.78
MR-6	83.58	240	42.63	-3319.2	-5.96	1	40564.58	1273.97	36167.89	37441.86
MR-7	218.27	240	42.63	-3302.76	-8.04	0	48424.09	6465.88	59991.15	66457.03
MR-8	218.27	146	41.34	-3552.42	-9.35	0	48424.09	37406.24	59706.93	97113.17
MR-9	83.58	146	41.34	-3822.78	-8.57	0	40564.58	24425.45	35890.79	60316.24
MR-10	83.58	134	40.09	-3860.07	-8.83	0	40564.58	28179.02	35613.13	63792.15
MR-11	83.58	118.04	3	-3860.07	-8.72	0.183	40564.58	50361.69	10719.11	61080.8
MR-12	83.58	125.98	2.91	-3743.54	-7.77	0.447	40564.58	36602.91	10419.08	47021.99
MR-13	218.27	141.34	2.91	-3552.42	-9.29	0.076	48424.09	75098.13	18480.75	93578.88
MR-14	301.84	135.13	2.91	-3605.33	-8.85	0.225	46234.84	113993.79	28915.64	142909.43
MR-15	301.84	238.57	2.82	-3009.96	-5.62	1	46234.84	3556.44	28059.32	31615.76
MR-16	301.84	300.95	7.5	-2908.57	-5.53	1	46234.84	7.35	54453.43	54460.78
MR-17	301.84	300.95	7.5	-2908.57	-5.53	1	46234.84	7.35	54453.43	54460.78
MR-18	301.84	361.72	17.5	-2800.92	-5.46	1	46234.84	3691.13	76447.39	80138.52
MR-19	301.84	305	17.33	-2916.4	-5.8	1	46234.84	46.17	76202.22	76248.39
MR-20	301.84	382.27	48.6	-2788.57	-5.72	1	46234.84	7234.18	99939.6	107173.78
PROP-1	81.1	238.5	1.3	-2471.72	-6.51	1	48847.39	868.98	1115.85	1984.83
PROP-2	81.1	265.43	2.5	-2434.21	-6.48	1	48847.39	256.27	4011.43	4267.7
PROP-3	141.82	253.91	2.5	-2452.42	-6.55	1	48847.39	831.14	7014.82	7845.97
PROP-4	222.92	258.13	2.5	-2445.8	-6.53	1	48847.39	1063.37	11026.26	12089.62
PROP-5	222.92	289.34	5.1	-2402.76	-6.49	1	48847.39	51.3	19436.6	19487.9
PROP-6	99.87	275.45	5.1	-2426.45	-6.58	1	48847.39	155.29	8707.27	8862.56

Table 5.3 – Thermodynamic base-case data of process material streams (continued)

Stream ID	m	T	p	h	s	x	e ^{CH}	E ^T	E ^M	E ^{PH}
	[kg/s]	[K]	[bar]	[kJ/kg]	[kJ/kg-K]		[kJ/kg]	[kW]	[kW]	[kW]
PROP-7	322.79	285.07	5.1	-2410.09	-6.52	1	48847.39	164.46	28143.87	28308.33
PROP-8	322.79	301.12	7.2	-2388.41	-6.5	1	48847.39	8.58	33766.01	33774.6
PROP-9	119.91	287.34	7.2	-2413.1	-6.59	1	48847.39	42.96	12543.78	12586.74
PROP-10	442.7	297.41	7.2	-2395.1	-6.53	1	48847.39	0.73	46309.8	46310.52
PROP-11	442.7	331.52	14.3	-2351.54	-6.5	1	48847.39	8842.66	52909.77	61752.43
PROP-12	442.7	305	14.3	-2722.83	-7.68	0	48847.39	101.36	52909.77	53011.13
PROP-13	442.7	287.34	7.2	-2722.83	-7.67	0.14	48847.39	5317.25	46309.8	51627.04
PROP-14	442.7	287.34	7.2	-2675.58	-7.5	0.271	48847.39	4530.39	46309.8	50840.18
PROP-15	322.79	287.34	7.2	-2773.09	-7.84	0	48847.39	4487.42	33766.01	38253.44
PROP-16	322.79	275.45	5.1	-2773.09	-7.84	0.084	48847.39	9723.83	28143.87	37867.69
PROP-17	322.79	275.45	5.1	-2687.94	-7.53	0.309	48847.39	7458.51	28143.87	35602.38
PROP-18	222.92	275.45	5.1	-2805.09	-7.95	0	48847.39	7303.22	19436.6	26739.82
PROP-19	222.92	253.91	2.5	-2805.09	-7.94	0.134	48847.39	15003.59	11026.26	26029.85
PROP-20	222.92	253.91	2.5	-2600.62	-7.14	0.636	48847.39	7062.07	11026.26	18088.33
PROP-21	81.1	253.91	2.5	-2859.76	-8.16	0	48847.39	6230.93	4011.43	10242.36
PROP-22	81.1	237.14	1.3	-2859.76	-8.15	0.095	48847.39	8964.62	1115.85	10080.46
NATGAS-1	158.42	300	65	-4073.8	-6.69	1	48072.16	2.35	86893.84	86896.19
NATGAS-2	158.42	291	63.05	-4095.02	-6.75	1	48072.16	35.98	86316.81	86352.79
NATGAS-3	158.42	279	61.16	-4124.35	-6.84	1	48072.16	267.98	85738.23	86006.21
NATGAS-4	158.42	257	59.33	-4182.6	-7.04	1	48072.16	1360.82	85158.75	86519.57
NATGAS-5	158.42	240	57.55	-4231.44	-7.23	1	48072.16	3002.06	84575.74	87577.79
NATGAS-6	158.42	146	55.82	-4756.18	-9.93	0	48072.16	48032.84	83989.64	132022.48
NATGAS-7	158.42	134	54.15	-4797.99	-10.23	0	48072.16	55971.07	83404.5	139375.56
NATGAS-8	158.42	113.15	1.22	-4797.99	-10.06	0.181	48072.16	127682.64	3918.38	131601.02

Table 5.4 – Energy consumption within the components of the C3MR process

Component ID	W_{net}	Unit
MR-C1	34.00	MW
MR-C2	36.11	MW
MR-C3	42.87	MW
PROP-C1	3.38	MW
PROP-C2	10.66	MW
PROP-C3	7.78	MW
PROP-C4	21.43	MW
Total Energy Consumption	156.22	MW
Specific Energy Consumption	986.13	MJ/t _{LNG}

Furthermore, the exergy analysis for each component within the process is tabulated in Table 5.5. In the base case, it was found that four components are exceeding 10 MW of exergy destruction: MHX-1, which is part of the main cryogenic heat exchanger; followed by MR-C1, MR-C2, and MR-C3, which are essentially the exergy destruction during MR compression stage. The exergy destruction rate y_k of these components are more than 40%, which signified the impact of MR cycle in terms of exergy. As expected, the MHX1 has the highest exergy destruction since the heat exchange process involve a large mass flow rate in a finite temperature difference (the pinch temperature is 1.5°C). Nonetheless, the exergy efficiency of MHX1 is 88.2%, which is already a high value compared to the other components. Significant amount of exergy destructions is also occurred in the aftercoolers (MRCOL-3 and PROPCOL), since both working fluids require a relatively high condensing pressure at environment temperature. Note that the MR-COL1 was not considered as a physical component and only used by virtue of simulation purpose.

The components described above can be aggregated since into a more generalized category, e.g., MR compressors (MRC) and precooling compressors (PROPC) serve the same purpose, which is designed in a multi-stage compression. When the components are classified into this category, the highest exergy destruction comes from MRC at 33.5 MW, followed by MHX at 16.5 MW and the precooling compressors (PHX) at 12.7 MW. Furthermore, the

exergy destruction caused by the reduced pressure at the NATGAS-8 stream is 7.8 MW. Overall, the MR cycle is responsible for 62% of the total exergy destructions, whereas 31% is generated by the pre-cooling cycle.

Table 5.5 – Exergy analysis of C3MR components

Component ID	E_F [MW]	E_P [MW]	E_D [MW]	ϵ %	y_k %	y^* %
PHX1	2.04	0.22	1.82	10.9%	0.8%	1.6%
PHX2	3.47	1.36	2.11	39.3%	0.9%	1.9%
PHX3	9.15	5.33	3.82	58.2%	1.6%	3.4%
PHX4	9.32	6.66	2.66	71.5%	1.1%	2.4%
MHX1	112.44	99.12	13.32	88.2%	5.6%	11.9%
MHX2	14.92	11.69	3.23	78.4%	1.4%	2.9%
PROP-TV1	2.90	2.73	0.16	94.4%	0.1%	0.2%
PROP-TV2	8.41	7.70	0.71	91.6%	0.3%	0.6%
PROP-TV3	5.62	5.24	0.39	93.1%	0.2%	0.4%
PROP-TV4	6.70	5.32	1.38	79.4%	0.6%	1.2%
MR-TV1	41.22	37.69	3.53	91.4%	1.5%	3.2%
MR-TV2	24.89	22.18	2.71	89.1%	1.1%	2.4%
NGTV	79.49	71.71	7.78	90.2%	3.3%	7.0%
PROP-C1	4.00	2.90	1.10	72.5%	0.5%	1.0%
PROP-C2	11.67	8.41	3.26	72.1%	1.4%	2.9%
PROP-C3	7.94	5.63	2.31	70.9%	1.0%	2.1%
PROP-C4	21.43	15.44	5.99	72.1%	2.5%	5.4%
MR-C1	37.56	26.40	11.16	70.3%	4.7%	10.0%
MR-C2	36.11	25.68	10.43	71.1%	4.4%	9.4%
MR-C3	42.88	30.93	11.95	72.1%	5.0%	10.7%
PROPMIX1	0.15	0.13	0.02	84.5%	0.0%	0.0%
PROPMIX2	0.10	0.06	0.04	59.7%	0.0%	0.0%
PROPMIX3	0.05	0.00	0.05	1.0%	0.0%	0.1%
MRMIX	485.29	483.66	1.64	99.7%	0.7%	1.5%
MRCOL-2	-	-	3.89	0.0%	1.6%	3.5%
MRCOL-3	-	-	7.34	0.0%	3.1%	6.6%
PROPCOL	-	-	8.74	0.0%	3.7%	7.8%
SYSTEM	239.20	127.68	111.52	53.4%	46.6%	100.0%

5.3. PEC Estimations

5.3.1. Compressors

The centrifugal-type compressor is the common choice for various high pressure and large-scale operation such as in the LNG plants. For a lower pressure and high flow rate, axial-type compressors are also commonly used [184]. Therefore, the centrifugal compressor is selected as the multi-stage compressors for precooling and MR refrigerants. It is also assumed that the compressors are driven by electric motors. Estimation of the PEC is determined by the size factor according to the net required work $W_{net,comp}$ of each compressor. Since the cost correlation is only convenient for a range of the size factor, the compressors are assumed to consist of three identical smaller coolers operating in parallel, although they are simulated as one single component [89]. PEC estimation is given by the following equation

$$C_{PE,comp} = f_D f_M C_{B,comp} \quad (5.18)$$

Where F_D is the driver selection factor assumed to be equal to 1, f_M is the material selection factor assumed to be 2.5. C_B is the base cost of the compressors based on the year of 2009 (CEPCI = 394) that extrapolated to the year 2012 (CEPCI = 584.6), which is the function of net required work in horsepower. The calculation results of all compressors are presented in the Table 5.6.

$$C_{BM,comp} = C_{B,comp} f_M = e^{(7.2223 + 0.8 \ln(W_{net,comp}))} f_M \quad (5.19)$$

5.3.2. Heat Exchangers

The main cryogenic heat exchanger is the most important component in the LNG process since this is the component where natural gas liquefaction is made possible. Along with the compressors, it is also known to be the most expensive, to which the material built for MHX should be able to withstand the high operating pressure and cryogenic temperature.

Globally, there are only a handful of companies that built MHX for LNG purposes (Linde and Air Product are the prime examples), which create difficulties in cost estimation since the data are strictly confidential. All heat exchangers considered in this case is a plate-fin type which can handle a temperature difference of less than 1 K [26,185,186].

Table 5.6 – Cost estimations of compressors

Component ID	W_{NET} MW	C_{BM} (2000) 10^6 US\$	C_{PE} (2000) 10^6 US\$	C_{PE} (2012) 10^6 US\$
PROP-C1	3.380	1.1526	2.88	4.28
PROP-C2	10.660	2.8891	7.22	10.72
PROP-C3	7.775	2.2444	5.61	8.33
PROP-C4	21.427	5.0504	12.63	18.73
MR-C1	34.002	7.3074	7.59	33.77
MR-C2	36.106	7.6668	7.96	35.43
MR-C3	42.872	8.7961	9.13	40.65

Based on the heat transfer coefficient times the surface area values (UA) from Aspen Plus simulation, whereas the base cost was calculated using according to the six-tenths rule with the sizing exponent $\alpha = 0.58$. The base cost reference is assumed to be 5.5 million US\$, which was obtained from an industrial consultant [89]. Since the reference cost has taken the material, pressure and temperature factor into consideration, the PEC is given by

$$C_{PE,HX} = f_{BM} C_{B,HX} \quad (5.20)$$

The surface areas were determined by taking the overall heat transfer coefficient (U) values from the reference [187,188]. Other important assumptions are:

1. The bare module factor f_{BM} is assumed to be 3
2. The heat exchangers are estimated based on cost index of 2009 with the CEPCI = 521.9, whereas in 2012 the CEPCI = 584.6. Accordingly, the cost index equation was applied. Similarly, the cost of pre-cooling heat exchangers is also estimated with the same assumptions with the detailed cost estimation are presented in Table 5.7.

Table 5.7 – Cost estimation of heat exchangers ($A_{\text{ref}} = 672.43 \text{ m}^2$)

Component ID	UA [kW/K]	U [W/m ² K]	A [m ²]	C _{PE} (2012) [10 ⁶ US\$]
PHX1	2809.53	1000	2809.53	42.36
PHX2	3341.80	1200	2784.83	42.14
PHX3	4240.85	1300	3262.19	46.19
PHX4	3567.80	1500	2378.53	38.46
MHX1	17221.70	2500	6888.68	71.26
MHX2	559.11	1700	328.89	12.21

5.3.3. Coolers

During the multi-stage compression, the refrigerants need to have the intercooling as well as after cooling process to reach the two-phase and/or liquid state at the ambient temperature. For this component, the kettle-type or shell and tube heat exchangers are considered. A chart-based approach used in the cost estimation with the cost index reference for the year 2000 ($\text{CEPCI} = 394$). The PEC is calculated by

$$C_{PE, cooler} = f_p f_M f_L C_{B, cooler} \quad (5.21)$$

Where f_L is the tube length correction factor, assumed to be equal to 1. f_M is the material factor given by the relationship of the heat exchange surface area requirement, and carbon steel/stainless steel constants with $a = 1.75$ and $b = 0.13$ [89,189].

$$f_M = a + \left(\frac{A}{100}\right)^b \quad (5.22)$$

Furthermore, the pressure factor f_p and $C_{B, cooler}$ is expressed by [189]

$$f_p = 0.9803 + 0.018 \frac{p}{100} + 0.0017 \left(\frac{p}{100}\right)^2 \quad (5.23)$$

$$C_{B, coolers} = e^{(11.0545 - 0.9228 \ln(A_{coolers}) + 0.08961 (\ln(A_{coolers}))^2)} \quad (5.24)$$

Taking all factors and the UA data from the coolers, the costs were calculated and summarized in Table 5.8 below. The values for U are adopted from the literature [190].

Table 5.8 – Cost estimation of coolers

Component ID	UA	U	A	C _{PE} (2012)
	[kW/K]	[W/m ² K]	[m ²]	[10 ⁶ US\$]
PROPCOL	12210.63	1200	10176	3.70
MR-COL2	1534.56	500	3069	1.00
MR-COL3	1985.99	500	3972	1.49

5.3.4. Vapor-Liquid Separators

In exergy analysis, the separators are considered to have negligible effects to the irreversibilities of the system. Regardless, they are physical components that need to be purchased and installed. The cost estimation is based on the volume requirement of the vessels, which was calculated from the volumetric flow rate of incoming streams, and its weight, based on the material density and pressure specification [89,189]

$$C_{PE,separator} = f_M C_{V,separator} + C_{PL,separator} \quad (5.25)$$

Where C_V is the purchased cost of hollow vessels and C_{PL} is the additional equipment such as heads, manholes, safety valves, etc. These variables are calculated by

$$C_{V,separator} = e^{(6.775 - 0.18255 \ln(Wt) + 0.02297(\ln(Wt))^2)} \quad (5.26)$$

$$C_{PL,separator} = 237.1(D)^{0.63316}(L)^{0.80161} \quad (5.27)$$

Where Wt , D , and L is the weight, diameter and length of the vessel, respectively. The weight of the vessel or tower depends on the wall thickness of the shell and the two heads. For cost estimation purposes it is sufficient to assume shell thickness equal to the head thickness [89].

$$Wt = \pi t_s \rho (D + t_s)(L + 0.8D) \quad (5.28)$$

where the term ρ is the density of the carbon steel and t_s is the shell thickness. The term t_s refers to the shell thickness, which is calculated from the empirical relationships of the vessel

diameter D , design pressure p_D , maximum allowable stress of the shell material at the design temperature S and fractional welding efficiency E [189].

$$t_s = \frac{p_d D}{2SE - 1.2p_D} \quad (5.295)$$

The holdup time is assumed to be 2 minutes. Additionally, the components are assumed to be made of carbon steel, which gives the value of $f_M = 1.2$. Table 5.9 summarizes the cost calculation with $\rho = 0.28$ lb/in³, $E=0.85$, $S=15000$ psi for propane vessels and 16000 psi for MR vessels. The cost estimation is based on year 2000, therefore the CEPCI value is equal to the cost index of compressors and coolers.

Table 5.9 – Cost estimation of vapor-liquid separators

Component ID	Q	V	D	L	t _s	W	C _V (2000)	C _{PL} (2000)	C _{PE} (2012)
	[m ³ /s]	[m ³]	[m]	[m]	[in]	[kg]	[10 ⁶ US\$]		
PF1	30329	1011	6.9	27.4	1.4	203.0	0.46	0.06	0.91
PF2	34228	1141	7.1	28.5	1.1	165.7	0.39	0.07	0.80
PF3	92107	3070	9.9	39.7	0.8	229.0	0.51	0.11	1.06
MRFL	7006	234	4.2	16.8	4.4	242.2	0.53	0.03	0.99

5.3.5. J-T Valves

By extracting the information of the mass flow rate from the related streams, the cost of J-T valves can be estimated. PEC was also calculated using the six-tenths rule, while the reference costs are taken from personal interviews, where PEC_{ref} is assumed to be 20,000 US\$, and the sizing exponent is 0.67 [89]. Additionally, the module and pressure factors are assumed to be negligible.

5.4. Economic Analysis

Along with the thermodynamic evaluation, the economic analysis is the cornerstone for the assessment of energy systems. The calculation of plant economics is based on the TRR method [67] which is initialized with the calculation of PEC. In the subsequent sections,

elements of TRR estimation which include the PEC, fuel costs, operation, and maintenance (O&M) costs will be discussed. Ultimately, the levelized carrying charges can be calculated using the levelized TRR estimation. All costs except fuel costs and the values of by-products are assumed to change annually with a constant average inflation rate (r_i), neglecting the real escalation rate. The reason that the fuel costs are excluded from this approach is that the increase in fuel costs are expected to be faster than the predicted constant inflation in the coming years [67,89]. The general assumptions for the economic parameters are summarized in Table 5.11. The cost of fuel (the work supplied to the LNG compressors) is based on the electricity price for industrial purposes in Malaysia [89], with the plant operational lifetime is assumed to be 20 years at 85% average capacity factor.

Table 5.10 – Cost estimation of J-T valves ($\alpha = 0.67$)

Component ID	m [kg/s]	C _{PE} (2012) Million US\$
PROP-TV1	81.10	0.24
PROP-TV2	222.92	0.47
PROP-TV3	322.79	0.60
PROP-TV4	442.70	0.75
MR-TV1	218.27	0.46
MR-TV2	83.58	0.24
NGTV	83.29	0.24

5.4.1. Fixed Capital Investment (FCI)

The FCI can be subdivided into direct costs, which are related to the equipment procurement and installation of the LNG plant, and indirect costs, which are related to the construction costs and engineering services. The cost structure of these items is fundamentally based on the PEC calculations. Several additional assumptions that were considered for the FCI are [67,89]:

1. PEC installation cost represents the expenses that are related to the freight, insurance during the transportation from where the equipment was produced, the

labor, unloading, handling, foundations, supports and all other costs which are relevant for the erection and the connections of the equipment. The average value of 45% may be used if any other information is not provided.

2. Piping costs covers the material and labor expenses for the construction of the entire piping network. The cost was assumed 35% of the total PEC.
3. Instrumentation and control costs are fundamentally an integral part of the system. The value assumed for this cost item is 20% of the total PEC.
4. Electrical equipment and materials costs were assumed to be 20% of the total PEC.
5. Offsite costs such as land cost, civil and structural, and service facilities work were neglected since the cost items depend on where the LNG plant is going to be located.
6. Engineering and supervision are indirect costs that occurred during plant construction. The value is assumed to be 35% of the total PEC.
7. Construction costs are assumed to be 15% of the direct costs, while contingencies are assumed to be 10% of FCI costs. The contingency accounts for work stoppages, weather uncertainties, sudden price changes, and transportation difficulties.
8. PEC index is based on 2012 CEPCI.

5.4.2. Other Outlays

Three items are defined as the other outlays are Startup costs (SC), working capital (WC) and the allowance for funds used during construction (AFUDC). SC is the expenses related to materials, equipment, and engineering service costs during the startup of the plant before the full operation is commenced. This can be expressed as a sum of the non-escalated overheads, which comprises monthly average fixed operation and maintenance costs (FC O&M), monthly average of variable operation and maintenance costs (VC O&M) calculated at full load, one week of fuel costs at full load operation and a 2 % supplementary cost from the plant facilities investment

$$SC_{2012} = \frac{Fixed_{O\&M,annual} + Var_{O\&M,annual}}{12} + \frac{FC_{annual}}{52} + 2\% (FCI_{2012} - Land Cost) \quad (5.30)$$

WC is the non-escalated fund allocation that is needed for the 2 months of fuel and O&M as well as 3 months of labor expenses with 25% additional contingency before sales revenue is received. It can be expressed as

$$WC_{2012} = \left(\frac{Fuel Cost_{annual}}{6} + \frac{Direct O\&M_{annual}}{4} \right) 1.25 \quad (5.31)$$

Table 5.11 – Parameters and assumptions used in TRR calculation [89]

Parameter (units)	Value
1a. Average general inflation rate (%)	5.0
b. Average nominal escalation rate of all costs except fuel (%)	5.0
c. Average nominal escalation rate of electricity (%)	6.0
2a. Beginning of the design and construction period	Jan.1, 2014
b. Date of commercial operation	Jan.1, 2016
3a. Plant operational lifetime (years)	20
b. Plant operational lifetime for tax purposes (years)	15
4. Plant financing fractions and required returns on capital:	
Type of financing	Common Equity Preferred Stock Debt
Financing fraction (%)	35.0 15.0 50.0
Required annual return (%)	15.0 11.7 10.0
Resulting average cost of money (%)	- - 12.0
5a. Average combined income tax rate (1994-2017) (%)	38
b. Average property tax rate (1994-2017) [% of PFI (in end-2015 dollars)]	1.5
c. Average insurance rate (1994-2017) [% of PFI (in end-2015 dollars)]	0.5
6. Average capacity factor (%)	85
7. Labor positions for operating and maintenance	30
8. Average labor rate (\$/h)	2.24
9. Annual fixed O&M costs at full capacity (10 ⁶ \$)	0.336
10. Annual variable O&M costs at full capacity (10 ⁶ \$)	0.031
11. Unit cost of fuel (MYR/kWh)	0.25
12. Allocation of plant facilities investment to the individual years of design and construction (%)	
Jan.1-Dec.31, 2014	40
Jan.1-Dec.31, 2015	60

The AFUDC represents the time value of money during construction which is based on an interest rate equal to the weighted cost of capital. By considering the construction period of a plant, part of the investment is required to assessment and detailed engineering designs, civil engineering work, purchase and installation of equipment without having any revenue from the plant [89]. The equation is expressed as the sum of all AFUDC within the duration of the construction as mentioned in point 2 in Table 5.11.

$$AFUDC = AFUDC_{ce} + AFUDC_{stock} + AFUDC_{debt} \quad (5.32)$$

Where y is the $AFUDC_{ce}$ is the AFUDC of common equity, $AFUDC_{stock}$ is the AFUDC of preferred stock and $AFUDC_{debt}$ is the AFUDC of debt. These variables are solely based on the plant facilities investment (PFI), which is given by

$$PFI_{2012} = FCI_{2012} - Land\ Cost \quad (5.33)$$

Since the land cost is assumed to be zero, PFI is equal to FCI. Accordingly, 40 % of the PFI should be escalated to the end of 2014 while 60% should be escalated to the end of 2015. The distribution values are based on the plant financing fraction, while the annual escalation rate is assumed to be constant at 5%.

$$PFI_{ce} = 35\% \times ((40\% PFI_{2012})(1 + i_n)^2 + (60\% PFI_{2012})(1 + i_n)^3) \quad (5.34)$$

$$PFI_{stock} = 15\% \times ((40\% PFI_{2012})(1 + i_n)^2 + (60\% PFI_{2012})(1 + i_n)^3) \quad (5.6)$$

$$PFI_{debt} = 50\% \times ((40\% PFI_{2012})(1 + i_n)^2 + (60\% PFI_{2012})(1 + i_n)^3) \quad (5.36)$$

Henceforth, the AFUDC at the end of the construction phase for each financing fraction can be calculated according to its respective required annual return rar_f as mentioned in point 4 in Table 5.11.

$$AFUDC_k = PFI_k \left((1 + rar_f) - 1 \right) \quad (5.37)$$

Where k represents either the common equity, preferred stock or debt. In order to match PEC calculations, the value has to be reverted back to 2012 with the resulting average cost of money at 12% [67,89]. The result of AFUDC calculations is shown in Table 5.12.

$$AFUDC_{k,2012} = AFUDC_k(1 + 12\%)^{-4} \quad (5.38)$$

Table 5.12 – Calculations of AFUDC in a million US\$

Year	US\$ Jan. 01, 2012	Escalated Investment	Common Equity		Preferred Equity		Debt	
			Escalated Investment	AFUDC	Escalated Investment	AFUDC	Escalated Investment	AFUDC
2014	545.609	601.533	210.537	31.581	90.230	10.557	300.767	30.077
2015	818.413	947.415	331.595	0.000	142.112	0.000	473.708	0.000
Subtotal	1364.021	1548.948	542.132	31.581	232.342	10.557	774.474	30.077
Total AFUDC			72.214					
Total AFUDC in 2012			45.893					

Based on the calculations for the FCI and other outlays described above, the total capital investment (TCI) estimation is summarized in Table 5.13. Accordingly, let the total non-depreciable investment (TNI) be defined as

$$TNI_{2012} = Land\ Cost + WC_{2012} + AFUDC_{ce} \quad (5.7)$$

While the total depreciable investment is given by $TDI = TCI - TNI$, which is used as the basis to estimate the total revenue requirement.

5.4.3. Fuel and O&M Costs

As previously mentioned, all compressors are supplied by electric motors; thus the fuel cost considered for the analysis is the electricity supplied to the system. The industrial electricity price for the analysis is assumed at 0.25 MYR/kWh [89], where the LNG plant is assumed to be located. Therefore, considering the capacity factor 85%, the economic life of the plant and the corresponding base case energy consumption, the total fuel costs were calculated in

2011 price at 98.16 million US\$. Since the plant was scheduled to run in 2016 according to its economic analysis parameters, the price has to be escalated with $i_n = 6\%$ growth.

Table 5.13 – Estimation of Total Capital Investment of the base case

Items		Cost in 10 ⁶ \$
I.	Fixed Capital Investment (FCI)	
A.	Direct costs (DC)	
1.	Onsite costs (ONSC)	
	Total purchased equipment cost (PEC)	417.63
	PEC installation (45% of PEC)	191.81
	Piping (35% of PEC)	149.19
	Instrumentation and control (20 % of PEC)	85.25
	Electrical equipment and materials (20% of PEC)	85.25
	Total onsite costs	918.78
2.	Offsite costs (OFSC)	
	Land (10% of PEC)	0
	Civil, structural and architectural work (50% of PEC)	0
	Service facilities (65% of PEC)	0
	Total offsite costs	0
	Total direct costs	918.78
B.	Indirect costs (IC)	
1.	Engineering and supervision (35% of PEC)	146.17
2.	Construction costs (15% of DC)	137.82
3.	Contingencies (10% of IC)	133.64
	Total indirect costs	417.63
	Fixed-capital investment (FCI)	1,336.41
II.	Other Outlays (OO)	
A.	Startup costs	28.65
B.	Working capital	20.50
C.	Cost of licensing, R&D	0.00
D.	Allowance for funds used during construction (AFUDC)	44.96
	Total other outlays	94.11
	Total capital investment (TCI)	1,430.52

Using the following equation, the fuel cost in the first year of operation is

$$FC_{2016} = FC_{2011}(1 + i_n)^5 = 131.36 \text{ million US\$}$$

The cost of operation and maintenance (O&M) is divided into two parts: The fixed costs and variable costs, which are derived from direct O&M costs. The direct costs include

workforce expenses during operation, spare parts and equipment maintenance, the administration and support, as well as the marketing and distribution expenses. The price assumption for the workforce in the analysis is 2.24 US\$/hour in the year of 2009 with an average annual working time of 2080 hours/year [89]. 30 labors are assumed for the operation and maintenance of the plant. The price was then escalated to 2011, at which the construction was assumed to be commenced.

$$Direct\ OMC_{2011} = 2.24 \frac{US\$}{h} \times 2080 \frac{h}{year} \times 30 = 0.154 \text{ million US\$}$$

Subsequently, the fixed O&M costs and the variable O&M costs are estimated. The costs are estimated at 85% capacity factor, which assumed to be 2.18 and 0.2 of the direct O&M costs, respectively.

$$Fixed\ OMC_{2011} = 2.18 \times 0.154 \times 10^6 = 0.286 \text{ million US\$}$$

$$Variable\ OMC_{2011} = 0.2 \times 0.154 \times 10^6 = 0.026 \text{ million US\$}$$

In order to obtain the O&M costs for the first year of the operation, the calculation above also needs to be escalated with a nominal escalation rate of 5 % per year to the year 2016.

$$Fixed\ OMC_{2016} = Fixed\ O\&M_{2011}(1 + i_n)^5 = 0.364 \text{ million US\$}$$

$$Variable\ OMC_{2016} = Variable\ O\&M_{2011}(1 + i_n)^5 = 0.033 \text{ million US\$}$$

5.4.4. Estimation of TRR

The estimation of TRR was carried out according to the method discussed in section 4.2.4. In summary, TRR is the sum of the eight annual amounts: total capital recovery (TCR); minimum return on investment (ROI) for common equity (ce), preferred stock (ps) and debt (d); income taxes (ITX); other taxes and insurance (OTXI); fuel costs (FC); and operating and maintenance costs (O&M). The values are summarized in Table 5.14, with further details on the methods to calculate TCR and ROI are explained The Levelized Costs of Fuel, O&M and TRR in [67].

The levelized fuel costs (FC_L) are calculated with the aid of the equation 3.25 to 3.29 in order to obtain the constant escalation levelization factor (CEL_F), with the average cost of money (i_{eff}) is assumed to be 12%. Note that for the fuel costs, the nominal escalation rate r_n is 6%.

$$k_F = \frac{1+0.06}{1+0.012} = 0.946$$

$$CRF = \frac{0.12(1+0.12)^{20}}{(1+0.12)^{20}-1} = 0.134$$

$$FC_L = \frac{131.36 \times 10^6}{1.06} \times \frac{(1-0.946^{20})(0.134)}{(1-0.946)} = 190.145 \text{ million US\$}$$

Likewise, the levelized annual operating and maintenance costs (OMC_L) are estimated using the same equations, with the nominal escalation rate r_n of 5%. Therefore,

$$k_F = \frac{1+0.05}{1+0.012} = 0.9375$$

$$OMC_L = 0.538 \text{ million US\$}$$

The expenses of plant O&M, fuel costs, and the carrying charges are levelized in order to obtain the net present value over the plant economic life. The TRR is calculated with the annual escalated amount of its elements, which are presented in Table 5.14. Based on the year-by-year analysis results, the levelized TRR (TRR_L) is estimated using equation 3.30 with the operational time of 20 years. Therefore, the TRR_L base case can be calculated using the constant dollar value

$$TRR_L = CRF \times \sum_{y=1}^N TRR_{y,const.dollar} = 0.134 \times 3408.38 = 456.31 \text{ million US\$}$$

By referring to Equation 3.26 the levelized carrying charges of the plant was calculated using the relationship of the levelized TRR, fuel cost and O&M costs. CC_L is estimated at 265.627 million US\$.

Table 5.14 – Year-by-year revenue requirement analysis in a million US\$

The Calendar Year	(1) Capital Recovery	(2) Return on Common Equity	(3) Preferred Stock Dividends	(4) Interest on Debt	(5) Income Taxes	(6) Other Taxes and Insurance	(7) Fuel Cost	(8) O&M Cost	(9) TRR _y in current \$	(9) TRR _y in constant \$
2016	72.271	75.102	25.106	71.526	63.586	32.488	131.364	0.398	471.841	421.3
2017	95.778	71.236	23.850	67.950	36.940	32.488	139.246	0.418	467.905	373.0
2018	90.815	66.135	22.183	63.198	37.754	32.488	147.601	0.439	460.612	327.9
2019	86.375	61.294	20.602	58.695	38.258	32.488	156.457	0.461	454.629	288.9
2020	82.353	56.687	19.099	54.413	38.536	32.488	165.844	0.484	449.903	255.3
2021	78.696	52.291	17.667	50.333	38.620	32.488	175.795	0.508	446.397	226.2
2022	76.972	48.087	16.299	46.435	36.929	32.488	186.342	0.533	444.085	200.9
2023	76.972	43.973	14.961	42.624	33.588	32.488	197.523	0.560	442.689	178.8
2024	77.024	39.859	13.623	38.812	30.194	32.488	209.374	0.588	441.964	159.4
2025	76.972	35.743	12.284	34.998	26.903	32.488	221.937	0.617	441.943	142.3
2026	77.024	31.629	10.947	31.187	23.510	32.488	235.253	0.648	442.686	127.3
2027	76.972	27.513	9.608	27.373	20.218	32.488	249.368	0.681	444.221	114.0
2028	77.024	23.399	8.270	23.562	16.825	32.488	264.330	0.715	446.613	102.4
2029	76.972	19.283	6.931	19.748	13.534	32.488	280.190	0.750	449.896	92.1
2030	77.024	15.169	5.594	15.936	10.140	32.488	297.001	0.788	454.141	83.0
2031	61.562	11.053	4.255	12.122	22.259	32.488	314.821	0.827	459.388	74.9
2032	46.152	7.748	3.188	9.081	34.989	32.488	333.711	0.869	468.226	68.2
2033	46.152	5.253	2.391	6.811	32.971	32.488	353.733	0.912	480.712	62.5
2034	46.152	2.757	1.594	4.541	30.953	32.488	374.957	0.958	494.400	57.4
2035	46.152	0.261	0.797	2.270	28.935	32.488	397.455	1.005	509.365	52.8

5.5. Exergoeconomic Analysis

The first step to exergoeconomic analysis is to use the calculation results of PEC, CC_L, and OMC_L to obtain the cost rate associated with the investment and O&M costs (\dot{Z}_k), as defined in equation 3.34. The calculation results of \dot{Z}_k is summarized in the pie chart illustrated in Figure 5.3. It can be seen that the biggest expenses are incurred by component MHX1, PHX3, PHX2, PHX1 and, MRC3, which constitute 61% of the total investment costs. Components such as compressors and heat exchangers are essentially designed in a multi-stage fashion, therefore it is more reasonable to categorize the sum of the costs of the same component as illustrated in Figure 5.3b. It is shown that 90% of the total \dot{Z}_k are incurred from PHX, MHX, MR compressors (MRC) and precooling compressors (PROPC). The components that are related to MR cycle accounts for 16902 \$/h, while precooling cycle requires 18568 \$/h or 52% from the total investment costs, therefore the proportion in the base case between the two cycles are approximately comparable.

Subsequently, the cost associated with the product and fuel of the component is determined according to the fuel and product rule [87,102] and the cost balance as given by

$$c_{P,k}\dot{E}_{P,k} = c_{F,k}\dot{E}_{F,k} + \dot{Z}_k \quad (5.40)$$

where the exergy of fuel and product of the respective component must be known prior to the exergoeconomic analysis. Initial values for the analysis is also taken based on the following assumptions:

1. The thermal and mechanical average costs of natural gas feed stream according to F rule is given by $c_{NG-1}^T = c_{NG-1}^M = c_{NG,feed}$. The split of the physical exergy streams into its mechanical and thermal parts was also applied in the exergoeconomic analysis, since the process involves streams that cross the ambient temperature.
2. The price of natural gas $c_{NG,feed}$ is assumed at 5.872 \$/GJ, whereas the specific cost of generating power for all compressors is assumed to be taken from the average cost of electricity with $c_W = 23.441$ \$/GJ [89].

3. The cost rate associated with the exergy losses is zero since the only effluent stream of the system (NATGAS-8) is related to the LNG product, whereas the exergy destruction from the dissipative coolers is assigned to the total product cost.

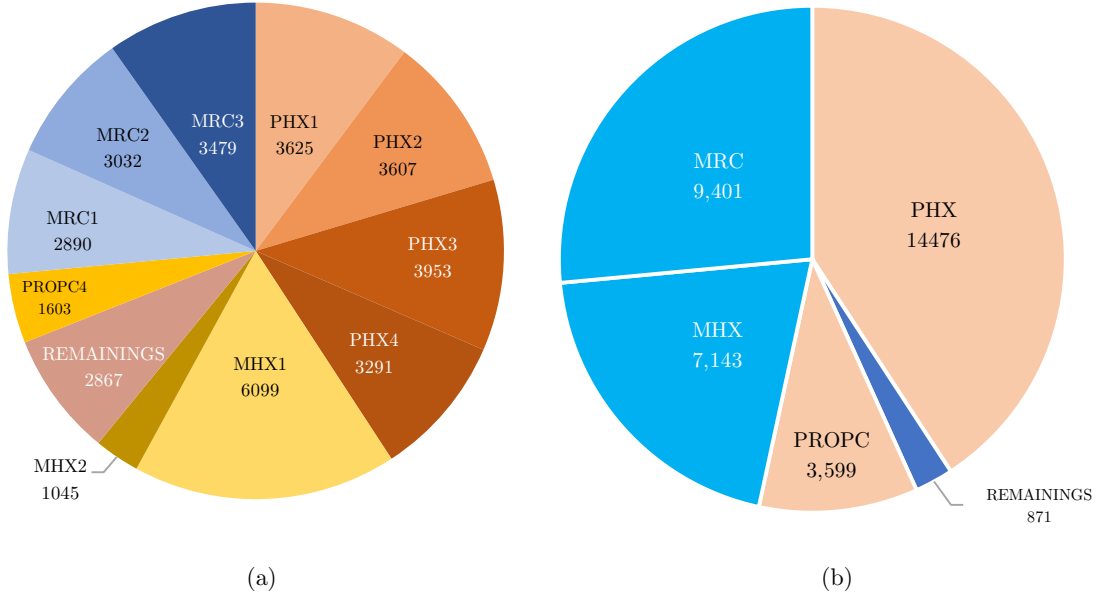


Figure 5.3 – Distribution of \dot{Z}_k at (a) component level and (b) group of components

Since the cost of natural gas is known, there are 99 streams in the system with 97 unknowns (the specific cost of mechanical and thermal exergy streams). The cost balances and the auxiliary equations of all components were listed in Appendix B: Exergoeconomic Balance. Note that the number of equations needs to be equal to the number of unknowns in order to solve the linear equations. The auxiliary equations were also required to solve the set of cost balance equations, through which the cost of each stream was obtained. The important assumptions to formulate the equations were considered [67,89]:

1. The specific costs associated with the inlet and the outlet of an exergy stream is equal to each other when the removal of mechanical exergy occurs in the process via expansion or friction through condensation at a pressure greater than the environment pressure. Thus, $c_e^M = c_i^M$ where the subscripts i and e represent the inlet and outlet state of the stream, respectively.

2. The mechanical and thermal exergies are supplied to the working fluid when vaporization and compression processes occur. Thus, the relationship is given by

$$\frac{\dot{C}_i^T - \dot{C}_i^T}{\dot{E}_i^T - \dot{E}_i^T} = \frac{\dot{C}_e^T - \dot{C}_e^T}{\dot{E}_e^T - \dot{E}_e^T} \quad (5.41)$$

The total cost of fuel and product of the overall system are defined respectively as

$$\dot{C}_{F,tot} = \sum_N c_w W_{comp,n} + c_{NG-1}^M \dot{E}_{NG-1}^M - c_{NG-8}^M \dot{E}_{NG-8}^M \quad (5.42)$$

$$\dot{C}_{P,tot} = c_{NG-8}^T \dot{E}_{NG-8}^T - c_{NG-1}^T \dot{E}_{NG-1}^T + \delta_{dissipative} \quad (5.43)$$

where the pressure difference between inlet and outlet of the feed gas and the work supplied to the compressors are considered as the driving force or fuel of the system. The product is the thermal exergy gained by the natural gas, which resulted in the form of LNG at the outlet of the system. Note that the cost of exergy destruction from coolers $\delta_{dissipative}$ must be assigned to the product of the system since they are dissipative components and therefore have no exergy of fuels nor products.

$$\delta_{dissipative} = \dot{C}_{D,MR-COL2} + \dot{C}_{D,MR-COL3} + \dot{C}_{D,PROPCOL} \quad (5.44)$$

The exergoeconomic analysis is calculated according to the base case inputs from Table 5.15. The output of the analysis is the specific thermal c_j^T and mechanical stream cost c_j^M , the specific cost of fuel $c_{F,k}$ and product $c_{P,k}$ of each component, and most importantly, the total cost fuel $c_{F,tot}$ and product of the system $c_{P,tot}$. The result obtained from the analysis for $c_{F,tot}$ is 17.2 \$/GJ and for $c_{P,tot}$ is 109.4 \$/GJ.

There are no exergy losses from the overall system since it is assumed that the end-flash system is neglected and therefore boil-off management is outside the scope of this study. The exergoeconomic analysis for component level is presented in Table 5.16. The results also provide information regarding the costs incurred as a result of exergy destruction. It is shown that MHX1 and propane cooler (PROPCOL) have the highest cost associated with its exergy destruction, followed by MHX2 and MR aftercooler (MRCOL3). Another useful parameter of the analysis is the term $\dot{C}_{D,k} + \dot{Z}_k$, which define the costs associated with

exergy destruction and investment at the component level. The opportunity for improvement can be seen using this parameter, particularly in order to identify the tradeoffs between exergy efficiency and economics of the system. When the components are grouped into a more general category, PHX have the biggest values of $\dot{C}_D + \dot{Z}$ at 17111 \$/h, followed by the MHX at 16861 \$/h and MR compressors at 12774 \$/h. These components are also the major expenditures in terms of \dot{Z}_k , as can be seen in Figure 5.3. The ratio of $\dot{C}_{D,k} + \dot{Z}_k$ between MR cycle and the precooling cycle is 1.4:1, indicating a more significant role in the MR cycle from the economics perspective.

Table 5.15 – Specific cost associated with thermal and mechanical exergy

Stream ID	m	T	p	c^T	c^M	c^T	c^M
	[kg/s]	[K]	[bar]	[kJ/kg]	[kJ/kg]	[\$/GJ]	[\$/GJ]
MR-1	301.84	305	48.2	0.21	330.55	63.76	76.81
MR-2	301.84	291	46.74	0.62	328.51	5069.35	76.81
MR-3	301.84	279	45.33	4.36	326.45	1494.91	76.81
MR-4	301.84	257	43.96	18.4	324.35	609.69	76.81
MR-5	301.84	240	42.63	35.03	322.24	434.97	76.81
MR-6	83.58	240	42.63	15.24	432.76	434.97	90.75
MR-7	218.27	240	42.63	29.62	274.85	434.97	90.75
MR-8	218.27	146	41.34	171.38	273.55	243.69	90.75
MR-9	83.58	146	41.34	292.26	429.44	215.77	90.75
MR-10	83.58	134	40.09	337.17	426.12	217.06	90.75
MR-11	83.58	118.04	3	602.59	128.26	166.43	90.75
MR-12	83.58	125.98	2.91	437.96	124.67	166.43	90.75
MR-13	218.27	141.34	2.91	344.06	84.67	171.35	90.75
MR-14	301.84	135.13	2.91	377.66	95.8	166.31	90.75
MR-15	301.84	238.57	2.82	11.78	92.96	166.31	90.75
MR-16	301.84	300.95	7.5	0.02	180.4	83	86.99
MR-17	301.84	300.95	7.5	0.02	180.4	83	86.99
MR-18	301.84	361.72	17.5	12.23	253.27	65.8	80.89
MR-19	301.84	305	17.33	0.15	252.46	65.8	80.89
MR-20	301.84	382.27	48.6	23.97	331.1	63.76	76.81
PROP-1	81.1	238.5	1.3	10.71	13.76	79.38	71.66
PROP-2	81.1	265.43	2.5	3.16	49.46	34.88	79.99
PROP-3	141.82	253.91	2.5	5.86	49.46	80	71.66
PROP-4	222.92	258.13	2.5	4.77	49.46	70.93	74.69
PROP-5	222.92	289.34	5.1	0.23	87.19	27.75	72.14
PROP-6	99.87	275.45	5.1	1.56	87.19	80.29	71.66
PROP-7	322.79	285.07	5.1	0.51	87.19	84.47	71.99
PROP-8	322.79	301.12	7.2	0.03	104.61	69.98	71.66

Table 5.16 – Specific cost associated with thermal and mechanical exergy (continued)

Stream ID	m	T	p	e ^T	e ^M	c ^T	c ^M
	[kg/s]	[K]	[bar]	[kJ/kg]	[kJ/kg]	[\$/GJ]	[\$/GJ]
PROP-9	119.91	287.34	7.2	0.36	104.61	81	71.66
PROP-10	442.7	297.41	7.2	0	104.61	5607.32	71.66
PROP-11	442.7	331.52	14.3	19.97	119.52	61.63	70.41
PROP-12	442.7	305	14.3	0.23	119.52	61.63	70.41
PROP-13	442.7	287.34	7.2	12.01	104.61	81	71.66
PROP-14	442.7	287.34	7.2	10.23	104.61	81	71.66
PROP-15	322.79	287.34	7.2	13.9	104.61	81	71.66
PROP-16	322.79	275.45	5.1	30.12	87.19	80.29	71.66
PROP-17	322.79	275.45	5.1	23.11	87.19	80.29	71.66
PROP-18	222.92	275.45	5.1	32.76	87.19	80.29	71.66
PROP-19	222.92	253.91	2.5	67.3	49.46	80	71.66
PROP-20	222.92	253.91	2.5	31.68	49.46	80	71.66
PROP-21	81.1	253.91	2.5	76.83	49.46	80	71.66
PROP-22	81.1	237.14	1.3	110.54	13.76	79.38	71.66
NATGAS-1	158.42	300	65	0.01	548.5	5.31	5.31
NATGAS-2	158.42	291	63.05	0.23	544.86	5069.35	5.31
NATGAS-3	158.42	279	61.16	1.69	541.21	1465.49	5.31
NATGAS-4	158.42	257	59.33	8.59	537.55	557.49	5.31
NATGAS-5	158.42	240	57.55	18.95	533.87	384.81	5.31
NATGAS-6	158.42	146	55.82	303.2	530.17	215.03	5.31
NATGAS-7	158.42	134	54.15	353.31	526.47	216.5	5.31
NATGAS-8	158.42	113.19	1.22	805.6	25.19	98.3	5.31

The main cost contributor to the total system is the sum of the components' investment costs (\dot{Z}_{tot}) with 70.6%, while the cost associated with the exergy destruction $\dot{E}_{D,tot}$ accounts for 13.7%, respectively. It implies that the investment costs of the components play a bigger role in the C3MR process and it has to be minimized, particularly for the heat exchangers, where the investment costs are directly related to the heat exchange area requirement. Reducing the exergy destruction might also a feasible approach to reduce the costs, however, it might be limited to a certain extent. Furthermore, since it is assumed that the C3MR plant operates in a steady state, the value of $\dot{E}_{P,tot}$ is constant. Thus, the cost improvement of the system could only be achieved by optimizing the investment costs and the cost associated with the overall exergy destruction.

Table 5.16 – The results of the exergoeconomic analysis for the base case

Component ID	c_F	c_P	\dot{Z}_k	\dot{C}_D	$\dot{C}_D + \dot{Z}_k$	r_k	f_k
	\$/GJ	\$/GJ	\$/h	\$/h	\$/h	%	%
PHX1	57.8	5069.3	3625	379	4004	8674	91
PHX2	67.1	906.6	3607	509	4115	1250	88
PHX3	75.0	334.8	3953	1033	4986	346	79
PHX4	74.6	241.6	3291	714	4005	224	82
MHX1	164.5	203.7	6099	7888	13987	24	44
MHX2	157.2	225.4	1045	1828	2872	43	36
PROPTV1	71.7	78.0	20	42	62	9	33
PROPTV2	71.7	79.7	40	183	223	11	18
PROPTV3	71.7	79.7	52	100	151	11	34
PROPTV4	61.6	81.0	64	307	371	31	17
MRTV1	90.8	99.6	40	1155	1194	10	3
MRTV2	90.8	102.1	21	886	907	13	2
NGTV	5.3	6.0	21	149	169	12	12
PROPC1	34.9	83.2	366	138	504	139	73
PROPC2	27.7	68.8	917	326	1243	148	74
PROPC3	24.7	70.0	713	205	918	183	78
PROPC4	23.6	61.6	1603	509	2112	161	76
MRC1	37.0	83.0	2890	1485	4375	125	66
MRC2	23.4	65.8	3032	880	3912	181	78
MRC3	23.4	63.7	3479	1008	4487	172	78
PROPMIX1	119.6	141.7	0	10	10	18	0
PROPMIX2	78.3	131.2	0	12	12	68	0
PROPMIX3	57.9	5607.3	0	11	11	9577	0
MRMIX	2.2	2.2	0	13	13	0	0
MRFL	0.9	0.9	84	0	84	0	100
MRCOL2	161.1		86	1020	1106	0	8
MRCOL3	38.6		127	1819	1947	0	7
PROPCOL	57.8		316	2256	2572	0	12
SYSTEM	17.2	109.3	35491	6886	42376	538	84

6. Single-Objective Optimization of C3MR

6.1. Optimization Workflow

The optimization was conducted by connecting the Aspen Plus process simulator as an ActiveX object with Microsoft Excel Visual Basic for Application (VBA), where it serves as the module for exergy analysis and the main data worksheet. Optimization module GA is programmed in programming language Python, which also acts as the main controller of the optimization procedure. The result of the exergy analyses was brought to Python where GA procedure was carried out in a specified number of iterations. Figure 6.1 illustrates the GA optimization procedure implemented for the C3MR process.

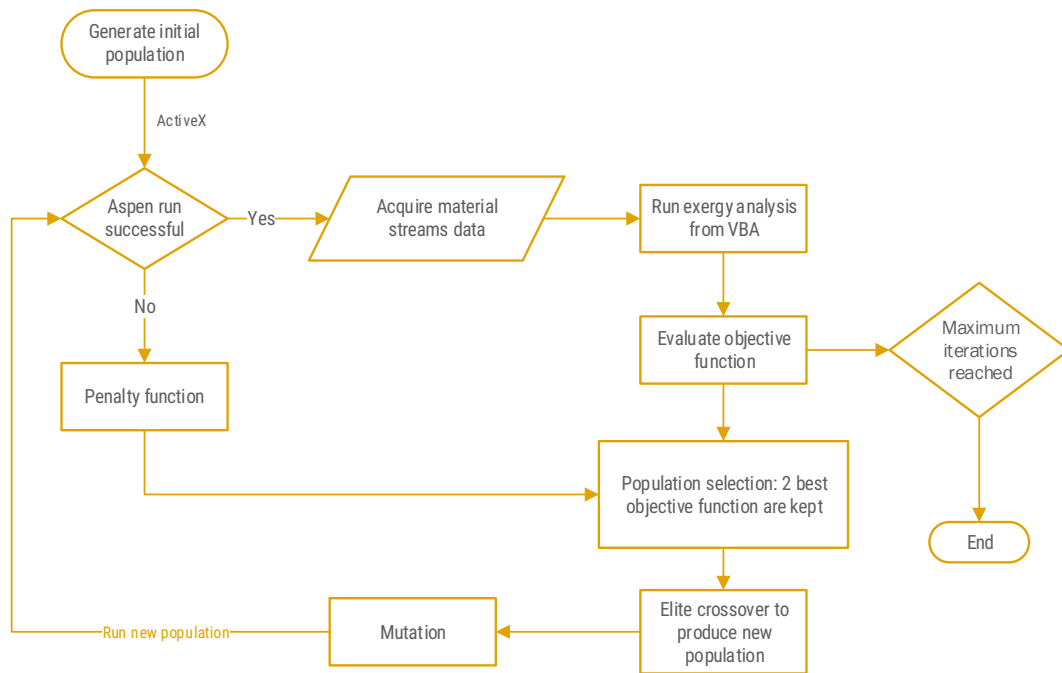


Figure 6.1 – Optimization workflow of GA using Python, VBA and Aspen Plus

As discussed previously in section 5.2.1, each GA iteration (population) consists of a number of individuals that contain unique design variables. The population size can be adjusted according to user preference and the complexity of the problem. A large number means more diversification but resulted in a slow computational time, whereas a small population size can limit the effectiveness of the algorithm. The optimization procedure starts with

Python that generates a random set of individuals and the initialization of Aspen Plus and Excel VBA to conduct the simulations and the exergy analyses. The simulation results are subsequently fed back to the main workflow to provide the information for GA regarding the objective functions. Due to the process constraints, each simulation would have unsuccessful individuals, meaning that the design variables are not converged in the process simulation. It can occur due to process feasibility reasons, such as temperature crossovers in the heat exchangers or when a fraction of liquid from the working fluid entering the compressors. These objective functions of these individuals are translated into the penalty function, which assigns them to undesirable values, e.g., a very low exergy efficiency so that they are to be eliminated in the succeeding iterations. On the other hand, the successful simulations are proceeded with exergy analysis to obtain their corresponding objective functions. In this case, an elitist strategy is imposed to retain four of the best objective functions for the next iteration. These individuals are not to be mutated until better individuals are found to ensure the intensification of the current best result. Furthermore, new offspring for the subsequent iteration is generated with crossover procedure, followed by random mutations are performed to create diversity in the variable space. This step is critical to avoid local minima and keeping the exploration principle of metaheuristics. The iteration loop continues until the specified number of iterations are reached.

6.2. Maximizing the Exergy Efficiency

6.2.1. Optimization of Mixed Refrigerant Cycle (OF1 and OF2)

Based on the base case result of the exergy analysis discussed in section 5.2, it was revealed that more than 62% of the overall exergy destructions are generated from MR-related components. The biggest irreversibilities come from MHX1 due to a finite temperature difference between the cold and hot streams involved. It is also clear that the exergy destructions from MR compression stage (MR-C1, MR-C2, and MR-C3) and their intercooling components (MRCOL-2 and MRCOL-3) can be minimized by reducing the mass flow rate of the MR. The throttling valve of natural gas (NGTV) is also responsible for about 7% of the overall exergy destructions. However, the NGTV pressure outlet is kept

constant at 1.2 bar due to the specification of the LNG storage. Hence, the design variables were selected according to the exergy analysis result of the base case.

In this section, optimizations are accomplished through two different approaches to compare the optimization performance:

1. OF1: To maximize the exergy efficiency, denoted by ε , by exclusively changing the MR stream properties. Therefore, 6 design variables were selected for the optimization including the mass fraction of the MR component (methane, ethane propane, isobutane, nitrogen) and the total mass flow rate of MR.
2. OF2: to maximize ε by changing all design variables that are corresponded with the MR cycle. These include MR composition, mass flow rate, pressure outlet of the throttling valves and the condensing pressure of MR. In total, 9 variables were selected in this objective function.

The objective function is defined as

$$\varepsilon_{tot} = \frac{\dot{E}_{P,tot}}{\dot{E}_{F,tot}} \quad (6.1)$$

where,

$$\dot{E}_{F,tot} = \sum_N \dot{W}_{comp,n} + \dot{E}_{NG-1}^M - \dot{E}_{NG-8}^M \quad (6.2)$$

$$\dot{E}_{P,tot} = \dot{E}_{NG-8}^T - \dot{E}_{NG-1}^T \quad (6.3)$$

GA is implemented in continuous variables with each of the iteration comprises 64 individuals. The other important parameters for the optimization are summarized in Table 6.1, and the lower- and upper bounds are specified in Table 6.2.

The crossover operator takes the previous generation as parents to produce new individuals, which are selected using the tournament selection. All individuals are randomly chosen and finally selected according to their objective functions. Individuals with better objective functions will be likely to be selected as parents. Subsequently, the offspring are generated using the following equations:

$$o_{1,k} = p_k^m - \beta(p_k^m - p_k^d) \quad (6.4)$$

$$o_{2,k} = p_k^d - \beta(p_k^m - p_k^d) \quad (6.8)$$

where $o_{i,k+1}$ is the i^{th} offspring, p_k^m and p_k^d are the selected parents from the k th generation and β is the random number from 0 to 1. The equation ensures the intensification principle, where the current best generation will likely to be selected and its property are to be inherited to the offspring.

Table 6.1 – Genetic algorithm parameters for the optimization

Parameter	OF1	OF2
Design variables	6	9
Number of iterations	100	100
Crossover points	3	5
Population size	64	64
Mutation rate	25%	25%

Furthermore, the mutation rate was set to 25% of the total number of variables to maintain the diversity of population selection without jumping too far from the elite individuals. Therefore,

$$N_{\text{mutated variables}} = \text{Mutation Rate} \times N_{\text{population}} \times N_{\text{design variables}} \quad (6.6)$$

Binary tournament selection was adopted as the crossover method since it is proven to be a robust GA approach to generate better offspring [149]. Individuals are randomly selected to compete head-to-head with the other individuals where parents are finally chosen based on their objective values. There were 30 crossovers in every iteration; each produced 2 new offspring to replace the low-ranked individuals. Furthermore, the lower and the upper bound of the design variables are set to $\pm 75\%$ from their base case, and the number of iterations is set to 100. The rest of the variables are retained as its base case according to Table 5.1.

Since the natural gas flow rate, pressure drops and the liquefaction temperature are kept constant; the exergy efficiency can only be maximized by reducing the exergy of fuel. This can be accomplished by reducing the flow rate of the working fluids, thus cutting the energy consumption of the compressors. The optimization of OF1 and OF2 resulted in the total energy consumption of 133.4 MW and 126.2 MW, respectively. This means that there is an

improvement of at least 15% from the base case scenario. Likewise, the specific power consumption of the system was reduced from 986 kJ/kg_{LNG} to 842 kJ/kg_{LNG} for OF1, and to 797 kJ/kg_{LNG} for OF2. The optimized scenario shows that OF1 has 59.0 % of exergy efficiency, while OF2 reached a slightly better efficiency at 61%. The new variables have improved the efficiency by more than 6% compared to the base case.

Table 6.2 – The lower and upper bound of the design variables for OF1 and OF2

Parameter	Unit	Aspen ID	Base case	LB	UB
Methane mass flow rate	kg/s	MR-1	74.83	18.71	130.95
Ethane mass flow rate	kg/s	MR-1	100.33	25.08	175.57
Propane mass flow rate	kg/s	MR-1	104.81	26.20	183.41
Isobutane mass flow rate	kg/s	MR-1	0	0.00	0.18
N-butane mass flow rate	kg/s	MR-1	0	0.00	0.18
Nitrogen mass flow rate	kg/s	MR-1	21.88	5.47	38.29
MR condensing pressure*	bar	MR-C3	48.6	12.15	85.05
Pressure outlet throttling valve 1*	bar	MRTV1	2.91	1.03	5.09
Pressure outlet throttling valve 2*	bar	MRTV2	3.00	1.12	5.25

*For OF1 these variables were kept at their base case values.

The results from exergy analysis indicate that the exergy destruction of MRC is 9% less than OF1, whereas from MR-TV1 and MR-TV2 combined it is almost 42 % smaller. The exergy destruction of MHX was also reduced from 16.5 MW in the base case to 2.7 MW in OF2 case, respectively. The total exergy destruction of the base case, OF1 and OF2 is equal to 111.5 MW, 88.6 MW, and 81.5 MW, respectively. By referring to Figure 6.2, it is shown that OF2 has the best result, which is particularly evident in MHX and MRC. The exergy efficiency of MHX is upgraded by more than 10% compared to its base case. Although MR compressors do not exhibit an improvement in exergy efficiency, the exergy destructions are still substantially reduced from 33.5 MW to 28.1 MW for OF1 and 25.5 for OF2. Since less MR mass flow rate required after the optimizations, the coolers, represented by MRCOL, were also improved. The reduction in exergy destructions has been essential in optimizing the exergy efficiency of the system since these components were initially contributed to the total exergy destructions by more than 60%. Furthermore, the progression of GA iterations is illustrated in Figure 6.3, where it can be seen that OF2 resulted in a better efficiency than OF1 by using more design variables.

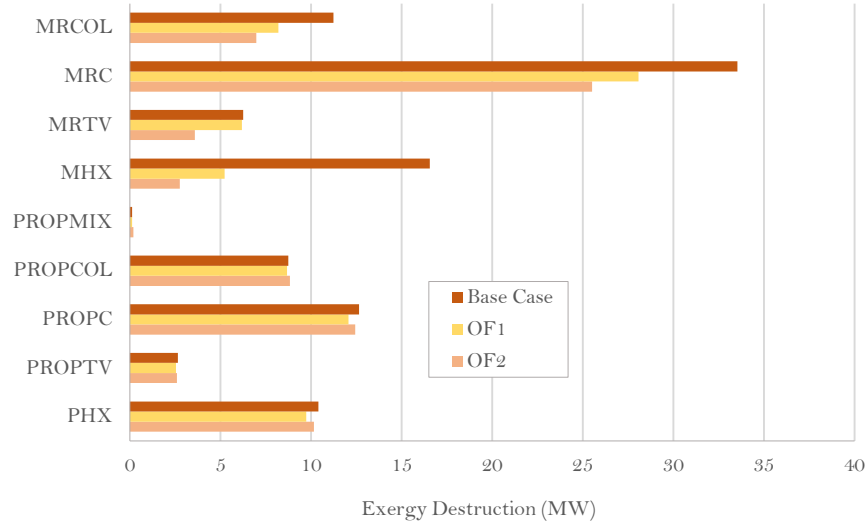


Figure 6.2 – Exergy destruction comparison between the base case, OF1, and OF2

Figure 6.2 shows that the most significant improvement is achieved by MHX, where exergy destructions are minimized from 16.5 MW to 5.7 MW and 2.7 MW for OF1 and OF2, respectively. The improvement is best illustrated in Figure 6.4 with a temperature-enthalpy (T-Q) diagram. The left side of the diagram represents the T-Q curve of MHX1, while the right side represents the T-Q curve of MHX2. It is shown that for the curve in the base case, there are still gaps between the hot and cold streams, indicating opportunities for improvements. The total cumulative duty in MHX1 is significantly higher than MHX2, meaning that even a small improvement that occurred in MHX1 would make a significant impact on the system. The minimum temperature of MHX1 for the OF1 and OF2 are 0.1 K and 1.5 K, respectively, while for the base case the value it was 1.5 K.

The solutions for the design variables are presented in Table 6.3. OF2 was able to find a lower condensing pressure and a higher outlet pressure for the MR throttling valves, therefore conserving more energy consumption than in OF1 case. Nonetheless, OF1 also revealed that the system could be significantly improved by only modifying MR composition and the mass flow rate. OF2 has a distinct advantage since more design variables were taken into account, with the throttling valve outlet pressure and MR condensing pressure were included. The outlet pressure of the throttling valves is slightly higher in OF2, which resulted in less mechanical exergy destructions. OF2 allows the system to have a lower MR

condensing pressure at 44.8 bar, since it has more propane and less ethane composition in the mixture compared to OF1. At 300 K, the vapor pressure of propane is around 10 bar, whereas for ethane it is around 43.5 bar [191]. OF1 was able to reduce the total MR flow rate by to 282.7 kg/s, whereas OF2 requires even less at 275.2 kg/s, implying a lower energy consumption by 6.4% than the base case.

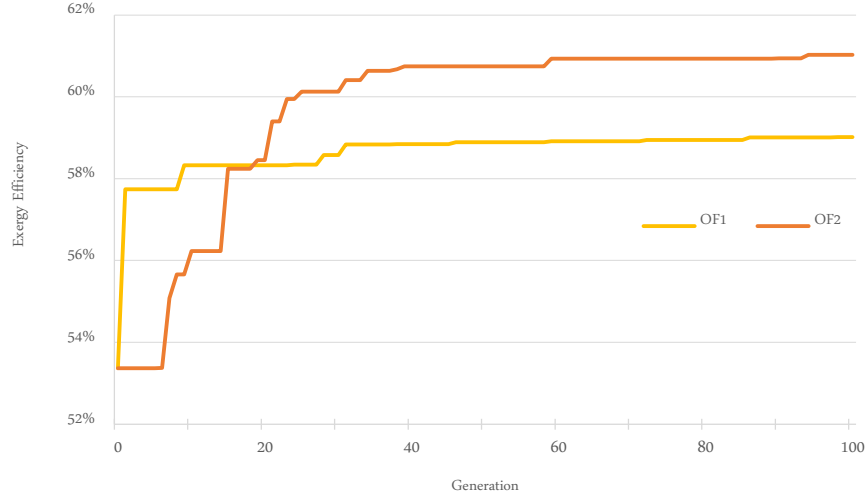


Figure 6.3 – Progress of the exergy efficiency optimization with OF1 and OF2

Table 6.3 – The solutions for design variables of OF1 and OF2

Variables	Aspen ID	Unit	OF1	OF2
MR Compressor outlet pressure	MR-C3	bar	48.6	44.8
MR flow rate	MR-1	kg/s	282.7	275.2
MR composition				
Methane	MR-1	mass fraction	0.12	0.25
Ethane	MR-1	mass fraction	0.50	0.35
Propane	MR-1	mass fraction	0.28	0.39
Isobutane	MR-1	mass fraction	0.00	0.00
n-Butane	MR-1	mass fraction	0.00	0.00
Nitrogen	MR-1	mass fraction	0.09	0.01
MRTV1 pressure outlet	MRTV-1	bar	2.9	3.9
MRTV2 pressure outlet	MRTV-2	bar	3.0	4.0

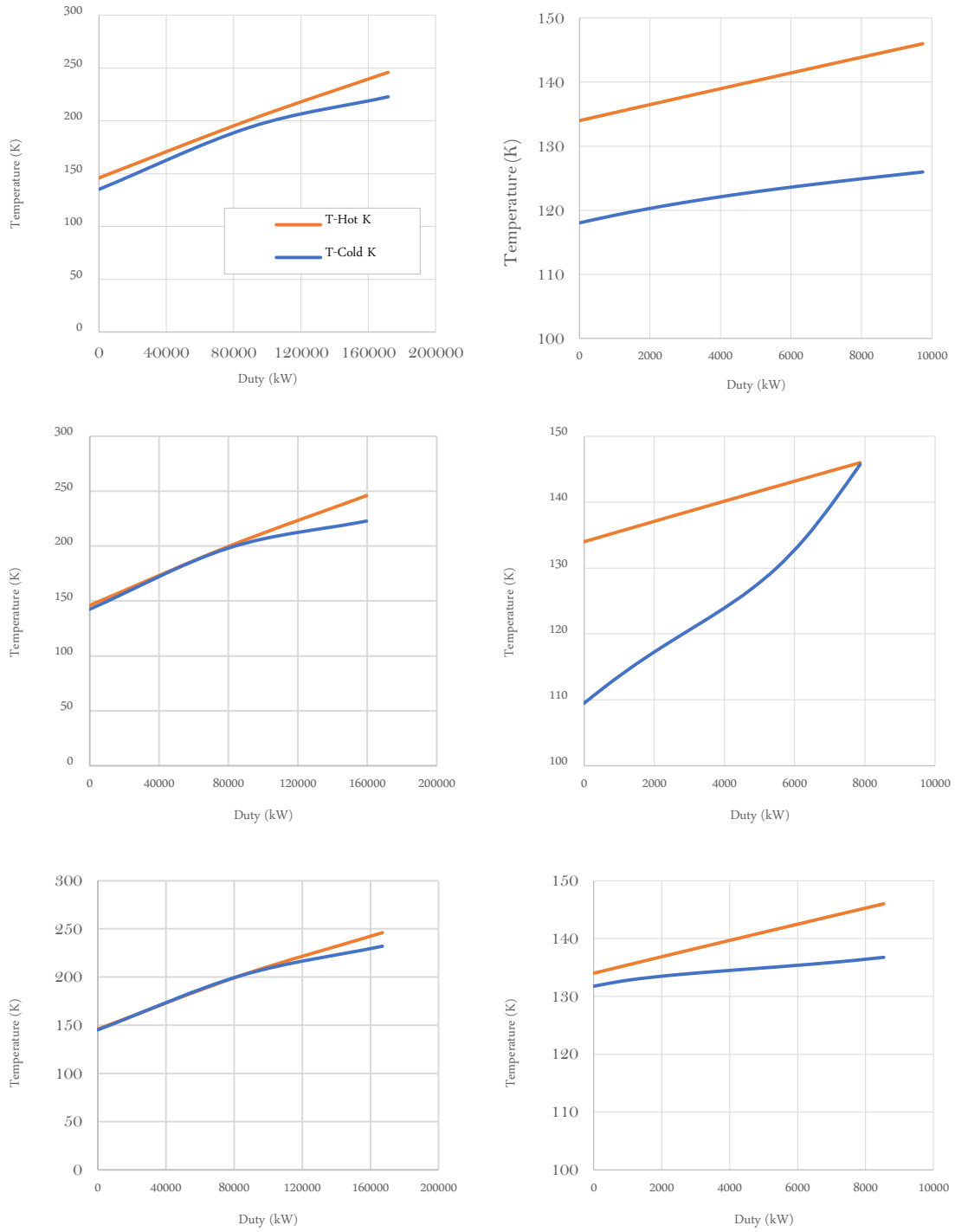


Figure 6.4 – T-Q diagram of MHX1 and MHX2 of base case (top), OF1 (middle) and OF2 (bottom)

6.2.2. Optimization of Precooling Cycle (OF3)

The previous optimization found that the maximum exergy efficiency was achieved using the solution of OF2. The optimization in this section is therefore called OF3. In this section, the pre-cooling cycle was optimized using the same approach by choosing the design

variables from precooling-related components. The difference is that, instead of the base case, the initial condition was adopted from the solutions of OF2. The variables include propane mass flow rate, the pressure outlet of all precooling compressors (PROP-C1, PROP-C2, PROP-C3, PROP-C4) and the pressure outlet of the last throttling valve (PROP-TV1), with the lower- and upper bounds are summarized in Table 6.4.

Table 6.4 – Lower and upper bound of the design variables for OF3

Parameter	Aspen ID	Base case	LB	UB	Unit
Precooling mass flow rate	PROP-12	442.7	110.7	774.7	kg/s
Pressure outlet precooling compressor 1	PROP-C1	2.5	1.5	4.4	bar
Pressure outlet precooling compressor 2	PROP-C2	5.1	2	8.9	bar
Pressure outlet precooling compressor 3	PROP-C3	7.2	2.5	12.6	bar
Pressure outlet precooling compressor 4	PROP-C4	14.3	10.7	25.0	bar
Pressure outlet throttling valve 1	PROP-TV1	1.30	1.03	2.28	bar

The pressure outlet of the other throttling valves (PROP-TV2, PROP-TV3, PROP-TV4) was not selected since the values are equivalent to pressure outlet of the precooling compressors, at which the streams are recycled to their respective compression stage. Note that only variables that are related to precooling cycle were selected for crossovers and mutation, while the rest of the variables are kept constant according to the optimized solution from OF2. Moreover, the optimization was performed in using the same GA parameters as in the previous optimizations.

OF3 was able to improve the exergy efficiency of the system compared to the previous optimizations since the MR cycle are already optimized in its initial condition. It has increased the exergy efficiency of the system to 63.9%, slightly better than OF2. This result implies that the MR cycle plays a more significant role in the exergetic performance of the system since more exergy destructions were reduced in the OF2 case. The impact is illustrated in Figure 6.5, where it is shown that the biggest improvement was achieved during OF2 optimization, particularly to MHX and MRC. In the base case, 34.6 MW of exergy destructions come from the pre-cooling cycle, in which the precooling compressors (PROPC) and precooling heat exchangers (PHX) being the largest contributors. OF3 result shows that the exergy destructions were reduced to 24.8 MW, with PROPC and PHX were

improved by 20% and 14%, respectively, with respect to OF2. According to the current results, MR compressors are still the major contributor with 25.5 MW or 35.3% from the total exergy destruction of the system.

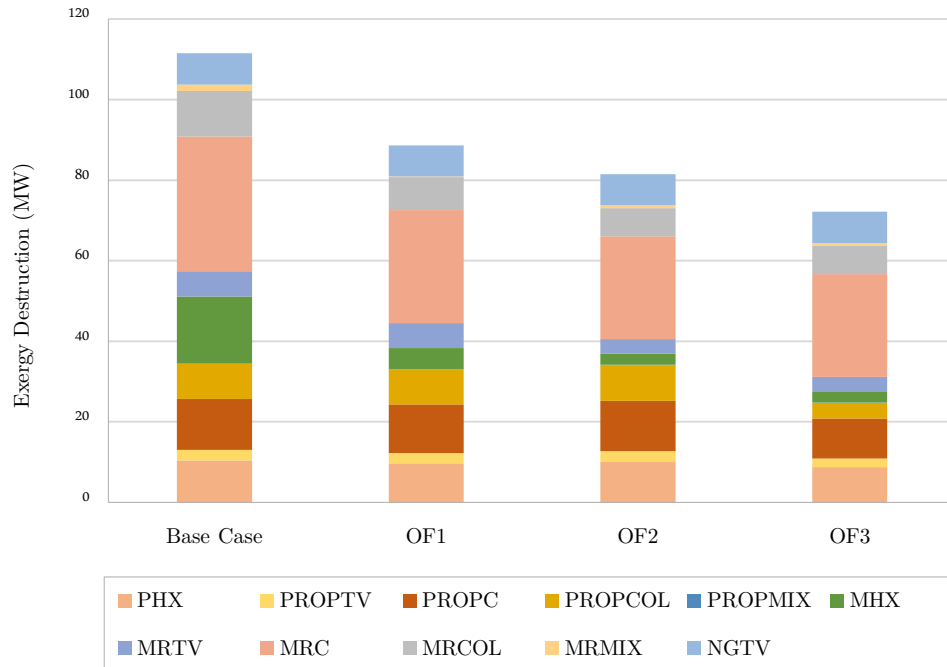


Figure 6.5 – Exergy destruction for the base case, OF1, OF2, and OF3

6.2.3. Conventional GA Optimization (OF4)

In the previous section, the systematic approach to C3MR optimization has been successfully demonstrated using the guidance from the exergy analysis. However, GA optimization also allows users to improve any system by selecting all potential design variables and let the stochastic nature to solve the optimization problem. This universal approach is indeed reasonable to select all relevant design variables in hope for the best solutions without any prior knowledge of the system. The purpose of this section is to see whether this approach can produce a better result than the previous optimizations, which were systematically guided by the exergy analysis. In order to create a fair comparison, the optimization OF4 was performed with the same GA parameter as OF3. The GA iterations for OF4 is set to 200, which is equal to the total number of iterations in OF2 and OF3

combined. All design variables from OF2 and OF3 were included in OF4 with the same lower and upper bounds.

Figure 6.6 illustrates the GA progression of OF4 and the combination of OF2 and OF3. The results clearly show that the simultaneous approach resulted in a slower optimization performance than the systematic one. The exergy efficiency of OF4 at 200th iterations was found at 60.7%, whereas OF2 and OF3 combined optimized the exergy efficiency to 63.9%. During the first 50 iterations, it can be seen that OF4 was struggling to find a better solution since the random combination of design variables were mostly violating the system constraints and therefore, most individuals during the early iterations are thermodynamically infeasible. Conversely, by taking a systematic approach with OF2 and OF3, it is easier for the system to search and explore new variables within the feasible space. The design variables, in this case, were selected systematically in relation to the exergy analysis and working fluids. In summary, the simultaneous approach does not necessarily provide a convenient way of optimizing a system that involves a high interaction between its components.

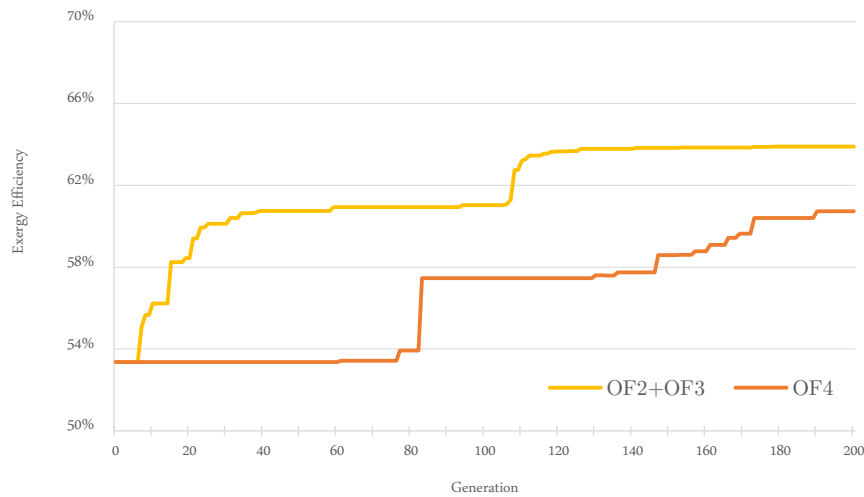


Figure 6.6 – GA progression of OF4 in comparison with OF2 and OF3

The exergy analysis result from OF4 solution is presented in Table 6.5. In this case, almost 60% of the total exergy destruction is caused by three components: MR compressors, precooling heat exchangers and precooling compressors. Since the system was already

optimized, MHX only contributes 6.3% of the total exergy destruction. The result in OF4 shows that the systems' exergy destruction is 10.3 MW greater than OF3. Furthermore, the exergy destruction of OF4 that caused by MR cycle is 45.2 MW, while the same cycle in OF3 generated 39.6 MW. The difference is due to the different MR composition and a lower MR mass flow rate and condensing pressure found in OF3 solutions. Figure 6.7 illustrates the comparison of the exergy destructions between OF3 and OF4, where it is shown that the solution of OF3 is more superior by a certain margin in all components.

Table 6.5 – Exergy analysis of the solution from OF4

Component ID	EF [MW]	EP [MW]	ED [MW]	ε %	y_k %	y^* %
PHX1	2.3	0.2	2.1	9.63%	1.01%	2.57%
PHX2	3.7	1.3	2.4	35.30%	1.16%	2.94%
PHX3	9.1	5.2	3.9	57.10%	1.86%	4.73%
PHX4	9.1	6.6	2.5	72.93%	1.17%	2.97%
MHX1	97.6	93.6	4.0	95.87%	1.92%	4.89%
MHX2	11.4	10.3	1.1	90.10%	0.54%	1.37%
PROP-TV1	2.5	2.4	0.1	94.92%	0.06%	0.15%
PROP-TV2	7	6.5	0.5	92.77%	0.24%	0.61%
PROP-TV3	6.5	6.0	0.5	92.83%	0.22%	0.56%
PROP-TV4	7.9	6.5	1.4	82.39%	0.66%	1.69%
MR-TV1	40.2	36.9	3.3	91.81%	1.57%	3.99%
MR-TV2	13.8	12.8	1.0	92.99%	0.46%	1.17%
NGTV	79.5	71.7	7.8	90.22%	3.70%	9.42%
PROP-C1	3.5	2.5	1.0	72.19%	0.46%	1.16%
PROP-C2	9.7	7.0	2.7	71.93%	1.30%	3.31%
PROP-C3	9.1	6.5	2.6	71.06%	1.25%	3.18%
PROP-C4	17.6	12.6	5.0	71.62%	2.37%	6.03%
MR-C1	23.5	16.8	6.7	71.36%	3.20%	8.15%
MR-C2	29.8	20.6	9.2	69.14%	4.38%	11.15%
MR-C3	40.1	28.9	11.2	72.10%	5.32%	13.54%
PROPMIX1	0.3	0.2	0.1	75.75%	0.03%	0.07%
PROPMIX2	0.2	0.1	0.1	62.05%	0.02%	0.06%
PROPMIX3	0.1	0.0	0.1	5.80%	0.03%	0.09%
MRMIX	79	78.3	0.7	99.13%	0.33%	0.83%
MRCOL-2	1	-	1.0	0.00%	0.46%	1.17%
MRCOL-3	7.1	-	7.1	0.00%	3.36%	8.55%
PROPCOL	4.7	-	4.7	0.00%	2.22%	5.64%
SYSTEM	210.2	127.7	82.5	60.74%	39.26%	100.00%

Likewise, the exergy destruction of OF4 caused by precooling cycle is 29.5 MW, while in OF3 has a lower value at 24.8 MW. The disparity can be analyzed in the design variables presented in Table 6.6, which shows the different MR composition, flow rate and condensing pressure of all working fluids. The pressure difference of the pre-cooling cycle in OF3 is lower than OF4, with addition to the lower propane mass flow rate it requires. The throttling valve outlet pressure in PROP-TV1 is also lower (the last throttling process before entering PHX4 and PROPC-1), conserving the precooling compression works. These variables are related to the throttling pressure of the precooling process, which ultimately determines the exergy efficiency of the pre-cooling heat exchangers. The exergy destruction generated by PHX components in OF4 is 5 MW more than OF3, while PROPC generates 2.2 MW more exergy destructions than the ones from OF3.

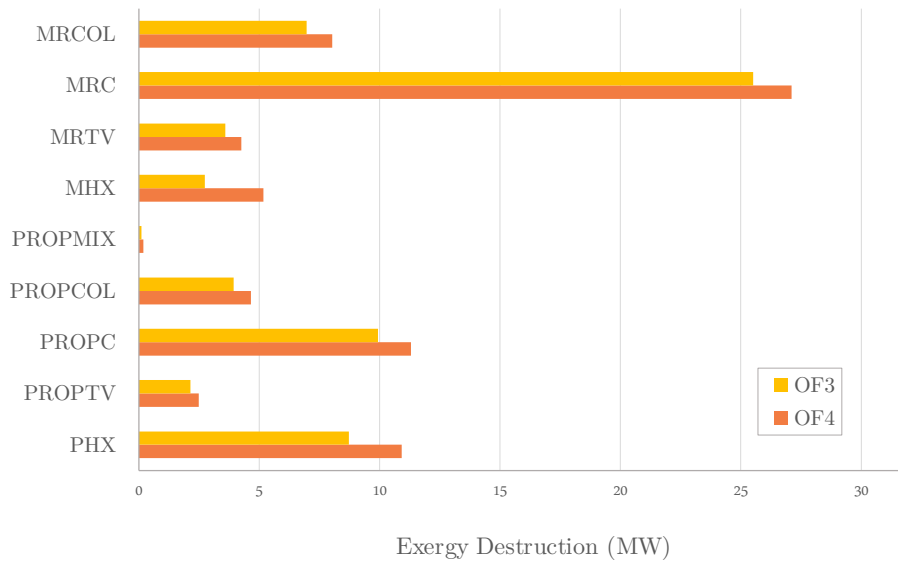


Figure 6.7 – Comparison of exergy destruction between OF3 and OF4

6.3. Minimizing the Total Cost of Product (OF5 and OF6)

In the practical application, it is essential to optimize not only from the thermodynamic perspective but also to minimize the economics of the plant. exergoeconomic analysis already shows that the costs related to the investment, operation, and maintenance can be associated with its components and the process streams. The outcome provides the costs of product and fuel associated with the components as well as the overall system. The optimization

was performed in this section with the basis of exergoeconomics. The goal is to minimize the total cost of product using a similar approach used in the previous sections. A sequential approach (OF5) was conducted by initially restricting the design variables solely to the MR cycle, followed by the optimization of the precooling cycle. Once again to compare the effectiveness of the approach, simultaneous optimization (OF6) was performed by selecting all design variables in both cycles in a single execution. The mutation rate, population size, and other GA parameters were applied according to 6.1, while the total number of iterations was set to 200.

Table 6.6 – The optimized design variables of OF3 and OF4

Variables	Aspen ID	Unit	OF3	OF4
MR Compressor inlet temperature	MR-COL3	K	305.0	305.0
MR Compressor outlet pressure	MR-C3	bar	44.8	48.9
MR flow rate	MR-1	kg/s	275.2	283.8
MR composition				
Methane	MR-1	mass fraction	0.25	0.26
Ethane	MR-1	mass fraction	0.35	0.35
Propane	MR-1	mass fraction	0.39	0.37
Isobutane	MR-1	mass fraction	0.00	0.00
n-Butane	MR-1	mass fraction	0.00	0.00
Nitrogen	MR-1	mass fraction	0.01	0.02
MRTV1 pressure outlet	MRTV-1	bar	3.9	4.1
MRTV2 pressure outlet	MRTV-2	bar	4.0	4.2
Precooling				
Propane flow rate	PROP-12	kg/s	442.7	446.7
Compressor 1 pressure outlet	PROP-C1	bar	2.7	2.4
Compressor 2 pressure outlet	PROP-C2	bar	5.7	4.5
Compressor 3 pressure outlet	PROP-C3	bar	7.9	6.8
Compressor 4 pressure outlet	PROP-C4	bar	11.5	11.8
Throttling valve pressure outlet	PROP-TV1	bar	1.5	1.3

As previously revealed in the exergoeconomic analysis of the base case, the components that have the largest value of $\dot{C}_{D,k} + \dot{Z}_k$ are the main cryogenic heat exchangers, MR compressors and the precooling heat exchangers. Therefore, the main consideration in OF5 was to find the optimized solution in two parts:

1. First, the optimization was focused on MR cycle consisting of the MR composition, mass flow rate, condensing pressure and the appropriate pressure at the outlet of throttling valves.
2. Second, the pre-cooling cycle was optimized by selecting the mass flow rate, condensing pressure of propane and the pressure at the outlet of throttling valves with minimum pressure losses.

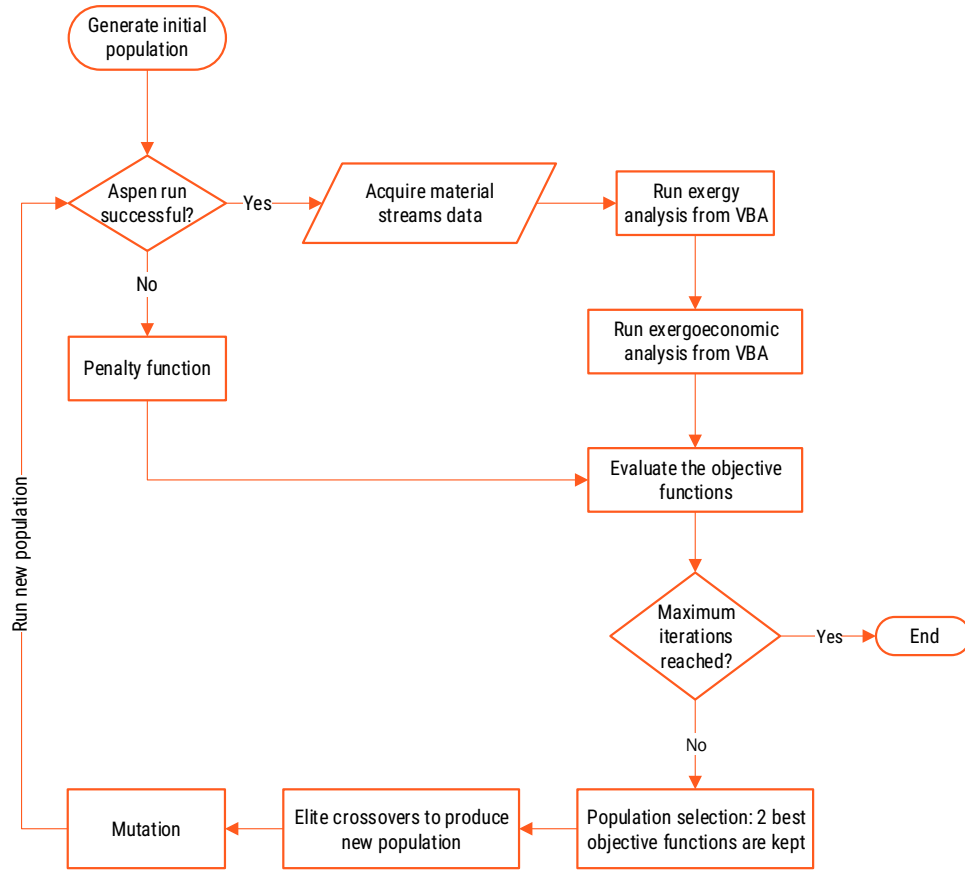


Figure 6.8 – Exergoeconomics optimization workflow

The objective function is defined as

$$c_P \dot{E}_{P,tot} = c_F \dot{E}_{F,tot} + \sum \dot{Z}_k \quad (6.7)$$

where,

$$\dot{C}_{F,tot} = \sum_N c_w \dot{W}_{comp,n} + c_{NG-1}^M \dot{E}_{NG-1}^M - c_{NG-8}^M \dot{E}_{NG-8}^M \quad (6.8)$$

The optimization workflow was implemented according to Figure 6.8. The process is similar to the exergy optimization with an additional exergoeconomic module. After process

simulation and exergy analysis were carried out, PEC calculation and economic analysis were performed using the data from the component variables. This was already explained in section 0 and 5.4. Subsequently, the exergoeconomic analysis was conducted by formulating the exergoeconomic cost balance of all components and solving the equations using the data from exergy and economic analyses.

The results of exergoeconomic optimization are shown in Table 6.7. In the exergy efficiency optimization, the main concern is to minimize the exergy destruction of the system without considering any economic effect. On the contrary, OF5 and OF6 focused on minimizing the total cost of product; therefore the algorithm focused on finding the best solution to save the costs. The results of the base case and OF3 are also presented here for the sake of comparison. OF3 is chosen since it was the best optimization result from the exergy efficiency point of view. Hence the effect of the exergy efficiency to the costs can also be identified.

Table 6.7 – Overview of the exergy and exergoeconomic optimization results

	Base case	OF3	OF5	OF6
Specific energy consumption ($\text{MJ}/\text{t}_{\text{LNG}}$)	986.1	737.7	862.3	986.5
Exergetic efficiency, ε (%)	53.4%	63.9%	58.1%	53.4%
Total exergy of fuel, $\dot{E}_{F,\text{sys}}$ (MW)	239.2	199.8	219.6	239.3
Total exergy of product, $\dot{E}_{P,\text{sys}}$ (MW)	127.7	127.7	127.7	127.7
Total exergy destruction, $\dot{E}_{D,\text{sys}}$ (MW)	111.5	72.2	91.9	111.6
Total cost rate of investment and O&M, \dot{Z}_{tot} (\$/h)	35491	66781	29606	29167
Total specific cost of fuel, $c_{F,\text{tot}}$ (\$/GJ)	17.2	15.9	16.6	17.2
Total specific cost of product, $c_{P,\text{tot}}$ (\$/GJ)	109.3	170.2	92.9	95.6

OF5 has the cheapest total cost of product ($c_{P,\text{tot}}$) with 92.9 \$/GJ by reducing the exergy destruction and the total cost associated with investment \dot{Z}_{sys} . The cost improvement from OF5 compared to the base case is 15%. The result from OF6 also exhibit an improvement in terms of costs with $c_{P,\text{tot}}$ is at 109.73 \$/GJ. However, the exergetic efficiency remains unimproved compared to the base case, since the exergy destruction in this case is almost comparable to the base case. All cases have the same LNG throughput at 158.42 kg/s, therefore the exergy of product is constant. The total cost of product from OF3 is 83% higher than the lowest cost of product found in OF5. On the contrary, the exergy efficiency

of OF5 is 6% less than the solution obtained in OF3, although it is still more effective than the base case. As expected, the costs of OF3 is much larger than the rest of the cases as a compromise to a high exergy efficiency, with its $c_{P,tot}$ nearly doubled the costs of OF5.

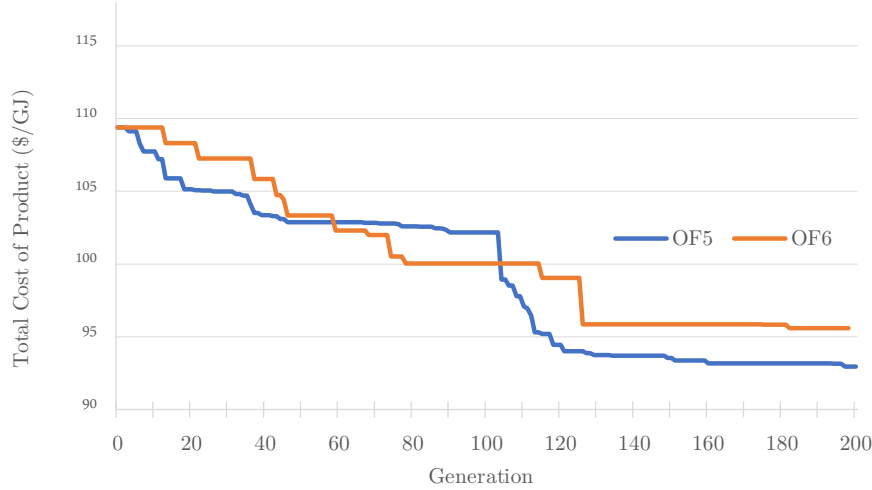


Figure 6.9 – The comparison of the objective functions between OF5 and OF6

In the base case analysis, the impact of \dot{Z}_{tot} to the total cost of product is clearly shown with 71% of the total cost of product. After the optimization in OF5 and OF6, the proportions were reduced to 69% and 66% respectively, with the former resulted in a lower total cost of product at 92.9 \$/GJ. Furthermore, the costs associated with the exergy destructions in the base case is 6886 \$/h, while in OF5 it was reduced to 5489 \$/h. In OF6, it was slightly increased to 6889 \$/h. In fact, these values only contribute around 15.6% to the total cost incurred by $\dot{C}_{D,k} + \dot{Z}_k$. It clearly indicates that the cost associated with the investment of a component (\dot{Z}_k) has a more substantial effect than the cost associated with its exergy destruction ($\dot{C}_{D,k}$). Again, the result also proves that the sequential approach (OF5) is more efficient than simply to throw all the design variables to the optimization. The comparison between of between the optimization performance of OF5 and OF6 can be seen in Figure 6.9.

Since OF5 has the best result amongst others, the detailed exergoeconomic analysis is presented in Table 6.8. The specific cost of fuel for MHX1 and MHX2 are relatively high with 141.7 \$/GJ and 133.1 \$/GJ, respectively, making them the largest contributor to the

$\dot{C}_{D,k}$ with the total of 4975 \$/h. Another major cost contributor comes from MRC and PHX, both have the same exergeconomic factor of 75% and the $\dot{C}_{D,k}$ value at 3484 \$/h and 2724 \$/h, respectively. The effect of exergy destruction to the costs of these components is moderate, since the specific cost of fuel is much lower than in MHX, albeit having significant exergy destructions. MHX, MRC and PHX are also the main contributors to the overall systems' investment with 85% from \dot{Z}_{tot} . Furthermore, the exergoeconomic factor (the ratio between \dot{Z}_k with $\dot{C}_{D,k} + \dot{Z}_k$) of these components when combined is almost proportional at 59%, which is an ideal scenario since MHX has a high impact relative to the system.

Table 6.8 – Exergoeconomic analysis of the solution from OF5

Component ID	E_D [MW]	c_f \$/GJ	c_p \$/GJ	C_D \$/h	$C_D + Z_k$ \$/h
PHX1	3.1	63.7	3707.1	713	3322
PHX2	3.3	69.0	642.5	821	2961
PHX3	4.3	74.3	305.4	1138	4287
PHX4	3.0	74.4	217.0	812	3110
MHX1	7.6	141.7	174.3	3867	9934
MHX2	2.3	133.1	195.9	1107	2100
PROPTV1	0.2	74.1	80.7	45	62
PROPTV2	0.3	74.1	80.5	68	104
PROPTV3	0.4	74.1	81.4	107	155
PROPTV4	2.3	61.9	77.4	506	570
MRTV1	2.3	82.3	86.9	692	732
MRTV2	0.6	82.3	88.4	181	191
NGTV	7.8	5.3	6.0	149	169
PROPC1	1.1	29.6	78.5	115	490
PROPC2	1.9	30.7	77.0	208	796
PROPC3	2.5	25.8	69.9	235	999
PROPC4	6.6	24.0	61.9	573	2296
MRC1	14.3	30.7	72.2	1584	5338
MRC2	8.1	23.4	65.6	679	3270
MRC3	5.5	23.4	71.0	461	2249
PROPMIX1	0.2	61.0	107.3	34	34
PROPMIX2	0.1	78.9	125.2	21	21
PROPMIX3	0.1	58.7	165.3	23	23
MRMIX	0.1	14.7	14.8	7	7
MRFL	0.0	0.7	0.7	0	45
MRCOL2	7.2	50.0		1841	1959
MRCOL3	2.5	203.0		701	759
PROPCOL	4.4	44.4		1289	1601
SYSTEM	91.9	16.6	92.9	5489	35095

6.3.1. Comparison between Base Case, OF3 and OF5

The lowest total cost of product in the exergoeconomic optimization was found in OF5. In order to analyze the changes that occurred in the C3MR components, it is convenient to compare it with the base case and OF3, since the latter has the best performance in terms of exergy efficiency. The detailed comparison at the component level between the three cases is presented in Table 6.9. The results reveal that the MR cycle has higher importance than the pre-cooling cycle in terms of the economics of the system. In the base case, the ratio of MR cycle to precooling cycle is 1.4:1, while in the OF5 the ratio was reduced to 1.3:1. Moreover, \dot{Z}_{tot} is also a critical indicator to evaluate exergoeconomic analysis, since its contribution in the base case is more than 70% of the total cost of product. The OF5 optimization was able to reduce \dot{Z}_{tot} from 35491 \$/h to 29606 \$/h, which also means a lower total cost of product at 92.9 \$/GJ. If the priority is to maximize the exergy efficiency as in OF3, \dot{Z}_{tot} is almost doubled to 66781 \$/h, with the total cost of product at 170.2 \$/GJ. Despite a higher exergetic performance and lower $\dot{C}_{D,tot}$, a higher \dot{Z}_{sys} value in OF3 case has surpassed the $\dot{C}_{D,tot}$ savings, resulting in a higher total cost of product. Another useful parameter that is worth mentioning in the analysis is the exergoeconomic factor f_k , where a small percentage indicates a more dominant $\dot{C}_{D,k}$ and a large percentage indicates a more dominant of \dot{Z}_k . In terms of optimization, the former implies that the exergy destruction has to be minimized whilst the latter requires process design changes in order to reduce the PEC of the respective component. Typically, when the exergy destruction is reduced, the cost of investment increases and vice versa. Overall, \dot{Z}_k is a more dominant factor for the cost formation of C3MR process. The proof can be seen in Table 6.9, which shows the dominant role \dot{Z} has, especially in the important components such as the pre-cooling heat exchangers and MR compressors. Another essential component, MHX has a relatively high \dot{C}_D , which becomes very high when the exergy efficiency is maximized.

The optimization in OF3 solely focused on the exergetic performance; therefore only the cost of exergy destruction is improved, mainly affecting the components that have the biggest irreversibilities such as MHX and MR compressors. Consequently, the total cost of product is increased because the process has to accommodate the design variables imposed

by the GA optimization, regardless of the investment costs required. The exergy destruction of MHX, for instance, is reduced from 16.5 MW in the base case to 2.7 MW in OF3. However, the value of $\dot{C}_{D,MHX} + \dot{Z}_{MHX}$ for MHX is 34536 \$/h, in which 93% comes from \dot{Z}_{MHX} alone. As a result, \dot{Z}_{MHX} in OF3 is approximately two times higher than the base case and five times higher than OF5. Similarly, in PHX the value of $\dot{C}_{D,PHX} + \dot{Z}_{PHX}$ is 26222 \$/h, with 91% contribution from the investment costs and doubled the costs compared to OF5. The MRC and PROPC component also have a significant contribution to the total cost of product, with the $\dot{C}_D + \dot{Z}$ value of 10317 \$/h and 3834 \$/h, respectively.

Table 6.9 – Comparison of exergoeconomic analysis between the optimized cases

Component ID	Base case			OF3			OF5		
	\dot{C}_D	$\dot{C}_D + \dot{Z}_k$	f_k	\dot{C}_D	$\dot{C}_D + \dot{Z}_k$	f_k	\dot{C}_D	$\dot{C}_D + \dot{Z}_k$	f_k
	\$/h	\$/h	%	\$/h	\$/h	%	\$/h	\$/h	%
PHX1	379	4004	90.5	366	6892	94.7	713	3322	78.5
PHX2	509	4115	87.6	408	8047	94.9	821	2961	72.3
PHX3	1033	4986	79.3	902	5423	83.4	1138	4287	73.5
PHX4	714	4005	82.2	567	5861	90.3	812	3110	73.9
MHX1	7888	13987	43.6	1731	31661	94.5	3867	9934	61.1
MHX2	1828	2872	36.4	826	2875	71.3	1107	2100	47.3
PROPTV1	42	62	32.9	36	56	35.3	45	62	28.6
PROPTV2	183	223	18.0	207	246	15.9	68	104	34.4
PROPTV3	100	151	34.2	96	146	34.2	107	155	30.5
PROPTV4	307	371	17.2	191	253	24.6	506	570	11.3
MRTV1	1155	1194	3.3	1080	1120	3.6	692	732	5.4
MRTV2	886	907	2.3	303	317	4.4	181	191	5.2
NGTV	149	169	12.3	149	169	12.0	149	169	12.3
PROPC1	138	504	72.6	125	455	72.5	115	490	76.5
PROPC2	326	1243	73.8	333	1264	73.6	208	796	73.8
PROPC3	205	918	77.6	191	857	77.7	235	999	76.4
PROPC4	509	2112	75.9	288	1257	77.1	573	2296	75.1
MRC1	1485	4375	66.1	1558	3388	54.0	1584	5338	70.3
MRC2	880	3912	77.5	750	3243	76.9	679	3270	79.2
MRC3	1008	4487	77.5	824	3686	77.6	461	2249	79.5
PROPMIX1	10	10	0.0	8	8	0.0	34	34	0.0
PROPMIX2	12	12	0.0	10	10	0.0	21	21	0.0
PROPMIX3	11	11	0.0	10	10	0.0	23	23	0.0
MRMIX	13	13	0.0	229	229	0.0	7	7	0.0
MRFL	0	84	100.0	0	63	100.0	0	45	100.0
MRCOL2	1020	1106	7.7	449	490	8.3	1841	1959	6.0
MRCOL3	1819	1947	6.5	1456	1558	6.6	701	759	7.6
PROPCOL	2256	2572	12.3	1215	1504	19.2	1289	1601	19.5
SYSTEM	6886	42376	83.8	4134	70916	94.2	5489	35095	84.4

The solution found in OF5 allows more exergy destruction from PHX and MHX, thus reducing the surface area and ultimately lowering the cost rate of investment of the respective component. According to the exergoeconomic analysis, these components have the biggest impact on the total cost of product. When it is compared to the base case, the exergy destruction in MHX is also improved while still keeping a reasonable surface area. According to the result from OF5, for MHX an increase of 1 \$/h in the costs of exergy destruction leads to a decrease in \dot{Z}_{MHX} value by more than 10 \$/h. This was particularly accomplished by employing less MR mass flow rate than in OF3. The new MR composition also enable a lower condensing pressure, hence resulted in a slightly lower $\dot{C}_{D,MRC}$. However, the \dot{Z}_{MRC} value is higher in OF5 compared to OF3, particularly at the component MRC1. This is due to lower outlet pressure at MRTV-1, which requires more energy at the beginning of the compression stage albeit a lower MR mass flow rate. Nevertheless, the impact of the component to the system is not as significant as MHX.

At the pre-cooling cycle, both optimizations found an optimum condensing pressure at 11.5 bar, while in OF5 the propane flow rate must be increased to 446.9 kg/s to accommodate the new throttling pressure configurations. In terms of the $\dot{C}_{D,k} + \dot{Z}_k$, the costs in the precooling-related components for OF5 are higher than OF3 with one exception in PHX. Since more propane used in the precooling cycle, the costs of exergy destruction in PHX from OF5 is higher than OF3. The solution is advantageous to the system since the costs of investments for PHX only requires half of the costs of OF3, as illustrated in Figure 6.10.

6.3.2. The Solutions to the Design Variables

The design variables from the optimized solution of OF3 and OF5 are presented in Table 6.10. Several notable differences occur to the optimization cases, such as for MR condensing pressure and MR mass flow rate. In OF3 the value is 44.8 bar and 275.2 kg/s, respectively, which is slightly smaller than the base case but higher compared to the same variables in OF5. As a result, the exergy destructions decrease and the exergetic efficiency increases, which in turn create a higher total cost of product due to higher investment costs required for the heat exchangers. Conversely, the MR mass flow rate in OF5 is 246.8 kg/s with lower

methane and slightly higher in ethane and propane composition in the mixture. The outlet pressure of MR throttling valves is also lower than OF3 and therefore require more energy in the first stage of compression. By doing so, the investment costs of MHX become much lower than OF3 by giving off more exergy destructions. Nevertheless, it does not generate a considerable gap in the cost structure of MR compressors, since the condensing pressure of MR can be lowered to 33.6 bar.

Table 6.10 – The optimized solutions for design variables OF3 and OF5

Variables	Aspen ID	Unit	OF3	OF5
MR Compressor inlet temperature	MR-COL3	K	305.0	305.0
MR Compressor outlet pressure	MR-C3	bar	44.8	33.6
MR flow rate	MR-1	kg/s	275.2	246.8
MR composition				
Methane	MR-1	mass fraction	0.25	0.15
Ethane	MR-1	mass fraction	0.35	0.41
Propane	MR-1	mass fraction	0.39	0.42
Isobutane	MR-1	mass fraction	0.00	0.00
n-Butane	MR-1	mass fraction	0.00	0.00
Nitrogen	MR-1	mass fraction	0.01	0.01
MRTV1 pressure outlet	MRTV-1	bar	3.9	1.4
MRTV2 pressure outlet	MRTV-2	bar	4.0	1.03
Precooling				
Propane flow rate	PROP-12	kg/s	442.7	446.9
Compressor 1 pressure outlet	PROP-C1	bar	2.7	2.2
Compressor 2 pressure outlet	PROP-C2	bar	5.7	3.6
Compressor 3 pressure outlet	PROP-C3	bar	7.9	5.5
Compressor 4 pressure outlet	PROP-C4	bar	11.5	11.5
Throttling valve pressure outlet	PROP-TV1	bar	1.5	1.0

Another vital component according to the base case analysis is PHX, of which the investment costs are the highest amongst other components. The exergy destructions generated by PHX from OF3 and OF5 are 8.7 MW and 13.7 MW, respectively. In order to lower the investment costs, the mass flow rate of pre-cooling refrigerant in OF5 needs to be slightly increased to 446.9 kg/s, while lowering the outlet pressure at each stage of the compressors. These variables are also equivalent to the outlet pressure of the throttling valves in the pre-cooling cycle, consequently reducing the heat exchanger area while still maintaining reasonable costs associated with their exergy destructions.

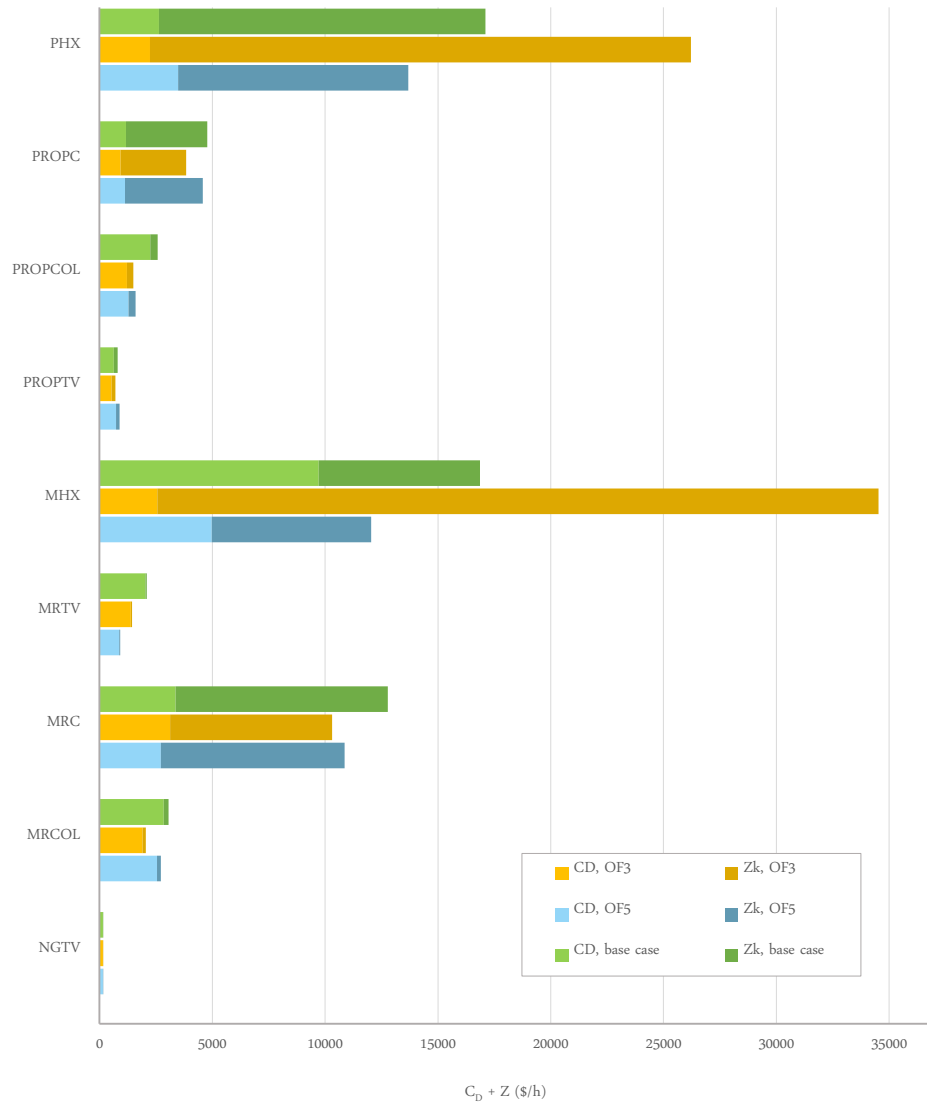


Figure 6.10 – Comparison of $\hat{C}_D + \hat{Z}$ between the base case, OF3, and OF5

7. Multi-Objective Optimization

Multi-objective optimization is an appropriate way to analyze the system when two or more objectives have equal importance and might be conflicting with each other. Theoretically, each objective can be easily combined into a single objective function. However, the result heavily relies on the weights that are assigned before the optimization and therefore resulted in a very subjective approach. Instead of referring to a single value solution, the purpose of multi-objective optimization should be presenting all of the available values in the given set of decision variables. The results should be able to explore the feasible solutions that lead to the optimality within the objective space. This condition is indicated when the solutions of an objective function cannot be improved further without worsening other objective functions. Each objective function is calculated separately and compared so that eventually all the non-dominated solutions are found and form the Pareto frontier, a term that bears a significant meaning in the multi-objective optimization study. Accordingly, the decision makers can acquire a complete insight into how an optimized system performs by considering all objectives and their tradeoffs.

7.1. Optimization Workflow

The multi-objective optimization workflow for C3MR process is illustrated in Figure 7.1. Although to some extent the metaheuristic algorithm of multi-objective is similar to the single-objective optimization, the sorting and selection method are modified in order to suits the purpose. The method that was applied to this study is based on the non-dominated sorting genetic algorithm II (NSGA-II) by Deb et al. [164]. The Sorting method carries the most important part of the algorithm. Instead of arranging the variable sets based on a single-objective approach, multi-objective optimization applies non-dominated sorting and assigns a parameter called crowding distances. The sorting procedure arranges the population based on the non-domination characteristic, while the crowding distance operator acts as a mechanism to ensure the exploration of the objective space. At a given number of

iterations, the population is ranked and selected accordingly, resulted in solutions from all frontiers including the Pareto frontier as the final result. The optimization and sorting algorithm is written in Python coupled with Aspen Plus as the process simulator and VBA for the exergy and exergoeconomic modules.

Unlike the single optimization workflow, the NSGA-II selection process is initiated by combining the old and new populations with the scheme previously shown in Figure 3.4. The objective results from new offspring are compared to the previous generation based on its non-domination rank and crowding distance parameters.

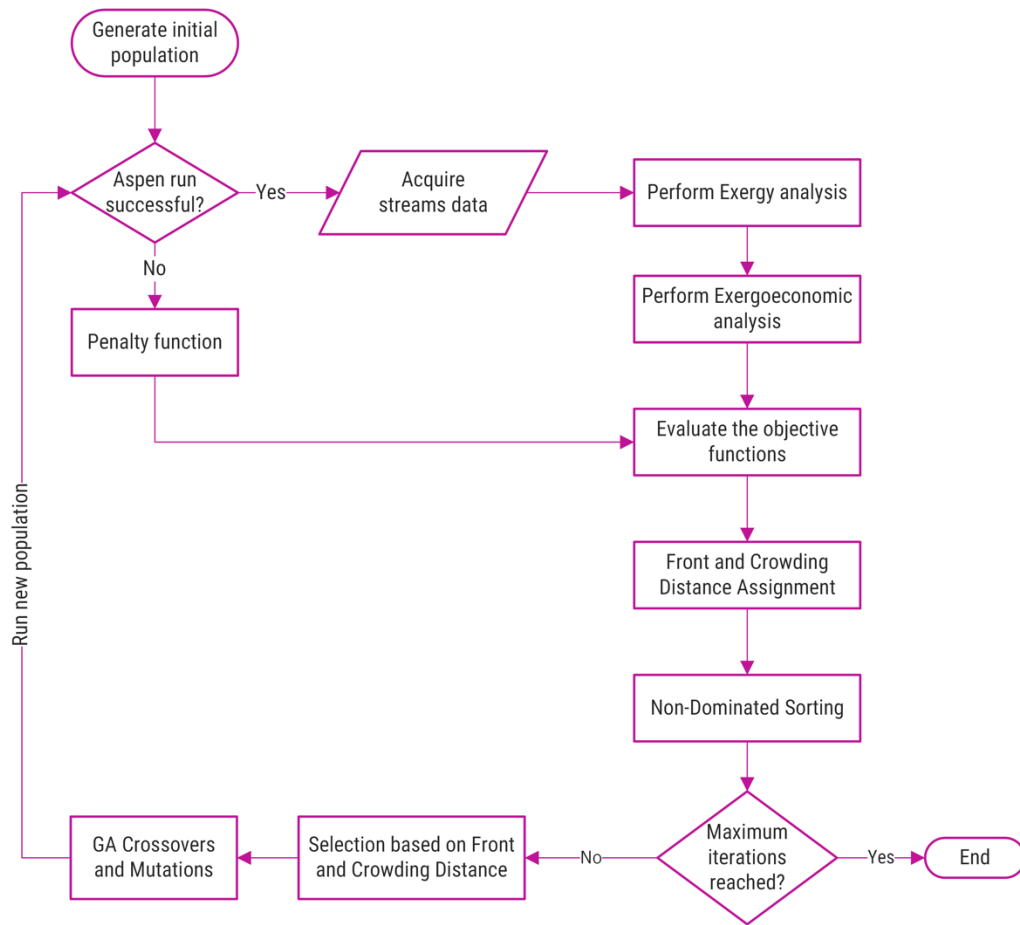


Figure 7.1 – Multi-objective optimization workflow

Thereafter, a Non-Dominated sort is performed iteratively according to the following steps:

1. For each individual p in the current iteration:
 - a. Define a variable $S_p = \emptyset$, which is a list that will contain individuals that are dominated by p .

- b. Define a variable $n_p = 0$, which is the individual counter that dominates p.
 - c. Add each individual q to S_p in the current iteration if q is dominated by p.
If this is the case, then $S_p = S_p \cup \{q\}$. Otherwise, $n_p = n_p + 1$.
 - d. If $n_p = 0$, it means there are no individuals that dominate p. Therefore, p is added to the 1st front, hence $F_1 = F_1 \cup \{p\}$.
2. If the 1st front is filled, define the front counter $i = 1$ and perform this operation to the entire population:
- a. Define $Q = \emptyset$. This will be a set for the subsequent $(i+1)^{\text{th}}$ front.
 - b. For each individual p in front F_i :
 - i. For each individual q in S_p from the current iteration:
 1. Subtract the domination counter $n_q = n_q - 1$
 2. If $n_q = 0$, it means that no individuals in the next front would dominate q. Thus, $\text{rank}_q = i+1$.
 3. Add q to the set of Q, where $Q = Q \cup \{q\}$.
 - c. Increment the front counter by one. $F_i = i + 1$. It will be defined as the subsequent front. Hence, set $F_i = Q$.

After obtaining the rank of each individual based on the non-domination method, a crowding distance parameter is assigned to compare the individual that belongs to the same front. The basic idea behind the crowding distance is finding the Euclidian distance between each individual in a front based on their m objectives in the m dimensional hyperspace. The individuals in the boundary are always selected since they have infinite distance assignment [164,192]. Note that the crowding distance parameter only compares the individuals within the same front. In this way, the selection process can prioritize the individuals that are not close to each other, ensuring a diversity to the NSGA-II result. The crowding distance value is assigned to individuals with the following steps:

1. For each objective function m:
 - a. Sort the individuals in front F_i according to its objective function results.
 - b. Assign infinite distance to boundary values (first and last rank) in F_i , such that $I(d_1) = \infty$ and $I(d_n) = \infty$

- c. For $k=2$ to $k=(n-1)$ calculate the crowding distance using the equation below:

$$I(d_n) = I(d_n) + \frac{I_m(n+1) - I_m(n-1)}{f_m^{max} - f_m^{min}}, \text{ where } I_m(k) \text{ is the distance of } n^{\text{th}} \text{ individual from } m^{\text{th}} \text{ objective function.}$$

After the front and the crowding distance are assigned to each individual, the selection process begins by sorting the individuals based on its front. Likewise, the rank of the individuals within the same front is decided by crowding distance values. Assigning the rank to the individuals are as follows:

- a. In the 1st front, set the rank of p so that $\text{rank}_p = 1$.
- b. Individuals that belong to the i^{th} front is set to $\text{rank} = i$.
- c. For crowding distance in the same front F_i , the individuals $p \prec_n q$ if $F_i(d_p)$ is higher than $F_i(d_q)$.

To summarize, the sorting and selection process in NSGA-II is accomplished by:

1. Comparing the objective results from the older and new generation. This will double the population.
2. Assigning the non-domination front and crowding distance to each individual
3. Rank the individual based on the front, and inside each front, the individual is sorted by its crowding distance.
4. Eliminate half of the population according to the ranking procedure in (3) and proceed to the next iteration.

7.2. Objective Functions and Decision Variables

Exergy efficiency maximization and cost of product minimization, which based on the exergy and exergoeconomic analyses, are chosen as the objective functions. The goal is to investigate the best tradeoffs between the exergy efficiency and the total cost of product that is expressed as

$$\epsilon_{tot} = \frac{\dot{E}_{P,tot}}{\dot{E}_{F,tot}} \quad (7.1)$$

where,

$$\dot{E}_{P,tot} = \dot{E}_{NATGAS-7}^T - \dot{E}_{NATGAS-1}^T \quad (7.2)$$

$$\dot{E}_{F,tot} = \sum_N \dot{W}_{comp,n} + \dot{E}_{NATGAS-1}^M - \dot{E}_{NATGAS-7}^M \quad (7.3)$$

The total cost of product is formulated using the exergoeconomic cost balance where it depends on the total cost rate of fuel and the cost rate associated with the investment, operation, and maintenance of the C3MR process.

$$c_P \dot{E}_{P,tot} = \dot{C}_{F,tot} + \sum \dot{Z}_k \quad (7.4)$$

Alternatively, the total cost rate of fuel and product can also be defined further formulated according to the fuel and product rule of the overall system using the following equations:

$$\dot{C}_{F,tot} = \sum_N (c_w \dot{W}_{comp,n}) + c_{NG-1}^M \dot{E}_{NG-1}^M - c_{NG-7}^M \dot{E}_{NG-7}^M \quad (7.5)$$

$$c_P \dot{E}_{P,tot} = c_{NG-7}^T \dot{E}_{NG-7}^T - c_{NG-1}^T \dot{E}_{NG-1}^T \quad (7.6)$$

Both objectives are conflicting to each other and at the same time strongly correlated, which is the primary motivation to conduct the multi-objective optimization.

Unlike the previous optimizations, it is more effective to choose all possible design variables and proceed with the optimization to obtain the desired results for the multi-objective purpose. This is because the goal of the multi-objective optimization is not only to find an optimum solution, but also to explore the objective space so that the Pareto frontier can be determined accordingly. Splitting the optimization based on the cycle could limit the possibility of diversification, which is essential in multi-objective optimization. Therefore, to ensure that the results can obtain the Pareto front, the total number of iterations, in this case, is set to 500. The decision variables include the most important parameters from the process, similar to in the case of OF6. In this case, each iteration consists of population consists of 128 individuals with the mutation rate of 35%.

7.3. Optimization results

During the early iterations, as illustrated in Figure 7.2, the optimization resulted in disperse solutions in the objective space, although as optimization progressed, they are more concentrated in either side of the higher exergy efficiency or on the lower cost of product. The intensification in GA has created this condition since more feasible results were found on both sides; it is more likely for the next offspring to be located around the previous best generations. The diversity of the solutions was also made possible by virtue of a mutation operator and the selection mechanism. In fact, the main distinction of the multi-objective with the single-objective optimization lies in how the selection procedure operates. Here, the selection mechanism guarantees a well-spread of solutions by assigning crowding distance to each individual. As the iteration progressed to 500th, it can be seen that the solutions became well-spread around the objective space whose exergy efficiency lies approximately between 58% to 64%. The search for Pareto front is ensured by comparing the objective functions using the non-domination rank; therefore the solution with low cost of product and high exergy efficiency as well as the opposite are regarded as the “best solution”. The result shows that the feasible solutions range approximately from 58% to 64% for exergetic efficiency and from 93 to 119 \$/GJ for the total cost of product.

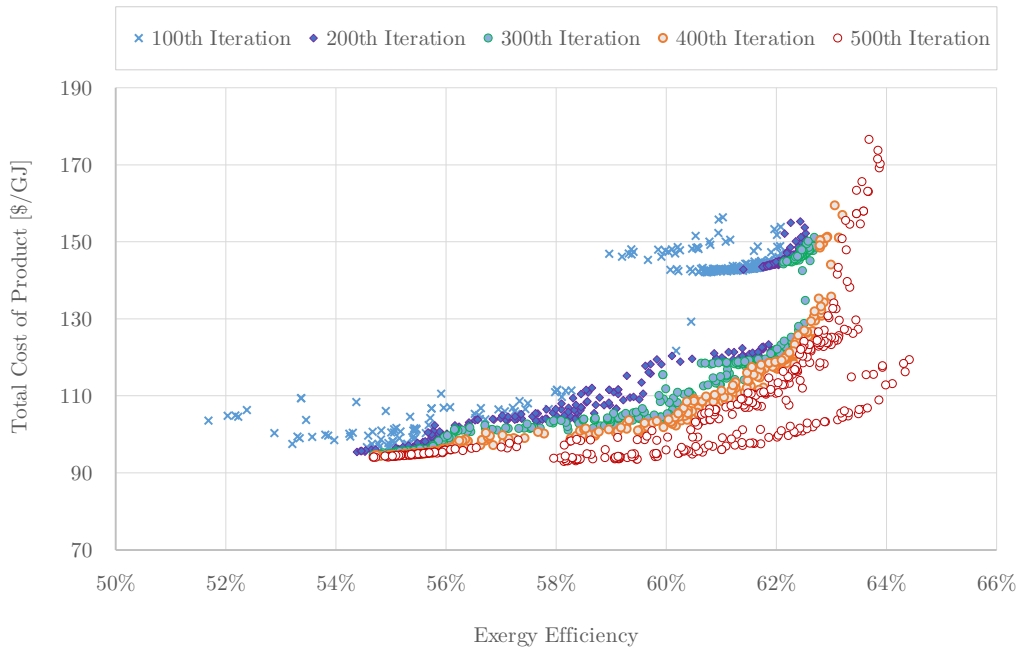


Figure 7.2 – Progression of C3MR multi-objective optimization towards Pareto front

The Pareto front curve provides the range of preference for decision-makers to enable them to choose the best tradeoffs between the exergetic efficiency and total cost of product. In this approach, a posteriori articulation of preferences was considered, where all results have to be initially quantified before the decision makers ultimately impose their preference. Start from the 200th iterations, the first front moves towards the x-axis, indicating that there is still a room of improvement in terms of the exergy efficiency. When the optimization approaches 500th iterations, it becomes apparent that the objective space is filled with more diverse solutions, slowly converged towards forming a curve-shaped Pareto front.

Additionally, a regression analysis was performed to the first and the second front, shown in Figure 7.3. These are the solutions, whose results are located in the near-optimum conditions. Note that the maximum exergy efficiency was obtained at 64.4%, which is a better result than the previous single-objective optimization. The efficiency improvement occurred due to a longer computational time since the GA performed with larger population size and a higher number of iterations. On the other hand, the total cost of product was not improved and obtained nearly at the same value as the previous result in OF5. All of the solutions of the exergy efficiency and the total cost of the product lies between OF7a and OF7c while between them the tradeoffs limit of the two conflicting objectives is drawn. The relationship between the cost of product ($\dot{C}_{P,sys}$) and exergetic efficiency (ϵ) of the system can be empirically established and the following equation is obtained:

$$\dot{C}_{P,tot} = 13220 \epsilon^3 - 15932 \epsilon^2 + 4995.9\epsilon \quad (7.9)$$

For the purpose of evaluation, the solutions that either produced the best exergy efficiency (OF7a), the least cost of product (OF7c) and the best trade-offs between two objectives (OF7b) are compared. These solutions are shown in Figure 7.3. Note that the selected solution does not imply that OF7b is the ultimate best solution from the Pareto front. The purpose of the selection is to show the tradeoff between the two objectives and showing the result of exergy-based analyses, which is presented in Table 7.1.

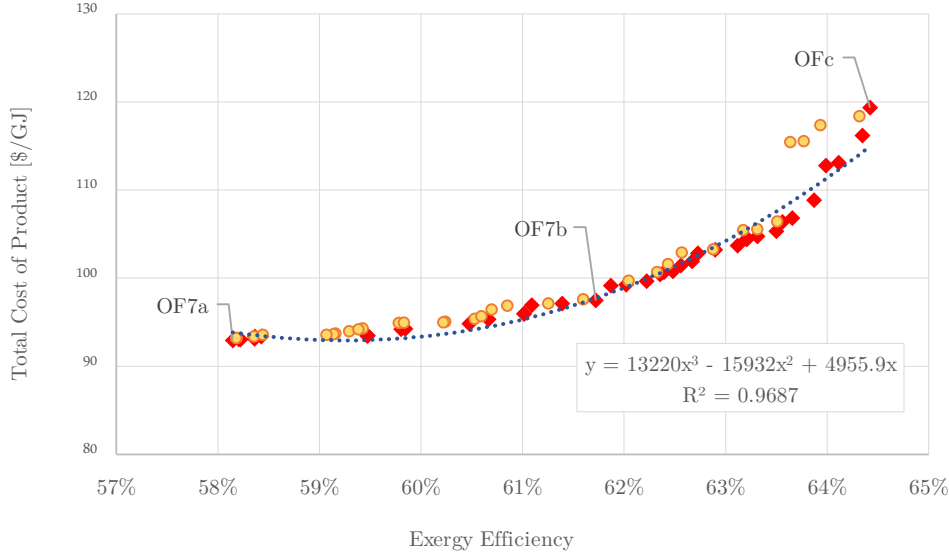


Figure 7.3 – Pareto frontier of multi-objective optimization for C3MR process

Table 7.1 – Overview of the analysis results of multi-objective optimization

	Base case	OF7a	OF7b	OF7c
Specific energy consumption (MJ/t _{LNG})	986.1	862.4	782.4	727.9
Exergetic efficiency, ε (%)	53.4%	58.2%	61.7%	64.4%
Total exergy of fuel, $\dot{E}_{F,tot}$ (MW)	239.2	219.5	206.9	198.2
Total exergy of product, $\dot{E}_{P,tot}$ (MW)	127.7	127.7	127.7	127.7
Total exergy destruction, $\dot{E}_{D,tot}$ (MW)	111.5	91.8	79.2	70.5
Total cost rate of investment and O&M, \dot{Z}_{tot} (\$/h)	35491	29603	32731	43131
Specific cost rate of of fuel, $c_{F,tot}$ (\$/h)	17.2	16.6	16.2	15.9
Specific cost rate of product, $c_{P,tot}$ (\$/h)	109.3	93.0	97.5	118.5

^a Maximum exergetic efficiency. ^b Minimum the cost of product. ^c Multi-objective optimization.

It was found that the highest exergy efficiency at 64.4% is obtained in OF7c, while OF7a produced the least total cost of product at 93 \$/GJ. As the number of population and the iterations are larger than the previous optimizations, the system now has different optimum solutions. This is, to some, one of the drawbacks of the metaheuristic optimization since there is no optimization path is repeatable due to its stochastic nature.

Regarding the cost of product, OF7a was able to achieve the lowest value compared to the other solutions. The exergy of fuel was also improved compared to the base case, although it is still lower than the OF7b and OF7c. The result is actually similar to the single-objective optimization in OF5, in which the exergy destruction increase is compensated by the reduction in \dot{Z}_{tot} . It also shows the importance of reducing the cost of investment in order to have a lower cost of product. On the contrary, OF7c has the highest efficiency the system

can achieve at 64.4%. The design parameter has improved the component that contributes the most largest exergy destruction (MHX), which was identified from the exergy analysis of the base case. The drawback of the solution is an increase of the cost of investment in MHX from 7065 \$/h in the OF7a to 18367 \$/h in OF7c. Consequently, the total system resulted in $c_{P,tot}$ of 118.5 \$/GJ, which is just slightly more expensive than the base case, yet about 24% higher when it is compared to OF7a.

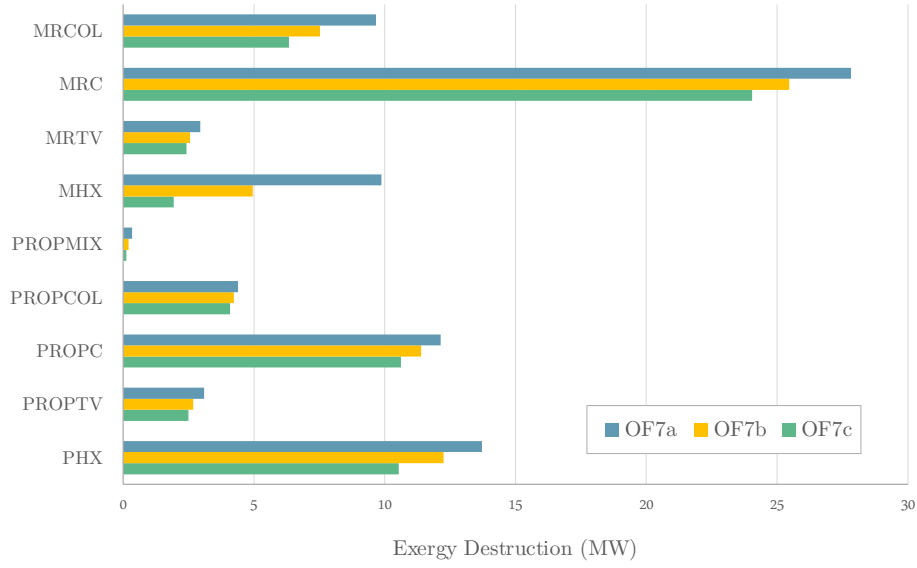


Figure 7.4 – Exergy destruction in selected multi-objective optimization results

OF7b is analyzed to see the “best” trade-off between the exergy efficiency and the cost of product. The comparison in terms of exergy destruction can be easily identified using the bar graph presented in Figure 7.4. It is evident that as the exergy efficiency increases, the exergy destruction in all components decreases. The reduction follows a similar pattern in all solutions. However, the most notable improvement in terms of magnitude occurred in MHX, where in each case the exergy destruction is almost cut into half. MHX in OF7b generates 5 MW of exergy destruction, while in OF7a, it is 9.9 MW. This indicates the critical importance of component MHX for the overall system. In addition, the exergy destruction difference of MR compressors between OF7a and OF7b are also among the highest, albeit not as significant as the impact of MHX.

The comparison of the economic performance for all cases that are mentioned in Table 7.1 is presented in Figure 7.5. In OF7c, PHX and MHX dominate the system over 75% from the total of investment costs, with MHX contributes the biggest portion with 43%. OF7b has the total investment cost 32731 \$/h, where MHX, PHX, and MR Compressors are the major cost contributors at 35%, 30%, and 23%, respectively. These three significant components also dominate the investment costs in OF7a with a more even distribution with 34%, 27%, and 24% from MHX, PHX and MR compressors, respectively. Furthermore, $\dot{C}_{D,tot}$ for OF7a is 5490 \$/h, which is 19% lower than OF7b and 36% lower than OF7c. It can be observed that with a higher exergy efficiency, the costs of the exergy destructions are reduced and at the same time, the costs of investment are likely to be increasing with the exception of the compressors. Since the cost of product in OF7a is optimized, the energy consumption of the compressors are slightly higher than other scenarios, which is proportional to the purchased equipment cost of the MR compressors.

Figure 7.6 shows the proportion of the important parameters in terms of the working fluids. The MR cycle overlooks the pre-cooling cycle in the total investment costs for OF7a, OF7b and OF7c with the value between 52%, 54%, and 59%, respectively. A similar pattern is also exhibited for the exergy destructions, where the solution with the least cost of product resulted in more irreversibilities. Solutions with a low cost of product are also characterized by a significant portion of \dot{C}_D from its MR cycle, as shown in OF7a with 62% of $\dot{C}_{D,total}$. In contrast, an even proportion of the investment costs between MR cycle and precooling cycle indicates a system with a lower cost of product.

7.3.1. The Effect of Design Variables

The results of multi-objective optimization also revealed that a slight increase in the MR mass flow rate strongly affect the economics of the system, where it can be seen clearly in MHX and PHX. As in the case of OF7c, the MR flow rate is only 1% higher than OF7b, yet the investment costs of MHX in this solution is 86% higher. On the other hand, the reduction in $\dot{C}_{D,MHX}$ is only 54% in a much smaller magnitude.

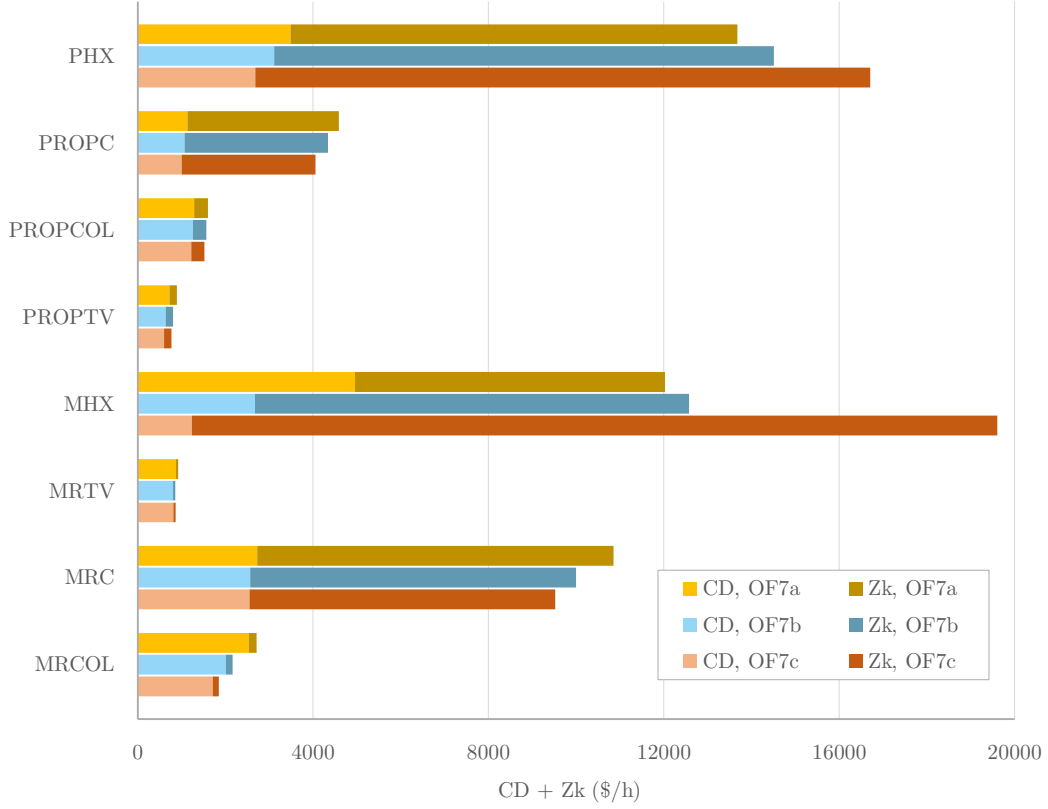


Figure 7.5 – Distribution of $\dot{C}_D + \dot{Z}_k$ from all OF7 scenarios

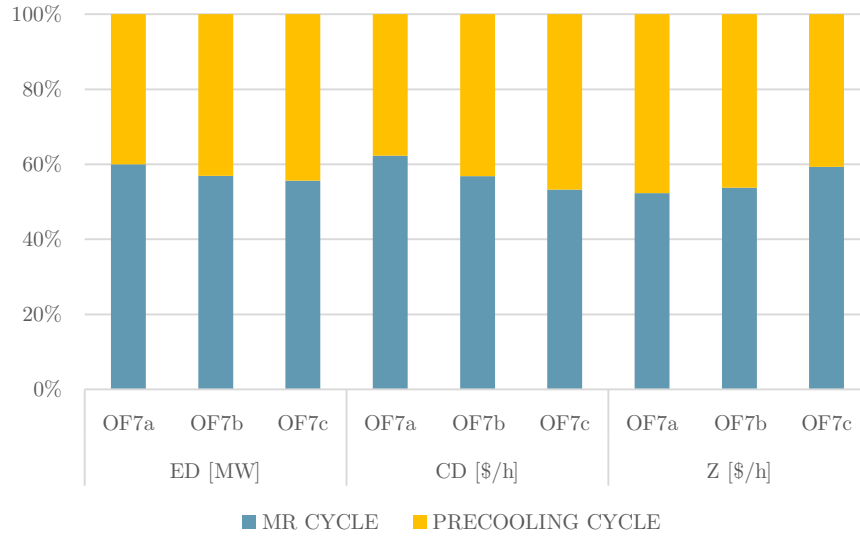


Figure 7.6 – Distribution of \dot{E}_D , $\dot{C}_{D,tot}$ and \dot{Z}_{tot} from all OF7 scenarios

The decision variables for the base case and all optimization scenarios are presented in Table 7.2. It was found that at Pareto front, the best MR composition is configured by around 40-41% ethane and propane, 15-16% methane, and a trace amount of nitrogen. Furthermore, maximizing the exergetic efficiency resulted in a higher MR mass flow rate than when the

primary concern in the total cost of product. The outlet pressure MR compressors also play a major role, where the value is found at 33.6 bar for all scenarios. This value has been a major improvement compared to the base case, where it was previously set at 48.6 bar. The key difference between these scenarios is in the pressure outlet of the MR throttling valves. A lower MR flow rate in OF7a is made possible by reducing the pressure in MRTV1 and MRTV2 to 1.4 and 1.5 bar, respectively, while the opposite case would minimize the exergy destruction. The mass flow rate of propane in all scenarios are found to be comparable; however it is slightly higher than in the base case so that a lower outlet pressure can be accommodated. The condensing pressure value is found to be equal in all optimization scenarios at 11.5 bar. The outlet pressure at each compression stage, which is equal to the pressure after throttling processes, are set to smaller values lower than other scenarios. These have allowed lower investment costs of PHX at the expense of exergy destructions.

Table 7.2 – Design variables from all multi-objective optimization scenarios

Variables	Unit	Base case	OF7a	OF7b	OF7c
MR Compressor outlet pressure	bar	48.6	33.6	33.6	33.6
MR flow rate	kg/s	301.8	246.8	249.0	251.3
MR composition					
Methane	mass fraction	0.25	0.15	0.16	0.16
Ethane	mass fraction	0.33	0.40	0.40	0.41
Propane	mass fraction	0.35	0.41	0.41	0.41
Nitrogen	mass fraction	0.072	0.01	0.01	0.01
MRTV1 pressure outlet	bar	2.9	1.4	1.9	2.3
MRTV2 pressure outlet	bar	3.0	1.5	2.0	2.4
Precooling					
Propane flow rate	kg/s	442.7	446.9	446.7	446.9
Compressor 1 pressure outlet	bar	2.5	2.2	2.4	2.6
Compressor 2 pressure outlet	bar	5.1	3.6	4.1	5.2
Compressor 3 pressure outlet	bar	7.2	5.5	6.2	6.6
Compressor 4 pressure outlet	bar	14.3	11.5	11.5	11.5
PROP-TV1 pressure outlet	bar	1.3	1.0	1.1	1.2
Natural Gas					
Feed flow rate	kg/s	158.4	158.4	158.4	158.4
PHX4 outlet temperature	K	240.0	240.0	240.0	240.0
LNG pressure outlet	bar	1.2	1.2	1.2	1.2

Table 7.3 – Exergoeconomic analysis results of all OF7 scenarios

Component ID	OF7a			OF7b			OF7c		
	\dot{C}_D	$\dot{C}_D + \dot{Z}_k$	f_k	\dot{C}_D	$\dot{C}_D + \dot{Z}_k$	f_k	\dot{C}_D	$\dot{C}_D + \dot{Z}_k$	f_k
	\$/h	\$/h	%	\$/h	\$/h	%	\$/h	\$/h	%
PHX1	712	3322	79	595	3562	83	535	3781	86
PHX2	821	2961	72	723	3138	77	497	4287	88
PHX3	1141	4283	73	1035	4575	77	920	5291	83
PHX4	814	3107	74	759	3231	76	734	3344	78
MHX1	3858	9931	61	1689	10487	84	209	17376	99
MHX2	1107	2100	47	988	2083	53	1025	2225	54
PROPTV1	45	62	29	47	65	28	56	75	25
PROPTV2	68	104	34	85	122	30	162	200	19
PROPTV3	108	155	30	116	164	29	51	100	49
PROPTV4	506	570	11	392	456	14	333	396	16
MRTV1	692	732	5	637	677	6	646	685	6
MRTV2	181	191	5	167	178	6	168	179	6
NGTV	148	169	12	148	169	12	148	169	12
PROPC1	115	490	77	127	501	75	147	540	73
PROPC2	209	798	74	224	863	74	292	1121	74
PROPC3	236	1000	76	236	1009	77	136	629	78
PROPC4	573	2296	75	480	1967	76	427	1767	76
MRC1	1583	5336	70	1424	4572	69	1411	4170	66
MRC2	679	3269	79	670	3155	79	666	3073	78
MRC3	461	2249	80	468	2267	79	476	2280	79
PROPMIX1	34	34	0	21	21	0	12	12	0
PROPMIX2	21	21	0	15	15	0	11	11	0
PROPMIX3	23	23	0	16	16	0	11	11	0
MRMIX	7	7	0	5	5	0	1	1	0
MRCOL2	1839	1957	6	1304	1398	7	998	1076	7
MRCOL3	701	759	8	707	765	8	715	773	7
PROPCOL	1291	1604	19	1260	1564	19	1224	1520	20
SYSTEM	5490	35093	84	4614	37344	88	4031	47161	91

8. Summary and Conclusions

Designing the liquefaction process involves several essential aspects including process design, thermodynamic evaluation, and economic assessment. The exergy-based analyses were applied to reveal the details of such aspects. In this study, the modeling, exergy-based analysis, and the optimization of the C3MR process are demonstrated and investigated. Subsequently, a multi-objective optimization was performed by implementing a genetic algorithm and a modified version of the selection system, tailored for the multi-objective purpose called NSGA-II. The objective functions were set to maximizing the exergetic efficiency and minimizing the total cost of product simultaneously, which assumed to be a posteriori approach, meaning that no particular preference is assigned to any of the objectives before results are obtained. Therefore, all solutions have to be initially calculated and only afterward decision makers can judge the design preference based on the optimum solutions. Regardless, the purpose of multi-objective optimization is not to find a single optimum solution, and instead, it is designed to find Pareto front within the objective space.

GA has successfully optimized the exergy efficiency of the system from 53.4% to 63.9% using the sequential approach, guided by the results of the exergy analysis. The overall exergy efficiency of the C3MR process largely depends on the MR compressors and the main cryogenic heat exchangers (MHX), which generate the most exergy destruction among other components. The exergy destruction for MHX can be minimized by changing the MR composition such that the minimum temperature is set to 0.1 K. However, it would also mean that the cost of investments of MHX significantly increases due to a very large heat exchange area. The result from OF3 optimization shows that the MR mass flow rate and its condensing pressure can be reduced to save energy consumption. Nonetheless, these variables still have a lower limit at 275.2 kg/s and 44.8 bar, respectively, due to the requirement of the liquefaction capacity.

In terms of the exergoeconomics, the sequential approach was able to reduce the $c_{p,tot}$ from 109.3 \$/GJ to 92.9 \$/GJ, which is proven to be 3% cheaper and 5% more efficient than the simultaneous approach. Without the aid of exergy-based methods, it was found that the optimization would be less superior in terms of the result and computational performance. There are three notable components that play significant roles to the total cost of product: MHX, PHX and MR compressors. The most significant improvement can be achieved by finding the right balance between the cost of investments and the costs associated with exergy destruction in the MHX. The optimization performed in OF5 reveals that in order to save costs, the MR composition needs to be changed with more ethane and propane, reducing the MR flow rate and condensing pressure. The outcome resulted in less investment costs as well as reducing the exergy destruction in MHX and PHX. The total cost of product in the base case is 109.3 \$/GJ, while in OF5 it was optimized to 92.9 \$/GJ. The biggest improvements occur in the investment costs of MHX and PHX, in which the costs are 53% and 40% lower, respectively, compared to the base case. The investment costs of MR compressors are also 27% lower than the base case due to a different mixture and a lower MR condensing pressure. In addition, shell and tube heat exchangers can replace the plate-fin type used in the precooling heat exchanger and might reduce the costs of investment. However, the process configuration needs to be altered accordingly and whether it resulted in a lower cost of product is subject to further investigation.

The multi-objective optimization technique demonstrated in this study is able to effectively find Pareto curve at near-optimum conditions, in which the exergetic efficiency ranges from 58% to 64% with the total cost of product obtained from ranges from 93 to 120 \$/GJ. Three scenarios are obtained to see the results of exergy-based analyses in depth. OF7a has the least cost of product with 92.9 \$/GJ, OF7c is the most efficient with the exergy efficiency at 64%, while OF7b is selected as the optimum tradeoff at the Pareto optimum curve. The exergy-based methods further revealed that when the priority is set to the total cost of product, a lower MR mass flow rate along with lower outlet pressure at all throttling

processes need to be applied to the system. On the other hand, a slight increase in the MR flow rate will significantly increase the investment costs of MHX, while higher pressure settings in the pre-cooling cycle will also increase the investment costs of PHX. In all scenarios, it was also shown that the cost contributors mainly come from MHX, PHX, and the MR compressors. Several important design variables such as the propane flow rate, MR condensing pressure, and the MR composition were found to be comparably equal at Pareto front. The system with a lower cost of product is characterized by a higher proportion of exergy destructions in the MR cycle while maintaining an equal proportion in terms of investments with the pre-cooling cycle. Ultimately, the solutions that lie at Pareto frontier can be used to establish the empirical relationship between exergetic efficiency and the cost of product, thus providing the decision makers with a wide range of optimality references to the C3MR process design.

Bibliography

- [1] International Gas Union. IGU World LNG report 2018.
- [2] S&P Global Platts. Opportunities and challenges of China's LNG expansion. 2018.
- [3] Hammer G, Lübcke T, Kettner R, Pillarella MR, Recknagel H, Commichau A, et al. Natural gas. Ullmann's Encycl Ind Chem 2000.
- [4] Tsatsaronis G. Thermoeconomic analysis and optimization of energy systems. *Prog Energy Combust Sci* 1993;19:227–57. doi:10.1016/0360-1285(93)90016-8.
- [5] Tsatsaronis G. Exergoeconomics: Is it only a new name? *Chem Eng Technol* 1996;19:163–9. doi:10.1002/ceat.270190210.
- [6] Chiu C-H. History of the Development of LNG Technology. Present. Annu. Conf. Years Adv. Fuels Petrochemicals Philadelphia (November 18, 2008), 2008.
- [7] Ahern JE. Applications of the second law of thermodynamics to cryogenics—A review. *Energy* 1980;5:891–7. doi:https://doi.org/10.1016/0360-5442(80)90104-8.
- [8] Zheng D, Uchiyama Y, Ishida M. Energy-utilization diagrams for two types of LNG power-generation systems. *Energy* 1986;11:631–9. doi:https://doi.org/10.1016/0360-5442(86)90111-8.
- [9] Liu H, You L. Characteristics and applications of the cold heat exergy of liquefied natural gas. *Energy Convers Manag* 1999;40:1515–25. doi:https://doi.org/10.1016/S0196-8904(99)00046-1.
- [10] Kanoğlu M. Exergy analysis of multistage cascade refrigeration cycle used for natural gas liquefaction. *Int J Energy Res* 2002;26:763–74. doi:10.1002/er.814.
- [11] Remelje CW, Hoadley AFA. An exergy analysis of small-scale liquefied natural gas (LNG) liquefaction processes. *Energy* 2006;31:1669–83. doi:10.1016/j.energy.2005.09.005.
- [12] Vatani A, Mehrpooya M, Palizdar A. Energy and exergy analyses of five conventional liquefied natural gas processes. *Int J Energy Res* 2014;38:1843–63. doi:10.1002/er.3193.
- [13] Vatani A, Mehrpooya M, Palizdar A. Advanced exergetic analysis of five natural gas liquefaction processes. *Energy Convers Manag* 2014;78:720–37. doi:https://doi.org/10.1016/j.enconman.2013.11.050.
- [14] Tsatsaronis G, Morosuk T. Advanced exergetic analysis of a novel system for generating electricity and vaporizing liquefied natural gas. *Energy* 2010;35:820–9.

doi:<https://doi.org/10.1016/j.energy.2009.08.019>.

- [15] Morosuk T, Tsatsaronis G, Boyano A, Gantiva C. Advanced exergy-based analyses applied to a system including LNG regasification and electricity generation. *Int J Energy Environ Eng* 2012;3:1.
- [16] Tsatsaronis G, Morosuk T. Advanced Exergoeconomic Evaluation and Its Application to Compression Refrigeration Machines 2007:859–68.
- [17] Morosuk T, Tsatsaronis G. Advanced exergetic evaluation of refrigeration machines using different working fluids. *Energy* 2009;34:2248–58.
- [18] Morosuk T, Tsatsaronis G. Comparative evaluation of LNG-based cogeneration systems using advanced exergetic analysis. *Energy* 2011;36:3771–8.
- [19] Morosuk T, Tsatsaronis G. A new approach to the exergy analysis of absorption refrigeration machines. *Energy* 2008;33:890–907. doi:<https://doi.org/10.1016/j.energy.2007.09.012>.
- [20] Kelly S, Tsatsaronis G, Morosuk T. Advanced exergetic analysis: Approaches for splitting the exergy destruction into endogenous and exogenous parts. *Energy* 2009;34:384–91.
- [21] Morosuk T, Tsatsaronis G. Splitting physical exergy : Theory and application. *Energy* 2019;167:698–707. doi:10.1016/j.energy.2018.10.090.
- [22] Lim W, Choi K, Moon I. Current status and perspectives of Liquefied Natural Gas (LNG) plant design. *Ind Eng Chem Res* 2013;52:3065–88. doi:10.1021/ie302877g.
- [23] Durr C, Coyle D, Hill D, Smith S. LNG technology for the commercially minded. *Proc, Gastech* 2005.
- [24] Mokhatab S, Mak JY, Valappil J V, Wood DA. Handbook of liquefied natural gas. Gulf Professional Publishing; 2013.
- [25] Wang M, Khalilpour R, Abbas A. Operation optimization of propane precooled mixed refrigerant processes. *J Nat Gas Sci Eng* 2013;15:93–105. doi:10.1016/j.jngse.2013.09.007.
- [26] Hill RWS. Exergy Analysis Applied to a C3MR Process for the Liquefaction of Natural Gas. Technische Universität Berlin, 2012.
- [27] Sanavandi H, Ziabasharhagh M. Design and comprehensive optimization of C3MR liquefaction natural gas cycle by considering operational constraints. *J Nat Gas Sci Eng* 2016;29:176–87. doi:10.1016/j.jngse.2015.12.055.
- [28] Faraday M. VI. On the liquefaction and solidification of bodies generally existing as gases. *Philos Trans R Soc London* 1845;135:155–77.

- [29] Noble PG. A Short History of LNG Shipping 1959-2009. Soc Nav Archit Mar Eng 2009. <https://higherlogicdownload.s3.amazonaws.com/SNAME/1dcdb863-8881-4263-af8d-530101f64412/UploadedFiles/c3352777fcaa4c4daa8f125c0a7c03e9.pdf>.
- [30] Foss MM. Introduction to LNG. Houston, Texas: 2012.
- [31] Kidnay AJ, Parrish WR, McCartney DG. Fundamentals of natural gas processing. CRC press; 2011.
- [32] Marques RM, Matos HA, Nauta KM. Modelling the natural gas sweetening and dehydration prior to liquefaction 2014.
- [33] Corvini G, Stiltner J, Clark K. Mercury Removal from Natural Gas and Liquid Streams. Houston, Texas, USA: n.d.
- [34] Yan TY. A novel process for Hg removal from gases. Ind Eng Chem Res 1994;33:3010–4.
- [35] Markovs J, Clark K. Optimized Mercury Removal in Gas Plants. Houston, Texas, USA: n.d.
- [36] Keller AB. NGL 101 - The Basics. NGL 101 - Basics 2012. https://www.eia.gov/conference/ngl_virtual/eia-ngl_workshop-anne-keller.pdf.
- [37] Timmerhaus KD, Reed RP. Cryogenic engineering: fifty years of progress. Springer Science & Business Media; 2007.
- [38] Venkatarathnam G, Timmerhaus KD. Cryogenic mixed refrigerant processes. vol. 100. Springer; 2008.
- [39] Dienel H-L. Carl Linde and His Relationship with Georges Claude: The Cooperation Between Two Independent Inventors in Cryogenics and Its Side Effects. Hist. Artif. Cold, Sci. Technol. Cult. Issues, Springer; 2014, p. 171–88.
- [40] Brodianski VM, Alexeev A. Cryogenics in Russia: development of basic cryogenic cycles. Proc. Twent. Int. Cryog. Eng. Conf., Elsevier; 2005, p. 11–8.
- [41] Eiksund O, Brodal E, Jackson S. Optimization of Pure-Component LNG Cascade Processes with Heat Integration. Energies 2018;11:202.
- [42] Jamieson D, Johnson P, Redding P. Targeting and achieving lower cost liquefaction plants. Twelfth Int. Conf. Exhib. Liq. Nat. Gas, Perth, Aust., vol. 7, 1998.
- [43] Andress DL. The Phillips Optimized Cascade LNG Process: A Quarter-of-a-Century of Improvements 1996.
- [44] Qualls WR, ConocoPhillips L, Hunter P. A Focus on Balance—A Novel Approach Taking the Phillips Optimized Cascade LNG Process Into the Future. AIChE 2003 Spring Natl. Meet., 2003.

- [45] Bauer HC. Mixed fluid cascade, experience and outlook. Pap. 25a, 12th Top. Conf. Gas Util. AIChE 2012 Spring Meet. Houston, Texas, vol. 2, 2012.
- [46] The Linde Group. LNG Technology: Optimised solutions for small- to world-scale plants. Munich, Germany: 2018.
- [47] Morosuk T, Tesch S, Hiemann A, Tsatsaronis G, Bin Omar N. Evaluation of the PRICO liquefaction process using exergy-based methods. J Nat Gas Sci Eng 2015;27:23–31. doi:10.1016/j.jngse.2015.02.007.
- [48] Black & Veatch. Small Scale PRICO LNG n.d. <https://www.bv.com/docs/energy-brochures/small-scale-prico.pdf>.
- [49] Bukowski JD, Liu YN, Pillarella MR, Boccella S, Kennington WA. Natural gas liquefaction technology for floating LNG facilities. IGRC, Seoul 2013.
- [50] Gaumer Jr LS, Newton CL. Liquefaction of natural gas employing multiple-component refrigerants, 1971.
- [51] Kinard GE, Gaumer LS. Mixed refrigerant cascade cycles for LNG, 1973.
- [52] Air Products. Large plant capabilities for capacity more than 2 MTPA: Benefit from economies of scale and proven technology 2013. <http://www.airproducts.com/~media/downloads/data-sheets/L/en-lng-large-medium-small-plant-capabilities.pdf>.
- [53] Roberts MJ, Chen F, Saygi-Arslan O. Brayton refrigeration cycles for small-scale LNG. Air Prod Chem INC, Allentown, USA, Spec Rep Small-Scale Process Solut 2015.
- [54] Kohler T, Bruentrup M, Key RD, Edvardsson T. Choose the best refrigeration technology for small-scale LNG production. Hydrocarbon Process 2014.
- [55] Forg W. Liquefaction of natural gas, 1978.
- [56] Liu Y-N, Pervier JW. Dual mixed refrigerant natural gas liquefaction, 1985.
- [57] Roberts MJ, Agrawal R. Dual mixed refrigerant cycle for gas liquefaction, 2000.
- [58] Nibbelke R, Kauffman S, Pek B. Double mixed refrigerant LNG process provides viable alternative for tropical conditions. Oil Gas J 2002;100:64.
- [59] Bradley A, Duan H, Elion W, Soest-Vercammen E van, Nagelvoort RK. Innovation in the LNG industry: Shell's approach 2009.
- [60] Yang YM, Kim JH, Seo HS, Lee K, Yoon IS. Development of the world's largest above-ground full containment LNG storage tank. 23rd World Gas Conf. Amsterdam, 2006, p. 1–14.
- [61] Sedlaczek R. Boil-Off in Large and Small Scale LNG Chains. MS Pet Eng Dep Pet

Eng Appl Geophys Nor Univ Sci Technol Trondheim 2008.

- [62] Weijts L. Shell DMR 2010. http://www.loekweijts.nl/infographics/shell_dmr.html.
- [63] Haley RM. LNG Line Blockages: Causes, Preventions and Cures. 17th Int. Conf. Exhib. Liq. Nat. Gas, Houston, Texas, USA: 2013.
- [64] Kurle YM, Wang S, Xu Q. Simulation study on boil-off gas minimization and recovery strategies at LNG exporting terminals. Appl Energy 2015;156:628–41. doi:10.1016/j.apenergy.2015.07.055.
- [65] Zellouf Y, Portannier B. First step in optimizing LNG storages for offshore terminals. J Nat Gas Sci Eng 2011;3:582–90.
- [66] Tsatsaronis G. Strengths and Limitations of Exergy Analysis. Thermodyn Optim Complex Energy Syst 1999;93–100. doi:10.1007/978-94-011-4685-2_6.
- [67] Bejan A, Tsatsaronis G, Moran M, Moran MJ. Thermal design and optimization. John Wiley & Sons; 1996.
- [68] Rant Z. Exergie, ein neues Wort fur ‘Technische Arbeitsfahigkeit’(Exergy, a new word for technical availability). Forsch Auf Dem Gebiet Des Ingenieurwesens A 1956;22:36–7.
- [69] Szargut J, Morris DR, Steward FR. Exergy analysis of thermal, chemical, and metallurgical processes 1987.
- [70] Hans-Georg P. Analysis of the Loss of Exergy Resulting from the Reactor Heat Transfer. Atomkernenergie (West Ger Merged with Kerntechnik to Form Atomkernenergie/Kerntechnik Acta Radiol Chang to Acta Radiol Oncol, Radiat Phys 1964;9.
- [71] Siegel K. Exergieanalyse heterogener leistungsreaktoren. Brennstoff-Warme-Kraft 1970;22:434–40.
- [72] Hendrix WA. Exergy optimization of regenerative feedwater heaters 1978.
- [73] Thirumaleshwar M. Exergy method of analysis and its application to a helium cryorefrigerator. Cryogenics (Guildf) 1979;19:355–61.
- [74] Maloney DP, Burton JR. Using second law analysis for energy conservation studies in the petrochemical industry. Energy 1980;5:925–30. doi:[https://doi.org/10.1016/0360-5442\(80\)90108-5](https://doi.org/10.1016/0360-5442(80)90108-5).
- [75] Flower JR, Linnhoff B. Thermodynamic analysis in the design of process networks. Comput Chem Eng 1979;3:283–91. doi:[https://doi.org/10.1016/0098-1354\(79\)80047-2](https://doi.org/10.1016/0098-1354(79)80047-2).
- [76] Shapiro HN, Kuehn TH. Second law analysis of the Ames solid waste recovery system.

- Energy 1980;5:985–91. doi:[https://doi.org/10.1016/0360-5442\(80\)90115-2](https://doi.org/10.1016/0360-5442(80)90115-2).
- [77] Gaggioli RA. The concept of available energy. *Chem Eng Sci* 1961;16:87–96.
 - [78] Haywood RW. A critical review of the theorems of thermodynamic availability, with concise formulations. *J Mech Eng Sci* 1974;16:160–73.
 - [79] Brzustowski TA, Golem PJ. Second-Law Analysis of Energy Processes Part I: Exergy—An Introduction. *Trans Can Soc Mech Eng* 1976;4:209–26.
 - [80] Ahern JE. Exergy method of energy systems analysis 1980.
 - [81] Szargut J. International progress in second law analysis. *Energy* 1980;5:709–18.
 - [82] Lee YD, Ahn KY, Morosuk T, Tsatsaronis G. Exergetic and exergoeconomic evaluation of a solid-oxide fuel-cell-based combined heat and power generation system. *Energy Convers Manag* 2014;85:154–64. doi:<https://doi.org/10.1016/j.enconman.2014.05.066>.
 - [83] Petrakopoulou F, Tsatsaronis G, Boyano A, Morosuk T. Exergoeconomic and exergoenvironmental evaluation of power plants including CO₂capture. *Chem Eng Res Des* 2011;89:1461–9. doi:10.1016/j.cherd.2010.08.001.
 - [84] Petrakopoulou F, Tsatsaronis G, Morosuk T, Carassai A. Conventional and advanced exergetic analyses applied to a combined cycle power plant. *Energy* 2012;41:146–52.
 - [85] Tsatsaronis G. Recent developments in exergy analysis and exergoeconomics. *Int J Exergy* 2008;5:489–99.
 - [86] Ahrendts J. Reference states. *Energy* 1980;5:666–77. doi:[https://doi.org/10.1016/0360-5442\(80\)90087-0](https://doi.org/10.1016/0360-5442(80)90087-0).
 - [87] Lazzaretto A, Tsatsaronis G. SPECO: A systematic and general methodology for calculating efficiencies and costs in thermal systems. *Energy* 2006;31:1257–89. doi:10.1016/j.energy.2005.03.011.
 - [88] Tsatsaronis G, Winhold M. Exergoeconomic analysis and evaluation of energy-conversion plants—I. A new general methodology. *Energy* 1985;10:69–80. doi:[https://doi.org/10.1016/0360-5442\(85\)90020-9](https://doi.org/10.1016/0360-5442(85)90020-9).
 - [89] Topal E. Exergoeconomic Analysis of a Plant for the Liquefaction of Natural Gas. Technische Universität Berlin, 2013.
 - [90] Tribe MA, Alpine RLW. Scale economies and the “0.6 rule.” *Eng Costs Prod Econ* 1986;10:271–8.
 - [91] Kreith F. CRC handbook of thermal engineering. CRC press; 1999.
 - [92] Frangopoulos CA. Thermo-economic functional analysis and optimization. *Energy* 1987;12:563–71.

- [93] Frangopoulos CA. Application of the thermoeconomic functional approach to the CGAM problem. *Energy* 1994;19:323–42.
- [94] Wall G. Thermoeconomic optimization of a heat pump system. *Energy* 1986;11:957–67.
- [95] Valero A, Munoz M, Lozano M. GENERAL THEORY OF EXERGY SAVING: III. ENERGY SAVING AND THERMOECONOMICS. vol. 2. 1986.
- [96] El-Sayed YM, Gaggioli RA. A Critical Review of Second Law Costing Methods—I: Background and Algebraic Procedures. *J Energy Resour Technol* 1989;111:1–7.
- [97] Hesselmann K. Waermeaustauschernetzwerke - eine exergoeconomische Betrachtung. RWTH Aachen, 1985.
- [98] Tsatsaronis G. A review of exergoeconomic methodologies. *Second Law Anal Therm Syst* 1987:81–7.
- [99] Tsatsaronis G, Tawfik T, Lin L, Gallaspy DT. Exergy analysis of an IGCC design configuration for Plant Wansley. United States: American Society of Mechanical Engineers; 1989.
- [100] Tsatsaronis G, Lin L, Pisa J. Exergy Costing in Exergoeconomics. *J Energy Resour Technol* 1993;115:9–16.
- [101] Tsatsaronis G, Pisa J. Exergoeconomic evaluation and optimization of energy systems — application to the CGAM problem. *Energy* 1994;19:287–321. doi:[https://doi.org/10.1016/0360-5442\(94\)90113-9](https://doi.org/10.1016/0360-5442(94)90113-9).
- [102] Tsatsaronis G. Design optimization using exergoeconomics. *Thermodyn. Optim. complex energy Syst.*, Springer; 1999, p. 101–15.
- [103] Wang L, Yang Y, Dong C, Morosuk T, Tsatsaronis G. Parametric optimization of supercritical coal-fired power plants by MINLP and differential evolution. *Energy Convers Manag* 2014;85:828–38.
- [104] Fazlollahi S, Maréchal F. Multi-objective, multi-period optimization of biomass conversion technologies using evolutionary algorithms and mixed integer linear programming (MILP). *Appl Therm Eng* 2013;50:1504–13.
- [105] Sirikum J, Techanitisawad A, Kachitvichyanukul V. A new efficient GA-benders' decomposition method: For power generation expansion planning with emission controls. *IEEE Trans POWER Syst PWRS* 2007;22:1092.
- [106] Young C-T, Zheng Y, Yeh C-W, Jang S-S. Information-Guided Genetic Algorithm Approach to the Solution of MINLP Problems. *Ind Eng Chem Res* 2007;46:1527–37. doi:10.1021/ie060727h.
- [107] Androulakis IP, Maranas CD, Floudas CA. α BB: A global optimization method for

- general constrained nonconvex problems. *J Glob Optim* 1995;7:337–63.
- [108] Moser I. Hooke-jeeves revisited. *Evol. Comput.* 2009. CEC'09. IEEE Congr., IEEE; 2009, p. 2670–6.
 - [109] Nelder JA, Mead R. A simplex method for function minimization. *Comput J* 1965;7:308–13.
 - [110] Shanno DF. Conditioning of quasi-Newton methods for function minimization. *Math Comput* 1970;24:647–56.
 - [111] Nocedal J. Updating quasi-Newton matrices with limited storage. *Math Comput* 1980;35:773–82.
 - [112] Han S-P. A globally convergent method for nonlinear programming. *J Optim Theory Appl* 1977;22:297–309.
 - [113] Nesterov Y, Nemirovskii A. Interior-point polynomial algorithms in convex programming. vol. 13. Siam; 1994.
 - [114] Boggs PT, Tolle JW. Sequential quadratic programming. *Acta Numer* 1995;4:1–51.
 - [115] Boggs PT, Tolle JW. Sequential quadratic programming for large-scale nonlinear optimization. *J Comput Appl Math* 2000;124:123–37.
 - [116] Benders JF. Partitioning procedures for solving mixed-variables programming problems. *Numer Math* 1962;4:238–52.
 - [117] Geoffrion AM. Generalized benders decomposition. *J Optim Theory Appl* 1972;10:237–60.
 - [118] Land AH, Doig AG. An Automatic Method of Solving Discrete Programming Problems. *Econometrica* 1960;28:497–520. doi:10.2307/1910129.
 - [119] Lawler EL, Wood DE. Branch-and-bound methods: A survey. *Oper Res* 1966;14:699–719.
 - [120] Gupta OK, Ravindran A. Branch and bound experiments in convex nonlinear integer programming. *Manage Sci* 1985;31:1533–46.
 - [121] Quesada I, Grossmann IE. An LP/NLP based branch and bound algorithm for convex MINLP optimization problems. *Comput Chem Eng* 1992;16:937–47.
 - [122] Duran MA, Grossmann IE. An outer-approximation algorithm for a class of mixed-integer nonlinear programs. *Math Program* 1986;36:307–39.
 - [123] Westerlund T, Pettersson F. An extended cutting plane method for solving convex MINLP problems. *Comput Chem Eng* 1995;19:131–6.
 - [124] Kelley James E J. The cutting-plane method for solving convex programs. *J Soc Ind*

Appl Math 1960;8:703–12.

- [125] Dauphin YN, Pascanu R, Gulcehre C, Cho K, Ganguli S, Bengio Y. Identifying and attacking the saddle point problem in high-dimensional non-convex optimization. *Adv. Neural Inf. Process. Syst.*, 2014, p. 2933–41.
- [126] Sahinidis N V. BARON: A general purpose global optimization software package. *J Glob Optim* 1996;8:201–5.
- [127] Belotti P, Lee J, Liberti L, Margot F, Wächter A. Branching and bounds tightening techniques for non-convex MINLP. *Optim Methods Softw* 2009;24:597–634.
- [128] Curtis FE, Overton ML. A sequential quadratic programming algorithm for nonconvex, nonsmooth constrained optimization. *SIAM J Optim* 2012;22:474–500.
- [129] Kocis GR, Grossmann IE. Global optimization of nonconvex mixed-integer nonlinear programming (MINLP) problems in process synthesis. *Ind Eng Chem Res* 1988;27:1407–21.
- [130] Viswanathan J, Grossmann IE. A combined penalty function and outer-approximation method for MINLP optimization. *Comput Chem Eng* 1990;14:769–82.
- [131] Holland JH. *Adaptation in natural and artificial systems: an introductory analysis with applications to biology, control, and artificial intelligence*. MIT press; 1992.
- [132] Schwefel H-P. *Evolutionsstrategie und numerische Optimierung*. 1975.
- [133] Rechenberg I. *Evolutionsstrategie--Optimierung technischer Systeme nach Prinzipien der biologischen Evolution* 1973.
- [134] Storn R, Price K. Differential Evolution – A Simple and Efficient Heuristic for global Optimization over Continuous Spaces. *J Glob Optim* 1997;11:341–59. doi:10.1023/A:1008202821328.
- [135] Ferreira C, Gepsoft U. *What is gene expression programming*. 2002 2008.
- [136] Kirkpatrick S, Gelatt CD, Vecchi MP. Optimization by simulated annealing. *Science* (80-) 1983;220:671–80.
- [137] Collet P, Rennard J-P. *Stochastic optimization algorithms. Intell. Inf. Technol. Concepts, Methodol. Tools, Appl.*, IGI Global; 2008, p. 1121–37.
- [138] Dorigo M, Birattari M, Blum C, Clerc M, Stützle T, Winfield A. *Ant Colony Optimization and Swarm Intelligence: 6th International Conference, ANTS 2008, Brussels, Belgium, September 22-24, 2008, Proceedings*. vol. 5217. Springer; 2008.
- [139] Gao Y, Guan H, Qi Z, Hou Y, Liu L. A multi-objective ant colony system algorithm for virtual machine placement in cloud computing. *J Comput Syst Sci* 2013;79:1230–42.

- [140] Kennedy J. Particle swarm optimization. *Encycl. Mach. Learn.*, Springer; 2011, p. 760–6.
- [141] Yang X-S. A new metaheuristic bat-inspired algorithm. *Nat. inspired Coop. Strateg. Optim. (NICSO 2010)*, Springer; 2010, p. 65–74.
- [142] Geem ZW, Kim JH, Loganathan GV. A new heuristic optimization algorithm: harmony search. *Simulation* 2001;76:60–8.
- [143] Cheng M-Y, Prayogo D. Symbiotic organisms search: a new metaheuristic optimization algorithm. *Comput Struct* 2014;139:98–112.
- [144] Brownlee J. *Clever Algorithms: Nature-Inspired Programming Recipes* 2015. http://www.cleveralgorithms.com/nature-inspired/evolution/genetic_algorithm.html.
- [145] Haupt RL, Haupt SE, Haupt SE. *Practical genetic algorithms*. vol. 2. Wiley New York; 1998.
- [146] Wright AH. Genetic Algorithms for Real Parameter Optimization. In: RAWLINS GJEFT-F of GA, editor. vol. 1, Elsevier; 1991, p. 205–18. doi:<https://doi.org/10.1016/B978-0-08-050684-5.50016-1>.
- [147] Adewuya AA. *New methods in genetic search with real-valued chromosomes* 1996.
- [148] Yadav SL, Sohal A. Comparative study of different selection techniques in genetic algorithm. *J Homepage Http//Www Ijesm Co* 2017;6.
- [149] Goldberg DE, Deb K. A comparative analysis of selection schemes used in genetic algorithms. *Found. Genet. algorithms*, vol. 1, Elsevier; 1991, p. 69–93.
- [150] Zhong J, Hu X, Zhang J, Gu M. Comparison of performance between different selection strategies on simple genetic algorithms. *Comput. Intell. Model. Control Autom. 2005 Int. Conf. Intell. Agents, Web Technol. Internet Commer. Int. Conf.*, vol. 2, IEEE; 2005, p. 1115–21.
- [151] Newcastle University Engineering Design Centre. Roulette Wheel Selection 2019. <http://www.edc.ncl.ac.uk/highlight/rhjanuary2007g02.php/>.
- [152] Messac A. Physical programming-effective optimization for computational design. *AIAA J* 1996;34:149–58.
- [153] Coello CAC. Evolutionary multi-objective optimization: a historical view of the field. *IEEE Comput Intell Mag* 2006;1:28–36.
- [154] Marler RT, Arora JS. Survey of multi-objective optimization methods for engineering. *Struct Multidiscip Optim* 2004;26:369–95. doi:10.1007/s00158-003-0368-6.
- [155] Das I, Dennis JE. Normal-boundary intersection: A new method for generating the

- Pareto surface in nonlinear multicriteria optimization problems. *SIAM J Optim* 1998;8:631–57.
- [156] Guenov M, Utyuzhnikov S, Fantini P. Application of the Modified Physical Programming Method to Generating the Entire Pareto Frontier in Multiobjective Optimization. *Evol. Determ. Methods Des. Optim. Control with Appl. to Ind. Soc. Probl. EUROGEN 2005*, Munich, Germany: 2005.
 - [157] Messac A, Ismail-Yahaya A, Mattson CA. The normalized normal constraint method for generating the Pareto frontier. *Struct Multidiscip Optim* 2003;25:86–98.
 - [158] Ismail-Yahaya A, Messac A. Effective generation of the Pareto frontier using the normal constraint method. 40th AIAA Aerosp. Sci. Meet. Exhib., 2002, p. 178.
 - [159] Schaffer JD. Some experiments in machine learning using vector evaluated genetic algorithms (artificial intelligence, optimization, adaptation, pattern recognition) 1984.
 - [160] Fonseca CM, Fleming PJ. Genetic Algorithms for Multiobjective Optimization: Formulation Discussion and Generalization. *Icga*, vol. 93, 1993, p. 416–23.
 - [161] Zitzler E, Thiele L. An evolutionary algorithm for multiobjective optimization: The strength pareto approach. *TIK-Report* 1998;43.
 - [162] Zitzler E, Laumanns M, Thiele L. SPEA2: Improving the strength pareto evolutionary algorithm. *TIK-Report* 2001;103. doi:10.3929/ethz-a-004284029.
 - [163] Srinivas N, Deb K. Multiobjective optimization using nondominated sorting in genetic algorithms. *Evol Comput* 1994;2:221–48.
 - [164] Deb K, Pratab S, Agarwal S, Meyarivan T. A Fast and Elitist Multiobjective Genetic Algorithm: NSGA-II. *IEEE Trans Evol Comput* 2002;6:182–97. doi:10.1109/4235.996017.
 - [165] Alabdulkarem A, Mortazavi A, Hwang Y, Radermacher R, Rogers P. Optimization of propane pre-cooled mixed refrigerant LNG plant. *Appl Therm Eng* 2011;31:1091–8.
 - [166] Al-Sobhi SA, Elkamel A. Simulation and optimization of natural gas processing and production network consisting of LNG, GTL, and methanol facilities. *J Nat Gas Sci Eng* 2015;23:500–8.
 - [167] Wang M, Khalilpour R, Abbas A. Thermodynamic and economic optimization of LNG mixed refrigerant processes. *Energy Convers Manag* 2014;88:947–61. doi:10.1016/j.enconman.2014.09.007.
 - [168] Hatcher P, Khalilpour R, Abbas A. Optimisation of LNG mixed-refrigerant processes considering operation and design objectives. *Comput Chem Eng* 2012;41:123–33.

doi:10.1016/j.compchemeng.2012.03.005.

- [169] Khan MS, Lee S, Lee M. Optimization of single mixed refrigerant natural gas liquefaction plant with nonlinear programming. *Asia-Pacific J Chem Eng* 2012;7:S62–70.
- [170] Xu X, Liu J, Jiang C, Cao L. The correlation between mixed refrigerant composition and ambient conditions in the PRICO LNG process. *Appl Energy* 2013;102:1127–36.
- [171] Ahmadi P, Dincer I. Thermodynamic and exergoenvironmental analyses, and multi-objective optimization of a gas turbine power plant. *Appl Therm Eng* 2011;31:2529–40. doi:10.1016/j.applthermaleng.2011.04.018.
- [172] Ahmadi P, Dincer I, Rosen MA. Exergy, exergoeconomic and environmental analyses and evolutionary algorithm based multi-objective optimization of combined cycle power plants. *Energy* 2011;36:5886–98. doi:10.1016/j.energy.2011.08.034.
- [173] Zhao H, Deng Q, Huang W, Wang D, Feng Z. Thermodynamic and Economic Analysis and Multi-objective Optimization of Supercritical CO₂ Brayton Cycles. *J Eng Gas Turbines Power* 2016;138:1–9. doi:10.1115/1.4032666.
- [174] Fergani Z, Touil D, Morosuk T. Multi-criteria exergy based optimization of an Organic Rankine Cycle for waste heat recovery in the cement industry. *Energy Convers Manag* 2016;112:81–90.
- [175] Wang L, Yang Y, Dong C, Morosuk T, Tsatsaronis G. Multi-objective optimization of coal-fired power plants using differential evolution. *Appl Energy* 2014;115:254–64.
- [176] Ghorbani B, Hamed M, Shirmohammadi R, Hamed M, Mehrpooya M. Exergoeconomic analysis and multi-objective Pareto optimization of the C₃MR liquefaction process. *Sustain Energy Technol Assessments* 2016;17:56–67. doi:10.1016/j.seta.2016.09.001.
- [177] Morosuk T. Thermal Design of Compression Refrigeration Machines - Notes for the Class. Berlin: Technische Universität Berlin; 2009.
- [178] Gaumer L, Newton C. Combined cascade and multicomponent refrigeration system and method 1973.
- [179] Peng D-Y, Robinson DB. A New Two-Constant Equation of State. *Ind Eng Chem Fundam* 1976;15:59–64. doi:10.1021/i160057a011.
- [180] Adewumi M. Peng-Robinson EOS. Phase Relations Reserv Eng 2018. https://www.e-education.psu.edu/png520/m11_p2.html.
- [181] Voulgaris ME, Peters CJ, de Swaan Arons J. Prediction of the Condensation Behavior of Natural Gas: A Comparative Study of the Peng–Robinson and the Simplified-Perturbed-Hard-Chain Theory Equations of State. *Ind Eng Chem Res*

- 1998;37:1696–706. doi:10.1021/ie970641b.
- [182] Elliott JR, Lira CT. Introductory chemical engineering thermodynamics. vol. 184. Prentice Hall PTR Upper Saddle River, NJ; 1999.
 - [183] Tsatsaronis G. Definitions and nomenclature in exergy analysis and exergoeconomics. *Energy* 2007;32:249–53.
 - [184] Ghizawi N, Pelagotti A, Grimaldi A, Guenard D, Giachi M. Compressor Aerodynamic Design for LNG Applications. *Proc. 3rd Gas Process. Symp.*, Elsevier; 2012, p. 231–40.
 - [185] Freko P, Hölzl R, Lehmacher A, Woitalka A, Todorov T. Lifetime Optimisation. *LNG Ind* 2017.
 - [186] The Linde Group. Aluminium plate-fin heat exchangers. Proven technology in a variety of designs. Pullach, Germany: n.d.
 - [187] Kakac S, Liu H, Pramuanjaroenkij A. Heat exchangers: selection, rating, and thermal design. CRC press; 2002.
 - [188] Al-Aidaroos S, Bass N, Downey B, Ziegler J. Offshore LNG Production. *Sr Des Reports* 2009:11.
 - [189] Seider WD, Seader JD, Lewin DR. Product and Process Design Principles: Synthesis, Analysis and Evaluation. John Wiley & Sons; 2009.
 - [190] Martin H, Gnielinski V, Mewes D, Steiner D, Stephan K, Schaber K, et al. VDI Wärmeatlas: Berechnungsblätter für den Wärmeübergang. Verein Dtsch Ingenieure 2002.
 - [191] Younglove BA, Ely JF. Thermophysical properties of fluids. II. Methane, ethane, propane, isobutane, and normal butane. *J Phys Chem Ref Data* 1987;16:577–798.
 - [192] Seshadri A. NSGA-II: A multi-objective optimization algorithm. 2007.

Appendix A: Exergy Balance Equations

Exergy of fuel and product of C3MR components are formulated as follows:

PHX1

$$\begin{aligned}\dot{E}_F &= \dot{E}_{NG-1}^T + \dot{E}_{MR-1}^T + \dot{E}_{PROP-13}^T - \dot{E}_{PROP-14}^T + \dot{E}_{NG-1}^M - \dot{E}_{NG-2}^T + \dot{E}_{MR-1}^T - \dot{E}_{MR-2}^T + \dot{E}_{PROP-13}^M - \dot{E}_{PROP-14}^M \\ \dot{E}_P &= \dot{E}_{NG-1}^T + \dot{E}_{MR-2}^T\end{aligned}$$

PHX2

$$\begin{aligned}\dot{E}_F &= \dot{E}_{PROP-16}^T - \dot{E}_{PROP-17}^T + \dot{E}_{NATGAS-2}^M - \dot{E}_{NATGAS-3}^M + \dot{E}_{MR-2}^M - \dot{E}_{MR-3}^M + \dot{E}_{PROP-16}^M - \dot{E}_{PROP-17}^M \\ \dot{E}_P &= \dot{E}_{NATGAS-3}^T - \dot{E}_{NATGAS-2}^T + \dot{E}_{MR-3}^T - \dot{E}_{MR-2}^T\end{aligned}$$

PHX3

$$\begin{aligned}\dot{E}_F &= \dot{E}_{PROP-19}^T - \dot{E}_{PROP-20}^T + \dot{E}_{NG-3}^M - \dot{E}_{NG-4}^M + \dot{E}_{MR-3}^M - \dot{E}_{MR-4}^M + \dot{E}_{PROP-19}^M - \dot{E}_{PROP-20}^M \\ \dot{E}_P &= \dot{E}_{NG-4}^T - \dot{E}_{NG-3}^T + \dot{E}_{MR-4}^T - \dot{E}_{MR-3}^T\end{aligned}$$

PHX4

$$\begin{aligned}\dot{E}_F &= \dot{E}_{PROP-22}^T - \dot{E}_{PROP-1}^T + \dot{E}_{NG-4}^M - \dot{E}_{NG-5}^M + -\dot{E}_{MR-5}^M + \dot{E}_{PROP-22}^M - \dot{E}_{PROP-1}^M \\ \dot{E}_P &= \dot{E}_{NG-5}^T - \dot{E}_{NG-4}^T + \dot{E}_{MR-5}^T - \dot{E}_{MR-4}^T\end{aligned}$$

MHX1

$$\begin{aligned}\dot{E}_F &= \dot{E}_{MR-14}^T - \dot{E}_{MR-15}^T + \dot{E}_{MR-14}^M - \dot{E}_{MR-15}^M + \dot{E}_{MR-6}^M - \dot{E}_{MR-9}^M + \dot{E}_{MR-7}^M - \dot{E}_{MR-8}^M + \dot{E}_{NG-5}^M - \dot{E}_{NG-6}^M \\ \dot{E}_P &= \dot{E}_{MR-9}^T - \dot{E}_{MR-6}^T + \dot{E}_{MR-8}^T - \dot{E}_{MR-7}^T + \dot{E}_{NG-6}^T - \dot{E}_{NG-5}^T\end{aligned}$$

MHX2

$$\begin{aligned}\dot{E}_F &= \dot{E}_{MR-11}^T - \dot{E}_{MR-12}^T + \dot{E}_{MR-11}^M - \dot{E}_{MR-12}^M + \dot{E}_{MR-9}^M - \dot{E}_{MR-10}^M + \dot{E}_{NG-6}^M - \dot{E}_{NG-7}^M \\ \dot{E}_P &= \dot{E}_{MR-10}^T - \dot{E}_{MR-9}^T + \dot{E}_{NG-7}^T - \dot{E}_{NG-6}^T\end{aligned}$$

PROPTV1

$$\begin{aligned}\dot{E}_F &= \dot{E}_{PROP-21}^M - \dot{E}_{PROP-22}^M \\ \dot{E}_P &= \dot{E}_{PROP-22}^T - \dot{E}_{PROP-21}^T\end{aligned}$$

PROPTV2

$$\begin{aligned}\dot{E}_F &= \dot{E}_{PROP-18}^M - \dot{E}_{PROP-19}^M \\ \dot{E}_P &= \dot{E}_{PROP-19}^T - \dot{E}_{PROP-18}^T\end{aligned}$$

PROPTV3

$$\dot{E}_F = \dot{E}_{PROP-15}^M - \dot{E}_{PROP-16}^M$$

$$\dot{E}_P = \dot{E}_{PROP-16}^T - \dot{E}_{PROP-15}^T$$

PROPTV4

$$\dot{E}_F = \dot{E}_{PROP-12}^T + \dot{E}_{PROP-12}^M - \dot{E}_{PROP-13}^M$$

$$\dot{E}_P = \dot{E}_{PROP-13}^T$$

MRTV1

$$\dot{E}_F = \dot{E}_{MR-8}^M - \dot{E}_{MR-13}^M$$

$$\dot{E}_P = \dot{E}_{MR-13}^T - \dot{E}_{MR-8}^T$$

MRTV2

$$\dot{E}_F = \dot{E}_{MR-10}^M - \dot{E}_{MR-11}^M$$

$$\dot{E}_P = \dot{E}_{MR-11}^T - \dot{E}_{MR-10}^T$$

PROPC1

$$\dot{E}_F = \dot{W}_{PROP-C1} + \dot{E}_{PROP-1}^T - \dot{E}_{PROP-2}^T$$

$$\dot{E}_P = \dot{E}_{PROP-2}^M - \dot{E}_{PROP-1}^M$$

PROPC2

$$\dot{E}_F = \dot{W}_{PROP-C2} + \dot{E}_{PROP-4}^T - \dot{E}_{PROP-5}^T$$

$$\dot{E}_P = \dot{E}_{PROP-5}^M - \dot{E}_{PROP-4}^M$$

PROPC3

$$\dot{E}_F = \dot{W}_{PROP-C3} + \dot{E}_{PROP-7}^T$$

$$\dot{E}_P = \dot{E}_{PROP-8}^T + \dot{E}_{PROP-8}^M - \dot{E}_{PROP-7}^M$$

PROPC4

$$\dot{E}_F = \dot{W}_{PROP-C4} + \dot{E}_{PROP-10}^T$$

$$\dot{E}_P = \dot{E}_{PROP-11}^T + \dot{E}_{PROP-11}^M - \dot{E}_{PROP-10}^M$$

MRC1

$$\dot{E}_F = \dot{W}_{MR-C1} + \dot{E}_{MR-15}^T$$

$$\dot{E}_P = \dot{E}_{MR-16}^T + \dot{E}_{MR-16}^M - \dot{E}_{MR-15}^M$$

MRC2

$$\dot{E}_F = \dot{W}_{MR-C2}$$

$$\dot{E}_P = \dot{E}_{MR-18}^T - \dot{E}_{MR-17}^T + \dot{E}_{MR-18}^M - \dot{E}_{MR-17}^M$$

MRC3

$$\dot{E}_F = \dot{W}_{MR-C3}$$

$$\dot{E}_P = \dot{E}_{MR-20}^T - \dot{E}_{MR-19}^T + \dot{E}_{MR-20}^M - \dot{E}_{MR-19}^M$$

PROPMIX1

$$\dot{E}_F = \dot{m}_{PROP-3} \cdot \dot{E}_{PROP-3}^T - \dot{m}_{PROP-3} \cdot \dot{E}_{PROP-4}^T$$

$$\dot{E}_P = \dot{m}_{PROP-2} \cdot \dot{E}_{PROP-4}^T - \dot{E}_{PROP-2}^T \cdot \dot{E}_{PROP-2}^T$$

PROPMIX2

$$\dot{E}_F = \dot{m}_{PROP-6} \cdot \dot{E}_{PROP-6}^T - \dot{m}_{PROP-6} \cdot \dot{E}_{PROP-7}^T$$

$$\dot{E}_P = \dot{m}_{PROP-5} \cdot \dot{E}_{PROP-7}^T - \dot{m}_{PROP-5} \cdot \dot{E}_{PROP-5}^T$$

PROPMIX3

$$\dot{E}_F = \dot{E}_{PROP-8}^T + \dot{E}_{PROP-9}^T - \dot{m}_{PROP-9} \cdot \dot{E}_{PROP-10}^T$$

$$\dot{E}_P = \dot{m}_{PROP-8} \cdot \dot{E}_{PROP-10}^T$$

MRMIX

$$\dot{E}_F = \dot{m}_{MR-13} (\dot{E}_{MR-13}^T - \dot{E}_{MR-14}^T) + \dot{m}_{MR-13} (\dot{E}_{MR-13}^M - \dot{E}_{MR-14}^M) + \dot{m}_{MR-13} (e_{MR-13}^{CH} - e_{MR-14}^{CH})$$

$$\dot{E}_P = \dot{m}_{MR-12} (\dot{E}_{MR-14}^T - \dot{E}_{MR-12}^T) + \dot{m}_{MR-12} (\dot{E}_{MR-14}^M - \dot{E}_{MR-12}^M) + \dot{m}_{MR-12} (e_{MR-14}^{CH} - e_{MR-12}^{CH})$$

MRFL (dissipative)

$$\dot{E}_D = \dot{E}_{MR-5}^{PH} - (\dot{E}_{MR-19}^{PH} - \dot{E}_{MR-19}^{PH})$$

MRCOL2 (dissipative)

$$\dot{E}_D = \dot{E}_{MR-18}^{PH} - \dot{E}_{MR-19}^{PH}$$

MRCOL3 (dissipative)

$$\dot{E}_D = \dot{E}_{MR-20}^{PH} - \dot{E}_{MR-1}^{PH}$$

PROPCOL (dissipative)

$$\dot{E}_D = \dot{E}_{PROP-11}^{PH} - \dot{E}_{PROP-12}^{PH}$$

SYSTEM

$$\dot{E}_F = \sum_N \dot{W}_{comp,n} + \dot{E}_{NG-1}^M - \dot{E}_{NG-7}^M$$

$$\dot{E}_P = \dot{E}_{NG-8}^T - \dot{E}_{NG-1}^T$$

Appendix B: Exergoeconomic Balance

PHX1**

$$\begin{aligned}\dot{C}_F &= c_{NG-1}^T \dot{E}_{NG-1}^T + c_{MR-1}^T \dot{E}_{MR-1}^T + c_{PROP-13}^T \dot{E}_{PROP-13}^T - c_{PROP-14}^T \dot{E}_{PROP-14}^T + c_{NG-1}^M \dot{E}_{NG-1}^M - c_{NG-2}^M \dot{E}_{NG-2}^M + \\ &\quad c_{MR-1}^M \dot{E}_{MR-1}^M - c_{MR-2}^M \dot{E}_{MR-2}^M + c_{PROP-13}^M \dot{E}_{PROP-13}^M - c_{PROP-14}^M \dot{E}_{PROP-14}^M \\ \dot{C}_P &= c_{NG-2}^T \dot{E}_{NG-2}^T + c_{MR-2}^T \dot{E}_{MR-2}^T\end{aligned}$$

Auxiliary equations:

$$c_{NG-1}^M = c_{NG-2}^M ; \quad c_{MR-1}^M = c_{MR-2}^M ; c_{PROP-13}^M = c_{PROP-14}^M ; c_{PROP-13}^T = c_{PROP-14}^T \quad (\text{F Rule})$$

$$c_{NG-2}^T = c_{MR-2}^T \quad (\text{P Rule})$$

PHX2

$$\begin{aligned}\dot{C}_F &= c_{PROP-16}^T \dot{E}_{PROP-16}^T - c_{PROP-17}^T \dot{E}_{PROP-17}^T + c_{NG-2}^M \dot{E}_{NG-2}^M - c_{NG-3}^M \dot{E}_{NG-3}^M + c_{MR-2}^M \dot{E}_{MR-2}^M - c_{MR-3}^T \dot{E}_{MR-3}^T + \\ &\quad c_{PROP-16}^M \dot{E}_{PROP-16}^M - c_{PROP-17}^M \dot{E}_{PROP-17}^M \\ \dot{C}_P &= c_{NG-3}^T \dot{E}_{NG-3}^T - c_{NG-2}^T \dot{E}_{NG-2}^T + c_{MR-3}^T \dot{E}_{MR-3}^T - c_{MR-2}^T \dot{E}_{MR-2}^T\end{aligned}$$

Auxiliary equations:

$$c_{PROP-16}^T = c_{PROP-17}^T ; \quad c_{PROP-16}^M = c_{PROP-17}^M ; \quad c_{MR-2}^M = c_{MR-3}^M ; c_{NG-2}^M = c_{NG-3}^M \quad (\text{F Rule})$$

$$\frac{c_{MR-3}^T - c_{MR-2}^T}{\dot{E}_{MR-3}^T - \dot{E}_{MR-2}^T} = \frac{c_{NG-3}^T - c_{NG-2}^T}{\dot{E}_{NG-3}^T - \dot{E}_{NG-2}^T} \quad (\text{P Rule})$$

PHX3

$$\begin{aligned}\dot{C}_F &= c_{PROP-19}^T \dot{E}_{PROP-19}^T - c_{PROP-20}^T \dot{E}_{PROP-20}^T + c_{NG-3}^M \dot{E}_{NG-3}^M - c_{NG-4}^M \dot{E}_{NG-4}^M + c_{MR-3}^M \dot{E}_{MR-3}^M - c_{MR-4}^M \dot{E}_{MR-4}^M + \\ &\quad c_{PROP-19}^M \dot{E}_{PROP-19}^M - c_{PROP-20}^M \dot{E}_{PROP-20}^M \\ \dot{C}_P &= c_{NG-4}^T \dot{E}_{NG-4}^T - c_{NG-3}^T \dot{E}_{NG-3}^T + c_{MR-4}^T \dot{E}_{MR-4}^T - c_{MR-3}^T \dot{E}_{MR-3}^T\end{aligned}$$

Auxiliary equations:

$$c_{PROP-19}^T = c_{PROP-20}^T ; \quad c_{PROP-19}^M = c_{PROP-20}^M ; \quad c_{MR-3}^M = c_{MR-4}^M ; c_{NG-3}^M = c_{NG-4}^M \quad (\text{F Rule})$$

$$\frac{c_{MR-4}^T - c_{MR-3}^T}{\dot{E}_{MR-4}^T - \dot{E}_{MR-3}^T} = \frac{c_{NG-4}^T - c_{NG-3}^T}{\dot{E}_{NG-4}^T - \dot{E}_{NG-3}^T} \quad (\text{P Rule})$$

PHX4

$$\begin{aligned}\dot{C}_F &= c_{PROP-22}^T \dot{E}_{PROP-22}^T - c_{PROP-1}^T \dot{E}_{PROP-1}^T + c_{NG-4}^M \dot{E}_{NG-4}^M - c_{NG-5}^M \dot{E}_{NG-5}^M + c_{MR-4}^M \dot{E}_{MR-4}^M - c_{MR-5}^M \dot{E}_{MR-5}^M + \\ &\quad c_{PROP-22}^M \dot{E}_{PROP-22}^M - c_{PROP-1}^M \dot{E}_{PROP-1}^M\end{aligned}$$

$$\dot{C}_P = c_{NG-5}^T \dot{E}_{NG-5}^T - c_{NG-4}^T \dot{E}_{NG-4}^T + c_{MR-5}^T \dot{E}_{MR-5}^T - c_{MR-4}^T \dot{E}_{MR-4}^T$$

Auxiliary equations:

$$c_{PROP-22}^T = c_{PROP-1}^T ; c_{PROP-22}^M = c_{PROP-1}^M ; \quad c_{MR-4}^M = c_{MR-5}^M ; c_{NG-4}^M = c_{NG-5}^M \quad (\text{F Rule})$$

$$\frac{\dot{c}_{MR-5}^T - \dot{c}_{MR-4}^T}{\dot{E}_{MR-5}^T - \dot{E}_{MR-4}^T} = \frac{\dot{c}_{NG-5}^T - \dot{c}_{NG-4}^T}{\dot{E}_{NG-5}^T - \dot{E}_{NG-4}^T} \quad (\text{P Rule})$$

MX1

$$\begin{aligned} \dot{C}_F &= c_{MR-14}^T \dot{E}_{MR-14}^T - c_{MR-15}^T \dot{E}_{MR-15}^T + c_{MR-14}^M \dot{E}_{MR-14}^M - c_{MR-15}^M \dot{E}_{MR-15}^M + c_{MR-6}^M \dot{E}_{MR-6}^M - c_{MR-9}^M \dot{E}_{MR-9}^M \\ &\quad + c_{MR-7}^M \dot{E}_{MR-7}^M - c_{MR-8}^M \dot{E}_{MR-8}^M + c_{NG-5}^M \dot{E}_{NG-5}^M - c_{NG-6}^M \dot{E}_{NG-6}^M \\ \dot{C}_P &= c_{MR-9}^T \dot{E}_{MR-9}^T - c_{MR-6}^T \dot{E}_{MR-6}^T + c_{MR-8}^T \dot{E}_{MR-8}^T - c_{MR-7}^T \dot{E}_{MR-7}^T + c_{MR-6}^T \dot{E}_{NG-6}^T - c_{NG-5}^T \dot{E}_{NG-5}^T \end{aligned}$$

Auxiliary equations:

$$c_{MR-14}^T = c_{MR-15}^T ; \quad c_{MR-6}^M = c_{MR-9}^M ; c_{MR-7}^M = c_{MR-8}^M ; c_{MR-7}^M = c_{MR-8}^M ; c_{NG-5}^M = c_{NG-6}^M \quad (\text{F Rule})$$

$$\frac{\dot{c}_{MR-9}^T - \dot{c}_{MR-6}^T}{\dot{E}_{MR-9}^T - \dot{E}_{MR-6}^T} = \frac{\dot{c}_{MR-8}^T - \dot{c}_{MR-7}^T}{\dot{E}_{MR-8}^T - \dot{E}_{MR-7}^T} = \frac{\dot{c}_{NG-6}^T - \dot{c}_{NG-5}^T}{\dot{E}_{NG-6}^T - \dot{E}_{NG-5}^T} \quad (\text{P Rule})$$

MX2

$$\begin{aligned} \dot{C}_F &= c_{MR-11}^T \dot{E}_{MR-11}^T - c_{MR-12}^T \dot{E}_{MR-12}^T + c_{MR-11}^M \dot{E}_{MR-11}^M - c_{MR-12}^M \dot{E}_{MR-12}^M + c_{MR-9}^M \dot{E}_{MR-9}^M - c_{MR-10}^M \dot{E}_{MR-10}^M + \\ &\quad c_{NG-6}^M \dot{E}_{NG-6}^M - c_{NG-7}^M \dot{E}_{NG-7}^M \\ \dot{C}_P &= c_{MR-10}^T \dot{E}_{MR-10}^T - c_{MR-9}^T \dot{E}_{MR-9}^T + c_{NG-7}^T \dot{E}_{NG-7}^T - c_{NG-6}^T \dot{E}_{NG-6}^T \end{aligned}$$

Auxiliary equations:

$$c_{MR-11}^T = c_{MR-12}^T ; \quad c_{MR-11}^M = c_{MR-12}^M ; c_{MR-9}^M = c_{MR-10}^M ; \quad c_{NG-6}^M = c_{NG-7}^M \quad (\text{F Rule})$$

$$\frac{\dot{c}_{MR-10}^T - \dot{c}_{MR-9}^T}{\dot{E}_{MR-10}^T - \dot{E}_{MR-9}^T} = \frac{\dot{c}_{NG-7}^T - \dot{c}_{NG-6}^T}{\dot{E}_{NG-7}^T - \dot{E}_{NG-6}^T} \quad (\text{P Rule})$$

PROPTV1

$$\begin{aligned} \dot{C}_F &= c_{PROP-21}^M \dot{E}_{PROP-21}^M - c_{PROP-22}^M \dot{E}_{PROP-22}^M \\ \dot{C}_P &= c_{PROP-22}^T \dot{E}_{PROP-22}^T - c_{PROP-21}^T \dot{E}_{PROP-21}^T \end{aligned}$$

Auxiliary equations:

$$c_{PROP-21}^M = c_{PROP-22}^M \quad (\text{F Rule})$$

PROPTV2

$$\begin{aligned} \dot{C}_F &= c_{PROP-18}^M \dot{E}_{PROP-18}^M - c_{PROP-19}^M \dot{E}_{PROP-19}^M \\ \dot{C}_P &= c_{PROP-19}^T \dot{E}_{PROP-19}^T - c_{PROP-18}^T \dot{E}_{PROP-18}^T \end{aligned}$$

Auxiliary equations:

$$c_{PROP-18}^M = c_{PROP-19}^M \quad (\text{F Rule})$$

PROPTV3

$$\dot{C}_F = c_{PROP-15}^T \dot{E}_{PROP-15}^M - c_{PROP-16}^T \dot{E}_{PROP-16}^M$$

$$\dot{C}_P = c_{PROP-16}^T \dot{E}_{PROP-16}^T - c_{PROP-15}^T \dot{E}_{PROP-15}^T$$

Auxiliary equations:

$$c_{PROP-15}^M = c_{PROP-16}^M \text{ (F Rule)}$$

PROPTV4**

$$\dot{C}_F = c_{PROP-12}^T \dot{E}_{PROP-12}^T + c_{PROP-12}^M \dot{E}_{PROP-12}^M - c_{PROP-13}^M \dot{E}_{PROP-13}^M$$

$$\dot{C}_P = c_{PROP-13}^T \dot{E}_{PROP-13}^T$$

Auxiliary equations:

$$\frac{c_{PROP-12}^M - c_{PROP-13}^M}{\dot{E}_{PROP-12}^M - \dot{E}_{PROP-13}^M} = c_{PROP-12}^T \text{ (F Rule)}$$

MRTV1

$$\dot{C}_F = c_{MR-8}^M \dot{E}_{MR-8}^M - c_{MR-13}^M \dot{E}_{MR-13}^M$$

$$\dot{C}_P = c_{MR-13}^T \dot{E}_{MR-13}^T - c_{MR-8}^T \dot{E}_{MR-8}^T$$

Auxiliary equations:

$$c_{PROP-8}^M = c_{PROP-13}^M \text{ (F Rule)}$$

MRTV2

$$\dot{C}_F = c_{MR-10}^M \dot{E}_{MR-10}^M - c_{MR-11}^M \dot{E}_{MR-11}^M$$

$$\dot{C}_P = c_{MR-11}^T \dot{E}_{MR-11}^T - c_{MR-10}^T \dot{E}_{MR-10}^T$$

Auxiliary equations:

$$c_{PROP-10}^M = c_{PROP-11}^M \text{ (F Rule)}$$

PROPC1

$$\dot{C}_F = c_W \dot{W}_{PROP-C1} + c_{PROP-1}^T \dot{E}_{PROP-1}^T - c_{PROP-2}^T \dot{E}_{PROP-2}^T$$

$$\dot{C}_P = c_{PROP-2}^M \dot{E}_{PROP-2}^M - c_{PROP-1}^M \dot{E}_{PROP-1}^M$$

Auxiliary equations:

$$\frac{c_{PROP-1}^T + c_W}{\dot{E}_{PROP-1}^T + \dot{W}_{PROP-C1}} = c_{PROP-2}^T \text{ (F Rule)}$$

PROPC2

$$\dot{C}_F = c_W \dot{W}_{PROP-C2} + c_{PROP-4}^T \dot{E}_{PROP-4}^T - c_{PROP-5}^T \dot{E}_{PROP-5}^T$$

$$\dot{C}_P = c_{PROP-5}^M \dot{E}_{PROP-5}^M - c_{PROP-4}^M \dot{E}_{PROP-4}^M$$

Auxiliary equations:

$$\frac{\dot{C}_{PROP-4}^T + \dot{C}_W}{\dot{E}_{PROP-4}^T - \dot{W}_{PROP-C2}} = c_{PROP-5}^T \quad (\text{F Rule})$$

PROPC3**

$$\dot{C}_F = c_W \dot{W}_{PROP-C3} + c_{PROP-7}^T \dot{E}_{PROP-7}^T$$

$$\dot{C}_P = c_{PROP-8}^T \dot{E}_{PROP-8}^T + c_{PROP-8}^M \dot{E}_{PROP-8}^M - c_{PROP-7}^M \dot{E}_{PROP-7}^M$$

Auxiliary equations:

$$\frac{\dot{C}_{PROP-8}^M - \dot{C}_{PROP-7}^M}{\dot{E}_{PROP-8}^M - \dot{E}_{PROP-7}^M} = c_{PROP-8}^T \quad (\text{P Rule})$$

PROPC4

$$\dot{C}_F = c_W \dot{W}_{PROP-C4} + c_{PROP-10}^T \dot{E}_{PROP-10}^T$$

$$\dot{C}_P = c_{PROP-11}^T \dot{E}_{PROP-11}^T + c_{PROP-11}^M \dot{E}_{PROP-11}^M - c_{PROP-10}^M \dot{E}_{PROP-10}^M$$

Auxiliary equations:

$$\frac{\dot{C}_{PROP-11}^M - \dot{C}_{PROP-10}^M}{\dot{E}_{PROP-11}^M - \dot{E}_{PROP-10}^M} = c_{PROP-11}^T \quad (\text{P Rule})$$

MRC1

$$\dot{C}_F = c_W \dot{W}_{MR-C1} + c_{MR-15}^T \dot{E}_{MR-15}^T$$

$$\dot{C}_P = c_{MR-16}^T \dot{E}_{MR-16}^T + c_{MR-16}^M \dot{E}_{MR-16}^M - c_{MR-15}^M \dot{E}_{MR-15}^M$$

Auxiliary equations:

$$\frac{\dot{C}_{MR-16}^M - \dot{C}_{MR-15}^M}{\dot{E}_{MR-16}^M - \dot{E}_{MR-15}^M} = c_{MR-16}^T \quad (\text{P Rule})$$

MRC2

$$\dot{C}_F = c_W \dot{W}_{MR-C2}$$

$$\dot{C}_P = c_{MR-18}^T \dot{E}_{MR-18}^T - c_{MR-17}^T \dot{E}_{MR-17}^T + c_{MR-18}^M \dot{E}_{MR-18}^M - c_{MR-17}^M \dot{E}_{MR-17}^M$$

Auxiliary equations:

$$\frac{\dot{C}_{MR-18}^T - \dot{C}_{MR-17}^T}{\dot{E}_{MR-18}^T - \dot{E}_{MR-17}^T} = \frac{\dot{C}_{MR-18}^M - \dot{C}_{MR-17}^M}{\dot{E}_{MR-18}^M - \dot{E}_{MR-17}^M} \quad (\text{P Rule})$$

MRC3

$$\dot{C}_F = c_W \dot{W}_{MR-C3}$$

$$\dot{C}_P = c_{MR-20}^T \dot{E}_{MR-20}^T - c_{MR-19}^T \dot{E}_{MR-19}^T + c_{MR-20}^M \dot{E}_{MR-20}^M - c_{MR-19}^M \dot{E}_{MR-19}^M$$

Auxiliary equations:

$$\frac{\dot{c}_{MR-20}^T - \dot{c}_{MR-19}^T}{\dot{E}_{MR-20}^T - \dot{E}_{MR-19}^T} = \frac{\dot{c}_{MR-20}^M - \dot{c}_{MR-19}^M}{\dot{E}_{MR-20}^M - \dot{E}_{MR-19}^M} \quad (\text{P Rule})$$

PROPMIX1

$$\begin{aligned} \dot{C}_F &= \dot{m}_{PROP-3} (c_{PROP-3}^T e_{PROP-3}^T - c_{PROP-4}^T e_{PROP-4}^T) \\ \dot{C}_P &= \dot{m}_{PROP-2} (c_{PROP-4}^T e_{PROP-4}^T - c_{PROP-2}^T e_{PROP-2}^T) \end{aligned}$$

Auxiliary equations:

$$\frac{\dot{c}_{PROP-2}^M + \dot{c}_{PROP-3}^M}{\dot{E}_{PROP-2}^M + \dot{E}_{PROP-3}^M} = c_{PROP-4}^M \quad (\text{F Rule})$$

PROPMIX2

$$\begin{aligned} \dot{C}_F &= \dot{m}_{PROP-6} (c_{PROP-6}^T e_{PROP-6}^T - c_{PROP-7}^T e_{PROP-7}^T) \\ \dot{C}_P &= \dot{m}_{PROP-5} (c_{PROP-7}^T e_{PROP-7}^T - c_{PROP-5}^T e_{PROP-5}^T) \end{aligned}$$

Auxiliary equations:

$$\frac{\dot{c}_{PROP-5}^M + \dot{c}_{PROP-6}^M}{\dot{E}_{PROP-5}^M + \dot{E}_{PROP-6}^M} = c_{PROP-7}^M \quad (\text{F Rule})$$

PROPMIX3

$$\begin{aligned} \dot{C}_F &= c_{PROP-8}^T \dot{E}_{PROP-8}^T + \dot{m}_{PROP-9} (c_{PROP-9}^T \dot{E}_{PROP-9}^T - c_{PROP-10}^T e_{PROP-10}^T) \\ \dot{C}_P &= \dot{m}_{PROP-8} \cdot c_{PROP-10}^T e_{PROP-10}^T \end{aligned}$$

Auxiliary equations:

$$\frac{\dot{c}_{PROP-8}^M + \dot{c}_{PROP-9}^M}{\dot{E}_{PROP-8}^M + \dot{E}_{PROP-9}^M} = c_{PROP-10}^M \quad (\text{F Rule})$$

MRMIX

$$\begin{aligned} \dot{C}_F &= \dot{m}_{MR-13} (c_{MR-13}^T e_{MR-13}^T - c_{MR-14}^T e_{MR-14}^T) + \dot{m}_{MR-13} (c_{MR-13}^M e_{MR-13}^M - c_{MR-14}^M e_{MR-14}^M) \\ \dot{C}_P &= \dot{m}_{MR-12} (c_{MR-14}^T e_{MR-14}^T - c_{MR-12}^T e_{MR-12}^T) + \dot{m}_{MR-12} (c_{MR-14}^M e_{MR-14}^M - c_{MR-12}^M e_{MR-12}^M) \end{aligned}$$

Auxiliary equations:

$$\frac{\dot{c}_{MR-12}^M + \dot{c}_{MR-13}^M}{\dot{E}_{MR-12}^M + \dot{E}_{MR-13}^M} = c_{MR-14}^M \quad (\text{F Rule})$$

Since the coolers are dissipative components, the cost rate of exergy losses caused by the intercoolers are set to zero and the difference \dot{C}_{Dis} is calculated to charge the dissipative outlet stream. Accordingly, the cost balances including the cost differences are formulated as

MRCOL2 (dissipative)

$$\begin{aligned} \dot{C}_{Dis} &= c_{MR-18} \dot{E}_{MR-18}^{PH} + \dot{Z}_{MRCOL2} - c_{MR-19} \dot{E}_{MR-19}^{PH} \\ c_{MR-18}^T &= c_{MR-19}^T ; \quad c_{MR-18}^M = c_{MR-19}^M \end{aligned}$$

MRCOL3 (dissipative)

$$\begin{aligned}\dot{C}_{Dis} &= c_{MR-20}\dot{E}_{MR-20}^{PH} + \dot{Z}_{MRCOL3} - c_{MR-1}\dot{E}_{MR-1}^{PH} \\ c_{MR-20}^T &= c_{MR-1}^T ; \quad c_{MR-20}^M = c_{MR-1}^M\end{aligned}$$

PROPCOL (dissipative)

$$\begin{aligned}\dot{C}_{Dis} &= c_{PROP-11}\dot{E}_{PROP-11}^{PH} + \dot{Z}_{PROPCOL} - c_{PROP-12}\dot{E}_{PROP-12}^{PH} \\ c_{PROP-11}^T &= c_{PROP-12}^T ; \quad c_{PROP-11}^M = c_{PROP-12}^M\end{aligned}$$

The exergy balance within phase separators do not produce any positive effect, nor any exergy destruction takes place. Therefore, the specific cost values between inlet and outlet streams remain constant, as given below

PF1

$$\begin{aligned}c_{PROP-14}^T &= c_{PROP-9}^T = c_{PROP-15}^T \\ c_{PROP-14}^M &= c_{PROP-9}^M = c_{PROP-15}^M\end{aligned}$$

PF2

$$\begin{aligned}c_{PROP-17}^T &= c_{PROP-6}^T = c_{PROP-18}^T \\ c_{PROP-17}^M &= c_{PROP-6}^M = c_{PROP-18}^M\end{aligned}$$

PF3

$$\begin{aligned}c_{PROP-20}^T &= c_{PROP-3}^T = c_{PROP-21}^T \\ c_{PROP-20}^M &= c_{PROP-3}^M = c_{PROP-21}^M\end{aligned}$$

MRFL

$$\begin{aligned}c_{MR-5}^T &= c_{MR-6}^T = c_{MR-7}^T \\ c_{MR-5}^M &= c_{MR-6}^M = c_{MR-7}^M\end{aligned}$$

Ultimately, the cost of fuel and product of the overall system are defined as

$$\begin{aligned}\dot{C}_{F,tot} &= \sum_N c_w \dot{W}_{comp,n} + c_{NG-1}^M \dot{E}_{NG-1}^M - c_{NG-8}^M \dot{E}_{NG-8}^M \\ \dot{C}_{P,tot} &= c_{NG-8}^T \dot{E}_{NG-8}^T - c_{NG-1}^T \dot{E}_{NG-1}^T\end{aligned}$$

Appendix C: Optimization Modules

8.1. Exergy and Exergoeconomic Analysis in VBA

```
Option Base 1
Global Aspen_Case As IHapp

Sub ExecuteAll()
    'FOR EXERGoeconomicS

    Path = "C:\Users\primabudi\PycharmProjects\GA_C3MR\aspen\AspenPlus_C3MR_7_Maret_2018.apw"
    Set Aspen_Case = GetObject(Path)
    Aspen_Case.SuppressDialogs = True
    Aspen_Case.Visible = False
    Application.DisplayAlerts = False

    Application.ScreenUpdating = False
    Application.Calculation = xlAutomatic

    Dim Population As Integer, Resultat() As String
    Dim EnConsum(), ExerResult() As Double

    'POPULATION VARIABLE FOR GA RUN
    Worksheets("Sheet1").Activate
    Population = Sheets("Sheet1").Range("O44")
    ReplaceSheet

    'Energy Consumption ID for the Result Sheet
    Set EnConID = Sheets("Sheet1").Range("N25:N31")
    EnConID.Copy
    Worksheets("Result").Range("B3").PasteSpecial Paste:=xlPasteValues

    For col = 1 To Population
        ro = 1
        'Put Decision Vars to the Excel Input
        Worksheets("Pops").Activate
        'DECISION VARIABLES MR TEMP and PRES
        Range(Sheets("Pops").Cells(ro + 1, col + 3), Sheets("Pops").Cells(ro + 2, col + 3)).Copy
        Worksheets("Sheet1").Range("B26:B27").PasteSpecial Paste:=xlPasteValues
        'DECISION VARIABLES MR FLOW
        Range(Sheets("Pops").Cells(ro + 3, col + 3), Sheets("Pops").Cells(ro + 8, col + 3)).Copy
        Worksheets("Sheet1").Range("B28:B33").PasteSpecial Paste:=xlPasteValues
        'DECISION VARIABLES PROPANE FLOW
        Range(Worksheets("Pops").Cells(ro + 9, col + 3), Worksheets("Pops").Cells(ro + 9, col + 3)).Copy
        Worksheets("Sheet1").Range("B34").PasteSpecial Paste:=xlPasteValues
        'DECISION VARIABLES PROPANE COMPRESSOR SETTINGS
        Range(Sheets("Pops").Cells(ro + 10, col + 3), Sheets("Pops").Cells(ro + 13, col + 3)).Copy
        Worksheets("Sheet1").Range("B35:B38").PasteSpecial Paste:=xlPasteValues
    Next col
End Sub
```

```

' DECISION VARIABLES PROPTV1 PRESSURE
  Range(Sheets("Pops").Cells(ro + 14, col + 3), Sheets("Pops").Cells(ro + 14, col + 3)).Copy
  Worksheets("Sheet1").Range("B39").PasteSpecial Paste:=xlPasteValues
' DECISION VARIABLES ALL MRTV PRESSURE
  Range(Sheets("Pops").Cells(ro + 15, col + 3), Sheets("Pops").Cells(ro + 17, col + 3)).Copy
  Worksheets("Sheet1").Range("B43:B45").PasteSpecial Paste:=xlPasteValues
' DECISION VARIABLES T PROPANE HEAT EXCHANGERS
  Sheets("Pops").Cells(ro + 18, col + 3).Copy
  Worksheets("Sheet1").Range("B46").PasteSpecial Paste:=xlPasteValues
  Sheets("Pops").Cells(ro + 19, col + 3).Copy
  Worksheets("Sheet1").Range("B48").PasteSpecial Paste:=xlPasteValues
  Sheets("Pops").Cells(ro + 20, col + 3).Copy
  Worksheets("Sheet1").Range("B50").PasteSpecial Paste:=xlPasteValues
  Sheets("Pops").Cells(ro + 21, col + 3).Copy
  Worksheets("Sheet1").Range("B52").PasteSpecial Paste:=xlPasteValues
' DECISION VARIABLES T MR HEAT EXCHANGERS
  Sheets("Pops").Cells(ro + 22, col + 3).Copy
  Worksheets("Sheet1").Range("B54").PasteSpecial Paste:=xlPasteValues
  Sheets("Pops").Cells(ro + 23, col + 3).Copy
  Worksheets("Sheet1").Range("B57").PasteSpecial Paste:=xlPasteValues

' Run Simulations & log energy consumption data to RESULT sheet
  RunAspen
  ReDim Preserve Resultat(col)
  Resultat(col) = Sheets("Sheet1").Cells(34, 15).Value
  Worksheets("Result").Cells(2, col + 2).Value = Resultat(col)
  For j = 1 To 7
    ReDim Preserve EnConsum(7, col)
    EnConsum(j, col) = Cells(j + 24, 15).Value
    Worksheets("Result").Cells(j + 2, col + 2).Value = EnConsum(j, col)
  Next j

' Run Exergy Analyses
  If Sheets("Sheet1").Range("O34").Value = "Success" Then
    ExergyAcq
    Matlabrequest

' Name of Components ID for the Result Sheet
  CompID = Range(Sheets("ExCon").Cells(289, 116), Sheets("ExCon").Cells(318, 116))
  Range(Sheets("Result").Cells(12, 2), Sheets("Result").Cells(41, 2)) = CompID
  Range(Sheets("Result").Cells(46, 2), Sheets("Result").Cells(75, 2)) = CompID
  Range(Sheets("Result").Cells(79, 2), Sheets("Result").Cells(108, 2)) = CompID
  Range(Sheets("Result").Cells(112, 2), Sheets("Result").Cells(141, 2)) = CompID

' Take Exergy Data per component
  Set WS = Sheets("Exergy Report")
  Set WR = Sheets("Result")
  ' eCH are not included therefore,
  WS.Range("C27:C28").Value = WS.Range("B27:B28").Value
  Range(WR.Cells(12, col * 2 + 1), WR.Cells(41, col * 2 + 2)).Value = Range(WS.Cells(3, 2), WS.Cells(32, 3)).Value
  WS.Cells(1, 1).Value = col
  Sheets("Result").Cells(11, col * 2 + 1) = "EF [MW]"

```



```
Sheets("Result").Cells(11, col * 2 + 2) = "EP [MW]"
```

Calculate the exergoeconomics matrix of streams

```
ExCon
```

Calculate the exergoeconomics per component

```
ExConComp_SinglePop
```

Summarize in RESULT worksheets, Put CF and CP result

```
Sheets("Result").Cells(44, col * 2 + 1) = "C(dot)F"
```

```
Sheets("Result").Cells(45, col * 2 + 1) = "$/s"
```

```
Sheets("Result").Cells(44, col * 2 + 2) = "C(dot)P"
```

```
Sheets("Result").Cells(45, col * 2 + 2) = "$/s"
```

```
CpCf = Range(Sheets("ExCon").Cells(289, 118), Sheets("ExCon").Cells(318, 119))
```

```
Range(Sheets("Result").Cells(46, col * 2 + 1), Sheets("Result").Cells(75, col * 2 + 2)) = CpCf
```

Solve specific cf and cp

```
Sheets("Result").Cells(77, col * 2 + 1) = "cf"
```

```
Sheets("Result").Cells(78, col * 2 + 1) = "$/GJ"
```

```
Sheets("Result").Cells(77, col * 2 + 2) = "cp"
```

```
Sheets("Result").Cells(78, col * 2 + 2) = "$/GJ"
```

```
For Row = 1 To 26
```

```
For k = 1 To 2
```

```
spec_c = Sheets("Result").Cells(45 + Row, col * 2 + k) / Sheets("Result").Cells(11 + Row, col * 2 + k) * 1000
```

```
Sheets("Result").Cells(78 + Row, col * 2 + k) = spec_c
```

```
Next k
```

```
Next Row
```

```
For Each Cell In Sheets("ExCon").Range(Sheets("ExCon").Cells(290, 115), Sheets("ExCon").Cells(293, 115))
```

```
If InStr(Cell.Formula, "#REF!") <> 0 Then
```

```
Cell.Formula = Replace(Cell.Formula, "#REF", "EXER")
```

```
End If
```

```
Next
```

cf of dissipative Components

```
For Row = 1 To 3
```

```
spec_ccol = Sheets("Excon").Cells(214 + Row, 116) / Sheets("Exergy Report").Cells(28 + Row, 4) * 1000
```

```
Sheets("Result").Cells(104 + Row, col * 2 + 1) = spec_ccol
```

```
Next Row
```

```
For Row = 30 To 30
```

```
For k = 1 To 2
```

```
spec_csys = Sheets("Result").Cells(45 + Row, col * 2 + k) / Sheets("Result").Cells(11 + Row, col * 2 + k) * 1000
```

```
Sheets("Result").Cells(78 + Row, col * 2 + k) = spec_csys
```

```
Next k
```

```
Next Row
```

Solve C(dot)d , CdotD_Zk, rk, and fk

```
Sheets("Result").Cells(110, col * 4 - 1) = "C(dot)D"
```

```
Sheets("Result").Cells(110, col * 4) = "CdotD + Zk"
```

```
Sheets("Result").Cells(110, col * 4 + 1) = "rk"
```

```
Sheets("Result").Cells(110, col * 4 + 2) = "fk"
```

```

Sheets("Result").Cells(111, col * 4 - 1) = "$/h"
Sheets("Result").Cells(111, col * 4) = "$/h"
Sheets("Result").Cells(111, col * 4 + 1) = "%"
Sheets("Result").Cells(111, col * 4 + 2) = "%"

```

ACTIVE COMPONENTS

For Row = 1 To 26

```

C(dot)D
CdotD = Sheets("Result").Cells(78 + Row, col * 2 + 1) / 1000 * (Sheets("Result").Cells(11 + Row, col * 2 + 1) -
    Sheets("Result").Cells(11 + Row, col * 2 + 2))
Sheets("Result").Cells(111 + Row, col * 4 - 1) = CdotD * 3600
C(dot)D + Zk
CdotD_Zk = (CdotD + Sheets("ExCon").Cells(288 + Row, 117))
Sheets("Result").Cells(111 + Row, col * 4) = CdotD_Zk * 3600
rk
rk = (Sheets("Result").Cells(78 + Row, col * 2 + 2) - Sheets("Result").Cells(78 + Row, col * 2 + 1)) /
    Sheets("Result").Cells(78 + Row, col * 2 + 1)
Sheets("Result").Cells(111 + Row, col * 4 + 1) = rk * 100
fk
fk = Sheets("ExCon").Cells(288 + Row, 117) / CdotD_Zk
Sheets("Result").Cells(111 + Row, col * 4 + 2) = fk * 100
Next Row

```

DISSIPATIVE COMPONENTS

For Row = 27 To 29

```

C(dot)D
CdotD = Sheets("ExCon").Cells(2 * Row + 287, 114).Value
Sheets("Result").Cells(111 + Row, col * 4 - 1) = CdotD * 3600
C(dot)D + Zk
CdotD_Zk = (CdotD + Sheets("ExCon").Cells(288 + Row, 117))
Sheets("Result").Cells(111 + Row, col * 4) = CdotD_Zk * 3600
rk
rk = 0
Sheets("Result").Cells(111 + Row, col * 4 + 1) = rk * 100
fk
fk = Sheets("ExCon").Cells(288 + Row, 117) / CdotD_Zk
Sheets("Result").Cells(111 + Row, col * 4 + 2) = fk * 100
Next Row

```

SYSTEM

For Row = 30 To 30

```

C(dot)D
CdotD = Sheets("Result").Cells(78 + Row, col * 2 + 1) / 1000 * (Sheets("Result").Cells(11 + Row, col * 2 + 1) -
    Sheets("Result").Cells(11 + Row, col * 2 + 2))
Sheets("Result").Cells(111 + Row, col * 4 - 1) = CdotD * 3600
C(dot)D + Zk
CdotD_Zk = (CdotD + Sheets("ExCon").Cells(288 + Row, 117))
Sheets("Result").Cells(111 + Row, col * 4) = CdotD_Zk * 3600
rk

```

```

rk = (Sheets("Result").Cells(78 + Row, col * 2 + 2) - Sheets("Result").Cells(78 + Row, col * 2 + 1)) /
      Sheets("Result").Cells(78 + Row, col * 2 + 1)
Sheets("Result").Cells(111 + Row, col * 4 + 1) = rk * 100
fk
fk = Sheets("ExCon").Cells(288 + Row, 117) / CdotD_Zk
Sheets("Result").Cells(111 + Row, col * 4 + 2) = fk * 100
Next Row
End If

Next col

End Sub

```

8.2. Aspen Plus Automation (VBA)

```

Option Base 1
Sub RunAspen()

' ----- DECISION VARIABLES SETUP -----
' Export Decision Variables from Excel to Aspen
Dim MR_Temp As IHNNode, MR_Pressure As IHNNode
Dim MR_CH4_Flow As IHNNode, MR_C2H6_Flow As IHNNode, MR_C3H8_Flow As IHNNode, MR_iC4H10_Flow
As IHNNode, MR_nC4H10_Flow As IHNNode, MR_N2_Flow As IHNNode
Dim Prop_Flow As IHNNode, Prop_C1_Pres As IHNNode, Prop_C2_Pres As IHNNode, Prop_C3_Pres As
IHNNode, Prop_C4_Pres As IHNNode
Dim PropTV1_Pres As IHNNode, PropTV2_Pres As IHNNode, PropTV3_Pres As IHNNode, PropTV4_Pres As
IHNNode
Dim MRTV1_Pres As IHNNode, MRTV2_Pres As IHNNode, NGTV_Pres As IHNNode
Dim T_NATGAS_2 As IHNNode, T_MR_02 As IHNNode, T_NATGAS_3 As IHNNode, T_MR_03 As IHNNode,
T_NATGAS_4 As IHNNode, T_MR_04 As IHNNode, T_NATGAS_5 As IHNNode, T_MR_05 As IHNNode
Dim T_NATGAS_6 As IHNNode, T_MR_08 As IHNNode, T_MR_09 As IHNNode, T_NATGAS_L As IHNNode,
T_MR_10 As IHNNode

' MR Initial Conditions
Set MR_Temp = Aspen_Case.Tree.FindNode("\Data\Blocks\MRCOL-3\Input\TEMP")
Set MR_Pressure = Aspen_Case.Tree.FindNode("\Data\Blocks\MR-C3\Input\PRES")

' Flowrate Settings
Set MR_CH4_Flow = Aspen_Case.Tree.FindNode("\Data\Streams\MR-1\Input\FLOW\MIXED\METHA-01")
Set MR_C2H6_Flow = Aspen_Case.Tree.FindNode("\Data\Streams\MR-1\Input\FLOW\MIXED\ETHAN-01")
Set MR_C3H8_Flow = Aspen_Case.Tree.FindNode("\Data\Streams\MR-1\Input\FLOW\MIXED\PROPA-01")
Set MR_iC4H10_Flow = Aspen_Case.Tree.FindNode("\Data\Streams\MR-1\Input\FLOW\MIXED\ISOBU-
01")
Set MR_nC4H10_Flow = Aspen_Case.Tree.FindNode("\Data\Streams\MR-1\Input\FLOW\MIXED\N-BUT-
01")
Set MR_N2_Flow = Aspen_Case.Tree.FindNode("\Data\Streams\MR-1\Input\FLOW\MIXED\NITRO-01")
Set Prop_Flow = Aspen_Case.Tree.FindNode("\Data\Streams\PROP-13\Input\TOTFLOW\MIXED")

' Pressure Settings
Set Prop_C1_Pres = Aspen_Case.Tree.FindNode("\Data\Blocks\PROP-C1\Input\PRES")
Set Prop_C2_Pres = Aspen_Case.Tree.FindNode("\Data\Blocks\PROP-C2\Input\PRES")
Set Prop_C3_Pres = Aspen_Case.Tree.FindNode("\Data\Blocks\PROP-C3\Input\PRES")
Set Prop_C4_Pres = Aspen_Case.Tree.FindNode("\Data\Blocks\PROP-C4\Input\PRES")
Set PropTV1_Pres = Aspen_Case.Tree.FindNode("\Data\Blocks\PROP-TV1\Input\P_OUT")
Set PropTV2_Pres = Aspen_Case.Tree.FindNode("\Data\Blocks\PROP-TV2\Input\P_OUT")
Set PropTV3_Pres = Aspen_Case.Tree.FindNode("\Data\Blocks\PROP-TV3\Input\P_OUT")
Set PropTV4_Pres = Aspen_Case.Tree.FindNode("\Data\Blocks\PROP-TV4\Input\P_OUT")
Set MRTV1_Pres = Aspen_Case.Tree.FindNode("\Data\Blocks\MRTV-1\Input\P_OUT")

```

```
Set MRTV2_Pres = Aspen_Case.Tree.FindNode("\Data\Blocks\MRTV-2\Input\P_OUT")
Set NGTV_Pres = Aspen_Case.Tree.FindNode("\Data\Blocks\NGTV\Input\P_OUT")
```

Propane Heat Exchanger Settings

```
Set T_NATGAS_2 = Aspen_Case.Tree.FindNode("\Data\Blocks\PHX1\Input\VALUE\NATGAS-1")
Set T_MR_2 = Aspen_Case.Tree.FindNode("\Data\Blocks\PHX1\Input\VALUE\MR-1")
Set T_NATGAS_3 = Aspen_Case.Tree.FindNode("\Data\Blocks\PHX2\Input\VALUE\NATGAS-2")
Set T_MR_3 = Aspen_Case.Tree.FindNode("\Data\Blocks\PHX2\Input\VALUE\MR-2")
Set T_NATGAS_4 = Aspen_Case.Tree.FindNode("\Data\Blocks\PHX3\Input\VALUE\NATGAS-3")
Set T_MR_4 = Aspen_Case.Tree.FindNode("\Data\Blocks\PHX3\Input\VALUE\MR-3")
Set T_NATGAS_5 = Aspen_Case.Tree.FindNode("\Data\Blocks\PHX4\Input\VALUE\NATGAS-4")
Set T_MR_5 = Aspen_Case.Tree.FindNode("\Data\Blocks\PHX4\Input\VALUE\MR-4")
```

MR Heat Exchanger Settings

```
Set T_NATGAS_6 = Aspen_Case.Tree.FindNode("\Data\Blocks\MHX1\Input\VALUE\NATGAS-5")
Set T_MR_8 = Aspen_Case.Tree.FindNode("\Data\Blocks\MHX1\Input\VALUE\MR-7")
Set T_MR_9 = Aspen_Case.Tree.FindNode("\Data\Blocks\MHX1\Input\VALUE\MR-6")
Set T_NATGAS_7 = Aspen_Case.Tree.FindNode("\Data\Blocks\MHX2\Input\VALUE\NATGAS-6")
Set T_MR_10 = Aspen_Case.Tree.FindNode("\Data\Blocks\MHX2\Input\VALUE\MR-9")
```

```
MR_Temp.Value = Sheets("Sheet1").Range("B26").Value
MR_Pressure.Value = Sheets("Sheet1").Range("B27").Value
MR_CH4_Flow.Value = Sheets("Sheet1").Range("B28").Value
MR_C2H6_Flow.Value = Sheets("Sheet1").Range("B29").Value
MR_C3H8_Flow.Value = Sheets("Sheet1").Range("B30").Value
MR_iC4H10_Flow.Value = Sheets("Sheet1").Range("B31").Value
MR_nC4H10_Flow.Value = Sheets("Sheet1").Range("B32").Value
MR_N2_Flow.Value = Sheets("Sheet1").Range("B33").Value
Prop_Flow.Value = Sheets("Sheet1").Range("B34").Value
Prop_C1_Pres.Value = Sheets("Sheet1").Range("B35").Value
Prop_C2_Pres.Value = Sheets("Sheet1").Range("B36").Value
Prop_C3_Pres.Value = Sheets("Sheet1").Range("B37").Value
Prop_C4_Pres.Value = Sheets("Sheet1").Range("B38").Value
PropTV1_Pres.Value = Sheets("Sheet1").Range("B39").Value
PropTV2_Pres.Value = Sheets("Sheet1").Range("B40").Value
PropTV3_Pres.Value = Sheets("Sheet1").Range("B41").Value
PropTV4_Pres.Value = Sheets("Sheet1").Range("B42").Value
MRTV1_Pres.Value = Sheets("Sheet1").Range("B43").Value
MRTV2_Pres.Value = Sheets("Sheet1").Range("B44").Value
NGTV_Pres.Value = Sheets("Sheet1").Range("B45").Value
T_NATGAS_2.Value = Sheets("Sheet1").Range("B46").Value
T_MR_2.Value = Sheets("Sheet1").Range("B47").Value
T_NATGAS_3.Value = Sheets("Sheet1").Range("B48").Value
T_MR_3.Value = Sheets("Sheet1").Range("B49").Value
T_NATGAS_4.Value = Sheets("Sheet1").Range("B50").Value
T_MR_4.Value = Sheets("Sheet1").Range("B51").Value
T_NATGAS_5.Value = Sheets("Sheet1").Range("B52").Value
T_MR_5.Value = Sheets("Sheet1").Range("B53").Value
T_NATGAS_6.Value = Sheets("Sheet1").Range("B54").Value
T_MR_8.Value = Sheets("Sheet1").Range("B55").Value
T_MR_9.Value = Sheets("Sheet1").Range("B56").Value
T_NATGAS_7.Value = Sheets("Sheet1").Range("B57").Value
T_MR_10.Value = Sheets("Sheet1").Range("B58").Value
```

Reinitialize and Run Aspen Plus Simulation

```
Aspen_Case.Reinit
Aspen_Case.Run
```

----- DISPLAYING THE RESULT -----

Returning the Aspen Plus Simulation Result back to Excel

```
Dim MR_1_Flowrate As INode
Dim MR_1_Pressure As INode
Dim PROP_13_Flowrate As INode
```

```

Dim LNG_Flowrate As IHNode, LNG_Temp As IHNode, LNG_Pressure As IHNode, LNG_LFrac As IHNode
Dim T_PROP_13 As IHNode, T_PROP_16 As IHNode, T_PROP_19 As IHNode, T_PROP_22 As IHNode
Dim T_MR_1 As IHNode, T_MR_11 As IHNode, T_MR_14 As IHNode
Set MR_1_Flowrate = Aspen_Case.Tree.FindNode("\Data\Streams\MR-1\Output\MASSFLMX\MIXED")
Set T_MR_1 = Aspen_Case.Tree.FindNode("\Data\Streams\MR-1\Output\TEMP_OUT\MIXED")
Set MR_1_Pressure = Aspen_Case.Tree.FindNode("\Data\Streams\MR-1\Output\PRES_OUT\MIXED")
Set PROP_13_Flowrate = Aspen_Case.Tree.FindNode("\Data\Streams\PROP-13\Output\MASSFLMX\MIXED")
Set PropTV1_Pres = Aspen_Case.Tree.FindNode("\Data\Blocks\PROP-TV1\Output\P_OUT_OUT")
Set PropTV2_Pres = Aspen_Case.Tree.FindNode("\Data\Blocks\PROP-TV2\Output\P_OUT_OUT")
Set PropTV3_Pres = Aspen_Case.Tree.FindNode("\Data\Blocks\PROP-TV3\Output\P_OUT_OUT")
Set PropTV4_Pres = Aspen_Case.Tree.FindNode("\Data\Blocks\PROP-TV4\Output\P_OUT_OUT")
Set NATGAS8_Flowrate = Aspen_Case.Tree.FindNode("\Data\Streams\NATGAS-8\Output\MASSFLMX\MIXED")
Set NATGAS8_Temp = Aspen_Case.Tree.FindNode("\Data\Streams\NATGAS-8\Output\TEMP_OUT\MIXED")
Set NATGAS8_Pressure = Aspen_Case.Tree.FindNode("\Data\Streams\NATGAS-8\Output\PRES_OUT\MIXED")
Set NATGAS8_LFrac = Aspen_Case.Tree.FindNode("\Data\Streams\NATGAS-8\Output\LFRAC\MIXED")
Set T_PROP_13 = Aspen_Case.Tree.FindNode("\Data\Streams\PROP-13\Output\TEMP_OUT\MIXED")
Set T_PROP_16 = Aspen_Case.Tree.FindNode("\Data\Streams\PROP-16\Output\TEMP_OUT\MIXED")
Set T_PROP_19 = Aspen_Case.Tree.FindNode("\Data\Streams\PROP-19\Output\TEMP_OUT\MIXED")
Set T_PROP_22 = Aspen_Case.Tree.FindNode("\Data\Streams\PROP-22\Output\TEMP_OUT\MIXED")
Set T_MR_11 = Aspen_Case.Tree.FindNode("\Data\Streams\MR-11\Output\TEMP_OUT\MIXED")
Set T_MR_14 = Aspen_Case.Tree.FindNode("\Data\Streams\MR-14\Output\TEMP_OUT\MIXED")
Worksheets("Sheet1").Activate

```

Place the result value in the workbook cells

```

Sheets("Sheet1").Range("T26") = MR_1_Flowrate.Value
Sheets("Sheet1").Range("T27") = T_MR_1.Value
Sheets("Sheet1").Range("T28") = MR_1_Pressure.Value
Sheets("Sheet1").Range("T29") = PROP_13_Flowrate.Value
Sheets("Sheet1").Range("T30") = T_PROP_13.Value
Sheets("Sheet1").Range("T31") = PropTV1_Pres.Value
Sheets("Sheet1").Range("T32") = PropTV2_Pres.Value
Sheets("Sheet1").Range("T33") = PropTV3_Pres.Value
Sheets("Sheet1").Range("T34") = PropTV4_Pres.Value
Sheets("Sheet1").Range("T35") = NATGAS8_Flowrate.Value
Sheets("Sheet1").Range("T36") = NATGAS8_Temp.Value
Sheets("Sheet1").Range("T37") = NATGAS8_Pressure.Value
Sheets("Sheet1").Range("T38") = NATGAS8_LFrac.Value
Sheets("Sheet1").Range("T39") = T_PROP_13.Value
Sheets("Sheet1").Range("T40") = T_PROP_16.Value
Sheets("Sheet1").Range("T41") = T_PROP_19.Value
Sheets("Sheet1").Range("T42") = T_PROP_22.Value
Sheets("Sheet1").Range("T43") = T_MR_11.Value
Sheets("Sheet1").Range("T44") = T_MR_14.Value

```

Place the Energy Consumption in the workbook cells

```

Dim W_PROP_C1 As IHNode, W_PROP_C2 As IHNode, W_PROP_C3 As IHNode, W_PROP_C4 As IHNode,
W_MR_C1 As IHNode, W_MR_C2 As IHNode, W_MR_C3 As IHNode
Set W_PROP_C1 = Aspen_Case.Tree.FindNode("\Data\Blocks\PROP-C1\Output\WNET")
Set W_PROP_C2 = Aspen_Case.Tree.FindNode("\Data\Blocks\PROP-C2\Output\WNET")
Set W_PROP_C3 = Aspen_Case.Tree.FindNode("\Data\Blocks\PROP-C3\Output\WNET")
Set W_PROP_C4 = Aspen_Case.Tree.FindNode("\Data\Blocks\PROP-C4\Output\WNET")
Set W_MR_C1 = Aspen_Case.Tree.FindNode("\Data\Blocks\MR-C1\Output\WNET")
Set W_MR_C2 = Aspen_Case.Tree.FindNode("\Data\Blocks\MR-C2\Output\WNET")
Set W_MR_C3 = Aspen_Case.Tree.FindNode("\Data\Blocks\MR-C3\Output\WNET")
Sheets("Sheet1").Range("O25") = W_MR_C1.Value / 1000
Sheets("Sheet1").Range("O26") = W_MR_C2.Value / 1000
Sheets("Sheet1").Range("O27") = W_MR_C3.Value / 1000
Sheets("Sheet1").Range("O28") = W_PROP_C1.Value / 1000
Sheets("Sheet1").Range("O29") = W_PROP_C2.Value / 1000
Sheets("Sheet1").Range("O30") = W_PROP_C3.Value / 1000
Sheets("Sheet1").Range("O31") = W_PROP_C4.Value / 1000

```

```

Place the COMPRESSORS aspen result in excelsheet
Dim INDPOWER, BRAKEPOWER, POWERLOSS, EFFISEN, EFFMECH, INPRES, POC, PRESRATIO, TOC, TOS,
BVFRAC As INode
Dim Compres As Variant
Compres = Array("PROP-C1", "PROP-C2", "PROP-C3", "PROP-C4", "MR-C1", "MR-C2", "MR-C3")
For x = 1 To 7
    Set INDPOWER = Aspen_Case.Tree.FindNode("\Data\Blocks\" + Compres(x) +
"Output" & IND_POWER")
    Set BRAKEPOWER = Aspen_Case.Tree.FindNode("\Data\Blocks\" + Compres(x) +
"Output" & BRAKE_POWER")
    Set POWERLOSS = Aspen_Case.Tree.FindNode("\Data\Blocks\" + Compres(x) +
"Output" & POWER_LOSS")
    Set EFFISEN = Aspen_Case.Tree.FindNode("\Data\Blocks\" + Compres(x) +
"Output" & EFF_ISEN")
    Set EFFMECH = Aspen_Case.Tree.FindNode("\Data\Blocks\" + Compres(x) +
"Output" & EFF_MECH")
    Set INPRES = Aspen_Case.Tree.FindNode("\Data\Blocks\" + Compres(x) +
"Output" & IN_PRES")
    Set POC = Aspen_Case.Tree.FindNode("\Data\Blocks\" + Compres(x) + "Output" & POC")
    Set PRESRATIO = Aspen_Case.Tree.FindNode("\Data\Blocks\" + Compres(x) +
"Output" & PRES_RATIO")
    Set BTEMP = Aspen_Case.Tree.FindNode("\Data\Blocks\" + Compres(x) +
"Output" & B_TEMP")
    Set TOC = Aspen_Case.Tree.FindNode("\Data\Blocks\" + Compres(x) + "Output" & TOC")
    Set TOS = Aspen_Case.Tree.FindNode("\Data\Blocks\" + Compres(x) + "Output" & TOS")
    Set BVFRAC = Aspen_Case.Tree.FindNode("\Data\Blocks\" + Compres(x) +
"Output" & B_VFRAC")
    Worksheets("Compressors").Cells(47, x + 2) = INDPOWER.Value
    Worksheets("Compressors").Cells(48, x + 2) = BRAKEPOWER.Value
    Worksheets("Compressors").Cells(51, x + 2) = POWERLOSS.Value
    Worksheets("Compressors").Cells(52, x + 2) = EFFISEN.Value
    Worksheets("Compressors").Cells(53, x + 2) = EFFMECH.Value
    Worksheets("Compressors").Cells(54, x + 2) = INPRES.Value
    Worksheets("Compressors").Cells(55, x + 2) = POC.Value
    Worksheets("Compressors").Cells(56, x + 2) = PRESRATIO.Value
    Worksheets("Compressors").Cells(57, x + 2) = BTEMP.Value
    Worksheets("Compressors").Cells(58, x + 2) = TOC.Value
    Worksheets("Compressors").Cells(59, x + 2) = TOS.Value
    Worksheets("Compressors").Cells(60, x + 2) = BVFRAC.Value
Next x

Place the heat exchangers aspen result in excelsheet
VARID = Array("FQ_OUTSTREAM", "FQ_SIDE_OUT", "IN_TEMP", "IN_PRES", "IN_VF", "B_TEMP",
"B_PRES", "B_VFRAC")
Dim streamID As String
Dim VAR_X, ZONE_X As INode
HXID = Array("PHX1", "PHX2", "PHX3", "PHX4", "MHX1", "MHX2")
PHX1 to PHX4
For ID = 1 To 4
    For Var = 1 To 8
        For x = 1 To 3
            kolom = ID * 2 - 1 + ID + x
            streamID = Worksheets("MHEATX").Cells(36, kolom)
            Set VAR_X = Aspen_Case.Tree.FindNode("\Data\Blocks\" + HXID(ID) +
"Output" & VARID(Var) + " " & streamID)
            Worksheets("MHEATX").Cells(36 + Var, kolom) = VAR_X.Value
        Next x
    Next Var
Next ID
MHX1
For ID = 5 To 5

```

```

For Var = 1 To 8
  For x = 1 To 4
    kolom = ID * 2 - 1 + ID + x
    streamID = Worksheets("MHEATX").Cells(36, kolom)
    Set VAR_X = Aspen_Case.Tree.FindNode("\Data\Blocks\" + HXID(ID) +
"Output" + VARID(Var) + " " + streamID)
    Worksheets("MHEATX").Cells(36 + Var, kolom) = VAR_X.Value
  Next x
Next Var
Next ID
' MHX2
For ID = 6 To 6
  For Var = 1 To 8
    For x = 1 To 3
      kolom = 18 + x
      streamID = Worksheets("MHEATX").Cells(36, kolom)
      Set VAR_X = Aspen_Case.Tree.FindNode("\Data\Blocks\" + HXID(ID) +
"Output" + VARID(Var) + " " + streamID)
      Worksheets("MHEATX").Cells(36 + Var, kolom) = VAR_X.Value
    Next x
  Next Var
Next ID
' ZONE ANALYSIS RESULT
ZONE_ID = Array("QCALC2", "UA", "LMTD", "MITA", "HSTA", "CSTA", "HSNTU", "CSNTU")
For ID = 1 To 6
  For Var = 1 To 8
    kolom = ID * 2 + ID
    Set ZONE_X = Aspen_Case.Tree.FindNode("\Data\Blocks\" + HXID(ID) +
"Output" + ZONE_ID(Var))
    Worksheets("MHEATX").Cells(46 + Var, kolom) = ZONE_X.Value
  Next Var
Next ID
' Place the COOLERS aspen result in excel sheet
COOLERS_VAR = Array("IN_TEMP", "B_TEMP", "IN_PRES", "B_PRES", "B_VFRAC", "QNET")
Dim COOL_X As IHNode
For ID = 1 To 3
  For Var = 1 To 6
    kolom = ID * 4 - 1
    cool_ID = Worksheets("Coolers").Cells(38, kolom)
    Set COOL_X = Aspen_Case.Tree.FindNode("\Data\Blocks\" + cool_ID + "Output" +
COOLERS_VAR(Var))
    Worksheets("Coolers").Cells(39 + Var, kolom) = COOL_X.Value
  Next Var
Next ID
' Place the FLASH VESSELS aspen result in excel sheet
FLASH_VAR = Array("B_TEMP", "B_PRES", "B_VFRAC", "Total Flow cum/hr ")
Dim FLASH_X As IHNode
For ID = 1 To 5
  For Var = 1 To 3
    kolom = ID + 2
    FLASH_ID = Worksheets("Flash Vessels").Cells(31, kolom)
    Set FLASH_X = Aspen_Case.Tree.FindNode("\Data\Blocks\" + FLASH_ID + "Output"
+ FLASH_VAR(Var))
    Worksheets("Flash Vessels").Cells(32 + Var, kolom) = FLASH_X.Value
  Next Var
  Dim Input_Flash As String
  kolom = ID + 2
  FLASH_ID = Worksheets("Flash Vessels").Cells(31, kolom)
  Input_Flash = Worksheets("Flash Vessels").Cells(32, kolom)
  Set FLASH_X = Aspen_Case.Tree.FindNode("\Data\Streams\" + Input_Flash +
"OutputVOLFLMXMIXED")
  Worksheets("Flash Vessels").Cells(36, kolom) = FLASH_X.Value

```

```

Next ID

' Place the VALVES aspen result in excelsheet
VALVE_VAR = Array("TOT_MASS_ABS")
Dim VALVE_X As IHNode
For ID = 1 To 6
    For Var = 1 To 1
        kolom = ID + 2
        valve_ID = Worksheets("Valves").Cells(11, kolom)
        Set VALVE_X = Aspen_Case.Tree.FindNode("\Data\Blocks\" + valve_ID + "Output"
+ VALVE_VAR(Var))
        Worksheets("Valves").Cells(12 + Var, kolom) = VALVE_X.Value
    Next Var
Next ID

' Updating Simulation Status
Dim StatusSim As IHNode
Set StatusSim = Aspen_Case.Tree.FindNode("\Data\Results Summary")
Sheets("Sheet1").Range("O34") = Status(StatusSim.AttributeValue(HAP_COMPSTATUS))
End Sub

```

8.3. Initialization of the Optimization

```

import sys, os
import timeit
import xlwings as xw
from numpy import asarray, nan, vstack, nanmin, nanmax
import FitnessFun as Fit
import GALoop as GA
import NSGALoop as N

# import os
import numpy as np

# import random as random
from pandas import DataFrame
import pandas as pd
import pythoncom

# Start timer
start = timeit.default_timer()

# Preparing the inputs for GA Loop
iteration = 100
MutationRate = 0.35
xoverpointsize = 9

# Excel File path
file = 'C3MR_Dashboard_Python.xlsm'

# Open the existing excel file
xw.Book(file)
Pops = xw.sheets('Pops')
Activebook = xw.books.active

# Find the appropriate index for Aspen Plus Input
index = Pops.range('A2:A24').value

# Import Initial Random Values
from Init_Var_OF4 import ListOfRandVar, popsize

```



```

# Sort the list based on the index
ListOfRandVar.sort(key=lambda x: index.index(x[1]))

# Convert to Panda DataFrame
df = DataFrame(ListOfRandVar)

# Extracting the initial random and base case variables
RandVar = [x[3] for x in ListOfRandVar]

# Write the init var values in Excel
Pops.range((2,4), (25,400)).clear_contents() # Change the column range to cell for more
robust coding.
Pops.range('E2').value = asarray(RandVar)
Pops.range((25,4), (25,4+popsiz-1)).value = 158.42 #4MTPA

# Summarize the decision variables
DecVar = Pops.range((2,4), (24,4+popsiz-1)).options(transpose=False).value
DecVarDf = DataFrame(DecVar) # cara lain: DecVarDf = list(map(list, zip(*1)))

# Run Exergy Analysis
#RunExergy = Activebook.macro('Run_Exergy_Analysis.Run_Exergy_Analysis')
#RunExergy()

# Run Exergoeconomic Analysis
RunExCon = Activebook.macro('Run_Exergoeconomics.ExecuteAll')
RunExCon()

# Import result of energy consumption to python
EnConResult = DataFrame(Activebook.sheets('Result').range((2,2), (9,2+popsiz)).value)
EnConResult.fillna(value=nan, inplace=True)

# Import result of exergy analysis to python
ExerCompResult =
DataFrame(Activebook.sheets('Result').range((11,2), (41,2+popsiz*2)).value)
ExerCompResult.fillna(value=nan, inplace=True)

# Import result of exergoeconomics to python
ExConCompResult =
DataFrame(Activebook.sheets('Result').range((44,2), (75,2+popsiz*2)).value)
ExConCompResult.fillna(value=nan, inplace=True)
ExConSpecific =
DataFrame(Activebook.sheets('Result').range((77,2), (108,2+popsiz*2)).value)
ExConSpecific.fillna(value=nan, inplace=True)
ExConDesResult =
DataFrame(Activebook.sheets('Result').range((110,2), (141,2+popsiz*4)).value)
ExConDesResult.fillna(value=nan, inplace=True)

# Evaluate the Fitness Functions
[FF2, FF4, FF2_index, FF4_index] = Fit.fitness(EnConResult, ExerCompResult, popsiz,
ExConSpecific, ExConCompResult, ExConDesResult, ExEnviroDes)

#----- Single GA optimization Loop-----
# Select objective function to evaluate, e.g. total cost of product (FF4)
idx = FF4_index
FF = FF4
BestFF = [min(FF)]

# Sorting the Decision Variables based on Fitness
DecVarRank = []
[DecVarRank.append(DecVarDf[i]) for i in idx]

# Entering GA Loop
GALoop.py

```

```

#----- End of single-objective GA -----

#----- Start of Multi-Objective GA -----
Objectives = 2

OF1 = FF2
OF2 = FF4

# Create Negative value for max. objectives
BestFFM = [[nanmin(OF1), nanmin(OF2)]]

# Preparing the Multi-objective Properties
FFMultiA = pd.DataFrame(OF1).transpose()
FFMultiB = pd.DataFrame(OF2).transpose()

# Replace nan with penalty value (0 for FF2, 5000 for FF5)
FFMultiA = FFMultiA.fillna(0)
FFMultiB = FFMultiB.fillna(5000)

# Setting Up Frontiers
Front = [nan for f in range(popsize)]
Front = pd.DataFrame(Front).transpose()

# Concatenate the variables
DecVarMulti = pd.concat([DecVarDf.copy(), FFMultiA, FFMultiB, FFMultiC, Front],
ignore_index=True)

# Define Object for NSGA properties
class PClass:
    def __init__(self, np, Sp, dist):
        self.np = np
        self.Sp = Sp
        self.dist = dist
    def __getitem__(self, i):
        return self.np[i]

class Frontier:
    def __init__(self, idx):
        self.idx = idx

Fronts = [Frontier([]) for F in range(popsize)]
# Non-Dominated Sorting: Finding first front
Indiv = []
for p in range(popsize):
    Indiv.append(PClass(0, [], 0))
    PQEqual = 0
    for q in range(popsize):
        m, n = range(Objectives)
        if (DecVarMulti.iloc[m+23][p] < DecVarMulti.iloc[m+23][q]
            and DecVarMulti.iloc[n+23][p] < DecVarMulti.iloc[n+23][q]):
            Indiv[p].Sp.append(q)
        elif (DecVarMulti.iloc[m+23][p] == DecVarMulti.iloc[m+23][q]
            and DecVarMulti.iloc[n+23][p] == DecVarMulti.iloc[n+23][q]):
            PQEqual = PQEqual + 1
        elif (DecVarMulti.iloc[m+23][p] > DecVarMulti.iloc[m+23][q]
            and DecVarMulti.iloc[n+23][p] > DecVarMulti.iloc[n+23][q]):
            Indiv[p].np = Indiv[p].np + 1
    if Indiv[p].np == 0:
        DecVarMulti.iloc[Objectives+23+1][p] = 1
        Fronts[1].idx.append(p)

# Non-Dominated Sorting: Subsequent Front
i = 1

```

```

LastFront = []
while Fronts[i].idx:
    Q = []
    for p in Fronts[i].idx:
        for q in Indiv[p].Sp:
            Indiv[q].np = Indiv[q].np - 1
            if Indiv[q].np == 0:
                Q.append(q)
    i = i + 1
    Fronts[i].idx = Q

# Assign front/rank in DecVarMulti
for item in range(1, len(Fronts)):
    for p in Fronts[item].idx:
        DecVarMulti[p][Objectives+23+1] = item

# Crowding Distance of individuals
# Sorting index by Front
SortByFront = []
for f in range(len(Fronts)):
    if Fronts[f].idx:
        for n in Fronts[f].idx:
            SortByFront.append(n)
# Sorting index by Objectives
for m in range(Objectives):
    alfa = DecVarMulti.iloc[m+23][:].values.tolist()
    beta = list(range(popsize))
    IndexByObjective = [x for _, x in sorted(zip(alfa, beta))]
    DecVarByObjective = []
    [DecVarByObjective.append(DecVarMulti[i]) for i in IndexByObjective]
    DecVarByObjective = DataFrame(DecVarByObjective).transpose()
    Indiv[IndexByObjective[0]].dist = Indiv[IndexByObjective[-1]].dist = float('inf')
    fmin = DecVarByObjective.iloc[m+23, 0]
    fmax = DecVarByObjective.iloc[m+23, -1]
    for o in range(1, popsize-1):
        Indiv[IndexByObjective[o]].dist += (DecVarByObjective.iloc[m+23, o+1] -
        DecVarByObjective.iloc[m+23, o-1]) / (fmax-fmin)

# Record the Crowding Distance in DecVarMulti (Bigger is Better)
Distance = [Indiv[o].dist for o in range(popsize)]
Distance_ = pd.DataFrame(Distance).transpose()
DecVarMulti = pd.concat([DecVarMulti, Distance_], ignore_index=True)

# Rename the index in DecVarMulti
DecVarMulti.rename(index={23:'ExEf', 24:'ExCon', 26:'Front', 27:'CrDist'}, inplace=True)

# Sorting based on 1:Front and then 2:Crowding Distances
idx_loop_ = []
DecVarRank = []
for f in range(len(Fronts)):
    if Fronts[f].idx:
        alfa = [Indiv[o].dist for o in Fronts[f].idx]
        idx_loop_ += [x for _, x in sorted(zip(alfa, Fronts[f].idx), reverse=True)]
    [DecVarRank.append(DecVarDf[i]) for i in idx_loop_]
DecVarRank = DataFrame(DecVarRank).transpose()
DecVarDf = DataFrame(DecVarRank.values)

# Saving the first front as the best individuals
f = Fronts[1].idx[0]
BestIndividuals = DecVarMulti[f]
for i in Fronts[1].idx:
    BestOfLoop = DecVarMulti[i]
    BestIndividuals = pd.concat([BestIndividuals, BestOfLoop], axis=1, ignore_index=True)

```

```

# Entering GA Loop with Non-dominated sorting and Crowding distance
NSGALoop.py

#----- End of Multi-Objective GA optimization Loop -----

```

8.4. Genetic Algorithm in Python

```

import numpy as np
import pandas as pd
import xlwings as xw
from random import random, randint
from pandas import DataFrame
from numpy import vstack, nan
import FitnessFun as Fit
import os, time

# Function of GA
def genetic(iteration, popsize, DecVarDf, DecVarRank, FF, BestFF, BestIndividuals,
xoverpointsize, MutationRate, DataSetFull, MutationLB=-0.75, MutationUB=0.75):

    # Reactivate Excel
    Pops = xw.sheets('Pops')
    Activebook = xw.books.active

    # Design Variables
    Keep = int(popsize/8) #some rate z.B. 25% in this case
    Children = popsize - Keep

    # Each Mating Produce 2 children
    MateSize = int(np.ceil(Children/2))

    # While loop for number of iteration
    iter = 0
    print('iteration: ', iter)

    while iter != iteration:

        # 1. SELECTION
        # Extracting kept variables from previous population
        DecVarKeep = DecVarRank.iloc[:, 0:Keep].copy()

        # Tournament Selection for Crossover:
        TourSize = 2
        mom = []
        dad = []

        # Selecting random candidates (index) for crossover with unique index
        while mom == [] or any([m == d for m, d in zip(mom, dad)]) is True:
            mom = []
            dad = []
            for i in range(MateSize):
                candidateMom = np.random.choice(np.arange(int(Keep)), replace=False,
                                                size=TourSize)
                if FF[candidateMom[0]] < FF[candidateMom[1]]:
                    WinMom = candidateMom[0]
                else:
                    WinMom = candidateMom[1]
            mom += [WinMom]

```

```

        candidateDad = np.random.choice(np.arange(int(Keep)), replace=False,
                                         size=TourSize)
        if FF[candidateDad[0]] < FF[candidateDad[1]]:
            WinDad = candidateDad[0]
        else:
            WinDad = candidateDad[1]
        dad += [WinDad]
    mom = np.asarray(mom)
    dad = np.asarray(dad)

# 2. CROSSOVER
OffspringList = []
for i in range(len(mom)):
    # Extracting offsprings from crossover
    Offspring1 = (DecVarDf[mom[i]].copy()).tolist()
    Offspring2 = (DecVarDf[dad[i]].copy()).tolist()
    # Generating random crossover points
    xoverpoint = np.random.choice(np.arange(1, len(DecVarDf)), replace=False,
                                   size=xoverpointsize)

    for j in range(xoverpoint.size):
        # Produce new crossover chromosome
        chromosome1 = DecVarDf[mom[i]][xoverpoint[j]] - random() * (
            DecVarDf[mom[i]][xoverpoint[j]] - DecVarDf[dad[i]][xoverpoint[j]])
        chromosome2 = DecVarDf[dad[i]][xoverpoint[j]] + random() * (
            DecVarDf[mom[i]][xoverpoint[j]] - DecVarDf[dad[i]][xoverpoint[j]])
        # Inserting new chromosomes for the offsprings
        Offspring1[xoverpoint[j]] = chromosome1
        Offspring2[xoverpoint[j]] = chromosome2

    # Collecting new population
    OffspringList.append(Offspring1)
    OffspringList.append(Offspring2)

# Adjusting MRTV1_Pres and MRTV2_Pres
if any(xoverpoint==14) is True:
    for i in range(len(OffspringList)):
        OffspringList[i][15] = OffspringList[i][14] - 0.09
elif any(xoverpoint==15) is True:
    for i in range(len(OffspringList)):
        OffspringList[i][14] = OffspringList[i][15] + 0.09
# Adjusting PROPTV1_Pres and MRTV3_Pres
elif any(xoverpoint==13) or any(xoverpoint==16) is True:
    for i in range(len(OffspringList)):
        OffspringList[i][13] = np.random.uniform(1.03125,1.5)
        OffspringList[i][16] = 1.2159

# Converting new Offsprings to Dataframe
OffspringDf = pd.DataFrame(OffspringList).T

# Converting the variables to list
DVKList = []
DVKList = DecVarKeep.values.tolist()
OFList = OffspringDf.values.tolist()

# Joining Kept variables and Offsprings from prev. population
DVKList = [DVKList[i] + OFList[i] for i in range(len(OFList))]

# Converting back to DataFrame.
DecVarXover = pd.DataFrame(DVKList)

# 3. MUTATION (Haupt, p.61)
# Generating random index for soon-to-be mutated variables. (

```

```

MutationSize = int(MutationRate * (Var_OF3*popsize))
MutRow = []
MutCol = []

# Mutation for all variables NO OF or OF4
MutRow = np.random.randint(1, high=15, size=MutationSize)

# First and Second Column (index 0 and 1) are be mutated due to elitism
MutCol = np.random.randint(2, high=popsize, size=MutationSize)

# Reset the existing values of DecVarDf
DecVarDf = DecVarXover.copy()

# Mutation Process
for i in range(MutationSize):
    alpha = np.random.uniform(MutationLB, MutationUB)
    DecVarDf[MutCol[i]][MutRow[i]] = (1 + alpha) *
DecVarXover[MutCol[i]][MutRow[i]]
    for i in range(len(DecVarDf.columns)):
        DecVarDf[i][14] = DecVarDf[i][15] - 0.09

# Return the variables to excel file
Pops.range('D2:ZZ24').clear_contents()
Pops.range('D2').value = DecVarDf.values

# Run Exergoeconomic Analysis
RunExCon = Activebook.macro('Run_Exergoeconomics.ExecuteAll')
RunExCon()

# Import the result to python
EnConResult = DataFrame(Activebook.sheets('Result').range
                        ((2,2),(9,2+popsize)).value)
EnConResult.fillna(value=nan, inplace=True)
ExerCompResult = DataFrame(Activebook.sheets('Result').
                        range((11,2),(41,2+popsize*2)).value)
ExerCompResult.fillna(value=nan, inplace=True)
ExConCompResult = DataFrame(Activebook.sheets('Result').range
                        ((44,2),(75,2+popsize*2)).value)
ExConCompResult.fillna(value=nan, inplace=True)
ExConSpecific = DataFrame(Activebook.sheets('Result').range
                        ((77,2),(108,2+popsize*2)).value)
ExConSpecific.fillna(value=nan, inplace=True)
ExConDesResult = DataFrame(Activebook.sheets('Result').range
                        ((110,2),(141,2+popsize*4)).value)
ExConDesResult.fillna(value=nan, inplace=True)
ExEnviroSpecific = DataFrame(Activebook.sheets('Result').range
                        ((177,2),(208,2+popsize*4)).value)
ExEnviroSpecific.fillna(value=nan, inplace=True)
ExEnviroDes = DataFrame(Activebook.sheets('Result').range
                        ((210,2),(241,2+popsize*4)).value)
ExEnviroDes.fillna(value=nan, inplace=True)

# Evaluate the Fitness Functions
[FF2, FF4, FF2_index, FF4_index] = Fit.fitness(EnConResult, ExerCompResult,
                        popsize, ExConSpecific, ExConCompResult,
                        ExConDesResult, ExEnviroDes)

# Select objective to evaluate: FF2, Exergy Efficiency, FF4 = Cost of Product
FF = FF4
idx_loop = FF4_index

# Maximize or minimize the objective
BestFF_loop = min(FF)

```

```

# Sorting the Decision Variables based on Fitness
DecVarRank = []
[DecVarRank.append(DecVarDf[i]) for i in idx_loop]
DecVarRank = DataFrame(DecVarRank).transpose()

# Store best individual of each iteration
BestOfLoop = DecVarRank.iloc[:,0].values
BestIndividuals = (np.vstack((BestIndividuals, BestOfLoop)))

# Store best fitness values of each iteration
BestFF.append(BestFF_loop)

# Save data sets for each iteration
DataSet = DecVarDf
DataSetResult = DataFrame([FF])
DataSet = DataSet.append(DataSetResult)
DataSetFull = pd.concat([DataSetFull,DataSet], axis=1)

# Iteration Count
iter += 1

BestIndividuals = BestIndividuals.transpose()

return DecVarRank, BestIndividuals, BestFF, DataSetFull

```